Deformation and diagenetic histories around foreland thrust faults

Gerald Patrick Roberts

DEFORMATION AND DIAGENETIC HISTORIES AROUND FORELAND THRUST FAULTS

GERALD PATRICK ROBERTS

A thesis submitted to the University of Durham for the degree of Doctor of Philosophy

Department of Geological Sciences

Commenced 1st September 1987
Submitted September 1990

DECLARATION

The content of this thesis is the original work of the author and has not previously been submitted for a degree at this or any other university. Other people's work is acknowledged by reference.

Gerald Roberts,
Department of Geological Sciences,
University of Durham.

COPYRIGHT

DEDICATED TO MY FAMILY.

ABSTRACT

This thesis is concerned with the relationship between deformation and fluid flow along thrust zones. The study was carried out in the Vercors, French Sub-Alpine Chains foreland thrust belt. Study of the thermal alteration of organic matter within the area suggests that prior to west-north-west directed thrusting within the Vercors basin in post middle Miocene times, the rocks now exposed at the surface had not been buried beneath a large thickness of foredeep sediments and remained within the diagenetic realm. Deeper buried levels within the stratigraphy passed into the hydrocarbon generation window prior to thrusting within the Vercors basin. The rocks presently exposed at the surface also remained in the diagenetic realm during and after the thrusting which suggests that thrust sheet loading did not significantly contribute to thermal alteration of organic matter. The structures of the thrust belt may have been possible structural traps for any hydrocarbons which underwent re-migration during the thrusting. The structures have been exhumed by erosion during isostatic uplift.

The Rencurel Thrust and overlying Rencurel Thrust Sheet were selected for special study as they are of regional structural importance. The thrust emplaces Urgonian limestones onto Miocene molasse sediments at present erosion levels. The thrust sheet is internally deformed by thrusts and folds. Structural data indicate that the deformation within the thrust sheet and within the Rencurel Thrust Zone occurred during one kinematically linked phase of thrusting. The Rencurel Thrust Zone itself is around 100 metres thick. The higher part of the thrust zone is composed of an array of minor faults developed within the Urgonian. These fault zones are generally less than 10cm wide and are coated in fault gouge. This array of faults is underlain by a gouge zone along the thrust contact between the Urgonian and the Miocene which is several metres thick. The gouge zones were all formed during the action of diffusive mass transfer (DMT) and cataclasis as deformation mechanisms. The wall-rocks to the gouge zones are relatively undeformed by the action of cataclasis. Cataclasis is dilatant and produces fracture porosity which increases the permeability of the fault zones whilst DMT reduces the porosity and permeability of the fault zones due to cement precipitation and pressure dissolution. Cross-cutting relationships between the microstructures indicating the action of cataclasis and DMT, suggest that the porosity and permeability of the fault rocks changed in a complex manner during the incremental deformation. This has important implications for assessing syn-kinematic fluid migration through fault zones. The fault rocks exposed at the surface today are relatively impermeable compared to undeformed wall-rocks away from the fault zone which have permeabilities comparable to those found within hydrocarbon reservoirs. The thrust zone may have been a seal in the sub-surface after the cessation of thrusting but prior to uplift and erosion.

Early distributed deformation produced an array of minor faults within the Urgonian. Cataclasis had ceased along these faults before later deformation became localised along the gouge zone which exists along the thrust contact between the Urgonian and the Miocene rocks. Early deformation was accompanied by the migration through fracture porosity of pore waters which were saturated with respect to calcite and had interacted with organic matter which was being thermally altered. This fluid flow system was not connected to fluid flow higher in the stratigraphy which resulted in the precipitation of ferroan calcite within fracture porosity in the Senonian limestones. Late deformation within the thrust zone was accompanied by the migration of hydrocarbons and pore waters saturated with respect to calcite and pyrite. All the pore waters involved in migration through the active thrust zone seem to have migrated up-dip. They migrated from levels in the stratigraphy where organic metamorphism and the maturation of hydrocarbons was occurring to levels in the deformed section which have always remained within the diagenetic realm. Ferroan calcite, pyrite and traces of hydrocarbons have not been found outside the gouge zone along the thrust contact between the Urgonian and Miocene. The fracturing which occurred to open this migration pathway did not re-fracture the inactive minor faults which were impermeable at this time. Fluid migration at this time was confined to beneath the zone of impermeable minor faults in the Urgonian and did not contribute to the diagenesis of the rocks above the thrust zone. Hydrocarbons could not have entered the hanging-wall anticline above the thrust zone from this migration pathway. The fracturing at this time did not produce connected fracture networks pervasively throughout the thrust zone which suggests that the deformation may not have released large amounts of energy in the form of seismic waves.

ACKNOWLEDGEMENTS

Firstly, I would like to thank my two supervisors Rob Butler and Maurice Tucker. Throughout my time as a PhD student they have been a constant source of help and encouragement. Special thanks to Maurice for dealing with administrative side of the studentship and for proof reading the manuscript.

I would like to acknowledge British Petroleum for the financing the studentship. I would also like to thank Rod Graham for helping to organise additional help from BP and its employees.

Special thanks are extended to James "Ned" Porter and Clare Milsom for their help during the fieldwork.

Assistance in the field was also recieved from Georgio Minelli and Max Barchi to whom I am grateful.

I would also like to thank the following people for their helpful comments and constructive criticism during the course of this study. Jonathan Henton, Dave Hunt, Rob Gawthorpe, Sue Bowler, Steve Moss, Steve Hall and Steve Jolley.

The following people were invaluable in their capacity as teachers of new techniques. Geoff Lloyd (cathodoluminescence), Andrew Peckett (microprobe and reflected light microscopy), Micky Jones (vitrinite reflectance, fluorescence microscopy, organic metamorphism and reflected light microscopy) and Ron Hardy (X-ray diffraction).

Technical assistance was provided by Dave Asbery, Paul Laverick, Gerry Dresser, George Ruth, Dave Stevenson, Karen Gittins, Carole Blair, Jeanette Finn, Lynne Gillchrist and M. Savell.

The mini-permeameter was borrowed from Shell Research B.V.

Special thanks are extended to George Randall and Ron Lambert for their patience in preparing thin sections of many descriptions.

I would like to thank all the students and members of staff who have passed through the Durham Geology department during my stay.

Further thanks are extended to Rob Gawthorpe, Rob Butler and Maurice Tucker for helping me to organise further research opportunities for after the end of my studentship.

DEFORMATION AND DIAGENETIC HISTORIES AROUND FORELAND THRUST FAULTS

GERALD PATRICK ROBERTS

CHAPTER 1 INTRODUCTION

In diagenetic studies and hydrocarbon exploration, fault zones are commonly cited as the primary conduits for the migration of hydrocarbons and sub-surface brines (Burley et al., 1989; Giroir et al., 1989; Dorobek, 1989). Conversely, fault zones are also invoked as impermeable seals to fluid migration, often helping to trap fluids such as hydrocarbons in the sub-surface (Smith, 1980; Harding & Tuminas, 1989).

Whether a fault is sealing or non-sealing is therefore an economically as well as an intellectually important question. The problem has generally been viewed in terms of the capillary pressure and pore fluid pressure differentials between the reservoir rock and the seal (Smith, 1966), the juxtaposition of certain lithologies combined with the lithology of the material smeared along the fault (Weber & Daukoru, 1975; Weber et al., 1978; Smith, 1980; Harding & Tuminas, 1989), and the finite state of the microstructures within the deformed rocks (Mitra, 1988). This approach to the problem, where the finite nature of the fault zone is considered to be of prime importance, has proved useful in hydrocarbon exploration.

However, it has been suggested that important episodes of migration of diagenetic solutions and hydrocarbons occur during fault displacements (Burley et al., 1989; Dorobek, 1989). This suggestion is backed up by changes in the discharge of streams closely associated with earthquake episodes (Briggs & Troxell, 1955) and the existence of minerals precipitated syn-kinematically within fault zones (Sibson et al., 1975; Sibson, 1981). One important mechanism producing the flow of fluids along fault zones during earthquake episodes is suggested to be seismic pumping, where earthquakes cause the collapse of dilatant fractures and the expulsion of the pore fluids they contain (Sibson et al., 1975). The episodic nature of fluid flow in these instances is not adequately described by the models mentioned above where only the finite nature of the fault zone is considered. For example deformation along fault zones at shallow crustal depths has been shown to involve fracturing and precipitation of new minerals. Fracturing allows fluid influx, whilst mineral growth occludes fracture porosity. The permeability of fault rocks therefore changes during the deformation. Also, along neotectonic fault zones surface ruptures caused by a single earthquake are discrete planes which cut through previously faulted zones which can be hundreds of metres wide. This suggests that temporal and spatial changes in the position of deformation and therefore structurally controlled fluid migration occur during incremental development of a fault zone.

This thesis investigates the relationships between deformation and fluid flow along fault zones. Thrust faults are investigated here, but the principles developed in this

thesis are equally applicable to normal or strike slip fault zones, and also areas such as hydrocarbon reservoirs which may have undergone deformation involving minor faulting. The aims of the study are listed below.

1) Can temporal and spatial changes in the permeability of fault zones be recognised from exhumed field examples? How does this compare with the finite permeability of the fault rocks which can be measured today?

2) What are the processes which induce changes in the permeability of fault zones during the deformation?

3) What is the nature of the fluids involved in migration along fault zones during the deformation?

4) Can the fluids which moved along the fault zones during the deformation be shown to have affected the diagenetic history of the rocks surrounding the fault zone? Is the pattern of wall-rock diagenesis in any way related to the geometrical development of the fault zone?

5) What are the processes which cause the migration of fluids along fault zones during the deformation?

The Vercors, French Sub-Alpine Chains which forms part of the foreland thrust belt on the western border of the Alps was chosen as the field area for the study. Chapter 2 introduces the geology of the Vercors. Stratigraphic studies and thermal alteration data (Section 2.5.4) are combined with structural data (Section 2.5) to provide an assessment of the burial history of the Vercors. These data suggest that the rocks exposed at the surface were generally never deeply buried by the emplacement of thrust sheets or during subsidence and sedimentation related to foreland basin development. Thus, the rocks at surface have remained within the diagenetic realm.

Chapter 3 introduces the geological background to the Rencurel Thrust Zone which was selected for special study as it is well exposed and is a structure of regional importance. The first part of the Chapter discusses the deformation which has occurred within the overlying Rencurel Thrust Sheet. The second part of the Chapter outlines the geometry of the Rencurel Thrust Zone. Section 3.5.4 presents structural data which indicate the kinematic links between different elements of the structural geometries present within the Rencurel Thrust Sheet. This allows conclusions about the geometrical development of the thrust sheet to be drawn.

The geological framework provided by Chapters 1 and 2 allow detailed studies to be placed into a regional context.

Chapters 4 and 5 are concerned with the links between deformation and fluid flow through the Rencurel Thrust Zone. Detailed outcrop descriptions are presented which aid the assessment of any temporal and spatial changes in the deformation and fluid flow which may have occurred within the thrust zone. Outcrop scale studies are also used to pin-point areas within the thrust zone which warrant more detailed study. Samples were taken from these areas. Microstructural studies are presented (Sections 4.1 to 4.3 and 5.1 to 5.2) which lead to two sets of conclusions. Firstly, concerning the links between microstructural evolution during incremental deformation and the changing porosity, permeability and fluid flow within the fault zone (Section 4.4 and 5.3). Secondly, concerning the faulting mechanisms derived from deformation mechanism studies (Sections 4.5 and 5.3.3). These two sets of conclusions lead to the presentation of a model for the migration of fluids through the fault zone which is shown to be directly linked to the geometrical development and microstructural evolution of the fault zone (Section 5.3.4). The implications which this model have for modelling arrays of minor faults are presented in Section 4.9. The processes leading to fault zone localisation are discussed in Section 5.3.6. The possible paleoseismicity of the fault zone is discussed in Section 5.3.7.

Chapter 6 presents the conclusions drawn from geochemical studies carried out on samples from the thrust zone which were shown to be important during structural studies presented in the previous Chapters. X-ray diffraction studies indicate the mineralogical signature of fluid flow through the thrust zone (Section 6.2). $\delta^{18}O$ and $\delta^{13}C$ stable isotopic studies are used to assess possible sources of the pore fluids, the physical and chemical nature of the fluids, flow directions, timing of fluid flow relative to basin scale processes and fluid flux within the fault zone (Section 6.3).

Chapter 7 is concerned with the relative permeabilities of the fault zone compared to the undeformed wall-rocks which exist today. A study using a mini-permeameter is presented.

Chapter 8 presents the conclusions of the study.

CHAPTER 2 INTRODUCTION TO THE GEOLOGY OF THE FRENCH SUB-ALPINE CHAINS

Section 2.1 INTRODUCTION

The Vercors is part of the French Sub-Alpine Chains whose structures form the most external part of the Western Alps (see Figure 2.1). The area is described in several classical alpine reviews by Trumpy (1960), Goguel (1963), Ramsay (1963), Debelmas & Lemoine (1970) and Debelmas & Kerchove (1980). Since the first classic descriptions of alpine geology (Heim, 1921; Argand, 1916; Collet, 1927), the understanding of the Western Alps has been developed and refined to an extent unrivalled by other mountain belts.

Section 2.2 ALPINE BACKGROUND: CRUSTAL STRUCTURE

The Western Alps is known to be an area of thickened continental crust since geophysical studies by Menard (1979) culminated in the production of a map of the depth to the Moho. (shown in Figure 2.2). This thickened crust has classically been explained by the stacking of large scale overthrust nappes. Pioneering work by Beach (1981a), Butler (1986) and Boyer & Elliott (1982) suggested that areas previously thought of as autochthonous are contained within thrust nappes which have been involved in large scale displacements (shown in Figure 2.3). Geophysical studies by Menard (1979) and Perrier & Vialon (1980) led to the presentation of a seismic velocity profile for the Western Alps shown in Figure 2.4. This showed that seismic velocities indicative of lower crustal rocks structurally overlie seismic velocities indicative of mid-crustal rocks. Also, seismic velocity profiles at depth suggest that upper mantle rocks structurally overlie rocks of the lower crust. This work led to the construction of crustal scale balanced sections which indicate that alpine collision led to the imbrication of the Tethyan passive margin along deeply penetrating thrusts which can be correlated with large scale thrusts exposed at the surface (Beach, 1981b; Butler, 1983; Menard & Thouvenot, 1984; Butler, 1986; Butler, 1988). Acquisition of the ECORS-CROP deep seismic reflection profile shown in Figure 2.5 (Bayer et al., 1987), led to the refinement of such crustal balanced sections, confirming that crustal thickening may have occurred by thrusting along large displacement low-angle thrusts which penetrate into the mantle and imbricate rocks from different crustal depths (Butler, 1989) (see Figure 2.3). The structures in the French Sub-Alpine Chains are thought to represent the western limit of this thrusting, where the thrusts have cut up section in their transport direction to detach along the basement-cover interface.

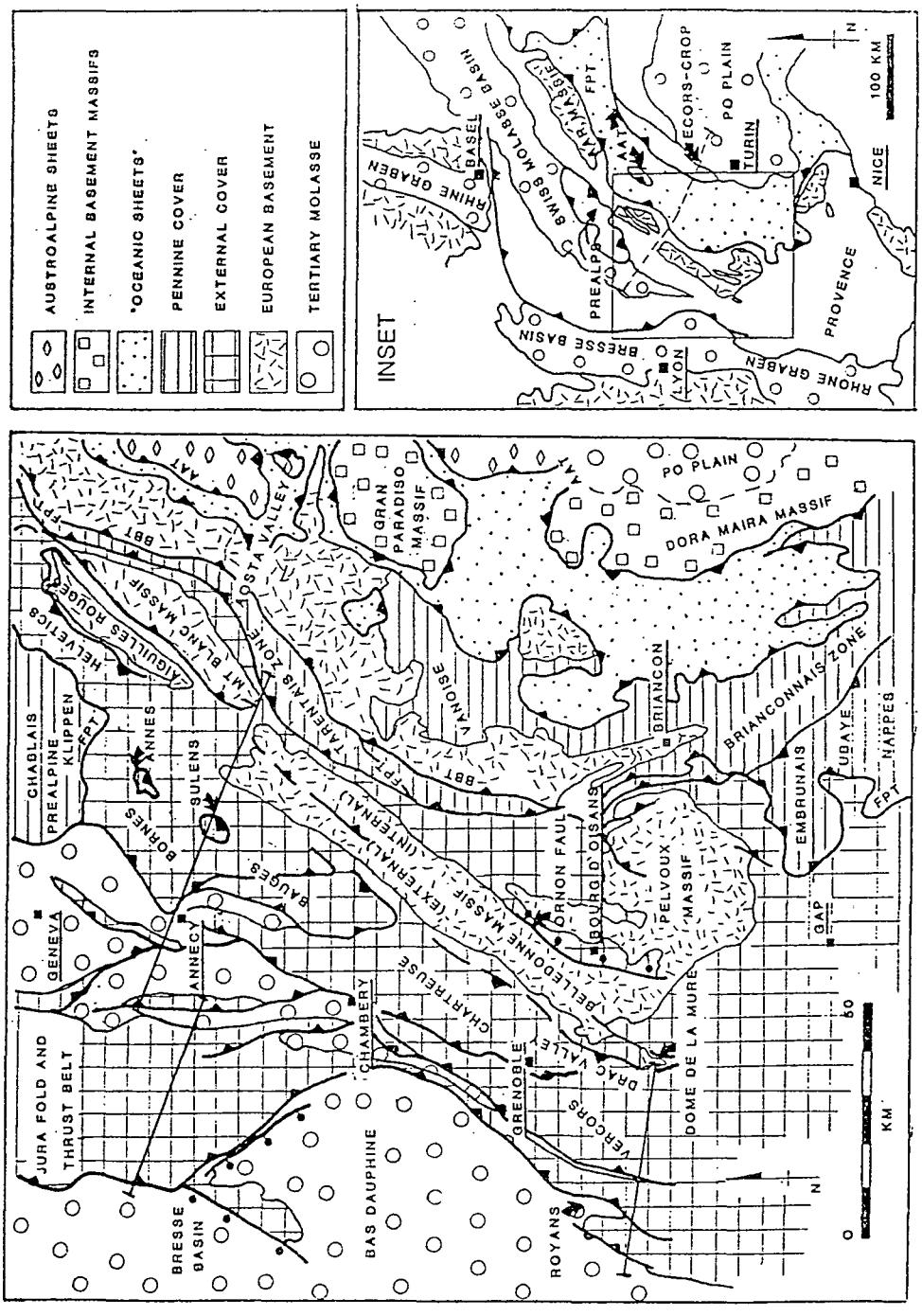

Figure 2.1. Simplified tectonic map of the NW Alps illustrating the main structural units and locations of detailed cross-sections (see Figure 2.9). FPT, Frontal Pennine Thrust; BBT, Basal Brianconnais Thrust; AAT, Austro-alpine Thrust. Location given by inset map of the Alps and adjacent European Basins (open circles). The line of the ECORS-CROP seismic experiment (Bayer et al., 1987, see Figure 2.5) is indicated. The basement of the European foreland is indicated by the random fleck ornament; the internal Alps are stippled. After Butler (1989).

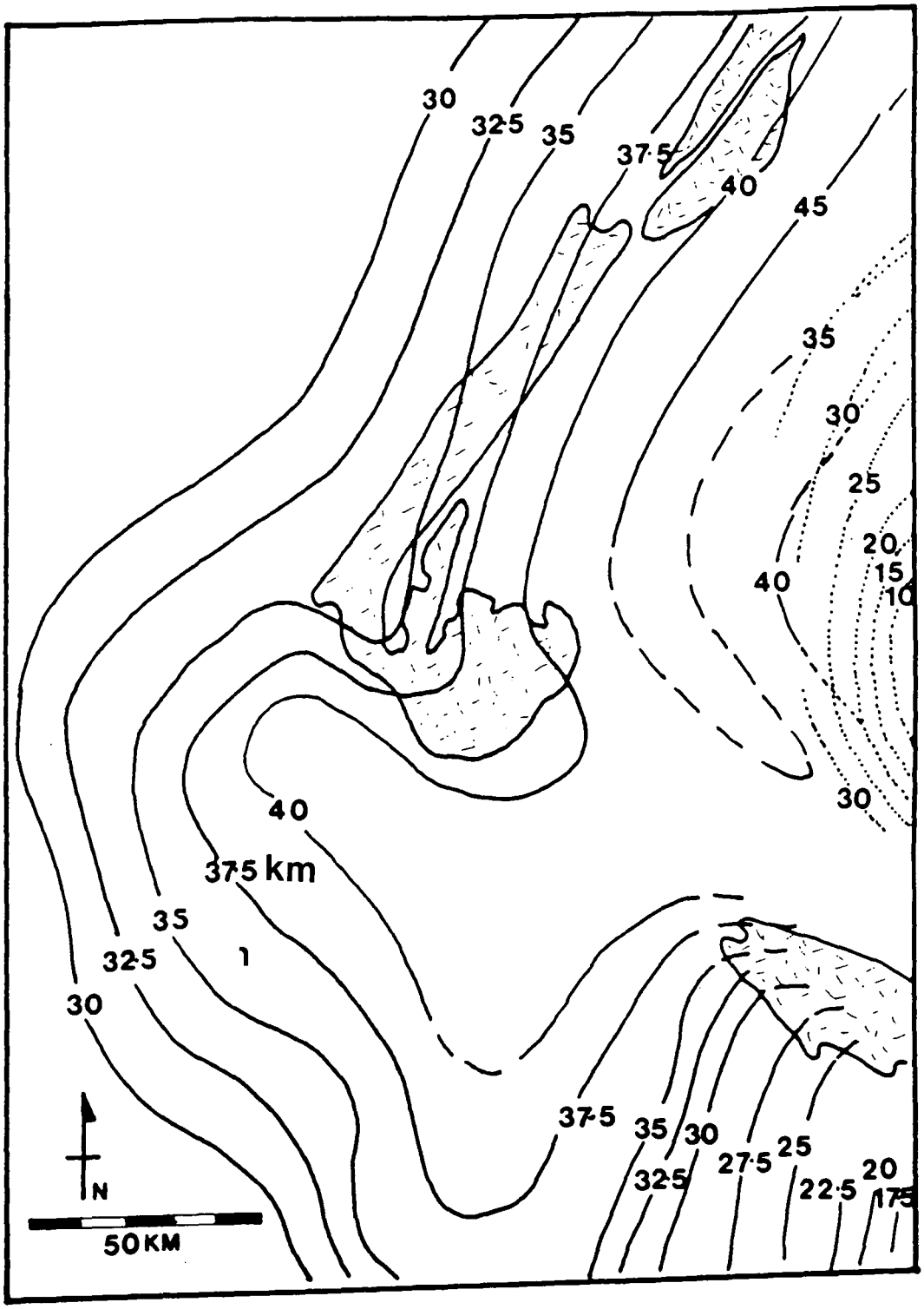

Figure 2.2. Contoured depth to Moho. in the Western Alps. After Menard (1979).

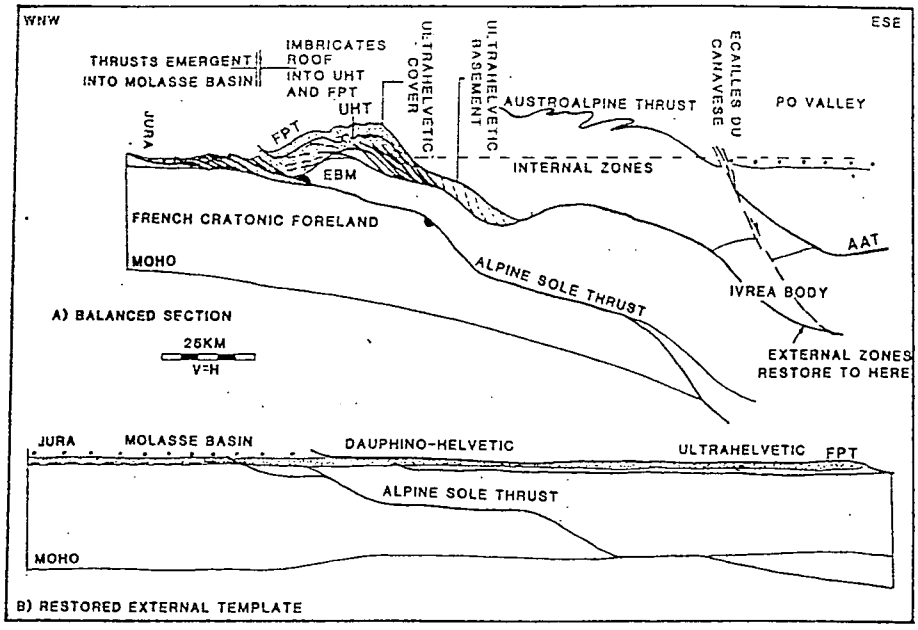

Figure 2.3. A balanced and restored section illustrating the deep structure of the NW external Alpine Thrust Belt. The external cover rocks are stippled. The position of the Moho. and the top of the Ivréa Body are after Menard, (1979) and Perrier and Vialon, (1980). The Section is located along the line indicated in Figure 2.1. EBM, External Belledonne Massif; FPT, Frontal Pennine Thrust; UHT, Ultrahelvetic Thrust; AAT, Austro-alpine Thrust (suture). After Butler (1986).

Figure 2.4. Seismic refraction through the Grenoble area of the Western Alps. After Menard (1979).

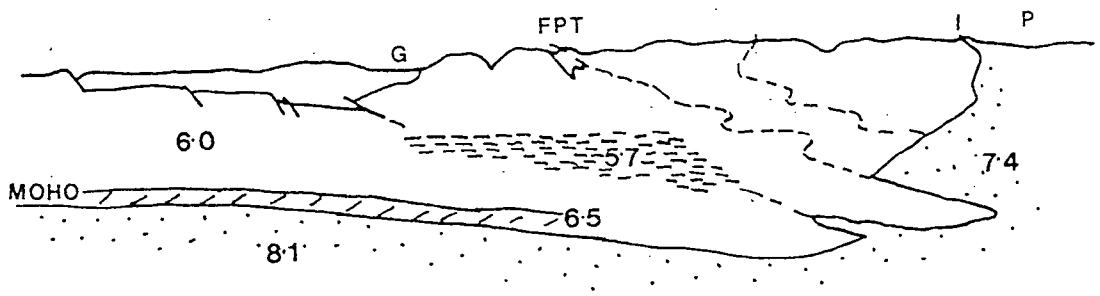

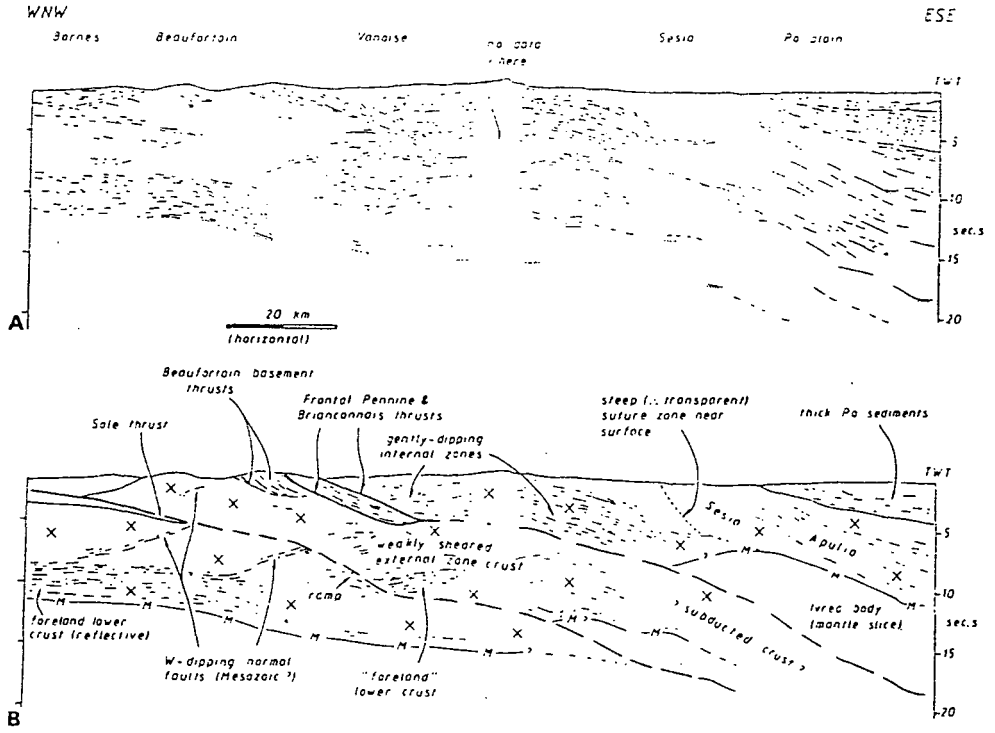

Figure 2.5. A: Line drawing of the ECORS-CROP deep seismic reflection profile (time section) through the Western Alps (location shown on Figure 2.1), incorporating the prominent events in dashed lines from the the wide angle reflection experiment (after Bayer et al., 1987). B: Interpretation of the line incorporating surface geology and using section balancing concepts (see Butler, 1986; Butler, 1988). Only the major thrusts are illustrated. There are substantial thrusts between the gently dipping reflective zone beneath the Vanoise.

Section 2.3 PALEOGEOGRAPHIC TEMPLATE BEFORE THRUSTING

The large displacements involved in this thrust system have presented difficulties in recognising the pre-thrusting template of the Western Alps.

Early in the history of alpine research it was realised that the Mesozoic stratigraphy shows large variations between different zones of the Western Alps (Trumpy, 1960; Goguel, 1963; Ramsay, 1963; Debelmas & Lemoine, 1970; Debelmas & Kerchove, 1980) as shown in Figure 2.6. It was then realised that these zones with different stratigraphies and basin histories are separated by the large displacement thrusts identified during structural studies (Lemoine et al., 1986).

The recognition of these paleogeographic domains allowed an assessment of the broader scale paleogeography. It was recognised that the Western Alps is composed of stratigraphy indicating the presence of a former Mesozoic ocean between two passive margins (Graciansky et al., 1979; Lemoine et al., 1986; Tricart & Lemoine 1986). Late Cretaceous and Tertiary closure of this Ligurian sea, a branch of the Tethys ocean, led to continental collision and the stacking of different elements of this former paleogeography by crustal-scale thrusting. Figures 2.7 and 2.5 show that the highest thrust sheets containing the Austro-Alpine stratigraphy represent the telescoped passive margin of the southern continent to the ocean. Lower in the nappe pile ultrabasic and basic rocks and their overlying sediments representing the oceanic areas are found within the Penninic Nappes. The northern-western passive margin of Ligurian Tethys is found in the lowest nappes and thrust sheets. The stratigraphy of the French Sub-Alpine Chains belongs to this latter paleogeographic domain. This has led to the comparison of the stratigraphy of the French Sub-Alpine Chains to that of the passive margin in the modern Bay of Biscay (Montadert et al., 1979; Graciansky et al., 1979; Lemoine et al., 1986).

Section 2.4 THE FRENCH SUB-ALPINE CHAINS

The stratigraphy of the French Sub-Alpine Chains forms part of the paleogeographic domain of the northern Tethyan passive margin. It can be divided into smaller domains defined by the varying stratigraphy which exists between small fault bounded platforms and basins which existed in Mesozoic times (Arnaud-Vanneau & Arnaud, 1990). Complex changes in thickness, geometry and facies are a result of the action of eustatically and tectonically driven relative sea-level change during the Mesozoic.

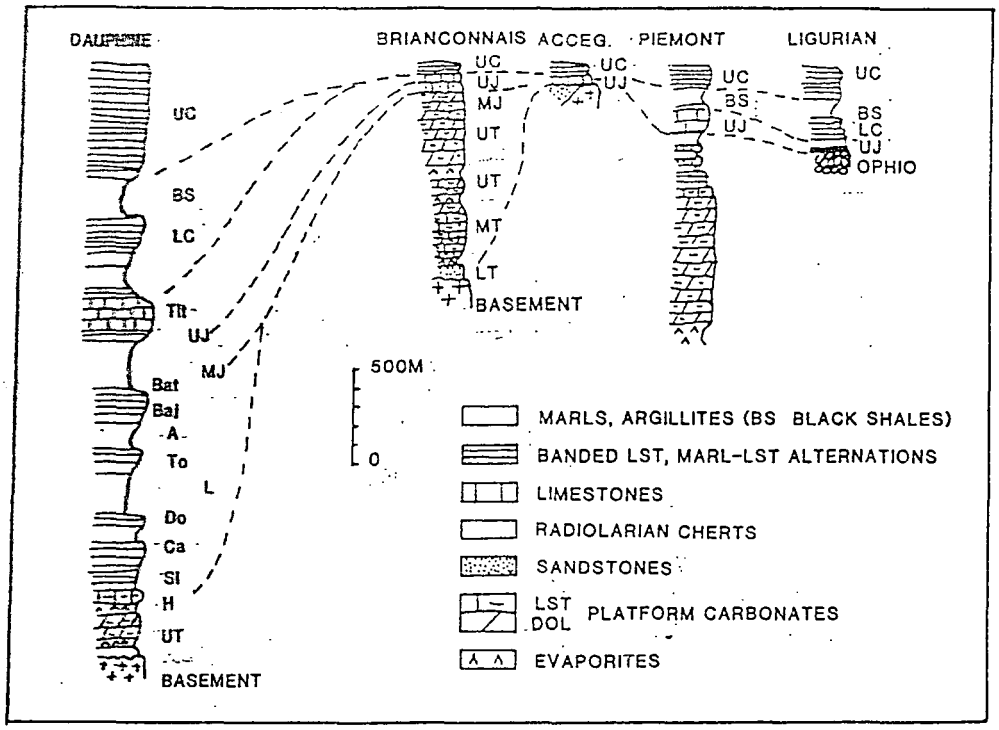

Figure 2.6. Simplified stratigraphic columns of the main types of sedimentary series in the Western Alps. Stratigraphy: LT,MT,UT, Lower, Middle, Upper Triassic. L, Liassic. H, Hettangian; Si, Sinemurian; Ca, Carixian; Do, Domerian; To, Toarcian. Mj, Middle Jurassic; Tit, Tithonian. Lc, Uc, Lower, Upper Cretaceous. Acceg.=Acceglio (eastern Brianconnais that underwent deep syn-rift erosion). After Lemoine et al. (1986).

Figure 2.7. Schematic section of the European passive margin in the Western Alps, assuming the presence of halokinetic structures. Crosses: Continental margin crust. Tr, Triassic (evaporites and dolomites in black). L, Liassic. MJ, Middle Jurassic. UJ, Upper Jurassic. (Ox,). UC, Upper Cretaceous. After Lemoine et al. (1986).

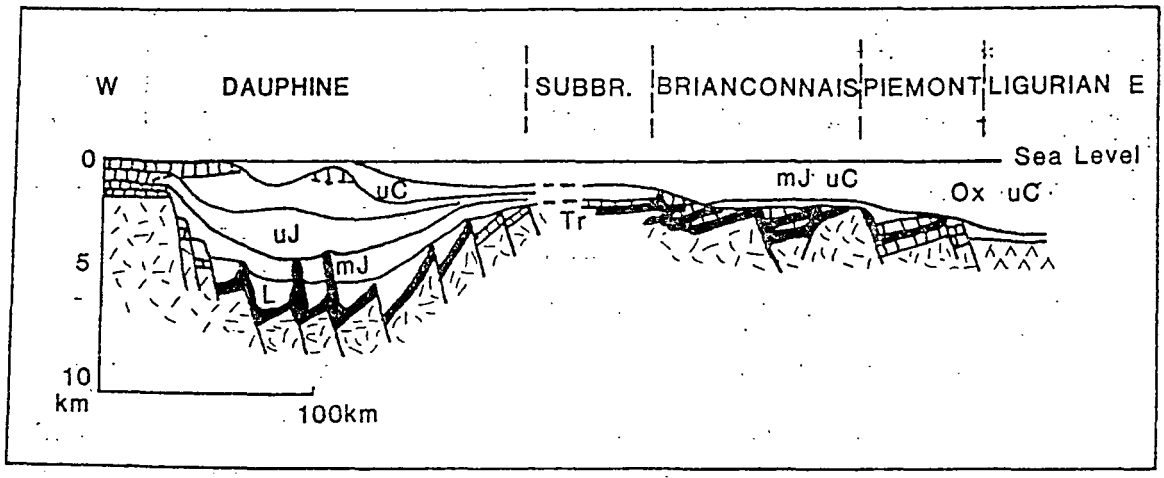

Section 2.4.1 Stratigraphy

Basement is generally termed to be anything pre-Triassic. Variscan schists, para- and orthogneisses, together with Stephanian and Permian sediments can all be found. Triassic sediments were deposited on a subsiding erosion surface and are composed of carbonates, sandstones and evaporites. Basaltic lava flows are intercalated with these sediments elsewhere in the external Alps, suggesting that crustal extension may have been initiated in the Triassic. Liassic times were marked by active extension which produced a basin and shoal paleogeography. Shallow-water limestones were deposited on the crests of the fault blocks, whilst the troughs in the hanging-walls to the extensional faults were marked by deep water pelagic carbonate deposition. By mid-Jurassic times the main phase of extension had ended but thick sequences of deep water carbonate mudrocks were deposited throughout the Oxfordian. It has been suggested that Tithonian times, marked by the deposition of a distinctive shallow water carbonate sequence, signifies the onset of the thermal subsidence phase of passive margin evolution (Lemoine et al., 1986). This phase of subsidence continued throughout the Cretaceous although local fault controlled subsidence also occurred. Despite the small scale stratigraphic complexity within the Sub-Alpine Chains, some regional trends can also be recognised. The Jura domain has a thinner stratigraphy than the adjacent Dauphinois domain. Also the Jura is dominated by stable platform carbonate deposition, whilst the Dauphinois has alternations of carbonate platform and deeper water pelagic carbonates. In the western Vercors the division between the two domains occurs across the buried Faille de l' Isére. This buried basement lineament, which has been suggested by borehole data and imaged by the geophysical studies of Menard (1979) is thought to separate the Jura stable platform from the Dauphinois fault bounded basin (shown in Figure 2.8).

Section 2.4.2 Alpine deformation

Tertiary times saw the development of a foreland thrust belt within the Sub-Alpine Chains.

Section 2.4.3 Large scale geometry of the French Sub-Alpine Chains

The Sub-Alpine Chains show large variations in structure along strike as shown in Figure 2.9. In the north the thrust belt is wide and can be divided into the outlying Jura hills in the west, which are separated from the Bornes-Aravis structures in the east by the Swiss Molasse Basin. The Sub-Alpine Chains are bounded in the east by the upthrusted External Belledonne Basement Massif. Farther south the outlying Jura

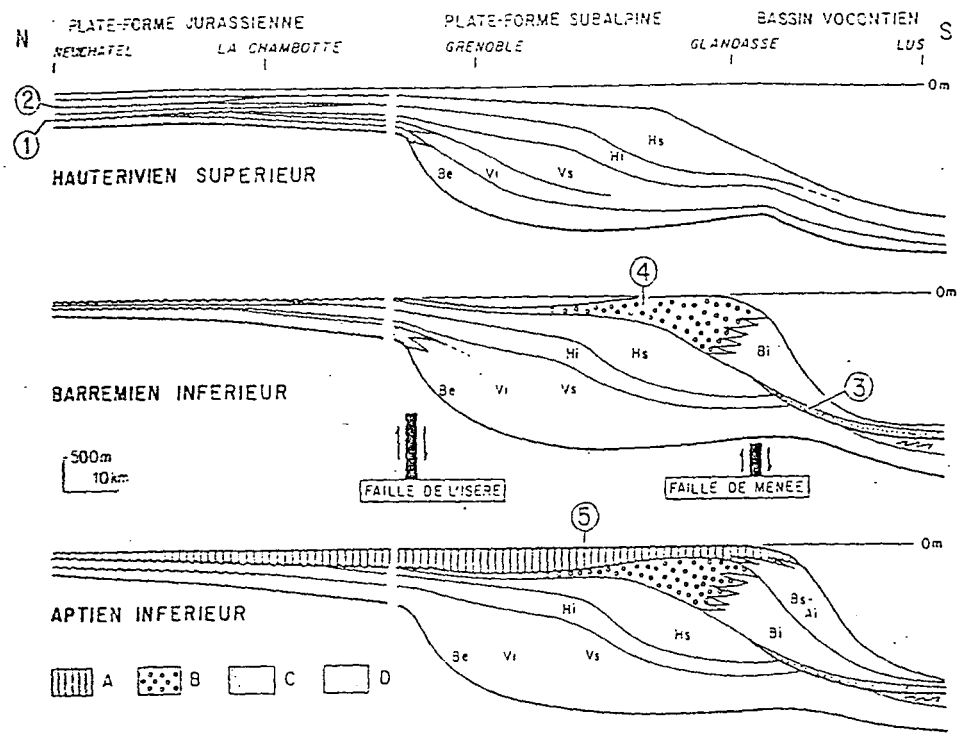

Figure 2.8. Schematic paleogeographic sections between Neuchatel and the southeastern Vercors. A: Urgonian Limestone Formation; B: Glandasse Bioclastic Limestone Formation; C: Berriasian-Hauterivian platform series; D: Basinal hemipelagic to pelagic facies. 1: Erosional surface of the Valanginian deposits in the Neuchatel area, Swiss Jura. 2: erosional surface of the Hauterivian deposits in the Jura domain. 3: Submarine syn-sedimentary erosion surface and submarine fan between Col de Menee and the Col de la Croix-Haute. 4: Lower Barremian Lowstand Wedge (Southern Vercors shoal); 5: Urgonian Platform Transgressive on the Jurassic domain). After Arnaud-Vanneau & Arnaud (1990).

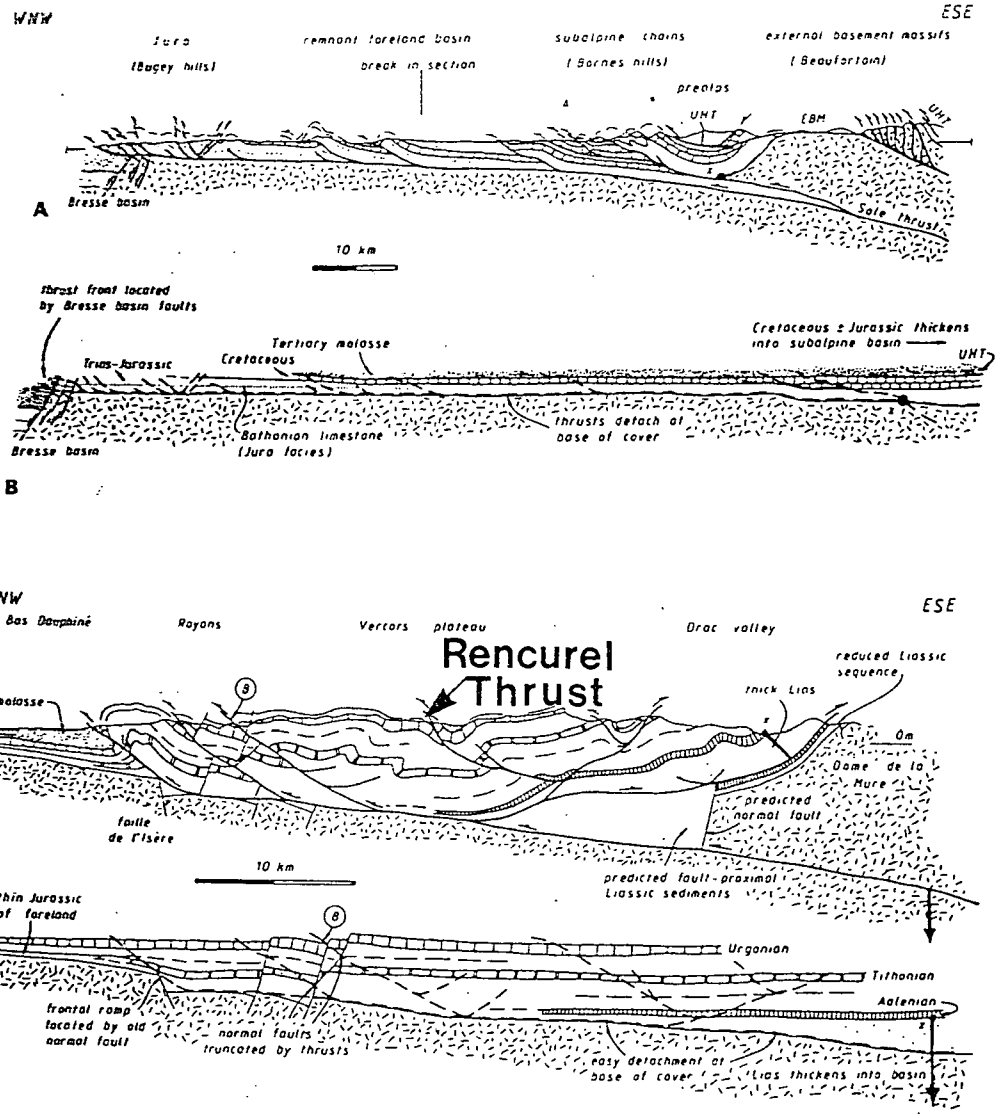

Figure 2.9. Cross-Sections across the Sub-Alpine Chains showing a constant 30km shortening ahead of the External Belledonne basement massif. Cross-Sections are located on Figure 2.1. After Butler (1989); Butler (in press).

structures merge with the main Sub-Alpine structures within the Chartreuse hills, with the southern termination of the Swiss Molasse Basin in the Voreppe Molasse furrow. In the Vercors, where the southern termination of the Jura structures occurs major backthrusts dominate the Sub-Alpine structure. The Chartreuse and Vercors are bounded on their western side by the Bas Dauphine Foreland Basin, and on their eastern side by the upthrusted External Belledonne Basement Massif.

The basement structure of the Sub-Alpine Chains is illustrated in the map of depth to pre-Triassic basement shown in Figure 2.10 (Menard, 1979). This map shows the depth to basement increasing from around 2km under the Jura to around 6km just to the west of the External Belledonne Basement Massif. Menard (1979) also suggested that the basement massif has been uplifted on a major thrust which emerges from basement to join with the Sub-Alpine Chain structures. These sub-surface data have been combined with surface geological data and published borehole data to construct a number of balanced sections across the Sub-Alpine Chains (Mugnier et al., 1987; Gillchrist et al., 1987; Butler, 1989). The sections of Butler (1989) and Butler (in press) show a constant 30km shortening within the Sub-Alpine Chains as shown in Figure 2.9. Restoration of the basement cover interface to regional levels within the Belledonne Basement Massif also suggests around 30km displacement on the thrust carrying the massif which is constant along its whole strike length (Butler, in press) as shown in Figure 2.3. The constancy of displacement within the Massif is backed up by other independent lines of evidence (Butler, in press). The uplift of the basement cover interface is constant relative to regional levels along the strike of the massif. Fault plane lineation data show a constant WNW-ESE orientation within the Sub-Alpine Chains from the Arve valley in the north to the Vercors in the south suggesting a continuous parallel thrust transport direction. Also, the basement massif is not cut by tear faults suggesting that the displacement is similar along the strike of the massif.

Section 2.5 STRUCTURAL GEOMETRIES WITHIN THE VERCORS, SOUTHERN SUB-ALPINE CHAINS

Figure 2.11 shows a map of the Vercors, French Sub-Alpine Chains.

Section 2.5.1 Western Vercors mountain front geometry: The role of pre-existing basin structure

The western Vercors contains the most westerly structures of the Sub-Alpine Chains which expose Mesozoic rocks at the surface. Certainly this represents a major structural divide between exposures of the foreland thrust belt and the Bas Dauphine

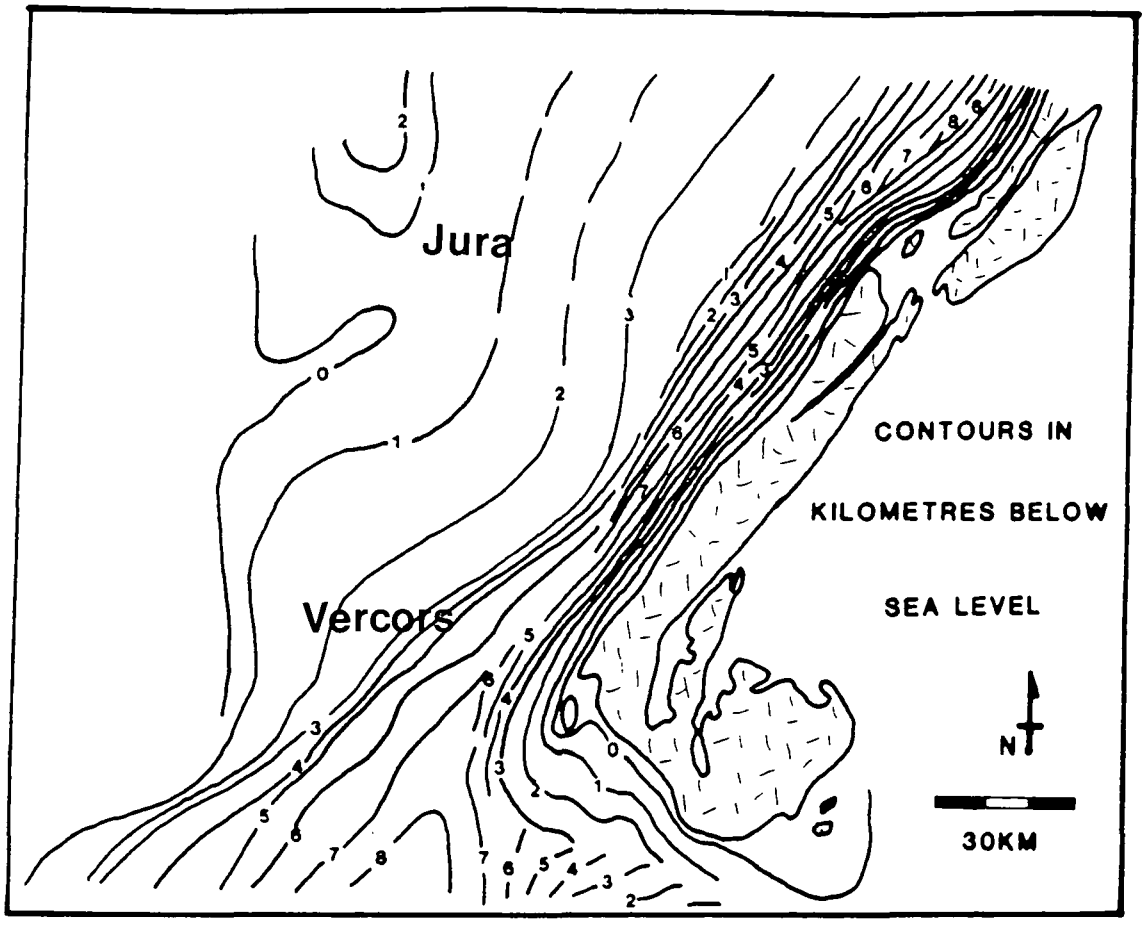

Figure 2.10. Map of the depth to pre-Triassic basement in the Western Alps. After Menard (1979).

foreland basin; however, the Alpine deformation front may lie further to the west within the poorly exposed Bas Dauphine. Pre-existing basin controlling faults are thought to have influenced the geometry of the later thrust structures, as discussed in the following sections.

Section 2.5.1.1 Faille de l'Isére

The structures at the mountain front where Mesozoic rocks are exposed at the surface are thrust-related anticlines arranged en echelon. In the south, the Beauregard-Baret Anticline is the frontal structure. This structure plunges to the north beneath the Royans area and the Bas Dauphine sediments. In Royans, the Pont en Royans Anticline forms the frontal structure. Well data from the Beauregard-Baret Anticline shown in Figure 2.12 (BRGM Romans-sur-Isére, 1975), indicate that the anticline is carried on a thrust which has a displacement in the order of a couple of kilometres. This thrust may emerge to the west in the poorly-exposed Bas Dauphine. The well data also show that 700 metres of Berriasian shales exist at depth within the anticline as well as 1km of Liassic rocks. To the west of this anticline however, the Mesozoic succession is relatively thin as shown in Figure 2.12. This change in stratigraphic thickness suggests the existence of a Mesozoic-age, basin-controlling fault, downthrowing to the east, located at depth beneath the current position of the mountain front anticlines within the Vercors. This important lineament, which as mentioned above, has been imaged by geophysical work and controlled Mesozoic paleogeographic domains, is termed the Faille de l'Isére (Figure 2.8) (BRGM Charpey, 1968). This basin controlling fault is likely to have a NNE-SSW orientation as suggested by the trend of the mountain front within the Vercors. This trend is parallel to the trend of the Menee fault system in the southern Vercors, which has also been suggested to be an important basin controlling fault, separating in mid-Cretaceous times, stable carbonate ramp and platform facies from the highly subsident Vocontian Basin marked by deeper water sedimentation (Figure 2.8) (Arnaud-Vanneau & Arnaud, 1990). These lineaments are suggested to be part of a strike-slip fault system which can be linked to the south-west to strike slip lineaments exposed in the Massif Central where local pull-apart basins exist which were active as far back as Carboniferous times (Figure 2.13). The present offsets of the frontal anticlines within the Vercors may mirror an en echelon arrangement of basement steps along the Faille de l'Isére, a feature so characteristic of strike slip fault systems.

This important lineament has been suggested to exert major control on the geometry of the western Vercors structure. Butler (1989) has suggested that this offset in the easy slip horizon which occurs at the basement-cover interface, has forced the detachment thrust to climb stratigraphy and produce a mountain front anticline

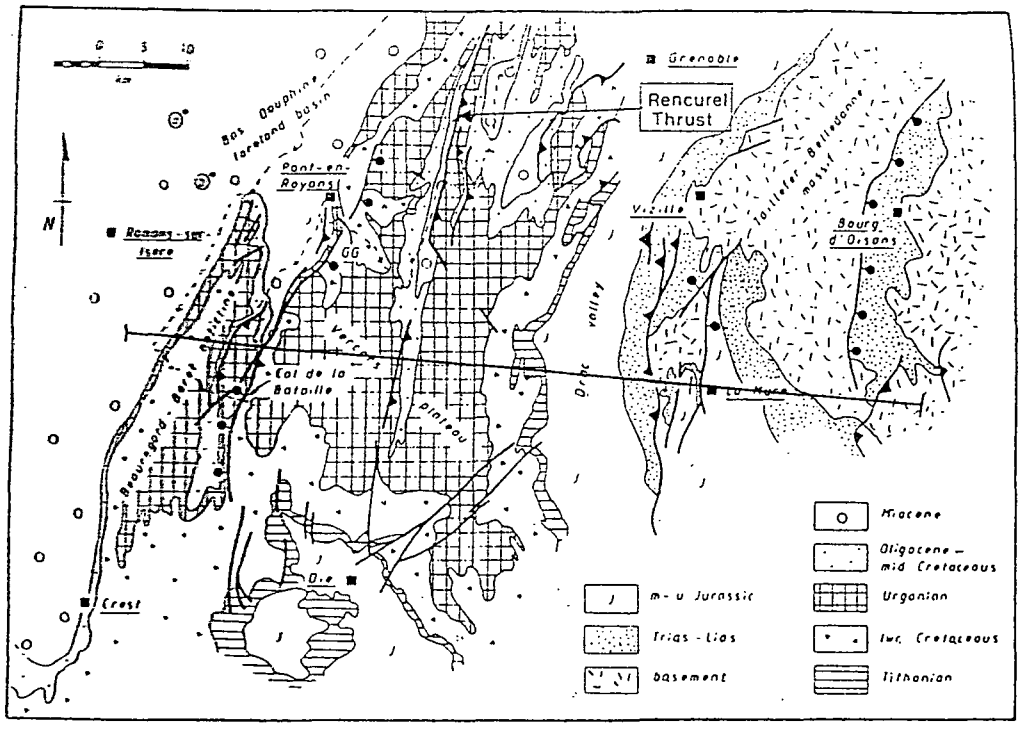

Figure 2.11. Simplified geological map of the Vercors and adjacent basement massifs with the location of the cross-section shown in Figure 2.14. GG, Grande Goulets. After Butler (in press).

Figure 2.12. The Vercors mountain front structure. After Gillchrist (1989).

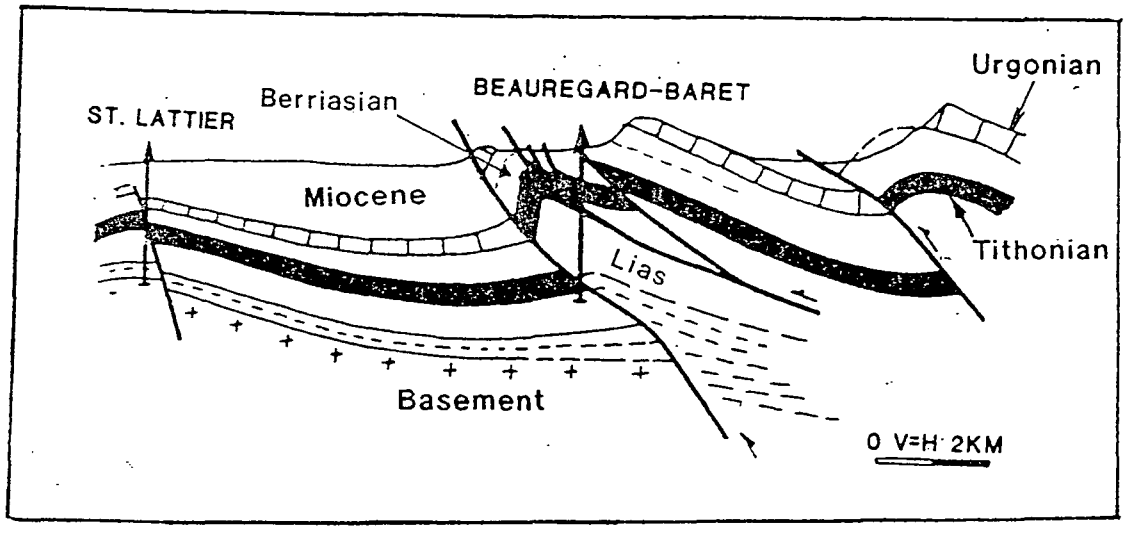

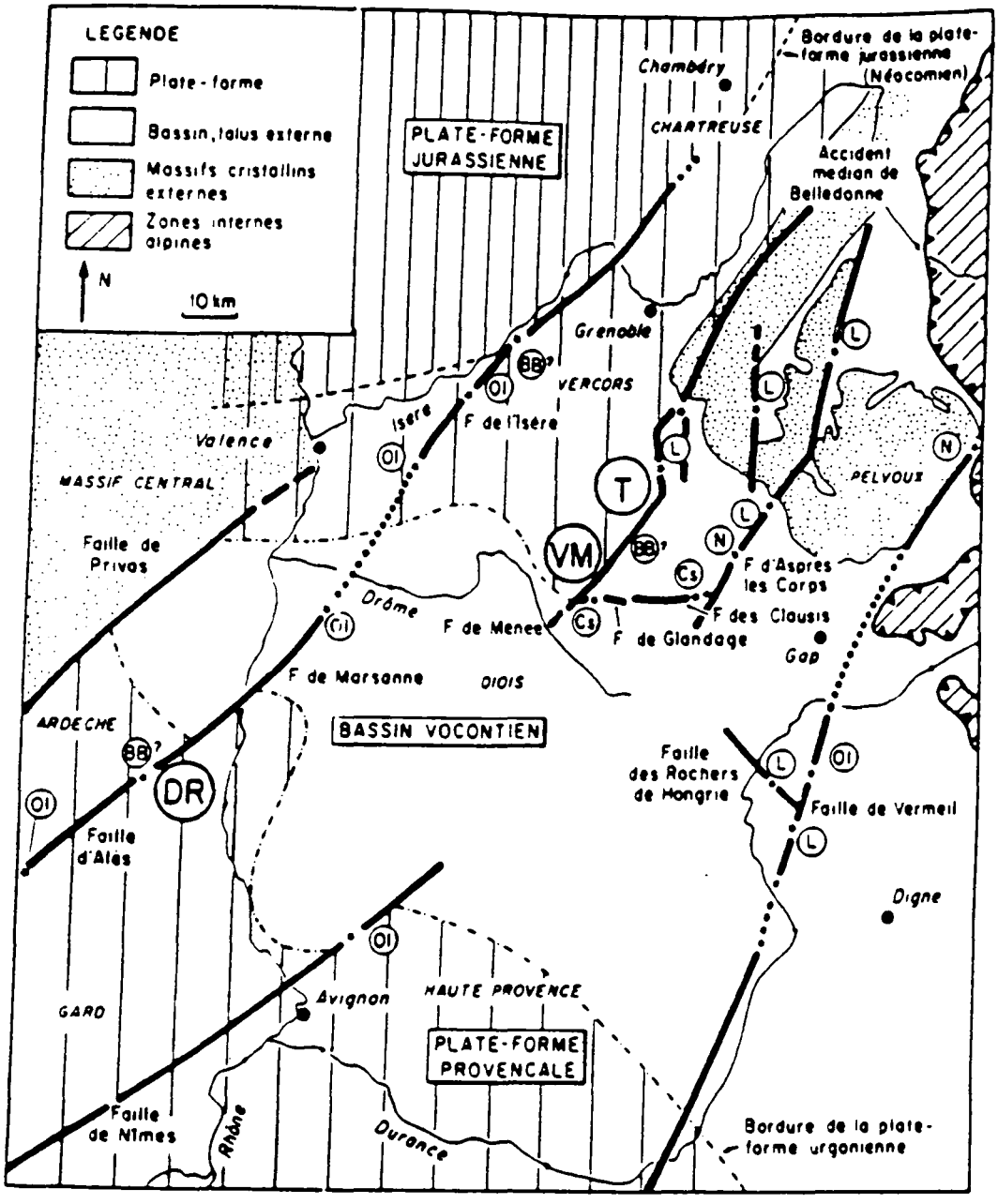

Figure 2.13. Mesozoic syn-sedimentary faults in the Western Alps. Faults known to be active- Lias (L), au Crétacé supérieur (Cs), au Nummulitique (N),a l Oligocène (01); Faults suggested to be active Barrémo-Bédoulien (BB). DR: haut-Fond de la Dent de Raz; T, haut-fond du Trieves; VM: haut-fond du Vercors méridional., After Arnaud (1981).

(Figures 2.14 and Figure 2.15). Basement steps which may occur along the Eocene/Oligocene faults are thought not to produce emergent anticlines because the faults downthrow basement towards the west such that the detachment would never propagate west into an upthrown basement block. Further evidence for the localisation of deformation associated with alpine thrusting along the Faille de l'Isére is the existence of extensive backthrusting within the forelimb of the Pont en Royans anticline. At the Petite Goulets, (Figure 2.16) major backthrust sense repetition of the Barremian to lower Aptian limestones, locally termed the Urgonian can clearly be seen in the high cliffs of the gorge walls. It has been suggested (Butler, 1989) that these faults formed before the growth of the frontal anticline. They may represent the re-distribution of displacement away from the basement-cover detachment into the hanging-wall cover rocks as the deformation becomes localised against the basement step along the Faille de l'Isére.

Section 2.5.1.2 Eocene/Oligocene growth faults

The western Vercors contains a set of N-S trending faults across which small extensional offsets of the stratigraphy exist (see Figure 2.11). Most of the faults cannot be dated stratigraphically because of uplift which occurred after the fault activity but prior to Miocene foredeep sedimentation. This resulted in the erosion of any basin filling sediments which may have existed. However, at St. Nazaire en Royans at the northern termination of the Beauregard-Baret Anticline, thickening of Oligocene continental deposits and uplift of a late-Cretaceous paleokarstic surface is associated with these faults (Butler, 1989). It has been suggested that these faults form part of a transtensional fault system which can be linked to the Rhone-Bresse Graben System (Butler, 1989).

These faults have influenced the development of structural geometries within the western Vercors. Butler (1989) has described cliff sections within the Grande Goulets Gorge. Thrusts can clearly be seen to cut across normal faults which downthrow Urgonian Limestones to the west against Hauterivian Shales as shown in Figure 2.17. Displacement remains localised on the thrust with no widespread deformation around the early normal fault.

However, farther south at the Col de la Bataille, (see Figure 2.11), Butler (1989) has described another westerly downthrowing normal fault which is situated within a zone of intense deformation where the fault is intersected by an alpine thrust. Foreland and hinterland directed thrusts are associated with upright folding. Stratigraphic relationships suggest that the early normal fault has downthrown massive Urgonian

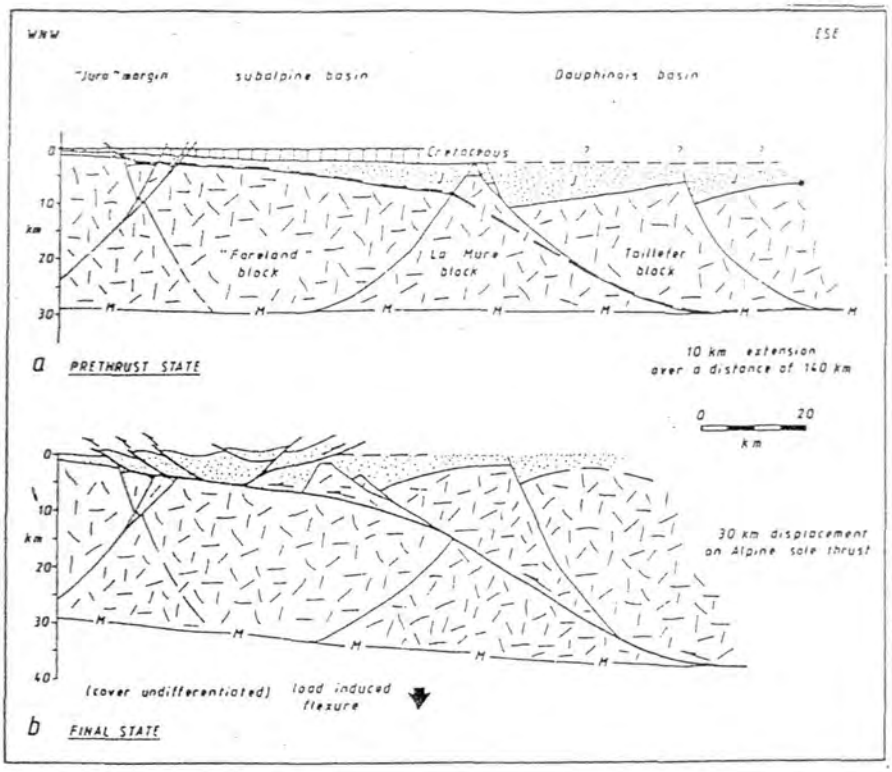

Figure 2.14. Cross-section through the Vercors. (Location shown on Figure 2.11). After Butler (1989).

Figure 2.15. A view looking northwards along the mountain front of the Vercors. At this location, near Pont en Royans (Grid reference 837 311), the Urgonian limestones are exposed within the mountain front monocline.

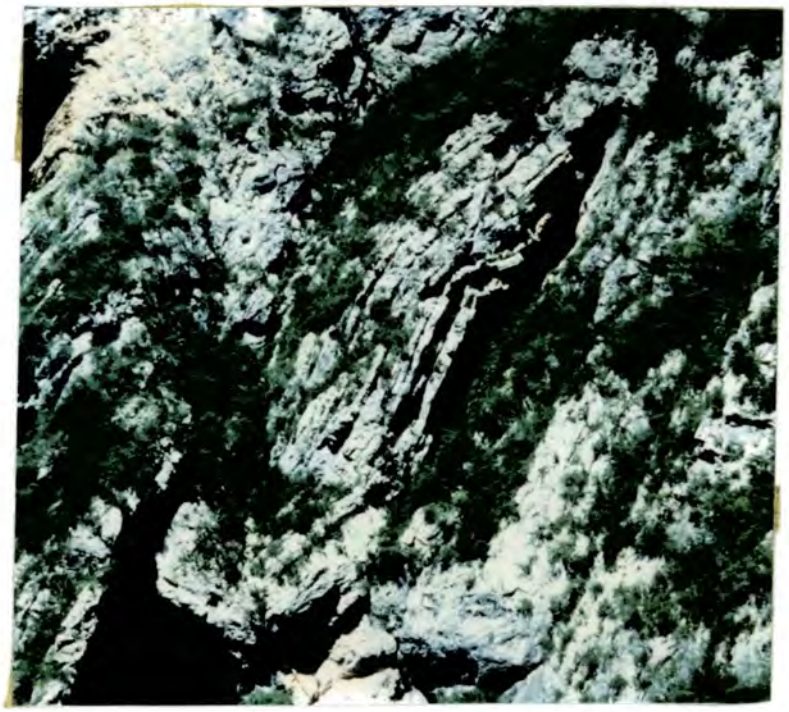

Figure 2.16. A view on to the northern side of the Petite Goulets Gorge where east vergent backthrusts cut a well bedded portion of the Urgonian Limestones. The cliffs are around 100 metres high. (Grid reference 837 310).

Figure 2.17. A view on to the southern side of the Grande Goulets Gorge where a west vergent thrust cuts across a pre-existing normal fault, repeating part of the Urgonian succession. The normal fault is probably of Eocene-Oligocene age, and downthrows Urgonian Limestones against the interbedded limestones and shales of the Hauterivian. The thrust geometry has not been influenced by the existence of the early normal fault. The cliffs are around 100 metres high. (Grid reference 841 310).

Limestones against Hauterivian limestones and shales. Butler, (1989) has suggested that as the thrust propagated to the west through the easily deformed limestones and shales and encountered the downthrown harder-to-deform massive Urgonian limestones, a zone of upright pure shear developed (Figure 2.18). This process has been termed Buttressing (Welbon, 1988; Butler, 1989).

Thus, it seems that it is the lithological contrasts across the normal faults rather than the existence of a pre-existing fault plane which exerts the most profound influence on later thrust geometries. At the Grande Goulets, easy-to-deform interbedded limestones and shales exist on both sides of the normal fault where the thrust intersects. The thrust can propagate easily across the normal fault which has little influence on the thrust geometry. At the Col de la Bataille the thrust crosses the normal fault where a large lithological contrast exists. The relatively hard-to-deform Urgonian limestones on the downthrown side of the fault causes the thrust displacement to become distributed into a zone of minor thrusting and upright folding. These ideas are drawn schematically in Figure 2.19.

Section 2.5.2 Eastern Vercors

In the eastern Vercors (see Figure 2.11), a complete succession from the Urgonian limestones down to the Triassic and into the basement is exposed in the Drac Valley. This valley separates the Belledonne Crystalline External Basement Massif in the east from the Mesozoic sedimentary rocks in the west which form the Vercors plateau. The Mesozoic succession is around 6km thick which is substantially thicker than in the western Vercors (Menard, 1979). The depth to pre-Triassic basement increases to around 6-7km in the eastern Vercors (Figure 2.10). This suggests that the Vercors is composed of a westward tapering wedge of stratigraphy. However, this pattern of an easterly thickening wedge does not continue across the Drac Valley, where important facies and thickness changes occur. Around 2km of Liassic basinal shales occur within the eastern Vercors. On the east of the Drac Valley, only 200 metres of Liassic shallow water crinoidal limestones occur. It has been suggested that this pattern of sedimentation is the result of the existence of a Liassic age extensional fault on the western side of the Belledonne Massif (Figure 2.20). This fault is suggested to have downthrown towards the west and separated the downthrown Vercors basin from the shoal paleogeography which existed on the upthrown footwall block (Lemoine et al., 1986; Butler, 1989). Westward downthrowing normal faults are exposed within the basement rocks of the Belledonne Massif (see Figure 2.11).

Menard (1979) suggested that the Belledonne massif was uplifted above its regional level on the large displacement Alpine Sole Thrust. As mentioned above this thrust is

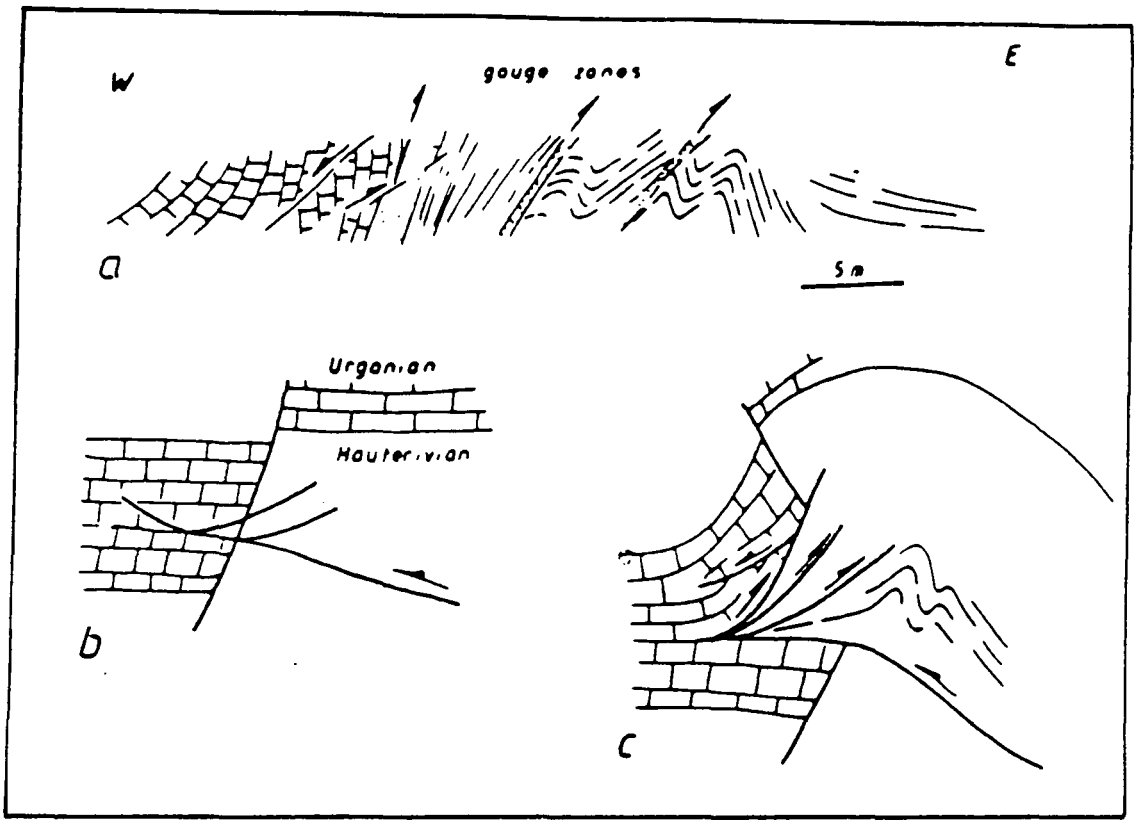

Figure 2.18. a: A sketch section through the Col de la Bataille at current exposure levels. b: and c: represent the pre-thrusting geometry and the final state Section respectively. After Butler (in press).

* Miocene sandstones and conglomerates in the Vexors contain clasts of gabbro and serpentinite, probably derived from the east where the internal zone thrust sheets exist.

thought to represent around 30km of displacement (Butler in press) (Figure 2.3). Thus, the position where alpine deformation responsible for basement imbrication and crustal thickening emerges into the Dauphinois stratigraphy coincides with the Jurassic age extensional fault in the eastern Vercors. Butler (1989) pointed out that the 30km of displacement on the Alpine Sole Thrust must also be present within the structures of the Sub-Alpine Chains. Butler (1989) suggested that the cover shortening has occurred by displacement along a large displacement backthrust located in the eastern Vercors. This backthrust transported the stratigraphy of the Vercors Basin eastward relative to the Belledonne basement rocks in the footwall to the backthrust. Backthrust-vergent structures have been described from the Drac Valley in the eastern Vercors (Gidon, 1979).

Thus, the structures within the eastern Vercors are complex. The area contains the eastward termination of the pre-thrusting Vercors basin which was controlled by a westward-downthrowing normal fault. Alpine shortening in the form of thrusting emerged into the Mesozoic Dauphinois cover rocks in this area. The cover shortening in the eastern Vercors is dominated by backthrusting. This polarity changes to foreland directed thrusting in the western Vercors.

Section 2.5.3 Timing of deformation within the Vercors

The thrust structures within the Sub-Alpine Chains involve Tertiary sediments. Eocene/Oligocene sediments were deposited along the Rhone/Bresse basin system. Miocene times saw the development of a foredeep succession where sediments derived from the growing Alpine mountains to the east were deposited in foreland basins (see Figure 2.21). Thrust loading resulted in the flexural downwarping of the French continental crust and foreland basin development. The sediments deposited within these basins are now found within the footwalls to thrusts within the Sub-Alpine Chains. Middle Miocene and younger proximal alluvial fan and fan delta, as well as distal lacustrine and marine facies are found within the foredeep succession. However, the molasse found within the footwall to individual thrusts are generally derived from more internal thrust sheets farther to the east within the mountain belt. The oldest proximal facies, such as the Voreppe conglomerates, are Burdigalian in age (Debrand-Passard et al., 1984) suggesting that the emergent thrust front was farther to the east before this time. So between 10 and 6 M.a. emergent thrusts existed within the vicinity of the Sub-Alpine Chains.

The proximal molasse derived from the emergent uplifted hanging-wall of an individual thrust will be higher in the stratigraphy than the molasse presently exposed in the footwall to the individual thrust. However this style of stratigraphic relationship

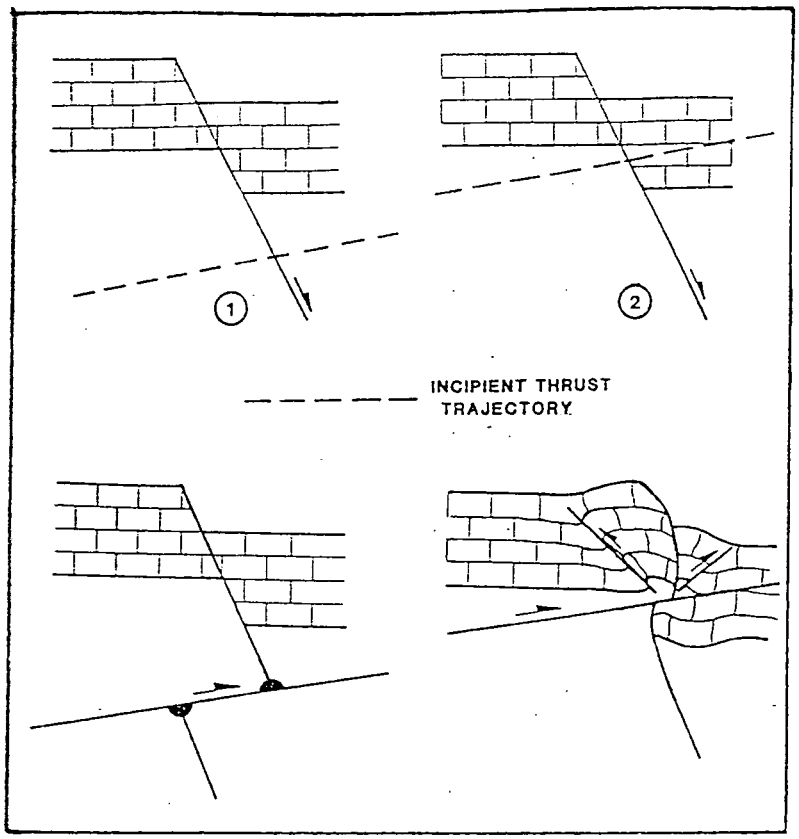

Figure 2.19. The effect of the pre-thrusting template on thrust geometry. 1: Southern side of the Grande Goulets Gorge. The thrust cuts a pre-existing normal fault where easy to deform limestones and shales exist on both sides of the fault. The thrust ignores the normal fault and develop a simple thrust geometry.
2: Col de la Bataille. The thrust cuts a pre-existing normal fault where competent Urgonian Limestones have been juxtaposed by the normal faulting against incompetent Hauterivian limestones and shales. The thrust cannot propagate as easily and developes a complex thrust geometry.

Figure 2.20. Schematic reconstruction of the eastern Vercors. The thickness and facies of carbonate deposition is controlled by the existence of a westward downthrowing normal fault on the western side of the External Belledonne Basement Massif. After Butler (in press).

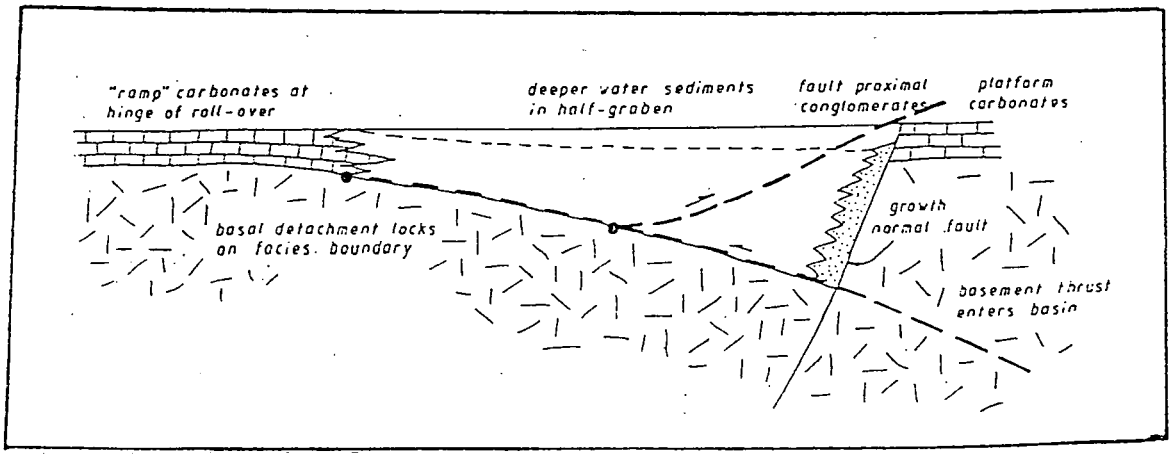

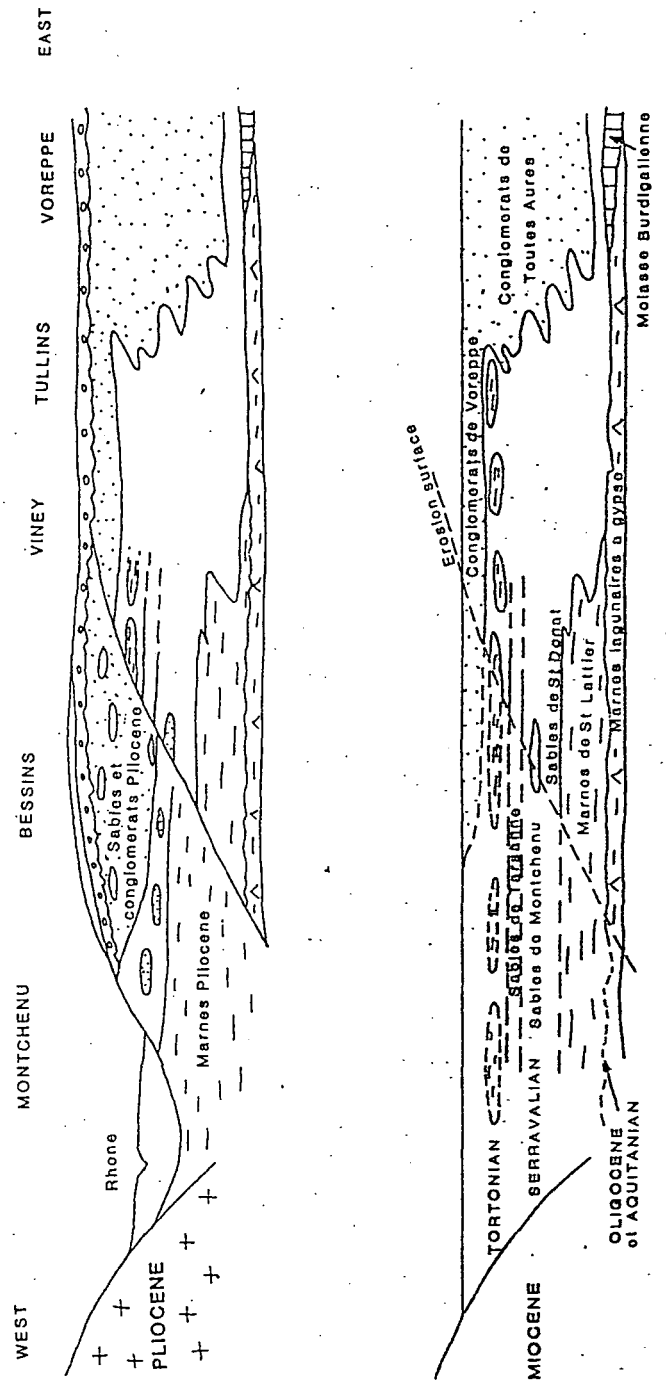

Figure 2.21. The Stratigraphy of the Bas Dauphine foredeep succession. After Debrand-Passard et al. (1984).

is generally not visible within the Sub-Alpine Chains as the area has undergone uplift due to the isostatic rebound of the lithosphere after the cessation of thrusting in post Miocene times. The higher parts of the molasse sequence and the structures within the foreland thrust belt have been uplifted and eroded.

In summary, a substantial thickness of foredeep sediments existed above the Mesozoic strata which were destined to become involved in foreland thrust belt structures. The thickness of this sequence is not presently known due to the uplift and erosion. Lower and middle Miocene sediments were certainly involved in the thrusting, and must have enclosed the Mesozoic rocks during the development of the folds and thrusts.

Section 2.5.4 Post Miocene uplift: Implications

After the cessation of thrusting, isostatic rebound of the lithosphere occurred, causing uplift and erosion of the Vercors structures. Figure 2.22 shows the spore colouration values of the Hauterivian rocks presently exposed within the Vercors. These indicate that the rocks have been buried and thermally altered. This thermal alteration is probably not the result of burial underneath thrust sheets as the area has not suffered large scale thrust translation causing stacking of the stratigraphic pile. Also the pattern of values does not mirror the structural trends within the Vercors, so that burial probably occurred beneath Miocene foredeep sediments.

The Miocene foredeep sediments provide a means to date the uplift and to assess the importance of isostatic versus thrust related uplift. The stratigraphy is shown in Figure 2.21. Within the Vercors plateau, Miocene sediments are involved in the thrust structures. In the footwall to the Rencurel Thrust (Figure 2.11), coarse to fine grained marine sands can be found. These rocks contain marine fossils such as Chlamys praescabriuscula and glauconite which is a marine authigenic mineral (Debrand-Passard et al., 1984). Also sedimentary structures such as tidally produced herringbone cross-stratification indicate shallow marine conditions. Sedimentation also occurred in Miocene times to the west of the present day thrust front, in the Bas Dauphine. Aquitanian times saw deposition of lacustrine limestones and shales. However from Burdigalian through to Tortonian times, the area experienced marine sedimentation, with storm influenced shelf sands, beach sands and biohermal build ups. In Serravalian and Tortonian times proximal alluvial fan/fan delta sediments were deposited. These Conglomerates de Voreppe indicate the presence of an emergent thrust front in the vicinity of the Vercors. The lateral equivalents to these conglomerates are the distal marine sands of the Sables de Montchenu. The marine Miocene sediments are now exposed within hills up to 450 metres above sea level in the Bas Dauphine. At the top of the Miocene in the Bas Dauphine there is an erosional

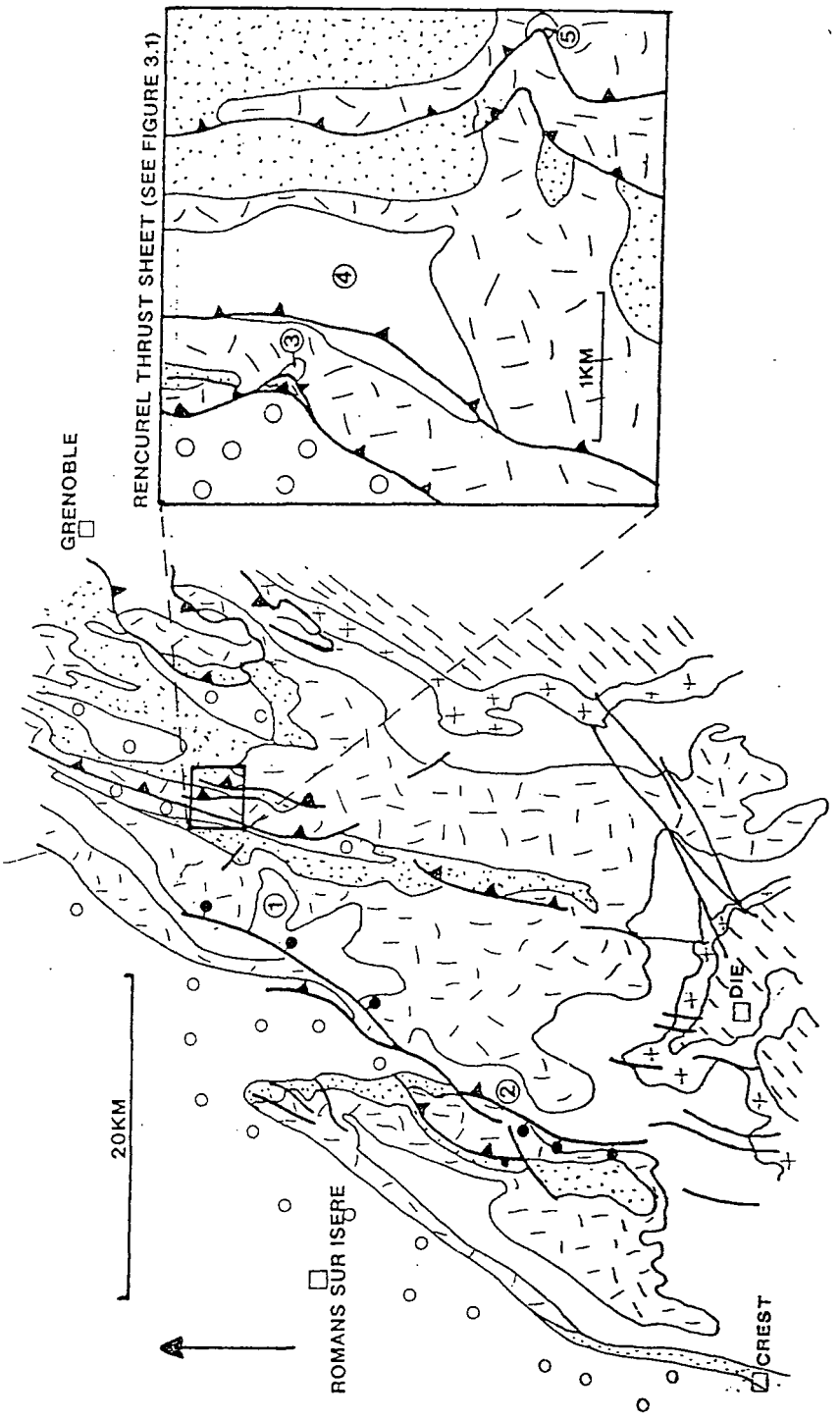

Location

Figure 2.22. A map of thermal maturity data indicated by spore colouration and vitrinite reflectance for the Vercors. All the five samples were taken from Hauterivian and Valanginian lime mudstones. They all contain spores which appear yellow to yellow-orange under fluorescent light. In addition a vitrinite reflectance value of 0.45% was obtained from sample (2). The samples were collected by the author. The thermal alteration data were collected by the author with the aid of M. Jones. Circles- Miocene; Dots- Senonian to Oligocene; Random fleck- Urgonian limestones; Un-ornamented- Lower Cretaceous; Crosses- Tithonian; Diagonal ornament- Middle to Upper Jurassic.

* If we take 40°C as the maximum burial temperature:-

For 35°C/Km geothermal gradient:-

Maximum burial = 1·14 Km

∴ Molasse thickness = 1·14Km − 0·7Km (Thickness of Mesozoic)

Molasse thickness = 440 metres

This figure is similar to that gained in Section 2·5·4 for the minimum uplift ie 300 metres.

For 25°c/Km geothermal gradient:-

Maximum burial = 1·6 Km

∴ Molasse thickness = 1·6 Km − 0·7 Km

" " = 900 metres

2 Km of thrust related uplift would have unroofed the Mesozoic rocks in both of these instances.

unconformity, with Pliocene rocks above. Messinian rocks are absent within the sequence but this may be the result of non-deposition due to the lowstand of sea level at this time (Haq et al., 1987), or post Messinian uplift and erosion prior to Pliocene sedimentation. The thickness of the Miocene foredeep succession prior to uplift and erosion is not known in the Sub-Alpine Chains. It is possible, however, to estimate amounts of uplift and the thickness of the Miocene sediments using indirect methods. At Montmiral, in the Bas Dauphine the youngest part of the Miocene sequence is exposed. These shallow-marine Helvetian sediments are presently exposed on the top of 450 metres high hills. In Helvetian times global sea level was around 100-150 metres higher than present levels (Haq et al., 1987). The minimum net uplift of these rocks since Helvetian times is therefore 450 metres minus 100-150 metres, that is, around 300 metres. If we assume that this uplift is isostatic then this minimum of 300 metres of uplift would have occurred across the foreland thrust belt. It is likely to be isostatic because no large displacement thrusts have been mapped within the Bas Dauphine. However, within the foreland thrust belt, this isostatic uplift occurred after thrust related uplift. The Vercors balanced cross section of Butler (1989) shows that up to 2km of relative uplift occurred locally between the hanging-wall cut off and the footwall cut off of individual stratigraphic markers along thrusts (Figure 2.9).

The thermal maturity of the Mesozoic rocks within the Sub-Alpine Chains can be used to give crude maximum burial depths and hence the thickness of the Miocene foredeep succession. Spore colouration within the Hauterivian rocks is yellow/yellow-orange which correlates with vitrinite reflectance values of around 0.3-0.4% (Figure 2.23) (Teichmuller, 1987). Such reflectance values are thought to indicate a maximum temperatures of around 40-80°C (Teichmuller 1987) (see Figure 2.24). If 80°C is taken as a maximum burial temperature and is used when trying to convert this to a burial depth by assuming a geothermal gradient, then a maximum burial depth for the Hauterivian and hence the thickness of the now eroded foredeep sediments above can be deduced. For a paleogeothermal gradient of 35°C/Km we get a maximum burial depth of the Hauterivian of around 2km. The thickness of Mesozoic stratigraphy above the Hauterivian is around 700 metres (BRGM Vif, 1983). This suggests that the foredeep succession was in the order of 1300 metres. This figure is of the correct order of magnitude as at least 700 metres of Miocene foredeep sediment exist at depth from well data at Montmiral (BRGM Romans-sur-Isére, 1975). 2km of thrust related uplift would have exposed the top of the Mesozoic succession at or above sea level during thrusting. If we take 25°C/Km as our paleogeothermal gradient, then this suggests a maximum burial depth of around 3.2km. The foredeep succession would be around 2.5km thick and the Mesozoic rocks would not have been unroofed by thrust related uplift.

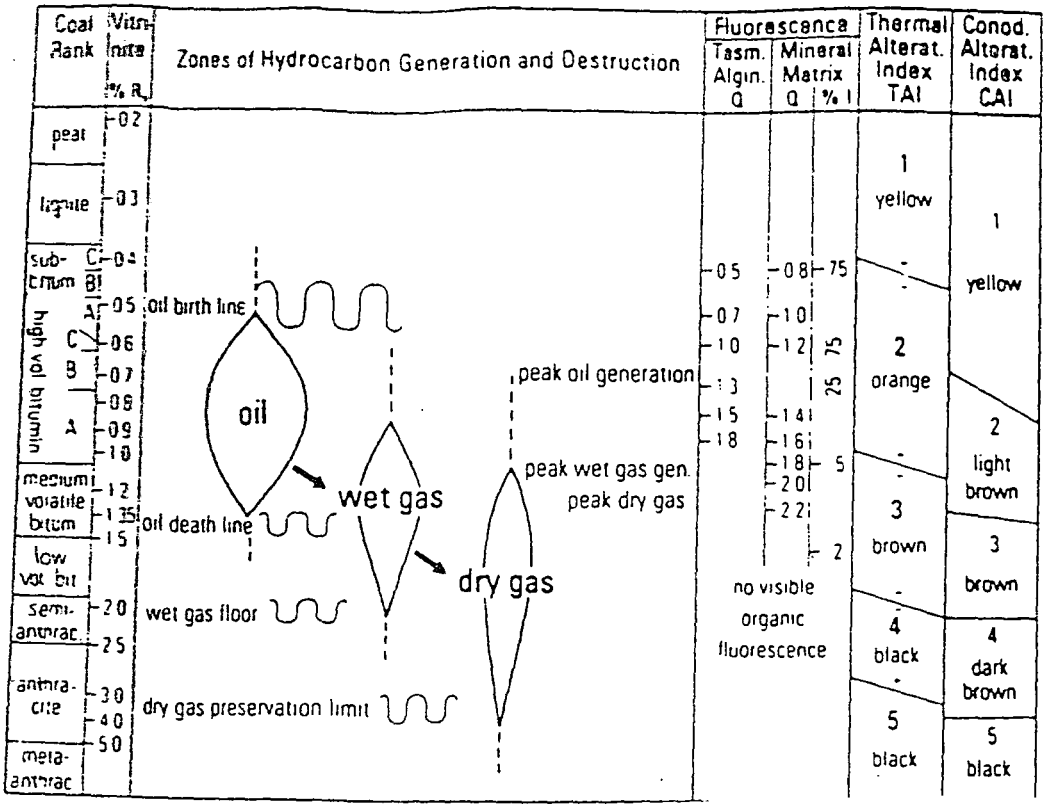

Figure 2.23. Correlation of rank stages through microscopic rank parameters in relation to oil and gas maturity. After Teichmuller (1987).

Figure 2.24. Increase in vitrinite reflectance with temperature in four boreholes in the upper Rhine Graben. After Teichmuller (1987).

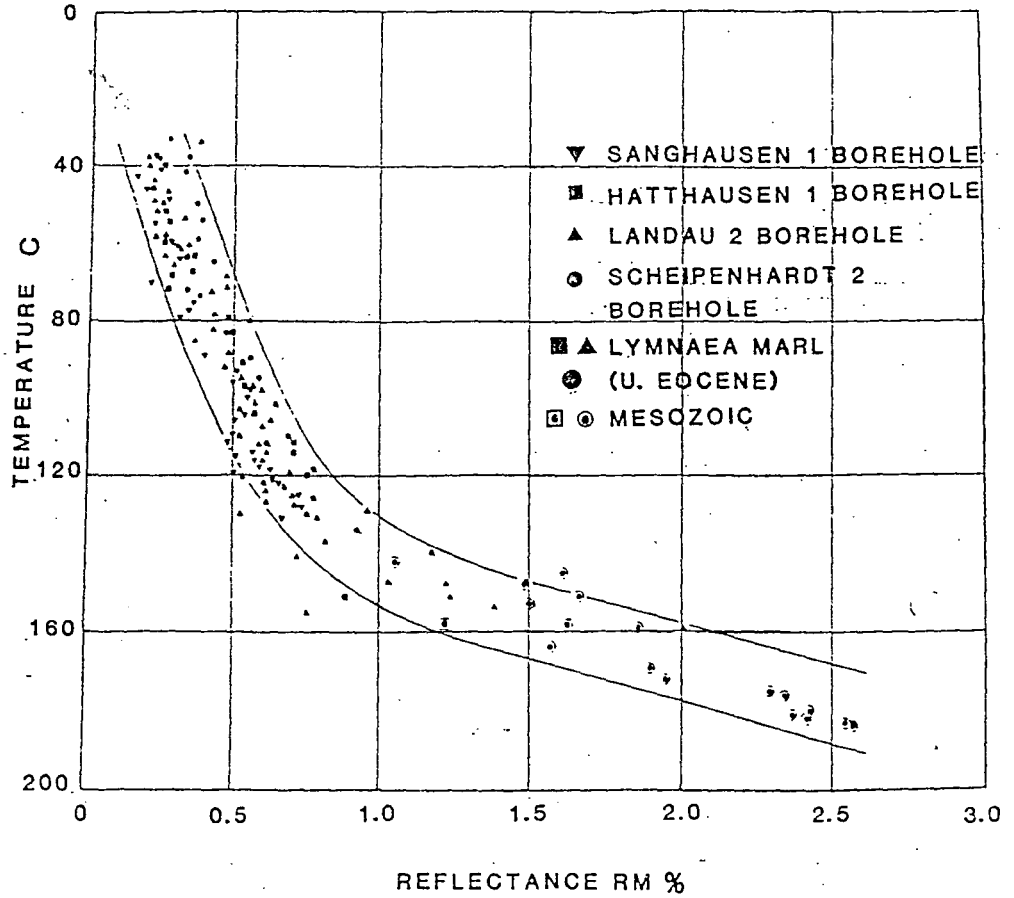

This discussion is based on the assumption that vitrinite reflectance values are mainly controlled by temperature (Teichmuller, 1987). However, the duration of burial is also thought to be an important control on thermal alteration and hence vitrinite reflectance values (Robert, 1988). The burial depths, stratigraphic thicknesses and paleogeographic information derived from this methodology are useful if used qualitatively. They can suggest scenarios such as the possible unroofing of Mesozoic strata during thrusting. The use of Apatite Fission-Track methods would produce more reliable results; however, the constraints of time and cost prohibited the use of this method during the course of this study.

Vitrinite reflectance values for rocks within the Drac Valley of around 1.45% suggest that burial depths within the deeper parts of the succession were great enough to cause thermal maturation of organic matter and hydrocarbon generation (see Figure 2.23). Bitumen seeps have been documented further north in the sector of the Sub-Alpine Chains. The bitumen has been trapped beneath the Miocene Foredeep rocks within Urgonian and Hauterivian reservoirs which have been uplifted to the surface. The hydrocarbons migrated prior to the thrusting and underwent re-migration during the thrusting (Zweidtler, 1985). The structures and sediments exposed today at the surface within the Vercors were possible structural traps and reservoir rocks prior to uplift and erosion brought them to the surface.

Section 2.5.5 Importance of the Vercors in studies of deformation and fluid flow around foreland thrust faults

The structures within the Vercors allow the study of the role of deformation in controlling sub-surface fluid migration within structural traps and reservoir rocks. The importance of sub-surface fluid migration during deformation has been emphasised in Chapter 1. With this in mind the Vercors was selected for this study. The area contains well exposed fault zones within the Urgonian limestones. The Urgonian has been locally dolomitized which has produced a secondary porosity. The Urgonian was a possible reservoir rock prior to uplift. The Urgonian is involved in thrust structures which are well exposed within deep gorge exposures which run east-west across the Vercors. The Rencurel Thrust and overlying thrust sheet is particularly well exposed within the upper part of the Gorges de la Bourne. The anticline in the hanging-wall to the thrust was a possible structural trap prior to uplift.

CHAPTER 3 STRUCTURAL GEOLOGY OF THE RENCUREL THRUST SHEET

Section 3.1 INTRODUCTION

In this Chapter, the structures within the Rencurel Thrust Sheet are discussed. General descriptions of these structures can be found in Debelmas (1983). Mapping at 1:10000 scale was carried out with the following aims.

1) To assess the geometry of the structures within the thrust sheet and to assess the temporal and spatial changes in the deformation.

2) To assess the regional significance of the structures in the mapped area.

3) To provide a large scale structural framework on which to base more detailed structural and geochemical studies.

4) To assess the movement directions and kinematic links between individual structures in the thrust sheet.

The results of the structural mapping are presented in Figure 3.1 which is contained inside the back cover of this thesis. A cross-section across the mapped area is presented in Figure 3.2.

The Rencurel Thrust which places Urgonian Limestones on to Miocene molasse clastic sediments is the most important structure on a regional scale. It can be traced to the north to merge with the Voreppe Thrust (BRGM Grenoble, 1978), and to the south into an area of large-scale gentle folds (BRGM La Chapelle en Vercors, 1967). For these reasons the Rencurel Thrust has been selected for a special study and also because it is well-exposed in the Gorges de la Bourne. The results of these studies are presented in the following Chapters. The rest of this Chapter first describes the structure of the Rencurel Thrust Sheet and then gives a detailed account of the geometry of the Rencurel Thrust Zone. Structural data which indicate the links between the structures within the Rencurel Thrust Sheet and the Rencurel Thrust Zone are presented and discussed in Sections 3.5.4. All the grid references quoted in this Chapter refer to Figure 3.1.

Section 3.2 OVERVIEW OF THE STRUCTURES IN THE RENCUREL THRUST SHEET

Figure 3.3 shows a panoramic view of the Rencurel Thrust Sheet looking north from Belv. de Valchevrière at grid reference 8487 3118. In the right of the view towards the east, the Ferrière Thrust is visible. Around grid reference 8490 3135, Urgonian limestones in the hanging-wall to the thrust can be seen structurally overlying

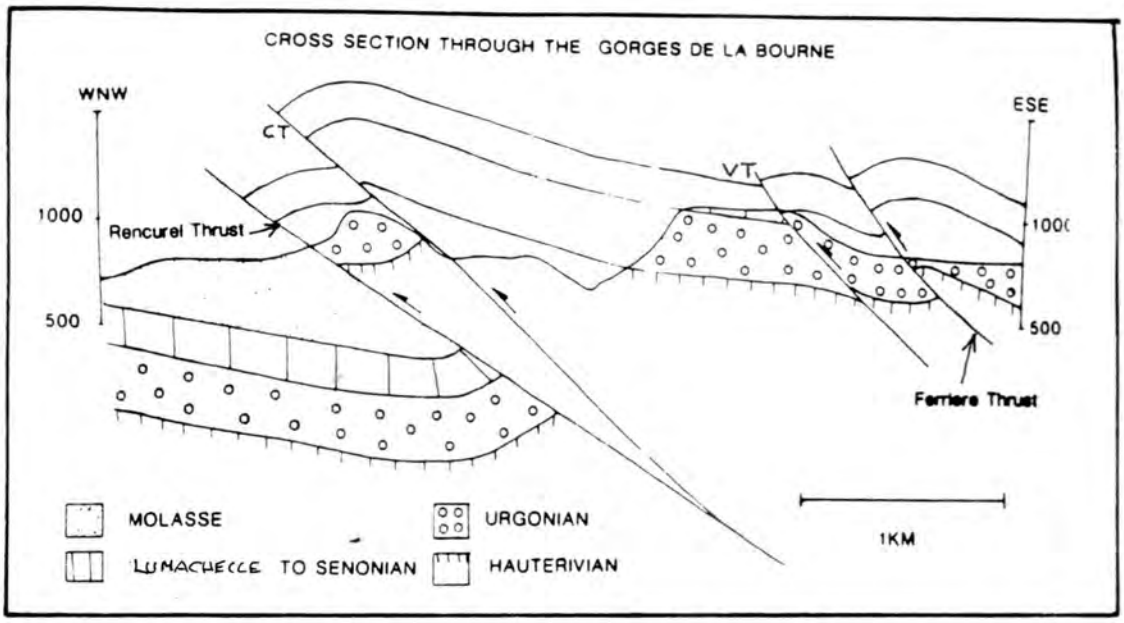

Figure 3.2 Cross section across the area south-east of La Balme de Rencurel. (See figure 3.1 for location). No sub-surface control.

Figure 3.3 View of the Rencurel Thrust sheet looking north from Belv. de Valchevriere. (Grid reference 8487 3118). See section 3.2 for explanation.

Senonian limestones in the footwall to the thrust. At grid reference 8498 3125 at the base of the Gorges de la Bourne not shown in the view, the thrust places Hauterivian limestones on to Urgonian limestones. Detailed mapping of this thrust has shown that the geometry of the thrust becomes more complicated towards the south. The single thrust in the north is replaced by a pair of thrusts in the south as indicated on BRGM Vif (1983). Mapping in the Gorges de la Bourne around Pont de Valchevrière (grid reference 8494 3125) shows that the two thrusts do not join in a simple manner but merge within a zone of minor thrusts. This area may be what would be termed a branch point in a regional scale structural study. In the south, the eastern-most thrust is exposed at grid reference 8492 3099 near Malaterre where Urgonian limestones in the hanging-wall to the thrust have been thrust upon Gargasian limestones locally termed the Lumachelle. The most westerly exposed thrust is at Belv. de Valchevrière (grid reference 8487 3118), where Urgonian limestones have been thrust on to the Lumachelle. This thrust probably runs farther south through Plateau de Chateau Julien where a hanging-wall anticline within the Urgonian is exposed near grid reference 8482 3105.

In the centre of the view in Figure 3.3, the Senonian limestones can be seen to be underlain by the Urgonian limestones exposed in the prominent cliffs which are in turn underlain by the Hauterivian limestones which are poorly exposed on the tree covered gentle slopes at the base of the Urgonian cliffs. Mapping of the Gorges de la Bourne shows that no major thrust exists within this stratigraphy. However, underlying this stratigraphy is the Chalimont Thrust. The thrust zone is not well exposed but runs north from Crete de Chalimont to the east of the hill Perrellier. The thrust emplaces Hauterivian limestones on to the Urgonian at present exposure levels.

To the extreme left of Figure 3.3 at grid reference 8471 3139, the Rencurel Thrust is exposed emplacing Urgonian limestones onto Miocene Molasse sandstones.

Section 3.3 STRUCTURAL TRAVERSE THROUGH THE GORGES DE LA BOURNE

The Gorges de la Bourne provides excellent exposures of the structures within the Rencurel Thrust Sheet. This Section describes the structures exposed within the gorge starting in the east with the highest structural levels and moving west towards the base of the thrust sheet were the Rencurel Thrust itself is exposed.

Section 3.3.1 Ferrière Thrust Zone

This thrust zone is the subject of a detailed study by Roberts (1990) which is included as an enclosure inside the back cover of this thesis. This Section is a brief summary of this paper.

The Ferrière Thrust Zone is well exposed in the road cut on the north side of the D531 road at grid reference 8498 3124. Figure 3.4 shows a field view of the geometry of the thrust zone. Figure 3.4 shows that both the hanging-wall Urgonian rocks and the footwall Hauterivian rocks contain minor faults. Cross-cutting relationships can be recognised between the faults. Figure 3.5 is a close-up view of the area indicated in Figure 3.4. The fault shown in Figure 3.5 and the other westward dipping faults within the Hauterivian rocks shown in Figure 3.4 are suggested to be early formed thrusts for the following reasons. The movement direction on the fault is known from the orientation of calcite steps on the fault plane shown in Figure 3.6. Using this evidence the fault can be seen to cut up-section along the movement direction placing older rocks on to younger rocks, indicating that the fault is a thrust. The faults exist within the western limb of the hanging-wall anticline to the Ferrière Thrust Zone. The faults seem to have formed early, before the folding rotated them into their present downward facing attitude. Figure 3.4 shows that the fold is cut by a set of faults dipping gently towards the east. These faults post-date the formation of the fold. Figure 3.7 shows a model for the deformation history within the Ferrière Thrust Zone. Deformation started with the formation of a set of minor thrusts. These faults were rotated into a downward facing attitude before later thrusts developed, cutting across the fold. Roberts (1990) outlined the structural controls on fluid migration through this thrust zone, utilising a combination of observations made using petrological and cathodoluminescence techniques.

Section 3.3.2 Valchevrière Thrust

The Valchevrière Thrust is to the west of the Ferrière Thrust described in Section 3.2. It is exposed at Belv. de Valchevrière (grid reference 8488 3120) and also in the northern side of the Gorges de la Bourne (grid reference 8492 3128). The thrust continues to the south and at Plateau de Chateau Julien, it emplaces Urgonian on to Senonian limestones. Figure 3.8 shows the Valchevrière Thrust at grid reference 8492 3128 in the Gorges de la Bourne. The thrust cuts through a fold within the Urgonian limestones.

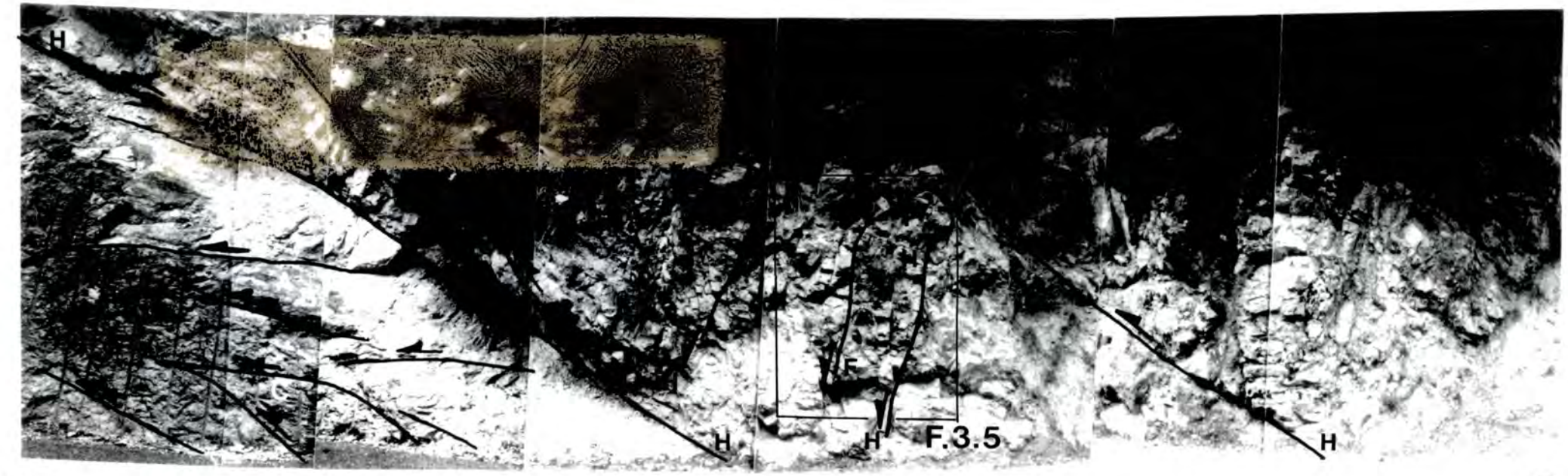

1m

Hangingwall ramp indicated by bedding plane cut offs.

H H

Footwall ramp indicated by bedding plane cut offs.

F F

Figure 3.4
Photo montage and structural interpretation of the Ferriere Thrust Zone. (From Roberts, 1990).

Figure 3.5 Downward facing thrust developed in Hauterivian interbedded limestones and lime-mudstones within the Ferriere Thrust Zone. For location see Figure 3.4.

Figure 3.6 Calcite steps on the fault plane shown in Figure 3.5.

Figure 3.7 The evolution of structural style seen in the Ferriere Thrust Zone. (From Roberts, 1990).

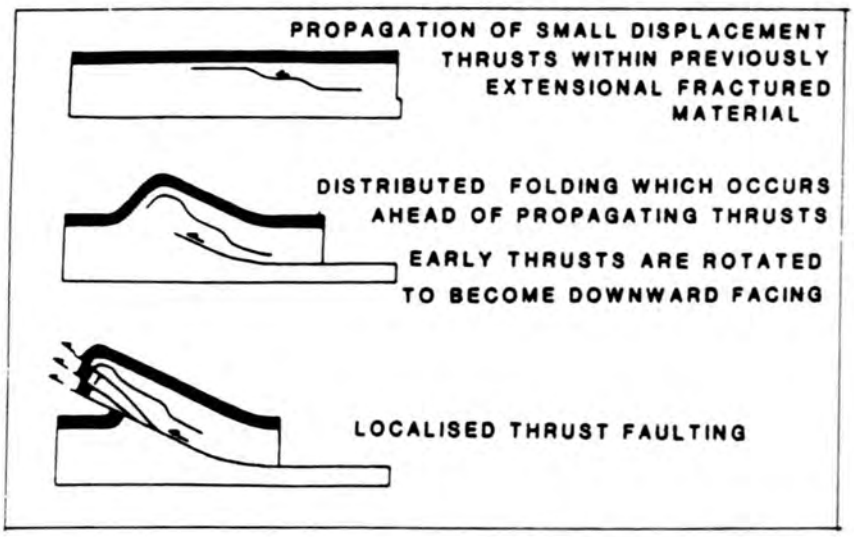

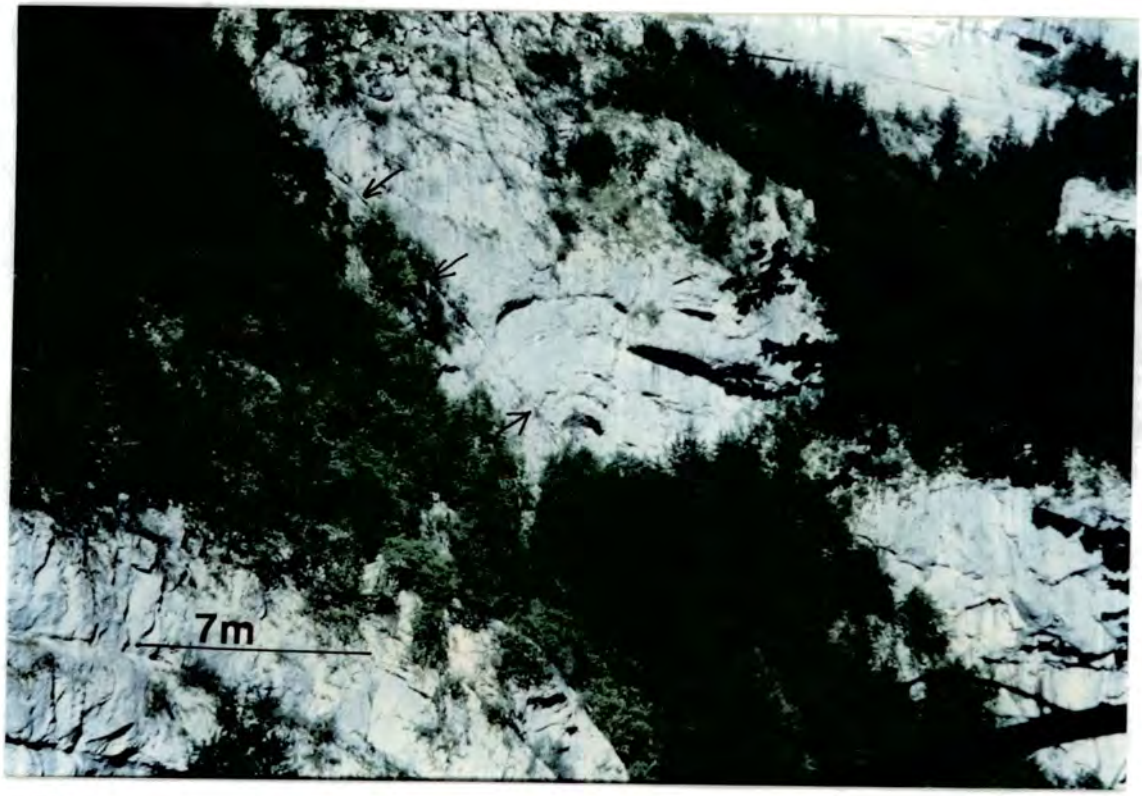

Figure 3.8 Valchevriere Thrust within the Urgonian limestones on the northern side of the Gorges de la Bourne. (Grid reference 8492 3128). (See section 3.3.2).

Section 3.3.3 Thrust at Grid reference 8492 3126

Figure 3.9 shows a footwall syncline developed in the gorge below the level of the road.

Section 3.3.4 Backthrust at grid reference 8490 3127

At this locality a backthrust is exposed which offsets some pre-existing faults. Figure 3.10 shows a view looking on to the northern side of the gorge from the road. A steeply dipping fault can be seen truncated in the footwall to a backthrust. The steeply dipping fault is probably of Eocene/Oligocene age formed during the development of the Rhone-Bresse Graben system. The Thrust is probably Miocene in age. The whole section has been tilted so that the thrust is now downward facing. The Eocene/Oligocene age fault is also exposed in the hanging-wall to the backthrust. The displacement on the backthrust can therefore be seen to be around 50 metres. The backthrust also shows a ramp-flat geometry as shown in Figure 3.11.

Section 3.3.5 Thrust at Grid reference 8484 3129

At this locality on the southern side of the gorge, an early normal fault is offset by a thrust as shown in Figure 3.11.

Section 3.3.6 Normal fault at grid reference 8483 3131

At this locality a normal fault offsets the base of the Urgonian (Figure 3.11). The stratigraphy consists of interbedded limestones and shales of the Hauterivian passing upwards across a non-conformity into the Upper Barremian where the Urgonian begins with 20 metres of massive dolomites passing upwards into thin-bedded limestones containing a paleokarst (Arnaud-Vanneau, 1980). The fault downthrows about 20 metres to the east placing the U. Barremian dolomites against the Hauterivian limestones and shales in the footwall.

Section 3.3.7 Rochers de Chalimont (grid reference 8480 3129)

This cliff contains exposures of the higher parts of the Urgonian stratigraphy. Figure 3.12 looking south on to the cliff, shows that a set of small displacement thrusts exists which display ramp-flat geometries controlled by the bedding.

Figure 3.9 Footwall syncline developed in the Urgonian limestones in the Gorges de la Bourne. The fold is exposed between the level of the road and the river. (Grid reference 8492 3126). (See section 3.3.3).

Figure 3.10 Early steeply-dipping fault exposed in the footwall to a backthrust developed in the Urgonian limestones. (Grid reference 8490 3127). (See section 3.3.4).

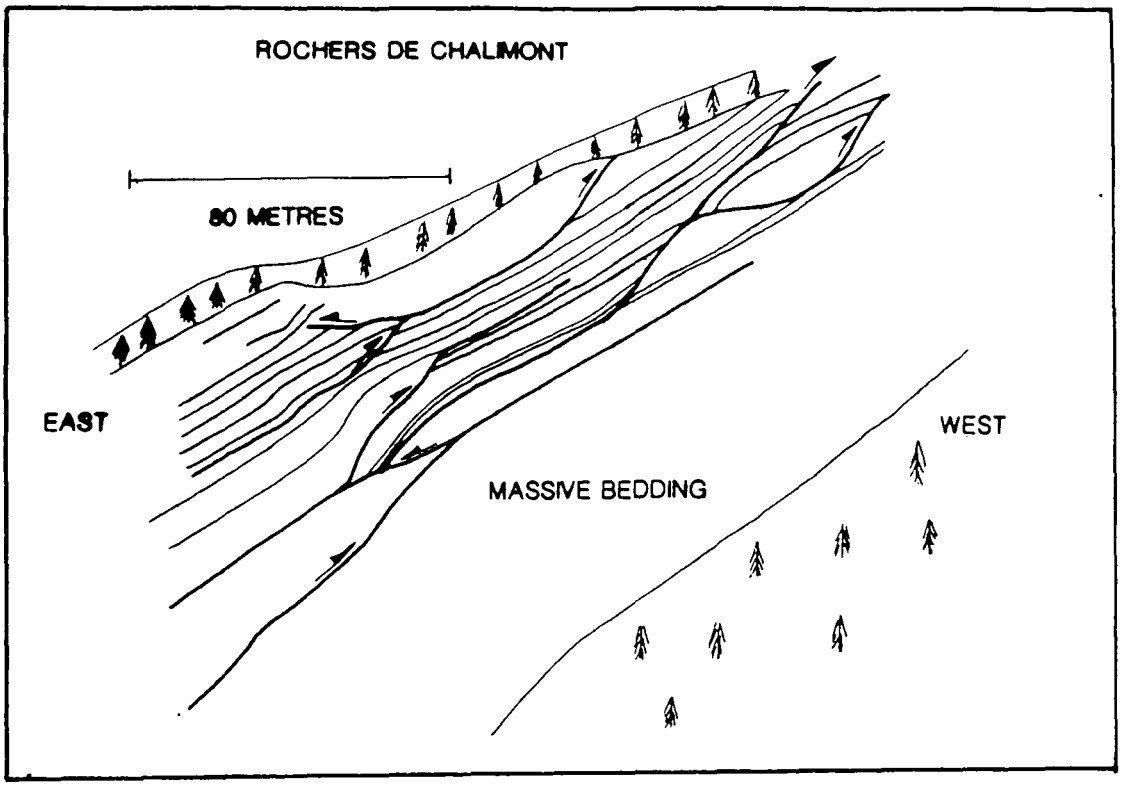

Figure 3.12 View looking south onto Rochers de Chalimont (grid reference 8480 3129). The structural interpretation shows a series of thrusts exhibiting ramp-flat geometries. (See section 3.3.7).

Section 3.3.8 Footwall to the Chalimont Thrust (grid reference 8476 3139)

The Chalimont Thrust is not exposed in the Gorges de la Bourne. However, the locality at grid reference 8476 3139 displays well the deformation which occurs in the footwall to this thrust. The contact between the Urgonian and the Hauterivian has been folded into a vertical attitude forming a footwall syncline to the thrust.. Bedding is cut across by a set of eastward vergent backthrusts which must have formed after the folding at a late stage in the deformation. Figure 3.13 shows the deformation along one of these fault zones which is typical of the deformation along the minor faults. The fault plane is coated in fine-grained fault gouge which cuts through a zone of coarse fault breccia. The wall-rocks to the thin fault zone seem to be relatively un-fractured.

Section 3.4 DISCUSSION OF STRUCTURES WITHIN THE RENCUREL THRUST SHEET

The structural traverse along the Gorges de la Bourne highlights three main aspects of the structural style within the Rencurel Thrust Sheet.

1) Early faults, probably of Eocene/Oligocene age existed in the area prior to the post mid-Miocene thrusting. These fault have throws of up to 20 metres. Oblique lineations exist on some of the fault planes suggesting that an important component of strike-slip was involved in the deformation which produced normal offsets in the stratigraphy. These early faults are simply truncated by the thrusts and do not localise zones of intense deformation involving upright pure shear and buttressing. This is probably because no significant lithologically-controlled rheological contrast was present across the early faults at the position where they were intersected by the thrusts (Section 2.5.1.2).

2) The minor thrusts display ramp-flat geometries in the well-bedded units of the Urgonian. Some of the minor thrusts cut through localised small scale folds. The minor thrusts have displacements generally less than 50 metres where visible*The minor thrust zones are composed of gouge and breccia accummulated to only a few centimetres in thickness. The wall-rocks around the faults are not penetratively deformed by fracturing.

3) The larger thrust zones such as the Ferrière Thrust and the footwall to the Chalimont Thrust are composed of an array of minor faults. These larger thrust zones show complex deformation histories with early minor thrusts being folded and rotated

* 5 THRUSTS WERE MEASURED.

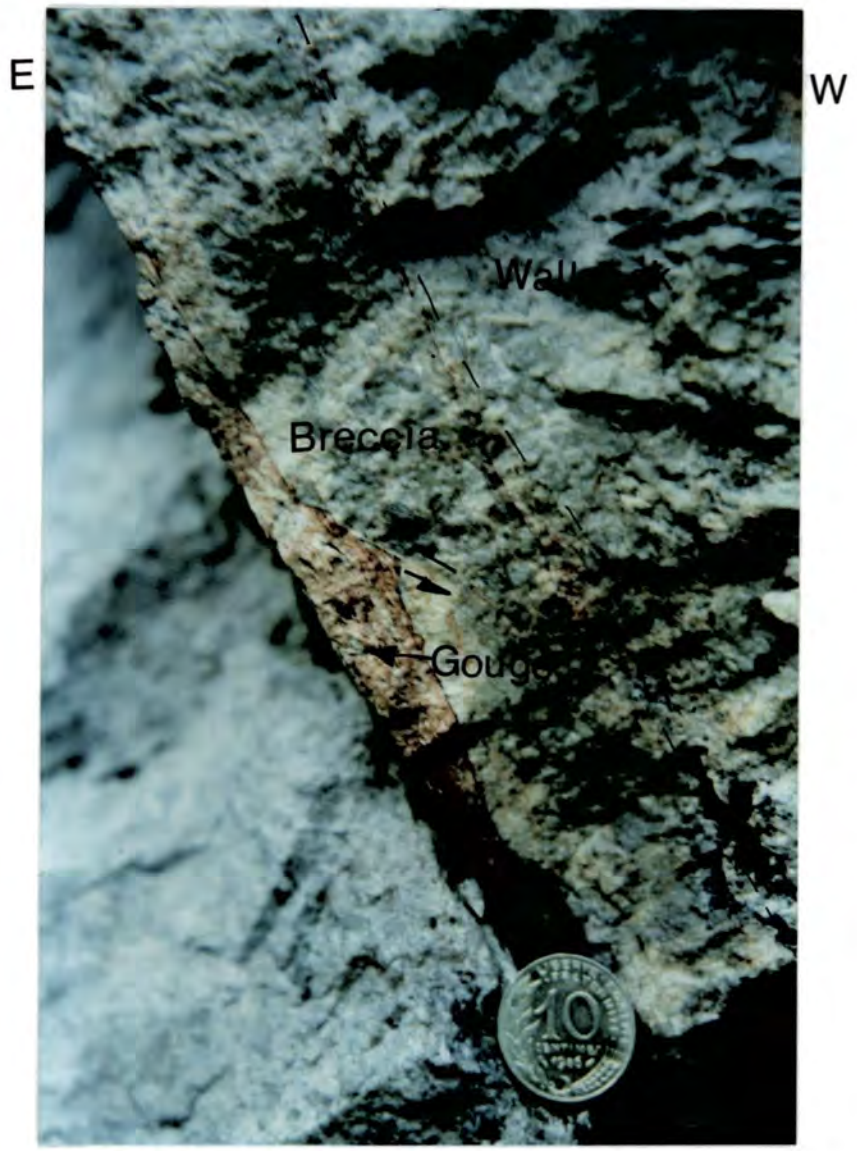

Figure 3.13 Discrete eastward-vergent backthrust developed in the Urgonian limestones in the footwall to the Chalimont Thrust Zone. A discrete fine-grained gouge zone cuts through a cemented fault breccia. The wall-rocks are relatively undeformed by fracturing. In thin section, recognisable wall-rock features can be seen such as limestone cements and allochems and dolomite rhombs. The rocks are not recrystallised but do display calcite twinning. (Grid reference 8476 3139). (See section 3.3.8).

before late minor thrusts develop.

Section 3.5 THE GEOMETRY OF THE RENCUREL THRUST ZONE

Fault zones are often represented on regional cross-sections as single fault breaks. However recent studies have shown that in areas where offsets in the stratigraphy occur due to faulting, the fault zone is in fact composed of an array of mesoscale faults. Fault densities increase into the centre of the fault zone where a zone of fault gouge often metres across exists. The fault zone can be up to a few hundred metres in thickness (Wojtal & Mitra, 1986; Woodward et al., 1988). Also single fault zones can divide to become separate fault splays. The areas where the faults diverge are known as branch lines, which are known as branch points after erosion across branch lines or in two dimensional cross-sections or maps. Fault separation at branch points can occur down or up-dip and along strike. Patterns of faults which display these geometries make up linked fault systems. These concepts are described in Butler (1982) and Boyer & Elliott (1982). In the following Sections, it will be shown that the Rencurel Thrust is composed of an array of mesoscale faults and changes its geometry along strike as revealed during structural mapping. It is important to understand the 3-dimensional geometry of the thrust zone as this gives insights into the style of deformation and also the geometry of potential seals or fluid migration pathways connected with the fault zone. This Section will describe the geometry of the Rencurel Thrust Zone as revealed by the structural mapping presented in Figure 3.1.

Section 3.5.1 Regional geometry of the Rencurel Thrust Zone

Figure 3.14 illustrates the geometry of the Rencurel Thrust Zone in grid square 347 313 as seen looking south from grid reference 8470 3160. The structure is exposed in the mountain Crete de Chalimont which is around 1600 metres high. The altitude at the village of La Balme de Rencurel seen in the foreground is around 700 metres. Each of the two distinct cliffs seen in the view is around 300 metres high. The cliffs are composed of Urgonian limestones which from regional considerations are known to be around 300 metres thick (BRGM Vif, 1983). In the centre of the view the gentle tree-covered slopes are formed on the Miocene molasse sediments. In the right of the view Senonian limestones are exposed in a gorge south-west of La Balme de Rencurel (BRGM Vif, 1983). The structure here is composed of two imbricate slices of Urgonian limestones separated by a thrust, here termed the Chalimont Thrust. At the base of the exposed structure where the Urgonian limestones structurally overlie the Miocene molasse sediments, another thrust exists which is termed the Rencurel Thrust. The Miocene rocks in the footwall to this thrust rest unconformably on the Senonian rocks exposed in the gorge to the west. In Figure 3.15, the geometry of the Rencurel Thrust

Figure 3.14 View looking south from 8470 3160 onto Crete de Chalimont. The Rencurel Thrust Zone runs at the foot of the hill beneath the lower cliff of Urgonian limestone. The Chalimont Thrust runs between the two cliffs of Urgonian linestones which are each around 300 metres high. (See section 3.5.1).

Figure 3.15 View looking north towards the Rencurel Thrust below Rochers de Gonson (1540 metres), from grid reference 8462 3135. The village of Rencurel is at around 780 metres. (See section 3.5.1).

just north of grid square 848 315 is shown as seen looking north from grid reference 8462 3135. The cliff of Rochers de Gonson is composed of around 300 metres of Urgonian limestones (BRGM Vif, 1983). At the base of the cliff the area of trees occurs on drift which may overlie Hauterivian limestones and shales. Exposures of Miocene molasse clastic sediments occur in the area of cultivated fields around the village of La Balme de Rencurel shown in the view. The Miocene rocks unconformably overlie Senonian limestones dipping gently east, which are exposed in the wood at the left of the view. The structure here is composed of a single main thrust which emplaces Cretaceous carbonates onto the Miocene molasse clastic sediments. Moving south from the Rochers de Gonson along the Rencurel Thrust, the thrust branches and becomes two imbricate thrusts each of which carries a slice of Urgonian limestones as shown in Figure 3.14 at Crete de Chalimont. The branch point must lie just to the north of grid square 847 315. In this grid square, the two imbricate slices still exist, the lower one exposed in the hill of Perrellier at grid reference 8475 3153 and the higher one in the cliff of Roche Chalve at grid reference 8488 3142. The area where the branch point exists is unfortunately poorly exposed (BRGM Vif, 1983). The geometry of the branch point between the Rencurel Thrust and the Chalimont Thrust is illustrated in Figure 3.16. The higher thrust splay is not marked on BRGM Vif, (1983), but is mentioned in Debelmas, (1983). The presence of this thrust is suggested by the double thickness of Urgonian limestones exposed in Crete de Chalimont (see Figure 3.14). Also, although the thrust is not well exposed, vertically bedded and highly deformed Hauterivian limestones and shales are exposed at 8478 3141 along the D531 road. These rocks are proposed to lie just into the hangingwall of the proposed Chalimont Thrust. This outcrop together with the vertically bedded and highly deformed transitional rocks between the Urgonian and Hauterivian which occur along the D103 road at 8476 3139 which are proposed to lie just in the footwall to the Chalimont Thrust, provide further evidence for the existence of a large thrust. These outcrops along the proposed Chalimont Thrust are described more fully in Section 3.3.8.

Section 3.5.2 Geometry of the Rencurel Thrust Zone.

This Section will describe the geometry of the Rencurel Thrust Zone as revealed by structural logging. The best exposures lie along the D103 and D531 roads.

Figure 3.17 shows the view looking south onto the Rencurel Thrust Zone where it is crossed by the D103 road at grid reference 8472 3139, as seen looking south from grid reference 8472 3145. The cliff is around 300 metres high and composed of Urgonian limestones which are locally dolomitized. In the higher parts of the cliff, bedding can be seen dipping gently towards the south-east. Lower in the cliff,

Figure 3.16 View looking north from grid reference 84 75 3128 towards Perrellier and the branch point between the Rencurel Thrust and the Chalimont Thrust. The road at the base of Perrellier is at around 660 metres, whilst the top of Perrellier is at around 1145 metres. (See section 3.5.1).

Figure 3.17 View looking south from grid reference 8472 3145 onto the Rencurel Thrust Zone where it is crossed by the D103 road at grid reference 8472 3139. The cliff of Urgonian limestone is around 300 metres high. The thrust carries the Urgonian onto Miocene molasse sandstones. (See section 3.5.2).

bedding cannot be seen clearly. Here, the Urgonian is dolomitized and cut by a dense array of mesoscale faults. In the wood at the extreme right of the view, a thrust contact is exposed between the older Urgonian limestones above the younger Miocene molasse along the D103 road. The Miocene in the footwall to the thrust is poorly exposed but at least 4 metres of highly deformed Miocene siltstone rock forms the lowest exposed portion of the Rencurel Thrust Zone. The base of the thrust zone is not exposed so its true thickness cannot be estimated. In this view the thickness is a minimum of 100 metres. The bedding in the higher parts of the cliff are parallel to the gentle dip of the fault zone to the south-east so that the fault zone has the geometry of a hanging-wall flat (Butler, 1982).

The fault zone is also partly exposed along the D531 road at the base of the hill Perrellier at grid reference 8474 3143. Figure 3.18 shows a view onto these exposures looking east-north-east from grid reference 8462 3141. The thrust contact between the Urgonian and the Miocene is not exposed here but there are good exposures of the array of minor faults in the Urgonian which form the higher parts of the Rencurel Thrust Zone. Bedding within the Urgonian limestones is gently folded into an anticline so that the fault zone here has the geometry of a hanging-wall ramp (Butler, 1982). The thrust cuts up section within the Urgonian towards the west-north-west. The thrust transport direction within the Vercors is towards the west-north-west as discussed in Section 3.5.4. The hanging-wall ramp within the Urgonian at this locality is therefore a frontal ramp (Butler, 1982). This frontal ramp would probably also have existed farther to the west of the outcrops of the thrust zone along the D103 road but it has now been eroded away.

The exposures along the D103 road were chosen for a detailed study as they allow examination of the detailed internal geometry of the fault zone, which can be placed into the context of the larger scale geometry discussed in Chapter 2 and Sections 3.1-3.5. The exposures are especially useful as they allow detailed structural logging, the collection of structural data and sample collection across a substantial portion of the thrust zone including the thrust contact of the Urgonian limestones and the Miocene molasse sediments.

Section 3.5.3 Detailed internal geometry of the Rencurel Thrust Zone along the D103 road

Preliminary study of the outcrops reveal that an array of minor faults is developed within the Urgonian. Individual faults within the array which exists within the Urgonian are coated in cataclastic fault gouge containing stylolitic seams produced by diffusive mass transfer (DMT). The faults have displacements in the order of less than

NNW SSE

Figure 3.18 View looking east-north-east from grid reference 8462 3141 onto the hill Perrellier (1145 metres). The road at the base of the cliff is at around 660 metres. The Rencurel Thrust is not exposed but probably runs close to the base of the cliffs. (See section 3.5.2).

a couple of metres. The thickness of cataclastic fault rock which exists along them is in the order of a couple of centimetres. Areas between the minor faults seem relatively undeformed by fracturing, pressure dissolution and veining. The thrust contact between the Urgonian and the Miocene is a zone of more pervasive deformation. A planar band of cataclastic fault gouge separates the Urgonian and Miocene rocks. The gouge is at least 40 centimetres thick and made of carbonate material derived from the Cretaceous rocks. In the footwall to this is a shear zone at least 4 metres wide, composed mainly of material derived from the Miocene clastic rocks, but also including blocks of carbonate material derived from the Cretaceous rocks.

It was decided that if these fault rock types are important in controlling fluid flow in the sub-surface, then understanding the spatial variations in the fault rocks would be important to assess fluid flow through the Rencurel Thrust Zone. This goal would be achieved by mapping the detailed geometry of the fault zone. Also understanding of the chronology of formation of different elements of the fault zone would highlight any temporal changes in the effect of porosity and permeability controlling deformation mechanisms. This goal would be achieved by searching for cross-cutting relationships within the fault zone.

The geometry of the fault zone was documented by mapping all the visible faults within the fault zone onto a black and white colour photo montage which is shown in (in enclosures) Figure 3.19. Only fractures which had visible fault rocks along them were marked on to this structural log. This avoids confusion as to whether a fracture is tectonic or produced by excavation and blasting of the road section or weathering but may bias the study. Black lines on the montage indicate the position of faults. Areas encircled by black lines indicate where fault planes are visible. This technique produces a minimum estimate of fault densities within the fault zone. Fault rocks may have been eroded from some fractures so that they cannot be positively identified as tectonic, and some faults may have been missed. A minimum estimate of fault densities is however still useful information to input into the fault zone models.

On this structural framework, more detailed studies were based.

1) The orientation of fault planes and fault plane lineations were measured in order to help characterise the deformation within the fault zone. The results of this are presented in Section 3.5.4.

2) Detailed outcrop descriptions were carried out to ascertain styles and spatial changes in deformation within the fault zone and to pin-point areas which warranted special study.

3) Samples were taken from areas which were indicated by the structural studies. This

was important so that laboratory based studies could be fitted into the context of the fault zone. All samples were orientated by marking a strike and dip on a prominent plane on the hand specimen.

4) Laboratory based studies began with petrological and microstructural analysis of the samples to evaluate deformation mechanisms and diagenetic histories. The results of studies 2, 3 and 4 are reported in Chapters 4 and 5.

Section 3.5.4 Structural data for the Rencurel Thrust Sheet: Movement directions and implications for the evolution of the thrust sheet.

Structural data were collected for the Rencurel Thrust Sheet. These data include the orientation of fault planes and lineations on the fault planes. Lineations on fault planes generally indicate the slip direction on a fault plane. Lineations on fault planes in the Rencurel Thrust Zone consist of striations, gouge grooves and the long axis of fault plane undulations. The lineations were measured using a compass clinometer and the data are presented in Figure 3.20. The data was converted into contoured stereographic projections using the STATIS programme. The stereographic projections presented in Figure 3.20 show that lineations are orientated west-north-west to east-south-east throughout the Rencurel Thrust Sheet. This is constant with the notion that all the faults are part of the thrust zone geometry and were formed during one kinematically linked phase of thrusting. Structural observations from all the elements of the thrust sheet can be used in constructing models of deformation and fluid migration through the Rencurel Thrust Sheet. Fault plane orientation data are presented in Figure 3.2 1. All the data collected are presented in Appendices 1.

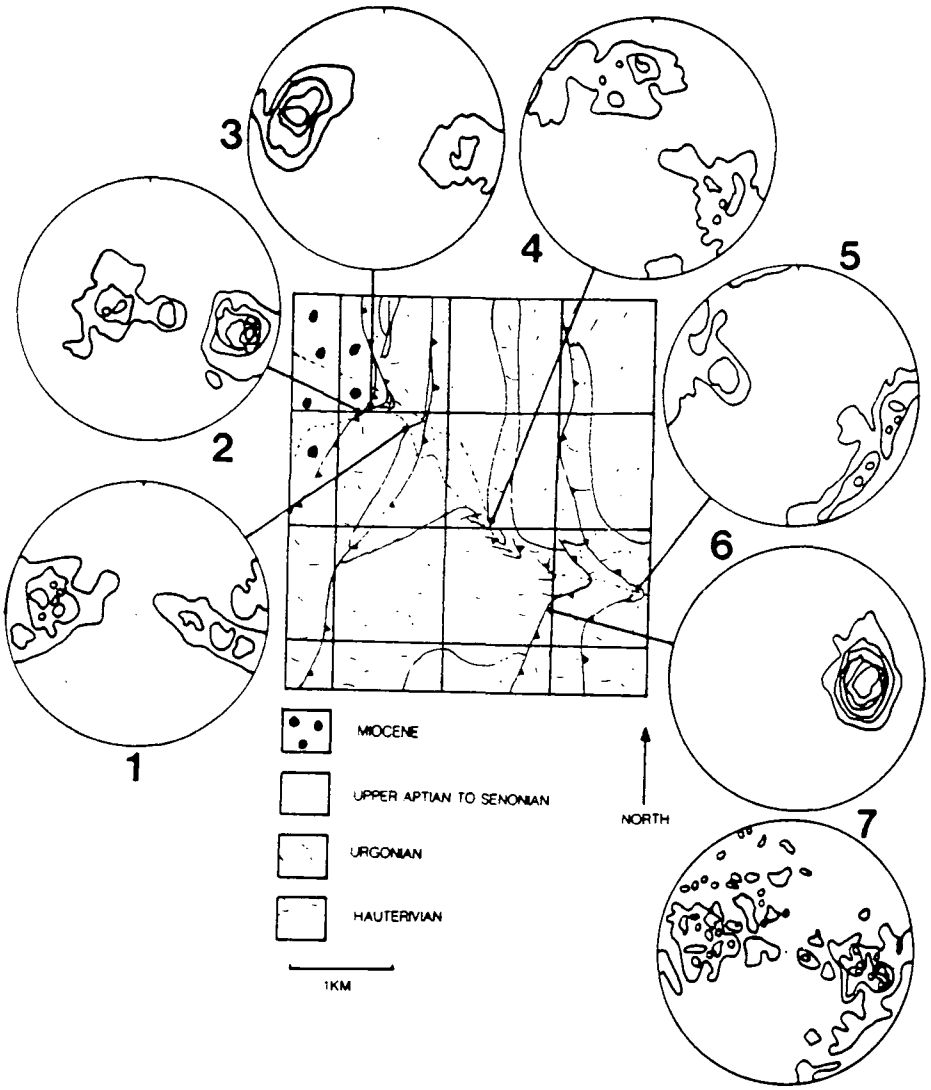

Figure 3.20 The orientation of lineations developed on fault planes in the Rencurel Thrust Sheet. (See section 3.5.4). 1- Footwall to the Chalimont Thrust; 2- Thrust contact between the Urgonian and the Miocene within the Rencurel Thrust Zone; 3- Array of minor faults in the Urgonian within the Rencurel Thrust zone; 4- Faults around Pont de Goule Noire; 5- Ferriere Thrust Zone; 6- Valchevriere Thrust Zone; 7- All the data for the Rencurel Thrust sheet. Contours represent <2%; >2%; >4%; >7%; >10%; >13% and >16% of the data plotting within the contoured area.

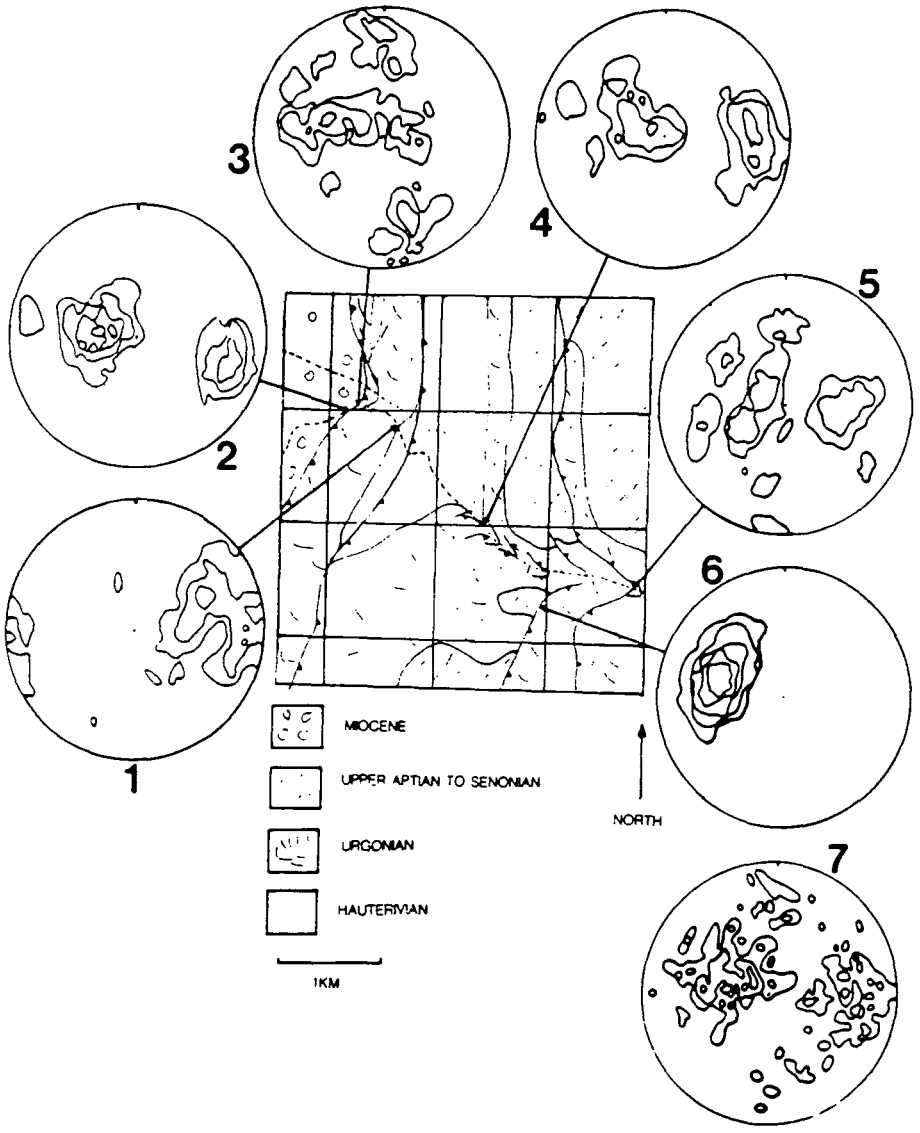

Figure 3.21 Fault plane orientations in the Rencurel Thrust Sheet. (See section 3.5.4). 1- Footwall to the Chalimont Thrust; 2- Thrust contact between the Urgonian and the Miocene within the Rencurel Thrust Zone; 3- Array of minor faults in the Urgonian within the Rencurel Thrust zone; 4- Faults around Pont de Goule Noire; 5- Ferriere Thrust Zone; 6- Valchevriere Thrust Zone; 7- All the data for the Rencurel Thrust sheet. Contours represent <2%; >2%; >4%; >7%; >10%; >13% and >16% of the data plotting within the contoured area.

CHAPTER 4 DEFORMATION OF THE URGONIAN LIMESTONES WITHIN THE RENCUREL THRUST ZONE

Section 4.1 INTRODUCTION

In Section 3.5.3 it was pointed out that the higher parts of the Rencurel Thrust Zone are composed of an array of minor faults cutting the Urgonian limestones. This Section describes the deformation associated with these faults. All the samples and observations mentioned in this Chapter are located on Figure 3.19.

Two main faulting styles seem to exist within the Urgonian:-

1) Breccia zones - Breccia zones are restricted to a small portion of the Rencurel Thrust Zone. They are described in Section 4.2.

2) Discrete gouge zones - Discrete gouge zones are by far the most common deformation features along the minor faults within the Urgonian involved in the Rencurel Thrust Zone. Several individual faults were singled out for special study, and these will be discussed in the following Sections. These faults are described in Section 4.3.

Section 4.2 BRECCIA ZONES.

Section 4.2.1 Observations

Figure 4.1 shows the style of deformation which occurs along the fault selected for a special case study. Around this fault fractures up to 5mm across are filled with very fine grained brown material (Figure 4.2). X-ray diffraction studies of this brown material have shown it to be a combination of smectite and montmorillonite, with small amounts of calcite and dolomite. Clasts of calcite and dolomite derived from the wall-rocks to the fractures are supported within the smectite and montmorillonite mixture. The edges of these fractures are sharp and not gradational. The carbonate wall rocks outside of the fractures show normal sedimentary and diagenetic textures and are relatively undeformed by fracturing. Some calcite crystals are however twinned.

These fractures grade into areas of breccia shown in Figure 4.1. The breccia clasts are isolated by similar fractures to those described above and are filled with the same mixture of smectite and montmorillonite, dolomite and calcite. These fractures are

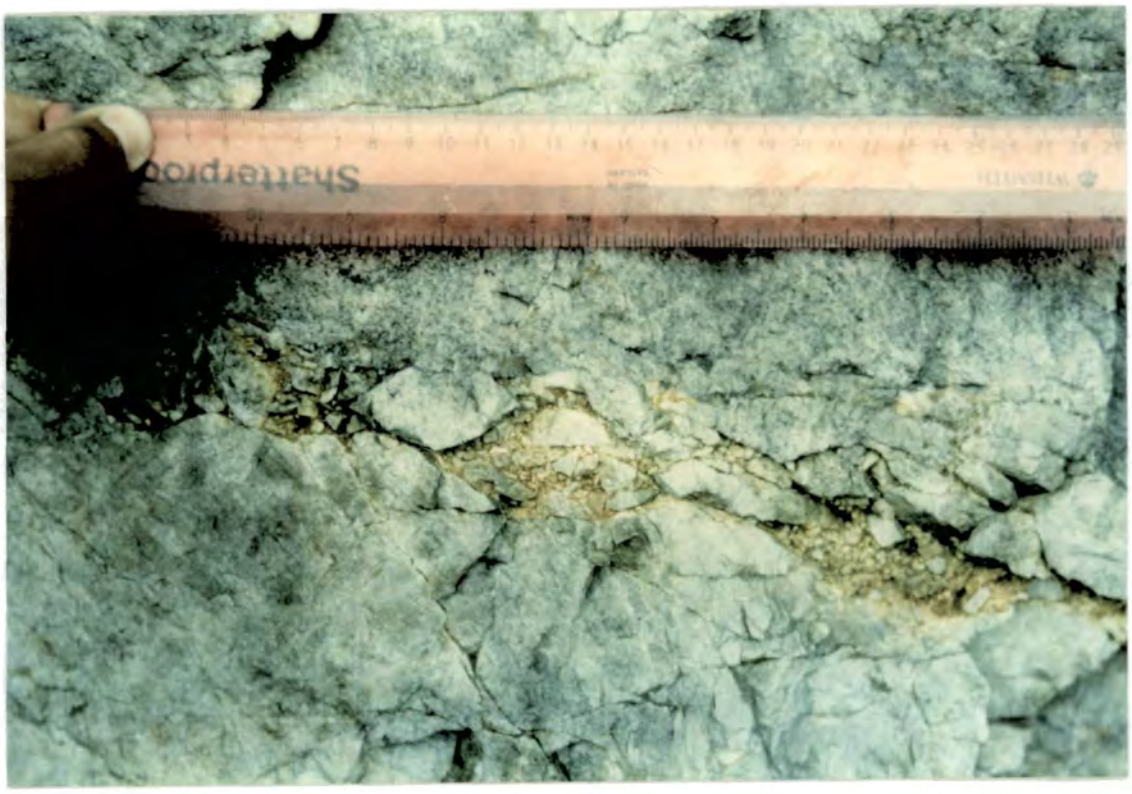

Figure 4.1 Deformation of the Urgonian limestones along the breccia zones (See Section 4.2). See Figure 3.19 for location.

Figure 4.2 Fracture associated with the breccia zones filled with a combination of smectite and montmorillonite (See Section 4.2).

however truncated by faults coated in fine-grained, red-stained carbonate fault gouge as illustrated in Figure 4.3. The rotation of the breccia clasts can be used to provide shear sense criteria for the fault zone which is top to the west. No fault plane lineations or extensional fractures filled with coarsely crystalline material are present.

The mixture of smectite and montmorillonite is also found within small areas of cave collapse material located on Figure 3.19. The areas contain chaotic breccias with smectite and montmorillonite filling the cavities between the clasts. These breccias are distinct from those found along the faults in that they do not occur in sub-planar zones. They also disrupt the fault geometries present indicating that they post-date the deformation.

Section 4.2.2 Discussion of the breccia zones.

Fracturing, which is a cataclastic process, was important during deformation along these fault zones. Cataclasis occurs at high strain rates at the temperatures and pressures which are suggested to have existed during this deformation by the burial history studies discussed in Section 2.5.4 (Sibson, 1977; Knipe 1989). Porosity would have been formed during this fracturing so that sub-surface fluids may have been able to move along these conduits. Evidence for this fluid flow would be fracture filling material which could unambiguously be shown to have been formed during the deformation. This is unfortunately not the case for the mixed smectite, montmorillonite, calcite and dolomite fill to these fractures. No deformation textures have been found within the fracture filling mixture which indicate syn-kinematic formation. Also the mixture is found within cave-collapse material which clearly post-dates the deformation. The smectite, montmorillonite, calcite and dolomite mixture in the cave-collapse material may have been re-mobilised after its syn-kinematic formation along the faults, but this has not been demonstrated by studies to date. The converse of this is also possible. The smectite and montmorillonite mixture may have formed during the development of the cave-collapse material and then been re-mobilised to be deposited within pre-existing tectonic fractures. Once again this relationship has not been clearly demonstrated to date by structural studies. The fracture-filling mixture cannot be used to demonstrate the presence of syn-kinematic fluids, and the faults were not studied further in terms of fluid migration through the Rencurel Thrust Zone. These faults characterised by the presence of breccias are found only in the small area indicated on Figure 3.19.

Section 4.3 DISCRETE GOUGE ZONES

In this Section the style of deformation along the discrete gouge zones is discussed.

Section 4.3.1 Case study of fault zone 2

Section 4.3.1.1 Outcrop observations and interpretation.

This sample site was selected because the fault zone 2 cuts across and truncates some earlier faults, and is composed of overlapping discrete fault strands, as shown in Figure 3.19. The fault zone dips at around 45° towards the east. At outcrop scale the fault appears as a discrete and planar fault break, coated in around 2-3cm of fine-grained, iron oxide-stained carbonate fault gouge. Away from the fault the wall-rocks are not heavily fractured and seem relatively undeformed. This was confirmed by examination of thin sections taken away from the fault zone. Lineations in the form of scratches or striations appear on this fault gouge. The fault is not continuous, but in the vicinity of sample site 2h (see Figure 3.19), the fault break cannot be traced far up-dip. A new fault break again dipping at around 45° can be found around 10-20cm to the east of the termination of the lower fault. This higher element of the fault zone overlaps with the lower fault break. At outcrop in the area between the two overlapping fault strands, fractures exist which are up to 2mm wide and filled with light coloured, fine grained material. Similar light coloured fractures can be found scattered along the trace of the fault zone, generally within 5-10cm of the fault break. Samples 2a, 2d, 2h and 2c located on Figure 3.19 all exhibit these fractures. These samples were sawn in half and the planar faces stained. The light coloured fractures can be seen to be filled with fine grained carbonate with clasts of grey carbonate wall-rock supported within it. The fractures form an anastomosing pattern which separate blocks of intact wall-rock. On the sawn face of sample 2h, this pattern of anastomosing fractures is cut by a planar zone of white fine grained carbonate material which is at least 1cm thick. The material is composed of angular clasts up to 5mm across supported in a fine-grained matrix. Clast sizes show a complete gradation in grain size from 5mm down to the size of the matrix. This is a cataclastic fault gouge formed by the fracturing and grain size reduction of the wall-rock during frictional slip along the fault. This gouge zone clearly post-dates the early fracturing and can be correlated with the gouge zone which exists along the main fault break. In thin section, the wall-rock lithology can be seen to change from a bioclastic grainstone at the bottom of the exposure in samples 2h, and 2d, to a coarse dolomite mosaic in samples 2a, 2c, and 2b (Figure 3.19).

Section 4.3.1.2 Sample 2d

Figure 4.4 shows a photomicrograph of sample 2d. The sample is a bioclastic grainstone which has been partially dolomitized. The dolomite rhombs have

Figure 4.3 Discrete gouge coated fault connecting two areas of breccia (See Section 4.2). See Figure 3.19 for location.

Figure 4.4 Photomicrograph of sample 2d (see Section 4.3.1.2). Field of view is 15mm.

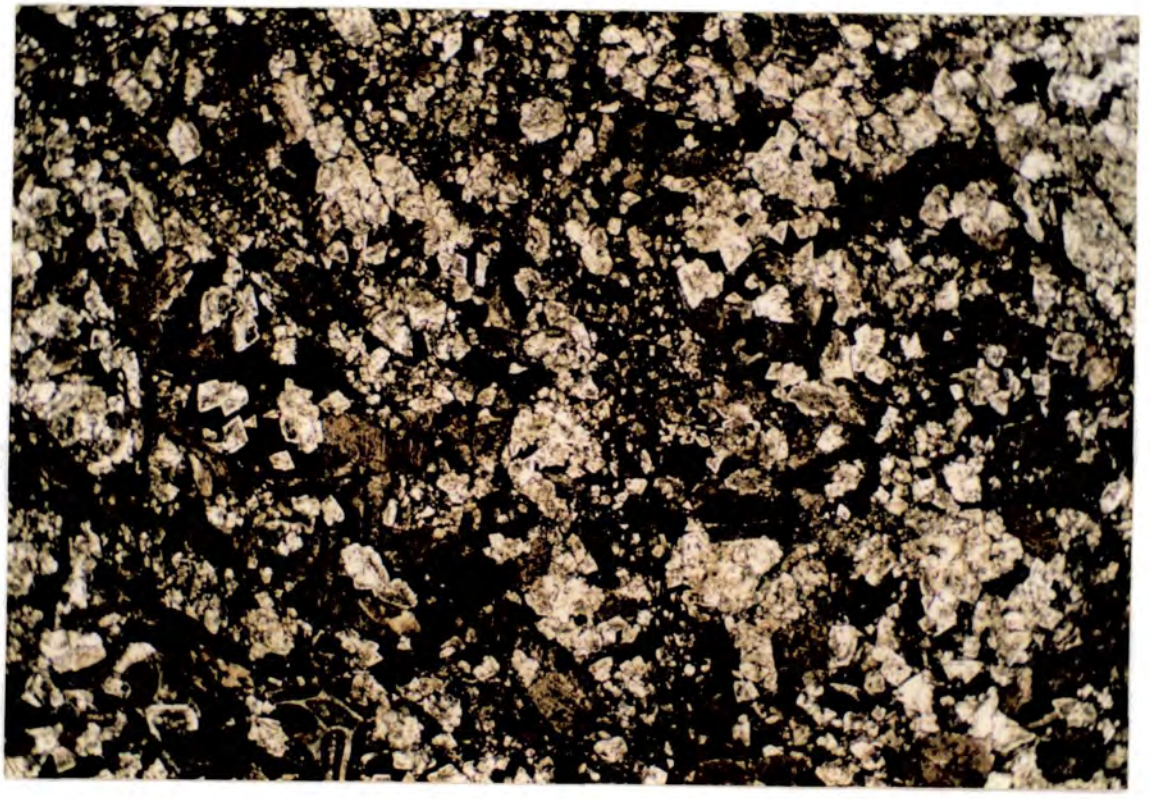

inclusion-rich centres surrounded by a syntaxial zone of clear, inclusion free dolomite. The sample is cut by a series of fracture zones. The fracturing cuts across the dolomite indicating that it is post-dolomitization. Within the fracture zones, the wall-rocks have undergone grain size reduction by fracturing to produce a fine-grained fault gouge. The visible clasts within the fault gouge are angular. The gouge is indurated but the extremely fine grain sizes within the gouge make it difficult to see textural evidence to indicate the lithification process even using a scanning electron microscope. These fracture zones can be correlated with the anastomosing fractures filled with white fine-grained material seen on the sawn faces of this specimen described above.

Section 4.3.1.3 Sample 2d- Discussion

The dominant deformation mechanism within this sample is fracturing which is a cataclastic process (Knipe, 1989). Fracturing has caused grain size reduction on the micron scale along sub-planar zones seen petrologically which can be correlated with the so-called fractures seen on the sawn face of the specimen. The so-called fractures seen in hand specimen are in fact fracture zones. These fracture zones interact to separate areas up to several centimetres across composed of intact wall-rock.
Thus, two scales of grain size reduction occur:-

1) Production of micron-scale clasts by the attrition of the wall-rocks along the thin fracture zones during frictional slip. The fine-grained fault rock is termed a fault gouge after Sibson (1977). Such gouge zones are formed during frictional slip along faults. During frictional slip, clast isolation by the breakage of asperities on the wall-rocks of the fault, and grain size reduction by clast breakage are the dominant processes (Sibson, 1986; Knipe, 1989).

2) Production of clasts on the centimetre scale by the interaction of fracture zones or gouge zones. When the density of fracture zones becomes great enough, areas of intact wall-rock become completely surrounded by fracture zones or gouge zones.

The fault rocks produced by this fracturing are now indurated and lithified. The fine-grained fault gouge is hard and does not crumble out of the fractures. The gouge may be cemented up by the precipitation of new minerals or compacted by pressure dissolution and locked together by the indentation of grains. The small grain sizes make it difficult to decide which of these two processes is dominant. Both of these processes are however characteristic of the action of diffusive mass transfer (DMT).

It is not clear if any strain was accommodated by grain boundary sliding without

fracture before induration of the fine-grained gouge occurred. This friction controlled deformation mechanism is termed independent particulate flow (Borradaille, 1981). The action of this deformation mechanism results in the re-packing of grains without reducing their grain sizes and is therefore difficult to recognise. The action of independent particulate flow is discussed more fully in Section 4.5.1.

Section 4.3.1.4 Sample 2a

Figure 4.5 shows a photomicrograph of sample 2a. The sample has been intensely deformed by fracturing to produce a fault gouge. The dolomite mosaic which made up the original wall-rock lithology can now only be seen within clasts within the fault gouge which are surrounded by poorly-sorted and fine-grained matrix. The clasts of original wall-rock contain fractures which are similar to those described from sample 2d in Section 4.3.1.2. Grain size reduction down to the micron scale and the production of a zone of sub-planar fault gouge has occurred in the wall-rocks prior to the formation of these clasts. These fractures divide up the wall-rock into a similar pattern as seen in sample 2d described in Section 4.3.1.2. The production of wall-rock clasts which are incorporated within the gouge textures of this sample clearly occurred after the intra-wall-rock clast fractures were formed. Some clasts within this sample are clearly composed of early lithified fine-grained fault gouge. The whole texture is cut across by extensional fractures filled with calcite which exhibits unit extinction and sub-planar crystal boundaries.

Section 4.3.1.5 Sample 2a- Discussion

Cross-cutting relationships within this fault rock suggest the deformation history illustrated in Figure 4.6. Stages 1 and 2 involved the division of the wall-rocks by gouge zones. Formation of at least 5mm of fine-grained fault gouge may have occurred contemporaneously as no clear cross-cutting relationship exists between them. Stage 3 clearly post-dates the induration and lithification of the textures produced in stages 1 and 2. Lithification must have occurred in order for the fine-grained gouges produced in stages 1 and 2 to obtain enough elastic strength so that brittle failure could occur and produce clasts which include their textures. The combined stages 1 and 2 are however likely to have had a more complicated history than discussed so far. The extreme grain size reduction which has taken place to produce their textures has destroyed any microstructural evidence for any earlier deformation. This may also be true of stage 3. Again the microstructural evidence has been destroyed by grain size reduction. The microstructures produced in stage 4, namely gouges and calcite-filled extensional fractures, again involved brittle failure processes. This suggests that the lithification processes which were active towards the

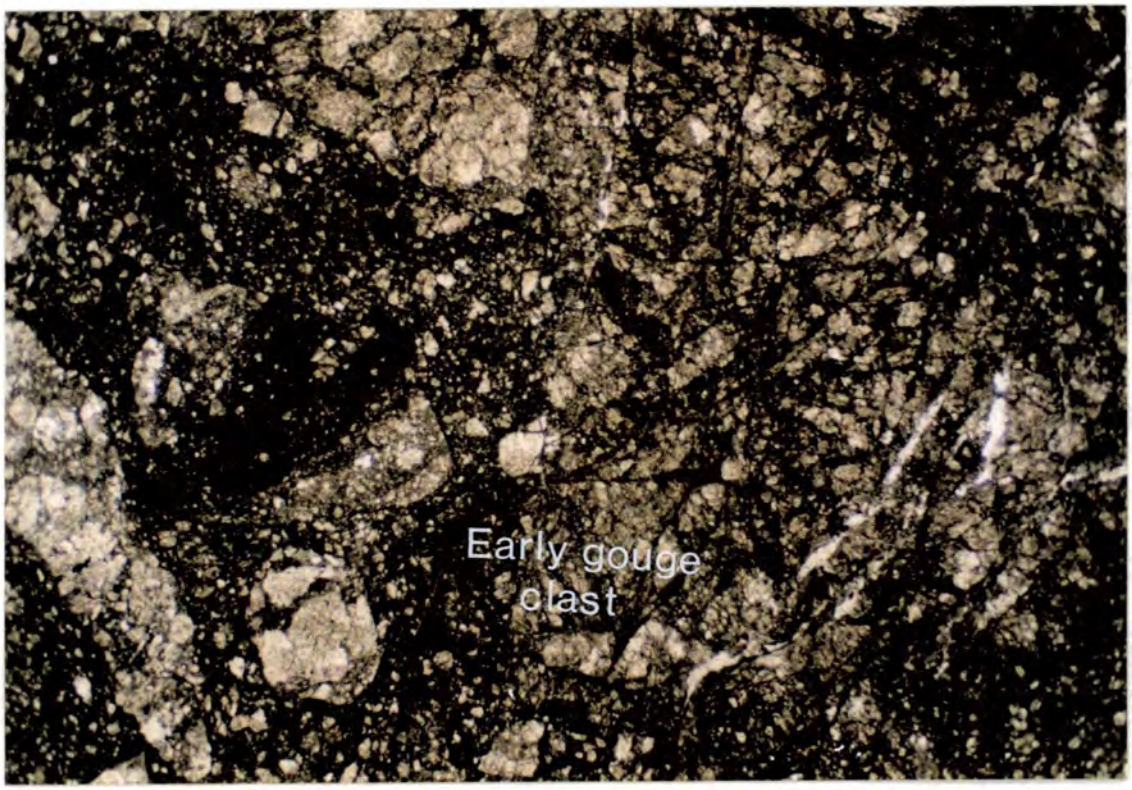

Figure 4.5 Photomicrograph of sample 2a (see Section 4.3.1.4). Field of view is 15mm.

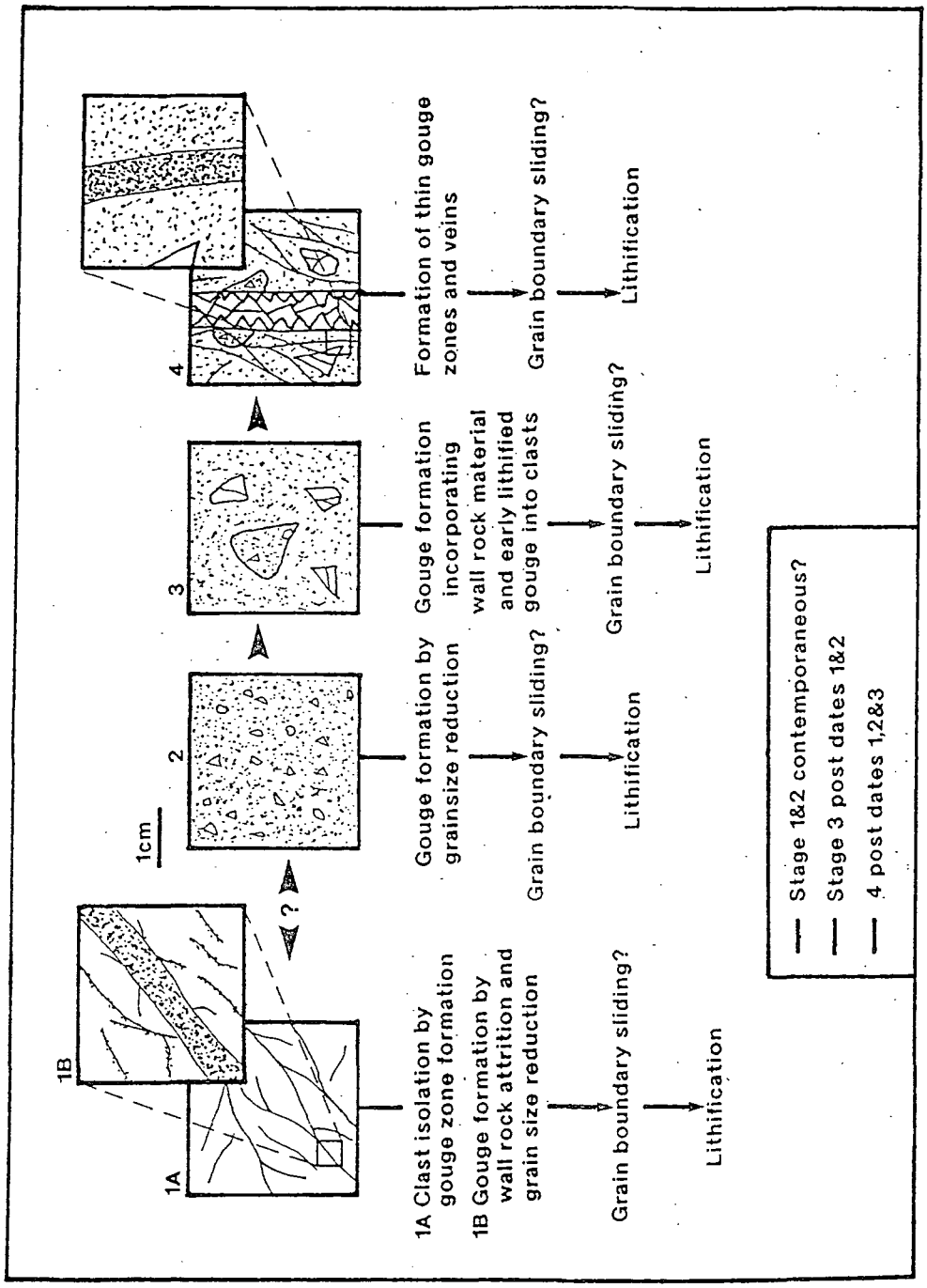

Figure 4.6 Deformation history displayed by sample 2a.

end of stage 3 had terminated before the cataclastic deformation in stage 4 began. The microstructures of stage 4 are now lithified and this lithification probably occurred at the same time as cement was being precipitated in extensional fractures. Again as in sample 2d (Section 4.3.1.3), the role of independent particulate flow as a deformation mechanism is not clear.

Section 4.3.2 Case study of fault zone 3

Section 4.3.2.1 Field observations and discussion.

This sample site was chosen because the fault zone is truncated by fault zone 2 as shown in Figure 3.19. It was hoped that a combined study involving both faults could be made using the cross-cutting relationships between them to give a time relationship. Figure 3.19 shows that the fault is composed of a single fault strand which at outcrop is seen to be coated in fine-grained fault gouge. Striations occur within the fault gouge indicating that fault displacements occurred along the line ESE-WNW. The wall-rocks to the fault zone are not fractured and seem relatively undeformed. This observation is confirmed by the examination of thin sections from the wall-rocks.

Section 4.3.2.2 Sample 3l

Figure 4.7 shows the microstructure of sample 3l. The sample is a bioclastic grainstone. The rhombs have inclusion-rich centres which are overgrown by syntaxial, inclusion-free, clear dolomite. The section is cut by a large fracture which is around 4mm wide and at least 3cm long. The fracture is filled with crudely stratified fine-grained material which under high power can be seen to be composed of angular clasts of dolomite and calcite. The fine-grained material is distinctly bimodal in its grainsize distribution, with over 90% of the material being extremely fine-grained, the remaining material composed of angular clasts up to 2mm long and 0.5mm wide. These clasts are composed of fragments of the wall-rock with both dolomite rhombs, allochems and calcite cement visible and also early lithified fine-grained material. The fracture margins are sharp and not gradational as are the margins of the fragments of wall-rock supported in the fine-grained material. The fracture margin is also irregular in morphology. The inside of the fracture is locally coated in a calcite cement. Stratification within the fine-grained material occurs through changes in the sorting of the material. The thin section is orientated and both the long axis of the fracture and the stratification of the fine-grained material occur within the horizontal plane. Also note the presence of a fracture which branches upwards from the main fracture. This shows a possible geopetal structure with the top of the

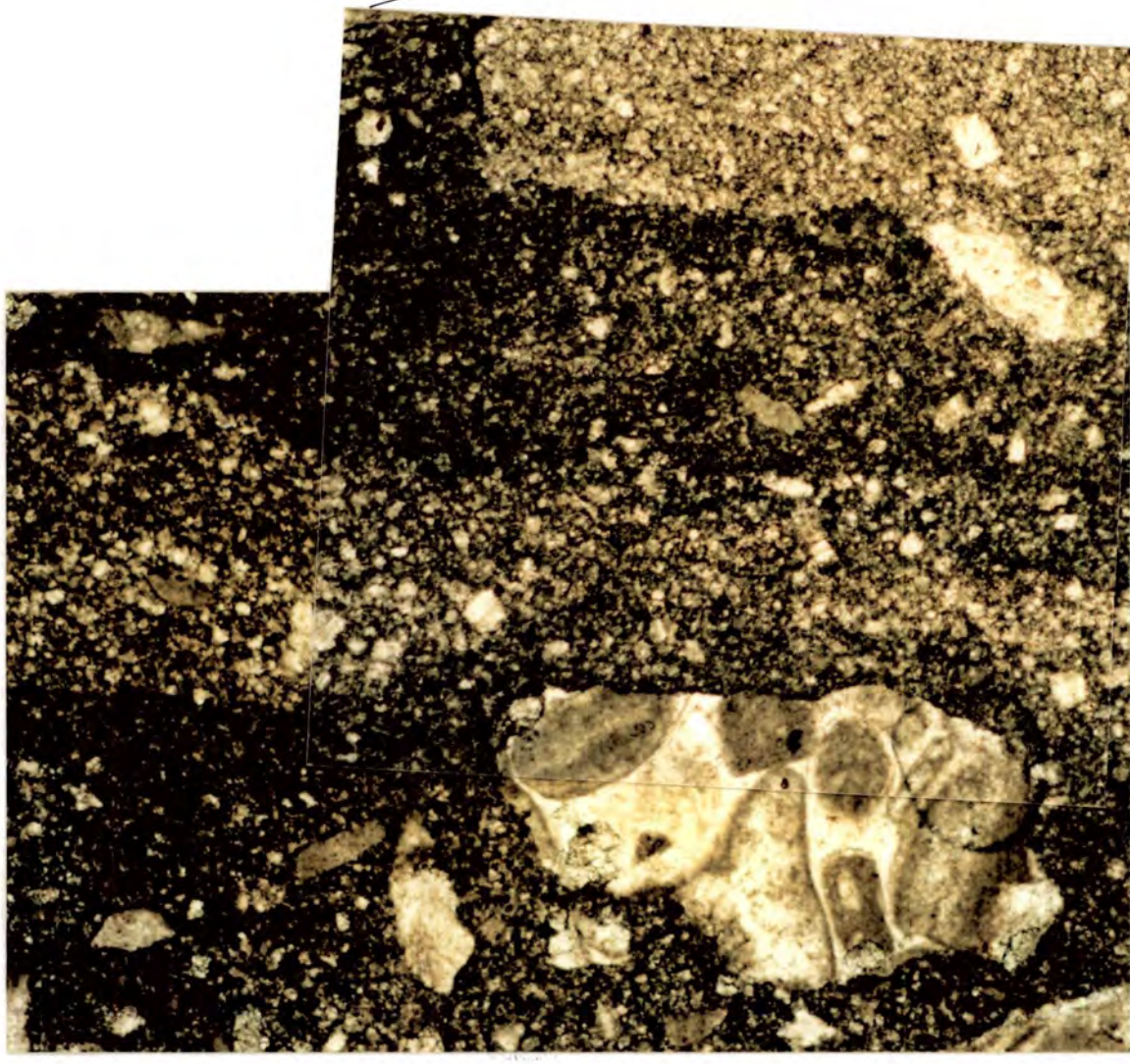

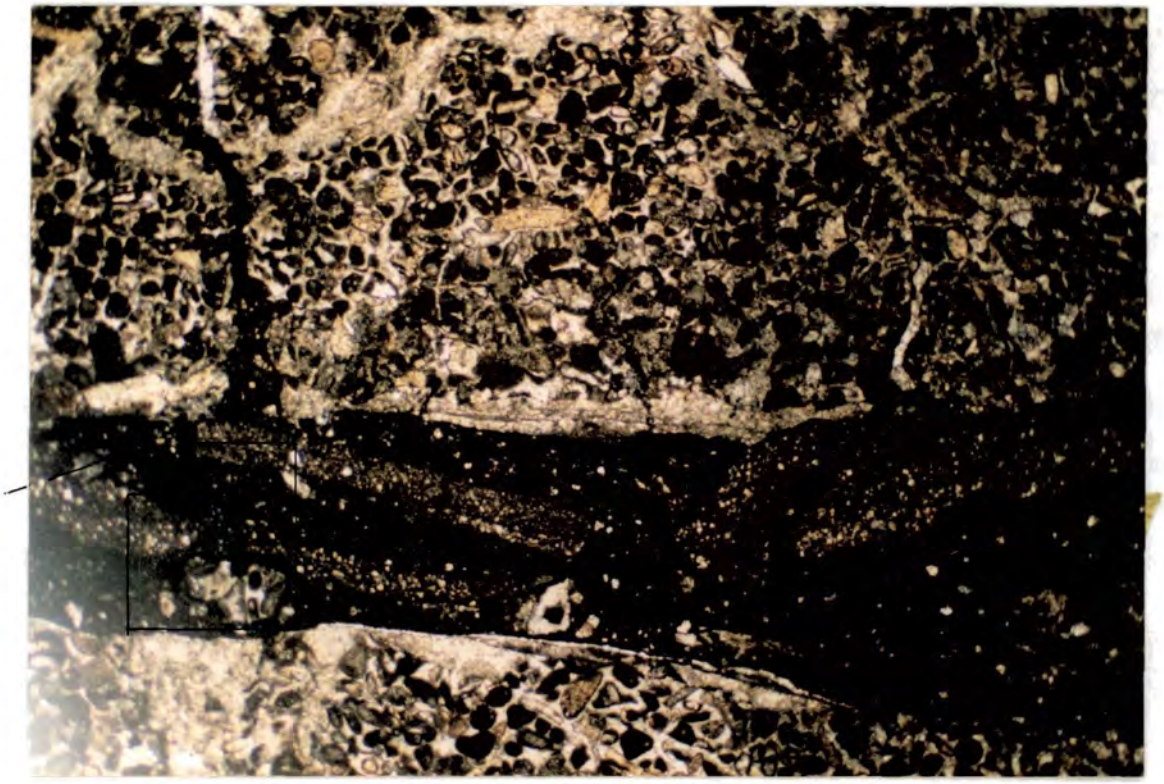

Figure 4.7 Photomicrograph of sample 31 (see Section 4.3.2.2). Field of view is 15mm.

former fracture porosity filled with calcite spar and the bottom with fine-grained material.

Section 4.3.2.3 Sample 3l- Discussion

The existence of calcite cement lining the insides of the fracture indicates that the fracture was filled with fluid during cement precipitation and was therefore a dilatant extensional fracture. The interpretation of this fracture as extensional is supported by the sharp and irregular nature of the fracture margin, and that the two sides of similar fractures interlock and can be fitted together. Shear fractures where gouge production occurs by grain size reduction during frictional slip generally have gradational and sub-planar margins. This occurs because the fracture margins are constantly degraded by cataclastic fracturing. The fine-grained fill to the fracture is also problematic. The angular clast shapes are reminiscent of those produced during cataclastic gouge production. Yet the material is well-sorted on a millimetre scale and stratification exists between areas of different sorting. This is not characteristic of the random textures and poor sorting of gouges produced by frictional slip in shear fractures. Also the large clasts have sharp margins and high aspect ratios. No intermediate clasts sizes exist. Poorly sorted gouges formed by frictional slip have a complete range of grain sizes which results from the attrition of large clasts to form small clasts during grain size reduction. Clasts are not characteristically elongate as they would be easily broken by fracturing during frictional slip. Also clasts within gouges formed by frictional slip often show gradational deformed edges due to the fracturing and plucking of material from the clast margin during deformation. It is suggested here that the fracture fill is not a cataclastic fault gouge produced by grainsize reduction during frictional slip. The presence of calcite cement indicates that fracture porosity and fluids existed within the fracture. It is suggested here that this fracture was an extensional fracture throughout its history and that the fine-grained material is re-worked gouge washed in by fluids migrating through the fracture. The change in grain size sorting between the different layers within the fine-grained material could reflect changes in the velocity of fluid migration through the fracture. The large wall-rock clasts were probably derived from degradation of the wall-rock to the fracture during fluid migration. The early-lithified, fine-grained material forming the clasts indicate that the material has been indurated and then re-worked. The horizontal attitude of both the stratification within the material and the fracture long axis supports this "sedimentary" origin for the fracture filling material. The gouge material may have been sourced from a nearby shear fracture whose cataclastic gouge fill had not been lithified at this time.

Deformation within this fault zone was accompanied by fluid migration. The fluid

migration velocity appears to have been great enough to cause the re-working, transportation and re-deposition of fine-grained gouge material. Fluid velocities may have fluctuated as suggested by the changes in grain size distribution of the fine grained material between different layers. Also early fluid migration resulted in calcite cement precipitation which indicates that large volumes of pore water migrated through the fracture.

Section 4.3.2.4 Sample 3D

Figure 4.8 shows the microstructures of sample 3D. The sample comes from the immediate hanging-wall to the fault and includes the fault break. The sample is a bioclastic grainstone overprinted by dolomite rhombs. At the bottom of the sample, grain size reduction by fracturing has produced a sub-planar zone of fault gouge. This gouge zone can be correlated with the gouge zone which exists at outcrop along the fault break. Here the total thickness of gouge preserved is only around 2-3mm. This gouge zone grades into a zone of fractures filled with fine-grained material. At the top of the Figure, a fracture is filled with a combination of fine grained material and larger wall-rock clasts. The fracture fill is bimodal. The fracture margins and margins of the large clasts are sharp and not gradational.

Section 4.3.2.5 Sample 3D- Discussion

This sample shows a combination of fracture types.The fault break is coated in fine-grained fault gouge where grain size reduction by fracturing has been an important deformation process. This gouge grades into an area of fractures filled with fine-grained material. The gouge is now lithified. At least some of the fractures in the hanging-wall to this gouge zone may be filled with washed in material and material derived from degradation of the fracture margin wall-rocks. As such they can be interpreted as extensional fractures. Fluid migration at significant velocities may have accompanied deformation. The other fractures may be small shear fractures which are filled with gouge derived from grain size reduction of the wall rocks to the fracture, or they all may be extensional fractures filled with fluid driven slurries of re-worked gouge material. Sample 31 and the individual samples from fault zone 2 showed only extensional or shear fracturing. This sample indicates that shear fracturing and extensional fracturing can occur along the same fault.

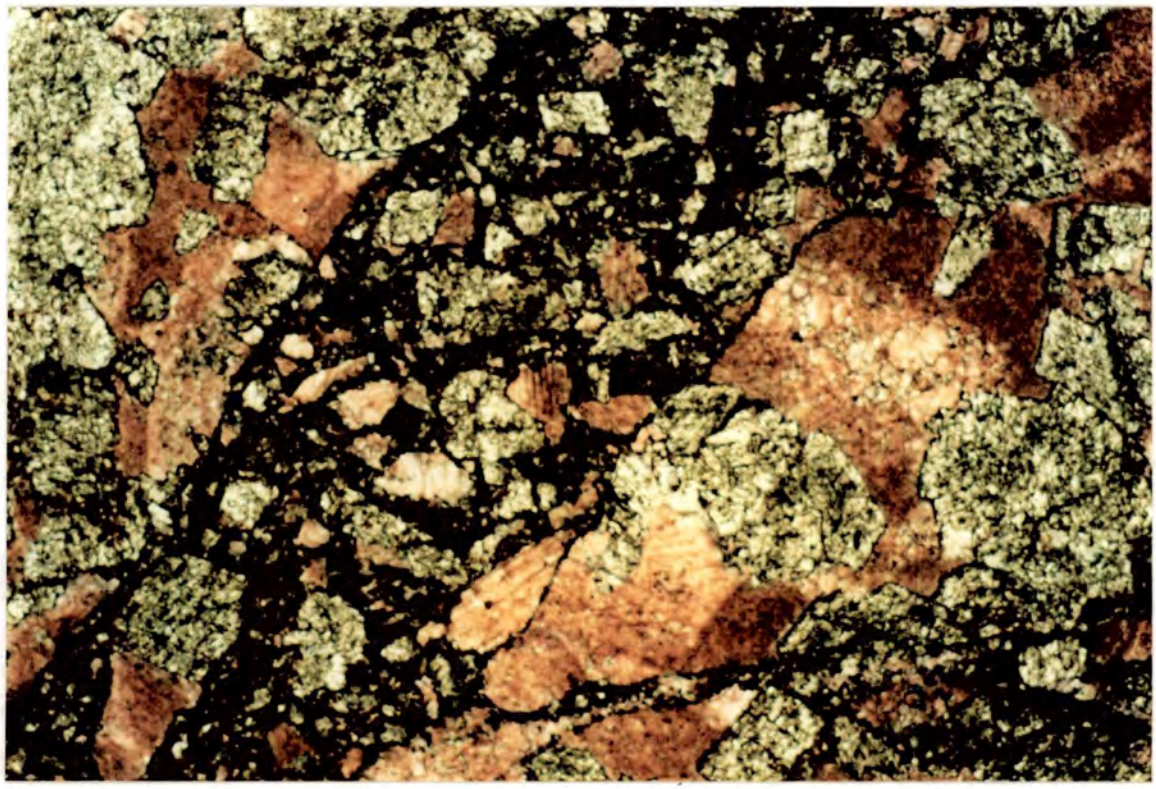

11A

Field of view is 15mm.

Figure 4.8 Photomicrograph of sample 3D (see Section 4.3.2.4).

Section 4.3.3 Fault zone 8

Section 4.3.3.1 Field observations and discussion

The position of fault zone 8 is indicated on Figure 3.19. The faults are discrete breaks which at outcrop can be seen to be coated in fine-grained fault gouge. The wall-rocks to the fault zone are relatively undeformed by fracturing. The fault zone differs from the other fault zones described so far in that the fault dips towards the west. This fault zone and the other westerly dipping faults marked on Figure 3.19 could be interpreted as backthrusts showing top to the east movement directions, or as extensional faults with top to the west movement directions. Kinematic indicators on these faults are not common. However, all of the three which were found showed top to the west movement directions so that these faults may be interpreted as extensional faults. Kinematic indicators included inclined pressure dissolution seams and calcite filled pull-aparts within the gouges. These kinematic indicators are discussed more fully in the following Sections. Minor extensional faults have been described from other foreland thrust zones (Wojtal & Mitra, 1986; Woodward et al. 1988). They are thought to form during thrust sheet translation in response to changes in the bulk rheology of the fault zone, working to thin the thrust zone (Wojtal & Mitra, 1986). They contribute to the deformation which occurs within thrust zones during bulk shortening and therefore must be included in studies of deformation and fluid flow histories through thrust zones.

Section 4.3.3.2 Sample 8a

Figure 4.9 shows the microstructures of sample 8a. The sample comes from the immediate hanging-wall to the fault and it includes the actual fault break. The microstructures consist of a gradation between deformed but recognisable wall-rock and fine-grained fault gouge. The dolomitic wall-rocks at the top of the specimen are cut by fractures filled with fine-grained fault gouge. These shear fractures surround blocks of intact wall-rock. As the gouge zone at the bottom of the specimen is approached, the areas of wall-rock between the shear fractures can be seen to become separated to form clasts in the basal gouge zone supported within fine-grained fault gouge. Two scales of clast formation can be seen to exist. Firstly, clasts up to 1cm across are formed by the interaction of thin shear fracture within the wall-rocks. Secondly, clasts less than 1mm across are formed within the shear fractures isolating the larger clasts and within the basal gouge zone by grain size reduction of the wall-rocks and pre-existing clasts during frictional slip. Lithification can be seen to have occurred between fracture events indicated by the presence of early gouges within wall-rock clasts now within the basal gouge zone. Red-stained, iron oxide-rich

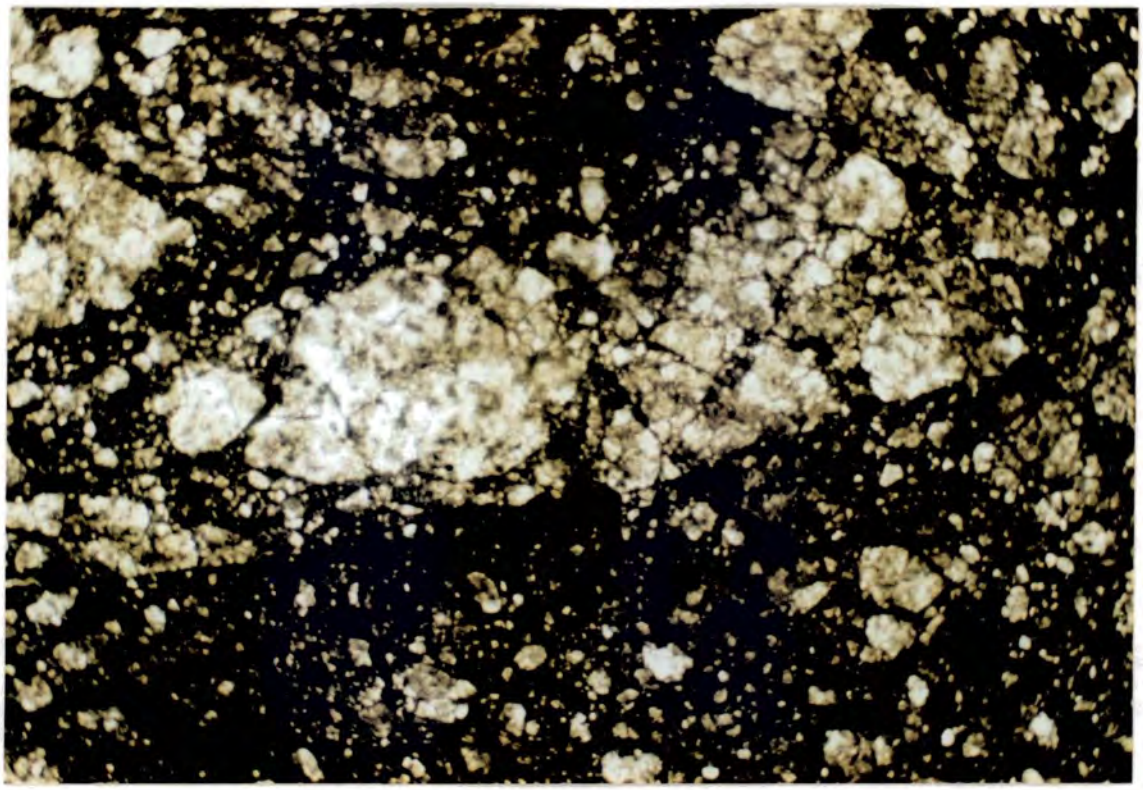

Figure 4.9 Photomicrograph of sample 8a (see Section 4.3.3.2). Field of view is 15mm.

pressure dissolution seams exist within the basal gouge zone. These indicate the action of DMT and the removal of material from along these seams. The thin section is orientated and the pressure dissolution seams dip towards the east.

Section 4.3.3.3 Sample 8a- Discussion

The easterly dipping pressure dissolution seams can be used as kinematic indicators. Pressure dissolution seams are thought to form orthogonal to the shortening direction in theoretical strain ellipsoids. As such they are inclined in shear zones such that their deflection is in accordance with the shear sense across the shear zone. The top of the pressure dissolution seams within this sample are deflected to the west so that the shear sense on these faults must be top to the west. This fault is an extensional fault zone during the action DMT.

The whole texture is remarkably similar to that of sample 2a described in Section 4.3.1.4. Sample 8a is thought to have undergone a similar style of deformation to that which occurred along fault zone 2. The discussion in Section 4.3.1.5 also applies to this fault zone so that the textures of sample 8a are not discussed further here.

Section 4.3.3.4 Sample 8c

Figure 4.10 shows the microstructure of sample 8c which was taken from the immediate hanging-wall to the fault zone. This sample shows extreme grainsize reduction within a gouge zone which is at least 5cm thick.

Pressure dissolution seams consisting of accumulations of red iron oxide can be seen dipping towards the east.

Section 4.3.3.5 Sample 8c- Discussion

The orientation of pressure dissolution seams in this sample indicates a shear sense of top to the west as discussed in Section 4.3.3.3. This backs up the interpretation of this fault zone as extensional in nature.

Section 4.3.3.6 Sample 8i

Figure 4.11 shows the microstructure of sample 8i which was taken from just into the hanging-wall to the fault break. The sample shows a transition between undeformed wall-rocks cut by a few gouge-coated shear fractures into the 5mm thick gouge zone which occurs along the fault break. In the hanging-wall to the 5mm thick gouge zone, the small gouge coated shear fractures form a "criss-crossing" pattern which separates

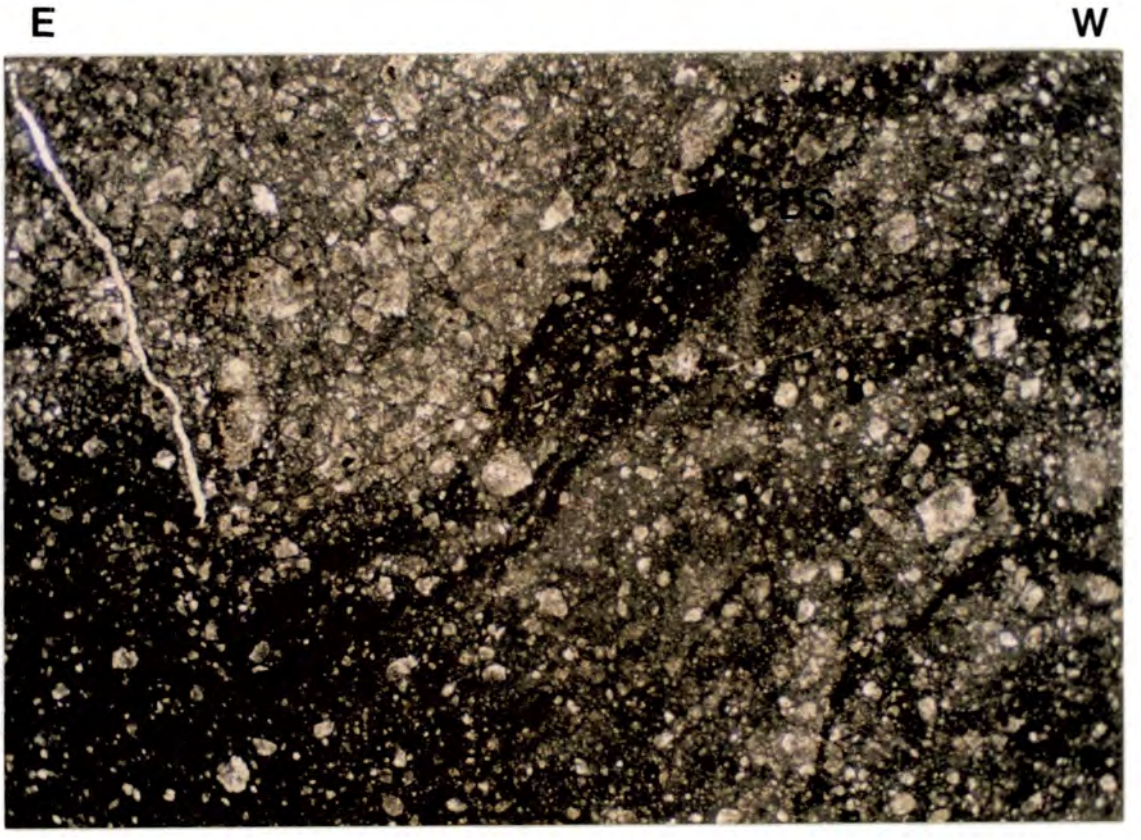

Figure 4.10 Photomicrograph of sample 8c (see Section 4.3.3.4). Field of view is 15mm.

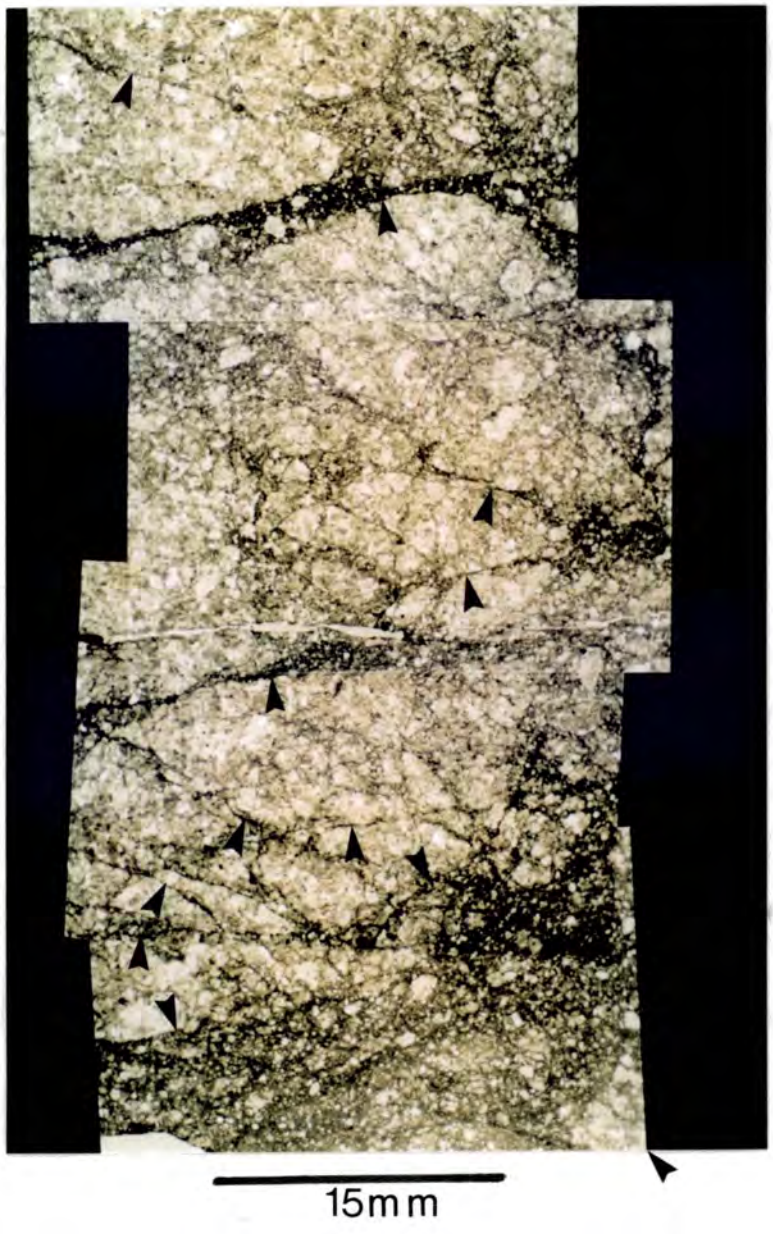

Figure 4.11 Photomicrograph of sample 8i (see Section 4.3.3.6). Field of view is 15mm.
The main gouge zones are arrowed.

blocks of intact wall-rock. Some shear fractures coated in up to 1mm thickness of fault gouge run parallel to the main basal gouge zone.

Section 4.3.3.7 Sample 8i- Discussion

This sample illustrates that the faults marked on Figure 3.19 are accompanied by a series of smaller faults which have not accumulated such a great thickness of gouge and are therefore difficult to spot at outcrop. This reinforces the idea suggested in Section 3.5.3, that Figure 3.19 shows only a minimum fault density. As discussed in Section 4.3.1.3, the role of independent particulate flow as a deformation mechanism is not clear.

Section 4.3.3.8 Sample 8h

Figure 4.12 shows the microstructure of sample 8h which is taken from the immediate hanging-wall of the fault. The sample is composed of a coarse dolomite mosaic which is cut by a series of gouge coated shear fractures. This texture is cut by a gouge zone which is at least 1cm wide, which can be correlated with the fault gouge coating the fault surface at outcrop. The fault zone is fine-grained and poorly-sorted, and contains a few clasts of intact wall-rock up to 8mm long and 3mm wide. The fault gouge is cut by a series of extensional fractures which are filled with crystalline calcite. The calcite is non-luminescent, displays unit extinction and is generally euhedral in crystal form. The calcite filled extensional fractures are arranged in a left-stepping en echelon arrangement.

Section 4.3.3.9 Sample 8h- Discussion

The texture described above is generally the same as the textures discussed in Sections 4.3.3.1-4.3.3.7. However in this sample, late extensional fracturing has occurred within the gouge zone. The left-stepping arrangement of the en echelon fractures suggests a shear sense of top to the west indicating that this is an extensional fault zone. The euhedral nature of the calcite fill suggests that the fractures may have been fluid filled cavities during the deformation. The fluids must have been migrating through this fracture porosity in order to have precipitated this cement.

Section 4.3.3.10 Sample 8e

Figure 4.13 shows the microstructure of sample 8e which is taken from 10-20cm away from the nearest gouge zone visible at outcrop. The sample shows no microstructural evidence for the existence of a zone of fault gouge. The sample is

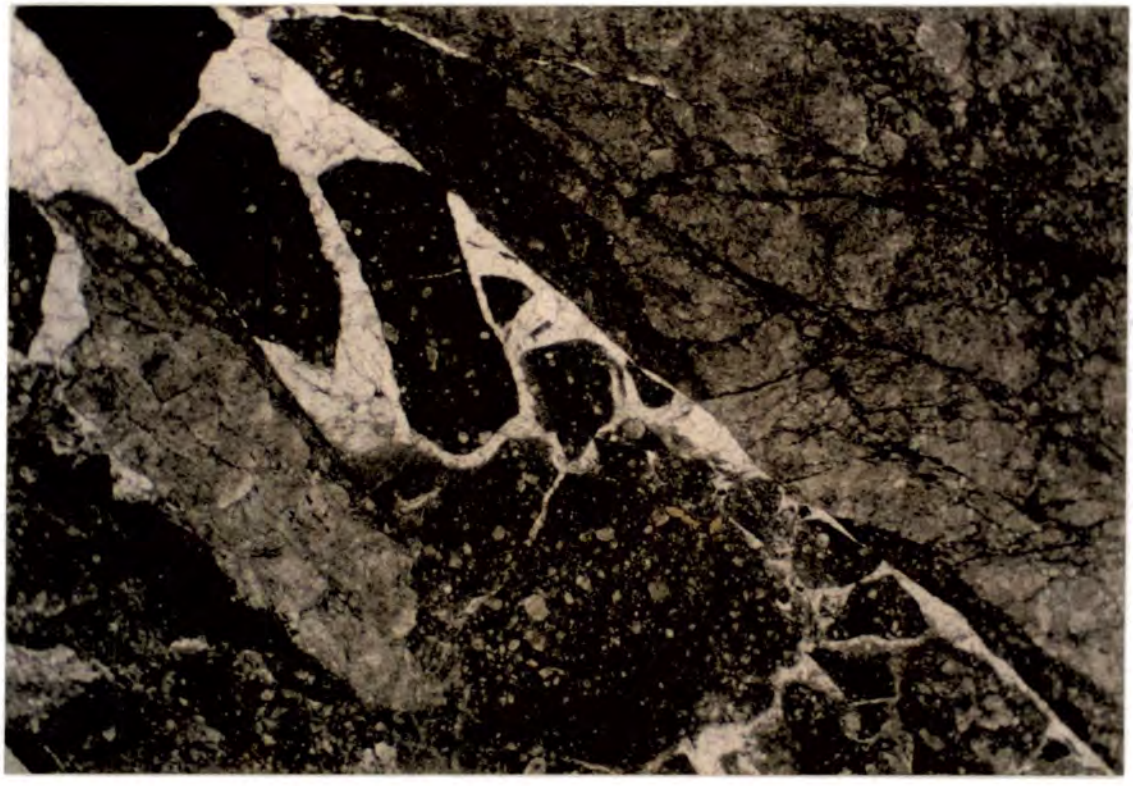

Figure 4.12 Photomicrograph of sample 8h (see Section 4.3.3.8). Field of view is 15mm.

Figure 4.13 Photomicrograph of sample 8e (see Section 4.3.3.10). Field of view is 15mm.

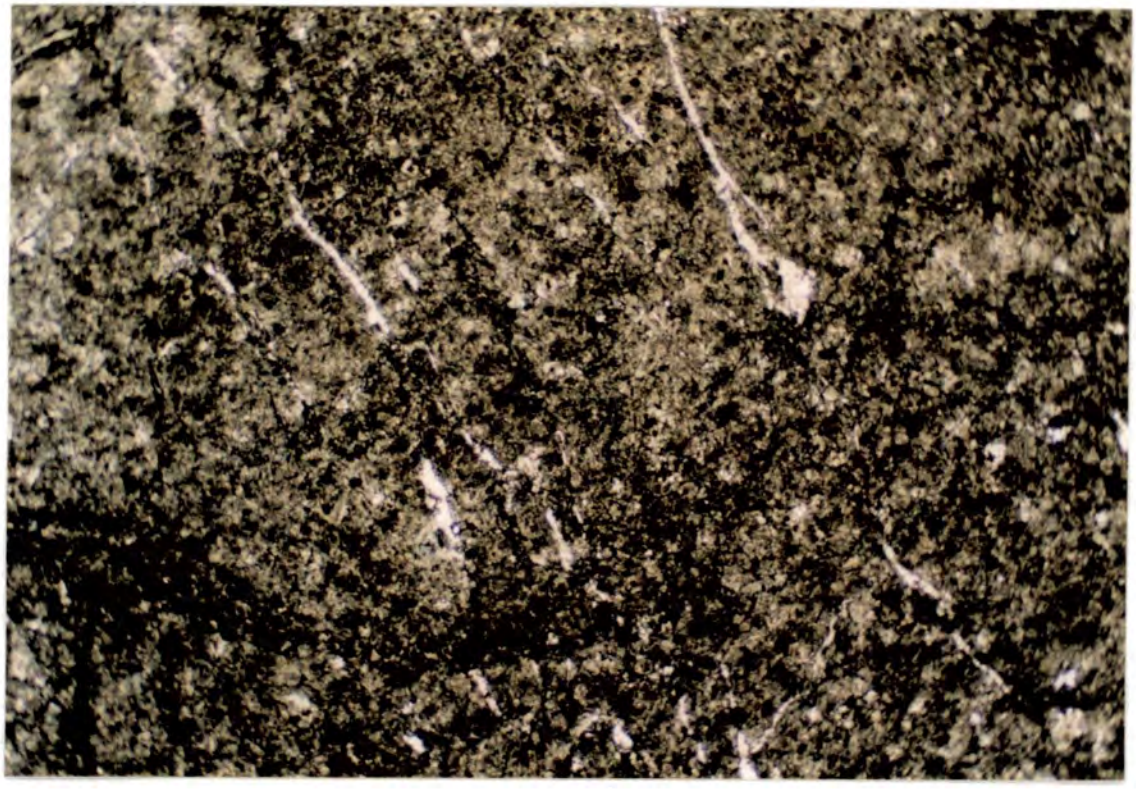

composed of a coarse iron oxide-rich dolomite mosaic which is cut by a series of extensional fractures filled with calcite cement. The calcite filling the fractures exhibits unit extinction and euhedral crystal shapes.

Section 4.3.3.11 Sample 8e- Discussion

Sample 8e displays well the deformation within the wall-rocks to the faults marked on Figure 3.19. The sample shows that the wall-rocks to a fault zone can be become deformed by extensional fractures. Cement precipitated from the pore waters which were migrating within these fractures, eventually occluding the fracture porosity.

Section 4.3.4 Fault zone 9

Section 4.3.4.1 Introduction

In this Section fault zone 9 will be described. The position of this fault zone is located on Figure 3.19. The fault zone is a discrete break which at outcrop is seen to be coated in up to 5cm of fault gouge as shown in Figure 4.14. The wall-rocks are not heavily fractured and seem relatively undeformed. Striations exist on the fault plane indicating displacements along the line ESE-WNW.

Section 4.3.4.2 Sample 9f

Figure 4.15 shows the microstructure of sample 9f which comes from the immediate hanging-wall to the fault and includes the gouge zone along the fault break. The sample is composed of a coarse dolomite mosaic which is cut by a series of gouge coated shear fractures. The bottom of the sample consists of a lithified fine-grained gouge zone which is at least 3cm thick. Higher in the sample the dolomite contains areas of calcite which are filling intercrystalline pore spaces (Figure 4.16). Filling the bottoms of the original intercrystalline pore spaces, are accumulations of fine-grained calcite crystals which have a rhombic shape. In some cases the size of the rhombs within the accumulation increases upwards. Coarse-grained idiotopic calcite infills the pore spaces between the rhombs and also fills the higher parts of the original intercrystalline pore spaces. All of the calcite is non-luminescent. The calcite is not cut by the gouge-coated shear fractures.

Section 4.3.4.3 Sample 9f- Discussion

This sample shows the same style of deformation as the other samples described in this Chapter. The grain size reduction due to fracturing which has occurred makes it

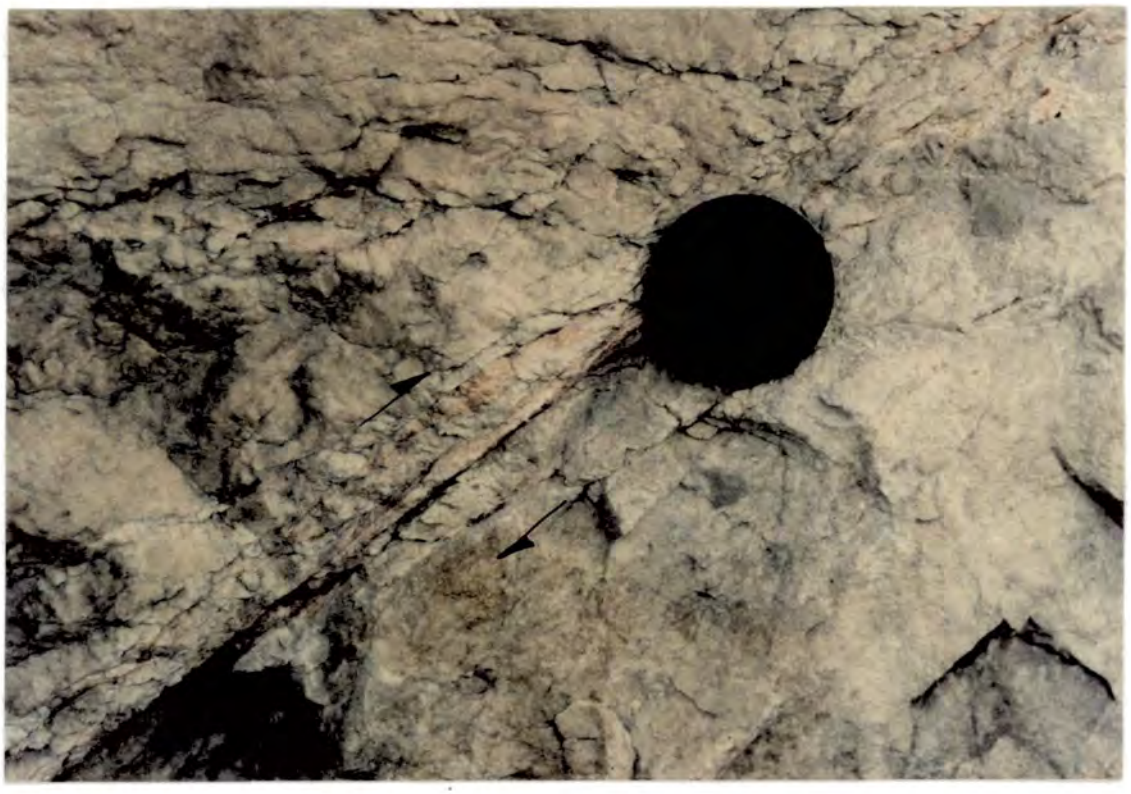

Figure 4.14 Field photo of fault zone 9. The fault is coated in cataclastic fault gouge which is red-stained due to the concentration of iron oxide along pressure dissolution seams. Lens cap is 50mm across (See Section 4.3.4.1). See Figure 3.19 for location.

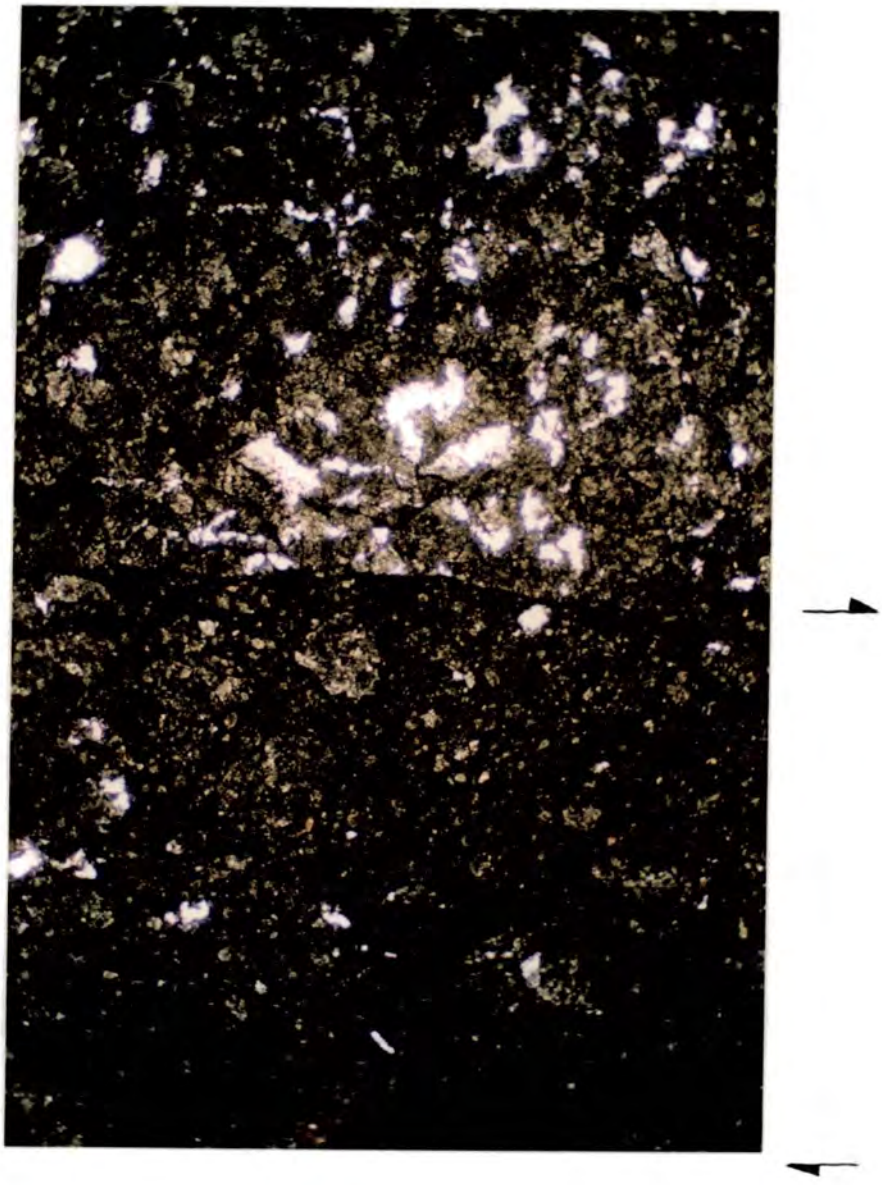

Figure 4.15 Photomicrograph of sample 9f (see Section 4.3.4.2). Field of view is 15mm.

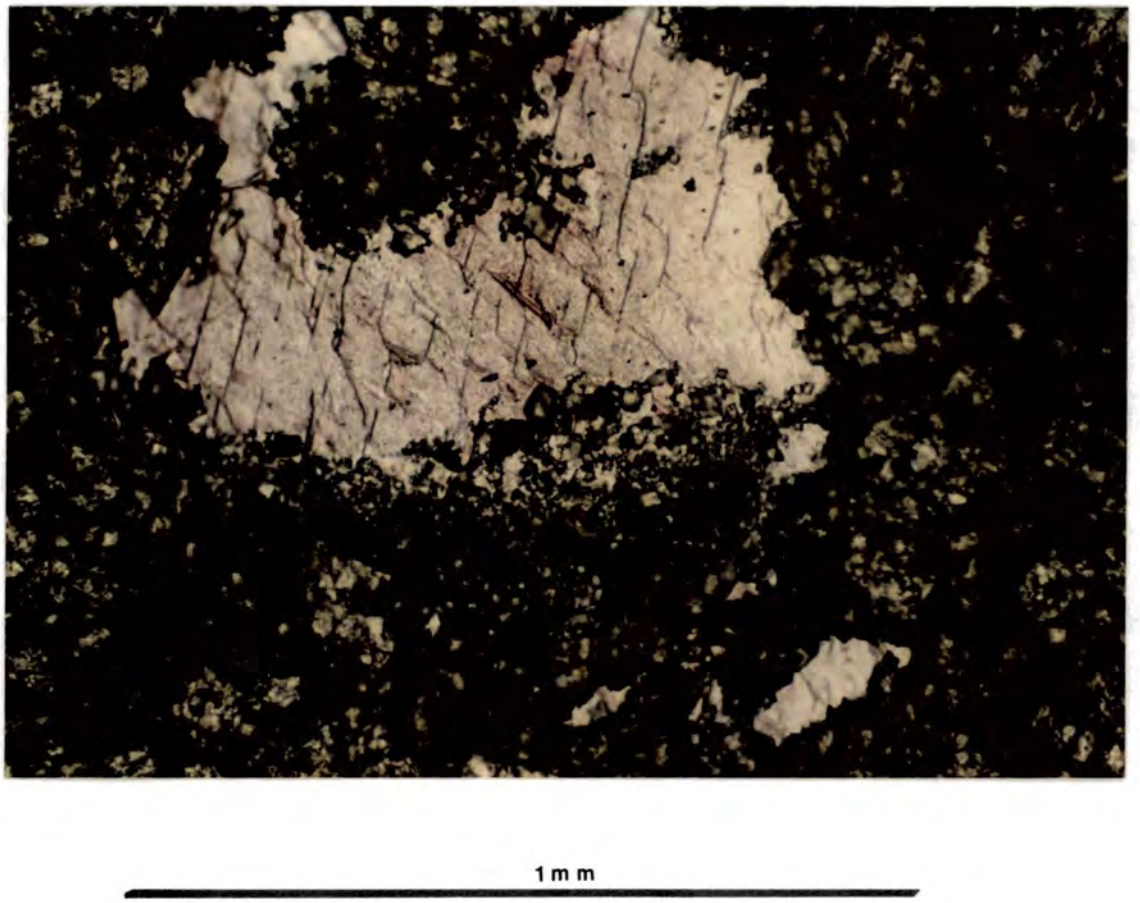

Figure 4.16 Photomicrograph of sample 9f (see Section 4.3.4.2).

difficult to demonstrate the time relationship between deformation and the precipitation of pore-filling calcite using textural criteria. In Section 6.3.3.3, stable isotopic methods are used to demonstrate that the calcite was probably precipitated during the deformation.

The structure of the calcite fill to the pore spaces can be used as geopetal structures. The section is orientated and the accumulations of fine calcite crystal occur at the bottom of the pore spaces. These accumulations may be analogous to crystal silts which form in the vadose zone. Crystal silts are accumulations of rhombic calcite crystals formed in the upper part of the vadose zone which can be transported in suspension and deposited in pore spaces, often exhibiting grading or even cross-lamination (Tucker and Wright, 1990). The geopetal structures described in Section 4.3.4.2 from sample 9f may have formed in the following way. Early relatively high flow rates may have been able to transport rhombic calcite crystals which were chemically precipitated in suspension. Flow rates may have dropped allowing the crystals to settle to the bottom of the cavities. Continued flow at lower flow rates will have allowed the precipitation of the idiotopic calcite cements within the pore spaces. In Section 6.3.3.4, ^{13}C and ^{18}O stable isotopic evidence will be presented which suggests that these cements are not however the product of vadose cementation as is the case of most crystal silts, but of cementation within the burial realm during faulting.

Section 4.4 SUMMARY OF THE MICROSTRUCTURES WITHIN THE DEFORMED URGONIAN LIMESTONES: IMPLICATIONS FOR FLUID FLOW

All the areas of deformation within the Urgonian share the same microstructures which indicate the importance of cataclasis and DMT as the dominant deformation mechanisms. This Section will summarise the microstructures characteristic of cataclasis and DMT and discuss their effect on fluid flow.

Section 4.4.1. Microstructures produced by cataclasis.

Cataclastic deformation is indicated by four main styles of microstructure:-

1) Thin zones of fine-grained fault gouge. - These zones are less than 2mm wide and have maximum grain sizes of less than 1mm. The gouges also contain a complete gradation of grain sizes down from this. The gouges are produced by grain size reduction of the wall-rocks during frictional slip along these thin gouge zones.

2) Wall-rock Breccias - These breccias occur in zones of varying shape and size. Maximum grain sizes of the breccias are around 1cm across so that the dimensions of the breccia zones are greater than 1cm. The maximum size of the breccia zones is hard to determine because as they occur associated with planar fault zones which are closely spaced, neighbouring breccia zones overlap with each other. This deformation style is developed almost ubiquitously in the wall-rocks within areas of high fault density. The breccias are formed when the shear fractures of (1) interact to isolate blocks of intact wall-rocks. More intense cataclastic deformation of these breccias occurs close to the minor faults marked on Figure 3.19. The result is the disaggregation and grain size reduction of the breccias and the production of sub-planar zones up to 10cm wide composed of poorly-sorted gouge which coat the faults marked on Figure 3.19. These gouges contain clasts of intact wall-rock up to 1cm in diameter. A complete range of grain sizes down from this occurs. The gouges are formed by disaggregation and grain size reduction of the wall-rocks to the fault zone during frictional fault slip. The wall-rocks already contain the smaller gouge-coated shear fractures summarised in (1).

These breccias are not to be confused with the breccias described in Section 4.2, whose clasts are isolated by extensional fractures filled with smectite and montmorillonite.

3) Single Extensional Fractures - This category refers to single isolated fractures which cut intact wall-rock or indurated fault rock. These fractures are dilational and formerly contained porosity which may now be filled with crystalline vein fill or wall rock debris. These fractures occur on a variety of scales. It must be stressed that the production of the features described in categories (1) and (2) involves the formation of extensional fractures but not as isolated fractures spatially separated from other fractures. Single extensional fractures may become veins if they are filled with crystalline material precipitated out of solution.

4) Re-packed grains - Re-packing of grains occurs during the action of independent particulate flow. Grain re-packing is, however, difficult to recognise.

The microstructural styles which indicate the action of cataclasis along the faults described in this chapter are summarised in Figure 4.17. The processes which produce these microstructures operate on a variety of scales. Using high-power objectives it can be seen that type (1) gouge zones are formed by the same processes outlined in the discussion of type (2) microstructures but on a smaller scale. The division of microstructures proposed here is designed to aid the interpretation of textures. It is not proposed here that type (1) and type (2) gouges represent fundamentally different

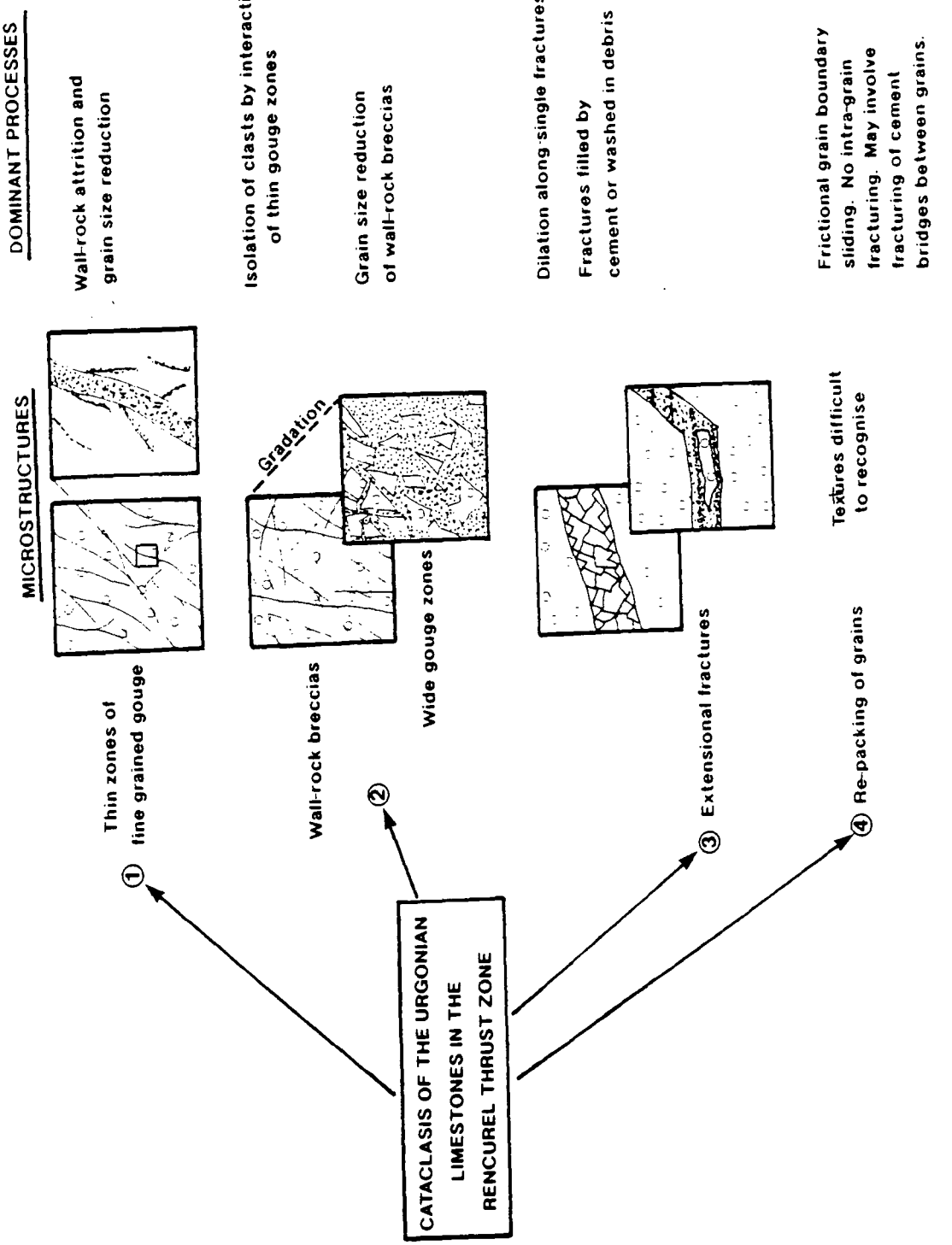

Figure 4.17 Summary of microstructures produced by cataclasis during the deformation of the Urgonian limestones in the Rencurel Thrust Zone.

types of deformation. This is also true of the extensional fracturing as discussed above.

These processes have one common feature in that they are all dilational in nature and therefore fracture porosity is produced. Cataclastic processes will increase the porosity and permeability of a fault zone promoting fluid flow.

This is however a rather simplistic view. Fracturing is the process by which grain size reduction occurs. With decreasing grain sizes, the size of intergranular pore spaces also decreases. It may be that the network of intergranular pore spaces produced by the grain size reduction may be less permeable than the arrangement of pore spaces which existed before the onset of cataclasis. Also the reduction in grain size reduces the distances over which diffusional processes occur (Knipe, 1989). This may lead to the enhanced action of DMT and the lithification and induration of the material by cement precipitation or by chemical compaction. This will reduce fluid flow, sealing the fault zone.

The influx of fluids which occurs during the cataclasis also ultimately leads to a porosity reduction. Migrating pore waters often allow cement precipitation to occur within the pore spaces. These cements occlude the original fracture porosity. Thus, cataclasis enhances fluid flow along these faults. However, the fracturing and fluid flow activate other processes which work towards retarding fluid flow. Each case involving cataclasis must be assessed individually.

Section 4.4.2 Diffusive Mass Transfer (DMT)

The action of DMT is indicated by three main styles of microstructure.

1) Areas of pressure dissolution. - These are areas where material is taken into solution due to high stresses. Insoluble residues are left behind producing pressure dissolution seams of which many different styles exist (Wanless, 1979; Bathurst, 1987). Fluids may be static or may be migrating along these seams (Knipe, 1989).

2) Fractures filled with fine-grained washed in material. - These microstructures are composite features. The fractures themselves and the fine-grained material are not formed by the process of DMT (except in the case of crystal silts discussed in Section 4.3.4.3). The existence of the fine-grained material in the extensional fractures does however indicate that fluid flow has occurred as discussed in Section 4.3.4.3. Fluid transport can sometimes be involved in the process of DMT. In this case diffusion of material as the transport mechanism is sub-ordinate to mass transport of the material

in a migrating solution. The microstructure described here is not formed by the process of DMT but indicates that fluid flow has occurred which in turn suggests that DMT is active.

3) Cements. - These are areas of newly precipitated crystalline material which exist within former pore spaces. They form as a result of the chemical precipitation of material out of solution. Accumulations of cement indicate that pore fluids were migrating, because many volumes of dilute pore fluid are needed to provide enough material to produce cement (Bathurst, 1975). Precipitation occurs because the pore fluids become saturated with respect to the precipitate which may be due to stress drops causing the release of CO_2, or chemical changes in the pore water (Bathurst, 1975).

The microstructures which indicate that DMT has been active are summarised in Figure 4.18.

These processes have one common feature in that they work towards the occlusion of porosity and hence reduce the permeability of the material. Pressure dissolution leading to chemical compaction together with cementation also cause induration of the material. Induration of the material must occur before it can become fractured. So in one respect, the action of DMT may promote the action of fracture processes.

All of the microstructures described above are today indurated. Thus DMT in the form of chemical compaction and cement precipitation seems to have been the final deformation mechanism which is active along these fault zones, before they ceased to deform. These faults become sealed to fluid migration at the end of their deformation history.

Section 4.5 INSIGHTS INTO FAULTING MECHANISMS FROM DEFORMATION MECHANISM STUDIES

The microstructures within the fault zones described above indicate that both cataclasis and DMT have both been active as deformation mechanisms. It is recognised that DMT dominates at low strain rates whilst cataclasis occurs at high strain rates (Rutter, 1976; White, 1976; Knipe, 1989). Composite microstructures such as those which exist within sample 2a (Section 4.3.1.4), indicate that cyclicity between DMT dominance and cataclasis occurs along these fault zones. This suggests that a range of strain rates great enough to activate cataclasis and DMT occurred and that in some cases strain rates varied in a cyclic pattern.

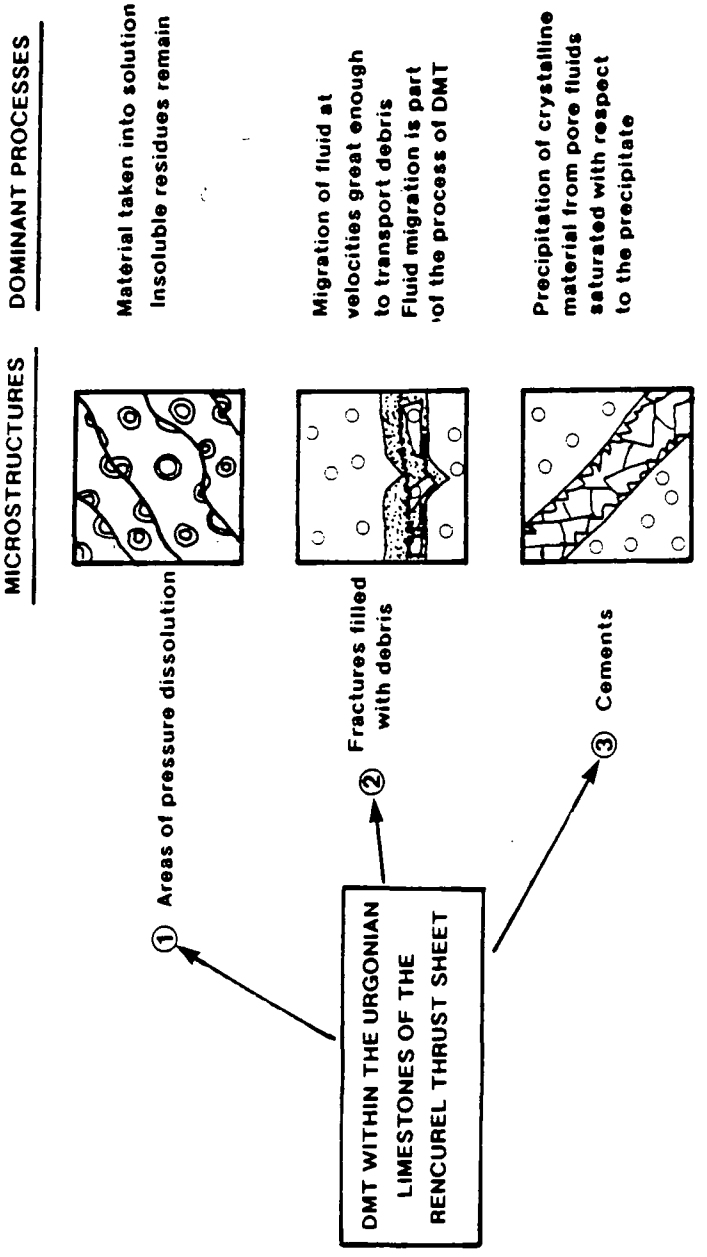

Figure 4.18 Summary of the microstructures produced by DMT during the deformation of the Urgonian limestones in the Rencurel Thrust Zone.

This much is clear from the microstructures preserved along the fault zones. Knipe, (1989) in his review paper on the recognition of deformation mechanisms from deformed rocks has pointed out that many more aspects of the deformation can be discussed after a microstructural study. The following Sections present a discussion of the fault zones of this Chapter using the guidelines suggested by Knipe (1989). It is hoped that the following discussion will highlight some of the problems which will have to be addressed if this particular study is to be continued beyond the scope of this thesis.

Section 4.5.1 Recognition of deformation mechanisms.

Knipe (1989) highlights the importance of careful assessment of deformation mechanisms in view of the problems of recognising the microstructures characteristic of grain boundary sliding processes. As discussed in Section 4.3.1.3 it is not clear what role if any frictional grain boundary sliding without fracture (independent particulate flow) played during the displacement along these gouge zones. This Section discusses the implications which result from the action of dependent versus independent particulate flow and highlights the importance of recognising all the deformation mechanisms which have been active, before a model for the fault zone development is proposed.

1) Dependent particulate flow: implications- Dependent particulate flow is a cataclastic deformation mechanism which involves the fracturing of grains in a gouge during displacement (Borradaille, 1981). Grain size reduction may lead to the strain hardening of a gouge zone deforming by dependent particulate flow. As grain sizes decrease, the stress concentration at point contacts between gouge clasts will decrease simply because there are more point contacts available to take up a given imposed stress. This will make it increasingly difficult to fracture the clasts and cause further grain size reduction. If pressure-sensitive, dependent particulate flow continues to be the dominant deformation mechanism, grain size reduction will strain harden the fault zone. This strain hardening may lead to the fault zone being abandoned, or continued displacement utilising a different deformation mechanism.

Also, the small grain sizes produced during dependent particulate flow will improve the efficiency of DMT as a deformation mechanism due to the relatively small diffusion distances which exist (Knipe, 1989). This will lead to greater lithification of fine-grained fault gouges which are under the influence of DMT. Faults zones undergoing the action of such processes may become relatively hard-to-deform and the deformation may be forced to change its position. Alternatively, individual faults may become the sites where stress build-ups during deformation are preferentially released,

perhaps because they are intrinsically easier to deform. Selection of individual faults for further deformation may be due to lithological contrasts within the wall-rocks or zones of anomalously high pore fluid pressures along the lithified and sealed faults. Both of these types of anisotropy may promote fracturing, so that the majority of displacement becomes localised within these zones. The relatively large displacements which will develop along these faults may in turn allow larger fragments of the wall-rocks to become disagreggated during frictional slip, which will increase the grain size of the gouge and make it relatively easier-to-deform. Also greater thicknesses of gouge will accumulate as the wall-rocks undergo disaggregation during displacement. The larger grain sizes and gouge thicknesses will increase the diffusion distances involved in DMT making it more difficult for the gouge to become lithified. The larger faults may also act as stress risers further concentrating applied stresses. The relatively strain hardened fine-grained gouge zones along small faults will be abandoned in favour of increasingly strain softened larger fault zones where greater grain sizes exist, promoting the localisation of displacement onto larger faults.

2) Independent particulate flow: implications- The increasing importance of fine-grained material in a gouge could promote the activation of grain boundary sliding without fracture. This deformation mechanism termed independent particulate flow (Borradaile, 1981), is important in unconsolidated material and in the presence of high fluid pressures. If the strength of the contacts between the grains in a gouge is less than the strength of the material which the clasts consist of, then continued deformation will result in grain boundary sliding of the gouge without further fracturing and grain-size reduction. Clasts will slide past each other and undergo re-organisation in their packing. This will lead to complex changes in the arrangement of pore spaces and dilatancy within the material. The strength of the contacts between the grains will be dependent on several things.

1) The state of lithification, that is, the strength of cement bridges or sutured contacts between the grains.

2) The fluid pressures in the intergranular pore spaces and their effect on the effective confining pressure. For example high fluid pressures in the intergranular pore spaces will decrease the effective confining pressure at point contacts between the grains decreasing the frictional resistance to slip and promoting grain boundary sliding.

3) The frictional resistance to slip will also be decreased in fine-grained materials. This occurs because of the greater number of grain-to-grain contacts.

So if fluid pressures remain high and the action of DMT is not sufficient to increase the strength of grain-to-grain contacts, fine-grained gouges in fault zones formed initially by fracturing may continue to deform by independent particulate flow involving grain boundary sliding without fracturing the grains. The fault zone may become strain softened by a change to this deformation mechanism, localising the displacement.

The important factors in controlling which of the alternative deformation mechanisms discussed above becomes prevalent are confining pressures, fluid pressures and the importance of gouge lithification. In the examples described here, the confining pressures and fluid pressures are not known. However, the microstructures do show evidence for lithification of the gouges before the action of further fracturing, with clasts in the gouges containing microstructures which were clearly lithified before the clasts were formed. This indicates that the faults under went deformation dominated by DMT, for a time great enough for the action of DMT to lithify the gouge. This confirms that the first alternative of dependent particulate flow outlined above certainly occurred. The second alternative of grain boundary sliding without fracture is however difficult to recognise as it involves only the re-arrangement of the clasts. This alternative may in fact have been more important than the first. In reality both of the processes outlined above are likely to have occurred. It is unreasonable to expect that the degree of lithification due to the action of DMT to be temporally and spatially uniform. This factor alone is likely to have been variable enough to allow both the activation of independent particulate flow causing strain softening, and/or lithification-induced strain hardening and fault zone abandonment. The variations in effective confining pressure caused by fluid pressure fluctuations may also have been great enough to allow both the alternatives outlined above to be viable. Figure 4.19 summarises the problem discussed here.

Section 4.5.2 Nature of the cyclic deformation

Knipe, (1989) has suggested that the preserved microstructures will have been influenced by the nature of the cyclic deformation which they have undergone. For example it is known that different deformation mechanisms operate at different strain rates, so that if all other factors are constant, a distinctive microstructure will be produced by a given strain rate. If a material undergoes deformation during changes in strain rate which occur in a cyclic pattern, it may be possible to model the form of the cycle by carrying out microstructural studies to propose deformation mechanism paths.

In the case of these fault zones which are small displacement, high level fault zones,

important details of the deformation include the following:-

1) Range of strain rates (Amplitude) - Deformation mechanism maps for material made of a combination of calcite and dolomite do not as yet exist for the complete range of strain rates needed to produce cataclasis and DMT. This is because there does not exist relevant experimental data on the deformation of combined calcite and dolomite rocks over the range of temperatures, pressures, grain sizes and fluid pressures which may have existed along the fault zones described above. These data will have to be collected before an actual range of strain rates for these fault zones can be suggested.

2) Form of the cyclic deformation - The time period over which certain strain rates act (wavelength), the exact form of variation (waveform), and the repeat time (frequency) of the cyclic strain rate variations should be important considerations in constructing deformation mechanism paths for the fault zones described in this Chapter. For example the strain accommodation along these faults may or may not be dominated by short wavelength but high amplitude deformation. The microstructures, however, may or may not be dominated by deformation which occurs over greater lengths of time but at lower strain rates. It must be decided which of these end members is most important (Knipe, 1989).

In the fault zones described in this Chapter, the greatest amount of strain within the material, is caused by the fracturing which has formed the fault gouges. The microstructures characteristic of DMT shown in Figure 4.18, cause a lesser degree of shape change. So in this case it seems that both the strain accommodation and the microstructures are dominated by the cataclastic deformation. However, this does not tell us about the periodicity of the fracture events, the absolute duration of the deformation at given strain rates or the rate of change between different levels of strain rate. Indeed because of the destructive nature of cataclasis, one cannot be certain what the dominant deformation mechanisms actually were during the early deformation. For example a simple scenario would be where the fault zones may have had an early history dominated by slow strain rate deformation of long duration where DMT was dominant. If this did occur, then it is difficult to recognise because the grain size reduction during late cataclastic activity has destroyed the microstructural evidence for the early deformation. More complex scenarios involving early cyclicity between cataclasis and DMT for example would also be difficult to recognise. The deformation mechanism path derived from microstructural studies may only be an approximation due to the loss of textural evidence for all deformation which occurred before a phase of grain size reduction. Another possibility is that frictional grain boundary sliding without fracture causing mass flow of pre-existing fine-grained

gouge material may have been an important process. Consider the position of the fine grained gouges described in this Chapter. The microstructures produced by independent particulate flow are difficult to spot; the shape change is accommodated by the re-packing of grains without intra-grain fracturing. If operation of this mechanism is not recognised then an incomplete deformation mechanism path may be proposed, and assessment of microstructurally controlled fluid migration cannot give absolute values for porosity and permeability, as these values will have changed in a manner corresponding to the microstructural changes which are not known.

Section 4.5.3 Spatial and temporal changes in the position of deformation

The role of changing the position of deformation must be considered. For example cyclicity at a point in space may be caused by migrating waves of deformation which contain gradients in strain rate. An example would be the repeated propagation of an earthquake rupture along a fault. An individual point on the fault trace would experience cyclic deformation dominated by short wavelength, high amplitude deformation but also involving longer periods of time where slower strain rates were active. However, areas away from the fault trace may only experience slow strain rate deformation. They undergo stress build-ups prior to earthquakes, but are never ruptured so that they never experience high strain rate deformation. This may be analogous to the fault zones described in this Chapter. Deformation of the tip zones and their fault zones may be manifestations of the same deformation. The tip zone may be the area which transmits the deformation which occurs in the fault zone into the wall-rocks. As such the deformation which occurs in the tip zone and the fault zone are kinematically linked. This is important for fluid flow in that a high strain rate event in the fault zone will be transmitted to the tip zone where the high strain rates may be maintained, so that fracturing occurs in both areas almost simultaneously. Fluid flow could occur between the two areas. Conversely the tip zone may be unaffected by the deformation which occurs within the fault zone. The deformation in the tip zone may have occurred at a different time from the fault zone deformation. For example it has been suggested that tip zone microstructures represent the last few increments of deformation along a fault when strain rates are decaying and the fault is about to be abandoned. The examples quoted are from the high level fault zones within the base of the Moine Thrust Belt (Knipe, 1989). In this example fracturing events or sealing events during the action of DMT may not have occurred simultaneously between the two areas. It is important to consider whether neighbouring areas exhibit textures which indicate that they reacted differently to the same deformation, or conversely, indicate the action of separate deformation events. This type of study will also indicate whether the microstructures were part of the same fluid flow system.

Section 4.5.4 The mechanical and chemical effects of fluid influx: implications for fluid flow and deformation style

The influence of fluid infiltration is also thought to be an important consideration (Knipe, 1989). It is not clear what influences fluid infiltration has on the next stage of the deformation mechanism cycle in terms of actually promoting a certain deformation mechanism. For example it is known that high fluid pressures promote fracturing (Knipe, 1989). If the fluid pressure approached lithostatic pressure in the fault zones described in this Chapter, hydraulic fracturing may have been an important mechanism. In this case the fluids would not be migrating passively in response to dilatancy, but would have been dynamically forcing open their own fractures. The fluid pressures involved in the deformation of the faults described in this Chapter are not known because of the lack of paleo-pore fluid pressure data. Indeed, fluctuating fluid pressures are likely to have occurred. For example the opening of dilatant fractures may have produced relatively low fluid pressures within the fractures. The resulting fluid pressure gradient may have promoted fluid migration.

These faults are likely to have been dominated by fracture processes. Elastic strain accumulation and the mechanical effects of the fluid migration are probably the most important factors in causing fracturing within these high level, low temperature fault zones (Knipe, 1989). These two factors have been combined by Sibson et al. (1975) into the seismic pumping model. Rising tectonic stresses cause the opening of dilatant fractures, within which relatively low fluid pressures exist. Fluids are drawn into these fractures by the low fluid pressures, decreasing the frictional resistance to fault rupture processes. When the fluid pressures in the fracture system reach sufficient levels, or stress reaches a critical level, fault rupture occurs causing a stress drop. The accumulated elastic strain is released and the dilatant fractures close. The fluids contained within the fractures are expelled and fluid migration occurs.

Also, high fluid pressures enhance the action of independent particulate flow by decreasing the frictional resistance to slip along the grain boundaries.

Another influence that fluid influxes may have is in helping to provide material which is used in the cementation of the fault zone (see Section 4.4.1). It has been suggested above in Section 4.5.1, that cyclic changes in deformation mechanism occur so that fracturing and fluid influx will occur episodically. Between the fracture events, the action of DMT may seal the fault zones to fluid flow. The precipitation of fracture filling cements within the fault zones described in this Chapter have caused the

induration of the deformation textures during low strain rate periods of the deformation. It has been suggested above in Section 4.4.2 that the low strain rate periods during which induration occurred, can be viewed as recovery periods where the elastic strength of the material was recovered after its disaggregation during fracturing. This highlights the important link between rheological cycles and lithological cycles (Knipe, 1989). For example if the microstructures had not become indurated between fracture events then renewed high strain rate deformation may have occurred by frictional grain boundary sliding as discussed above in Section 4.5.1. Induration which causes a lithological change, influences how the gouges react to the next increment of deformation. This ultimately controls the involvement of fluids during the next increment of deformation and can lead to rheological cycles controlled by lithological cycles (See Figure 4.19).

With these points in mind a model will be proposed for the fault zones described in this Chapter.

Section 4.6 FAULT ZONE MODEL

Fault zone 2 which is composed of two overlapping fault strands provides an ideal opportunity to study the processes which occur at a fault tip. In the vicinity of sample 2h which lies at the junction between the two fault strands, deformation takes the form of the fine grained gouges summarised in Figure 4.17. This style of gouge can also be found within the textures of the fault rocks collected from along fault zone 2. They exist in the wall-rocks close to the central gouge zone, and also within clasts within the gouge zone. All the other fault zones show similar features in the fault zones, but it was impossible to examine the terminations of the fault due to the state of exposure. The fine grained gouge zones always exhibit textures which suggest that they became lithified before being cut by the central gouge zone. The cross-cutting relationships outlined above suggest that the fine-grained gouge zones which seem to characterise the deformation around fault terminations, may form contemporaneously with growth in the dimension of the fault zones. The fault zones grow into areas previously affected by tip zone style deformation. Tip zone style deformation has ceased and the textures are lithified before the localised fault zone grows into them. As such the fault zone deformation may be kinematically linked to the deformation which occurs in the tip zone at the termination of the faults. Dilational events may have occurred simultaneously in the tip zone and the fault zone so that they may have formed part of the same fluid flow system. The microstructures indicating the action of dilatant processes are summarised in Figure 4.17. Similarly, sealing of the fault zone and fault tip are likely to have occurred simultaneously. The microstructures indicating the action of DMT which caused the sealing are summarised in Figure 4.18.

Indurated and sealed microstructures will exist within the wall-rocks as a central gouge zone develops. The fault zone gouge which would undergo episodic dilation would at times be relatively more permeable than the wall-rocks, causing localisation of fluid flow within the fault zone.

As the fault zone stops deforming at the end of its life cycle, the action of DMT would work towards finally sealing the fault to fluid flow.

Section 4.7 DEFORMATION MECHANISM PATH

Fracturing processes were important during the deformation. They allowed the influx of fluids by opening fracture porosity. The elastic strain accumulation and the mechanical effects of the fluids may have combined to provide a mechanism to drive fluid migration, known as seismic pumping (Sibson, et al. 1975). Fracturing also enhances the action of DMT because it allows the infiltration of fluid and also reduces the distances involved in diffusion processes (see Section 4.4.1). Cyclicity between these two deformation mechanisms occurred which allowed episodic fluid migration. This cyclicity may have been enhanced by the involvement of fluids which may have promoted the action of both fracturing and DMT. This may have led to lithological and rheological cycles (see Section 4.5.4). The periodicity, duration and rate of change of deformation mechanisms is as yet unknown. The actual range of strain rates was great enough to activate both DMT and cataclasis as deformation mechanisms. Spatial changes in the finite deformation do occur. For example the tip zone and fault zone textures are different, but they may have developed simultaneously. They may represent two manifestations of the same applied deformation but have developed different microstructures due to different rheologies of the two areas. The tip zone develops in undeformed wall rock whereas the fault zone develops within material previously deformed by the tip zone style deformation. The deformation mechanism path outlined above represents a "simplest case scenario" due to the loss of textural evidence for early deformation events along the fault zone due to grain size reduction.

Section 4.8 DISCUSSION OF THE FAULT ZONE MODEL: POSSIBILITIES PRODUCED

It is interesting to speculate as to why deformation becomes localised on to a thin fault zone after the deformation is originally taken up by distributed deformation. It has been suggested that fracturing causes fluid infiltration and that the fluids may instigate the action of processes leading to induration and reduction in permeability. It has also been suggested that cyclic deformation then occurs involving fracturing and fluid influx, followed by the action of DMT causing induration and permeability

reduction. It may be that repeated fracturing and sealing events lead to increased fluid pressures on a small scale in the centre of a deforming zone. This may occur because the increasing density of sealed microstructures with time will make it increasingly difficult for fluids to escape from the zone after they are drawn in during fracture events. The high fluid pressures in such a zone would enhance fracturing by increasing the effective stress within the zone. Fracturing may become localised within this zone of high fluid pressures and the growth of a localised fault zone may then occur.

This localisation process may be aided by the relative strain hardening of the gouge along the small shear fractures during grain size reduction. Conversely strain softening of fault gouges due to a change in the deformation mechanism to independent particulate flow may work against fault zone localisation (see Section 4.5.1). As discussed in Section 4.5.1, the action of these two processes which lead to strain hardening and strain softening respectively, are in reality probably competing processes. Temporal and spatial changes in the dominance of these two processes is likely to be the rule.

The geometries of these two styles of deformation may also encourage localisation. For a given applied bulk strain rate, a wide zone of deformation will experience a lower bulk strain rate than a thin zone of deformation. Thin zones of deformation are therefore more likely to experience fracture processes. This will promote an increased fluid flux in the thin deforming zone, further promoting fracture processes.

Increasing fluid pressures and grainsize changes in gouges within zones undergoing cyclic deformation involving the action of DMT and cataclasis may induce the localisation of displacement. When a localised deformation zone is formed, the partitioning of bulk strain rates causes fracturing, fluid influx and DMT to become localised. This localisation is further enhanced by the high fluid pressures which may develop within this zone.

Section 4.9 IMPLICATIONS FOR MODELLING ARRAYS OF FAULTS

Minor fault arrays within large fault zones have been described. The fault arrays exhibit a non-linear relationships between the dimensions and displacements of individual faults (Walsh & Watterson, 1988). Strain profiles across arrays of faults indicate that displacements are localised in the centre of the arrays (Wojtal & Mitra, 1986). It may be that the displacement distributions which can develop in fault zones may be controlled by the action of the processes discussed above in Sections 4.5.1. to 4.8.

CHAPTER 5 THE THRUST CONTACT BETWEEN THE URGONIAN AND MIOCENE ROCKS

Section 5.1 INTRODUCTION

The thrust contact between the Miocene and the Urgonian rocks is shown in Figure 5.1. This Chapter describes and discusses the rocks from this contact. The samples described are located on Figure 3.19.

Section 5.2 OBSERVATION AND DISCUSSION OF THE ROCKS ALONG THE THRUST CONTACT BETWEEN THE URGONIAN AND THE MIOCENE

Section 5.2.1 Sample 12s

Figure 5.2 shows the microstructure of sample 12s which is located in Figure 3.19. The sample comes from 10-20cm into the hanging-wall of a minor fault. The sample is a foraminiferal grainstone which is overprinted by dolomite rhombs. The deformation within the sample is generally not intense, but is restricted to the occurrence of thin fractures, less than 0.5mm wide which are filled with fine-grained material, pressure dissolution seams, and some calcite filled extensional fractures. Displacement of the wall-rock textures occurs across some of the fractures filled with fine-grained material, indicating that they are shear fractures. These fractures generally have sub-planar fracture margins and the fine-grained material is rarely accumulated to a thickness greater than 0.02mm. Other fractures have thicker accumulations of fine-grained material up to 0.7mm wide and have fracture margins which interlock. These fractures can often be traced along their length into fractures filled with crystalline calcite cements. The fine-grained material is composed of angular clasts of carbonate, some of which can be recognised as fragments of the calcite cements lining the fractures. The fine-grained material can also be found lining the bottoms of the calcite-filled fractures. These fractures are interpreted as extensional fractures filled with calcite cements and washed in re-worked gouge and wall-rock debris. The pressure dissolution seams within the sample are lined with dolomite rhombs, and are generally cut by all the fracture types described above. The dolomite rhombs along the pressure dissolution seams are petrographically indistinguishable from the dolomite rhombs which occur scattered within the wall-rocks. The pressure dissolution seams do not have large volume losses across them, because often portions of the same individual allochem in the limestone can be seen on both sides of the pressure dissolution seam.

Figure 5.1 Thrust contact between the Urgonian and the Miocene rocks.

Figure 5.2 Photomicrograph of sample 12s (see Section 5.2.1). Field of view is 15mm.

Section 5.2.2 Sample 12s- Discussion

It is suggested that the pressure dissolution seams within this sample have not collected their dolomite lining by the preferential dissolution of the calcite leaving the dolomite rhombs as relatively insoluble residues. This can be suggested because the rhombs are widely scattered within the undeformed rock and large volume losses are not displayed across the pressure dissolution seams. The pressure dissolution seams seem to have acted as pathways for the fluids which caused the dolomitization of the sample. The occurrence of these pressure dissolution seams may be due to chemical compaction during burial of the Urgonian limestones, or due to a phase of pressure dissolution during the early deformation history of the fault zone. Certainly the pressure dissolution seams pre-date the fracturing which occurred during the development of the Rencurel Thrust Zone. The fluid flow system must have been large scale in order to provide enough material to precipitate the dolomite along the pressure dissolution seams. If this fluid flow system was active during the deformation which formed the Rencurel Thrust Zone, it is surprising that no dolomite has been found filling tectonic fractures within the thrust zone. It is also surprising that petrographically indistinguishable dolomites are widespread in occurrence across the Vercors, even in areas away from faults (Vieban, 1983). It is suggested here that the dolomitization of the Urgonian occurred prior to the deformation associated with post mid-Miocene thrusting. The dolomitizing fluids often utilised inactive pressure dissolution seams as conduits for migration. The pressure dissolution seams were probably formed during the burial and chemical compaction of the Urgonian limestones. The fracture types within this sample are similar to those described from the fault zones in Chapter 4.

Section 5.2.3 Sample 12q

Figure 5.3 shows the microstructure of sample 12q, which comes from a minor fault as shown in Figure 3.19. The sample includes part of the fault gouge zone developed along this fault.

Starting at the bottom, the sample is composed of a peloidal grainstone with scattered dolomite rhombs which is cut by a set of thin calcite filled extensional fractures which are less than 0.1mm wide. Also a set of fractures filled with fine-grained material cuts across the wall-rock texture. These fractures are similar to those described from sample 12s, with fine-grained material associated with shear fractures, and also with extensional fractures which display calcite cement fills with fine-grained material at their bases. Higher in the sample, textures described from the bottom of the sample can be seen within clasts which exist within a coarse-grained poorly-sorted fault

Figure 5.3 Photomicrograph of sample 12q (see Section 5.2.3).
Field of view is 15mm.

gouge. The largest clasts are up to 1.5mm across and a complete range of grain sizes down from this seems to exist. The fault gouge texture is cut by a set of calcite-filled extensional fractures. Cross-cutting relationships are ambiguous so that this set of calcite-filled extensional fractures may have formed synchronously to the calcite-filled extensional fractures lower in the sample. In any case the calcite-filled extensional fractures higher in the specimen are cut by a set of fractures filled with a combination of fine-grained material and calcite cement with fine-grained material at its base. These fractures are interpreted as dilatant extensional fractures. These fractures can be traced to the top of the specimen where they link into a zone of poorly sorted fault gouge which cuts across all of the earlier textures. Clasts up to 1.5mm across exist and are composed of the early formed fault gouge and the wall-rocks which occur lower in the sample. The lower margin of this late gouge zone is lined with calcite cement.

Section 5.2.4 Sample 12q- Discussion

The sample exhibits microstructures which indicate the cyclic nature of deformation involving both DMT and cataclasis as deformation mechanisms. Cross cutting relationships suggest that the deformation textures become progressively younger towards the centre of the gouge along the minor fault. Early deformation involved cataclasis producing extensional fractures and fine-grained fault gouge along shear fractures. The influx of fluids along these fractures allowed the precipitation of calcite cements and the washing-around and re-deposition of fine-grained fault gouge within the fracture porosity. These deformation textures became indurated before cataclasis produced extensional fractures which became filled with calcite cements and fine-grained, washed-in material as a result of fluid migration through the fracture porosity. This texture became indurated before further cataclasis produced a younger fault gouge texture at the top of the specimen. This fault gouge texture is also indurated. The existence of calcite cements on the margin of this gouge zone suggests that the gouge zone developed along the site of a pre-existing extensional fracture which had become filled with calcite. These textures are similar to those discussed in Chapter 4.

Section 5.2.5 2nd thin section from Sample 12q

This sample (Figure 5.4) displays more of the texture of the final gouge zone described from the 1st thin section made from sample 12q described in Section 5.2.3. The gouge is poorly sorted with the largest clasts composed of wall-rock lithologies and re-worked, indurated gouge. The maximum clast size is around 1.75mm across. The clasts containing gouge textures are probably derived from the gouge zone which

occurs in the footwall to this gouge zone in sample 12q (see description of the first thin section from sample 12q in Section 5.2.3). The large clasts in the gouge have stained mostly pink indicating calcite with unstained areas indicating the presence of dolomite. However, the fine-grained portions of the fault gouge have stained blue indicating that they are iron-rich.

Section 5.2.6 2nd thin section from sample 12q- Discussion

The change in composition of the fault gouges indicates that the composition of the fluids has changed during the deformation.

Section 5.2.7 Sample 12i

Figure 5.5 shows the microstructure of sample 12i (see Figure 3.19 for location). This sample shows that the textures described from sample 12q have undergone further cataclastic deformation. The pink-staining textures similar to those in 12q occur within clasts in a later gouge zone. The fine-grained portion of this late gouge zone is stained blue. This late gouge zone is cut by some poorly displayed extensional fractures filled with ferroan calcite.

Section 5.2.8 Sample 12i- Discussion

The early lithified pink-staining gouges which now appear as clasts within the blue-stained gouge zones were impermeable during the migration of the fluid which infiltrated the blue-stained gouge. The whole texture became lithified before a stage of late extensional fracturing and fluid infiltration.

Section 5.2.9 Sample 12x

Figure 5.6 shows the microstructure of sample 12x which comes from the 60cm thick gouge zone which occurs just in the hanging-wall to the contact between the Urgonian and Miocene rocks (Figure 3.19). At outcrop the gouge zone is cut by a set of discrete minor faults (Figure 5.7). The fault planes are striated and in section seen on the sawn faces of samples the faults zones are marked by grain size reduction of the pre-existing indurated gouges. This sample includes the microstructures which occur along one of the discrete minor faults within the gouge zone. At first sight the whole sample appears to be composed of a fine-grained fault gouge. Only after staining the thin section can it be seen that the gouge contains large clasts up to 1cm across composed of an early lithified fine-grained carbonate fault gouge. This gouge texture became indurated before renewed cataclasis along the discrete minor fault isolated the

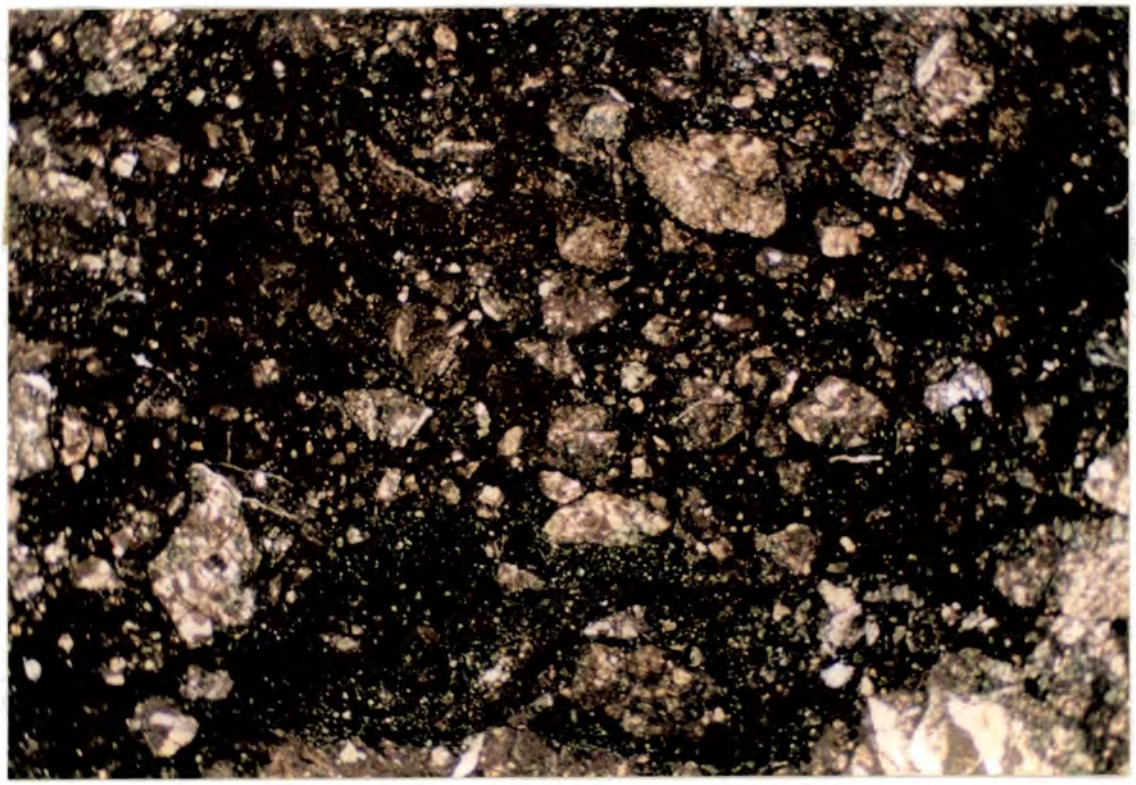

Figure 5.4 Photomicrograph of sample 12q, 2nd thin section (see Section 5.2.5). Field of view is 15mm.

Figure 5.5 Photomicrograph of sample 12i (see Section 5.2.7). Field of view is 15mm.

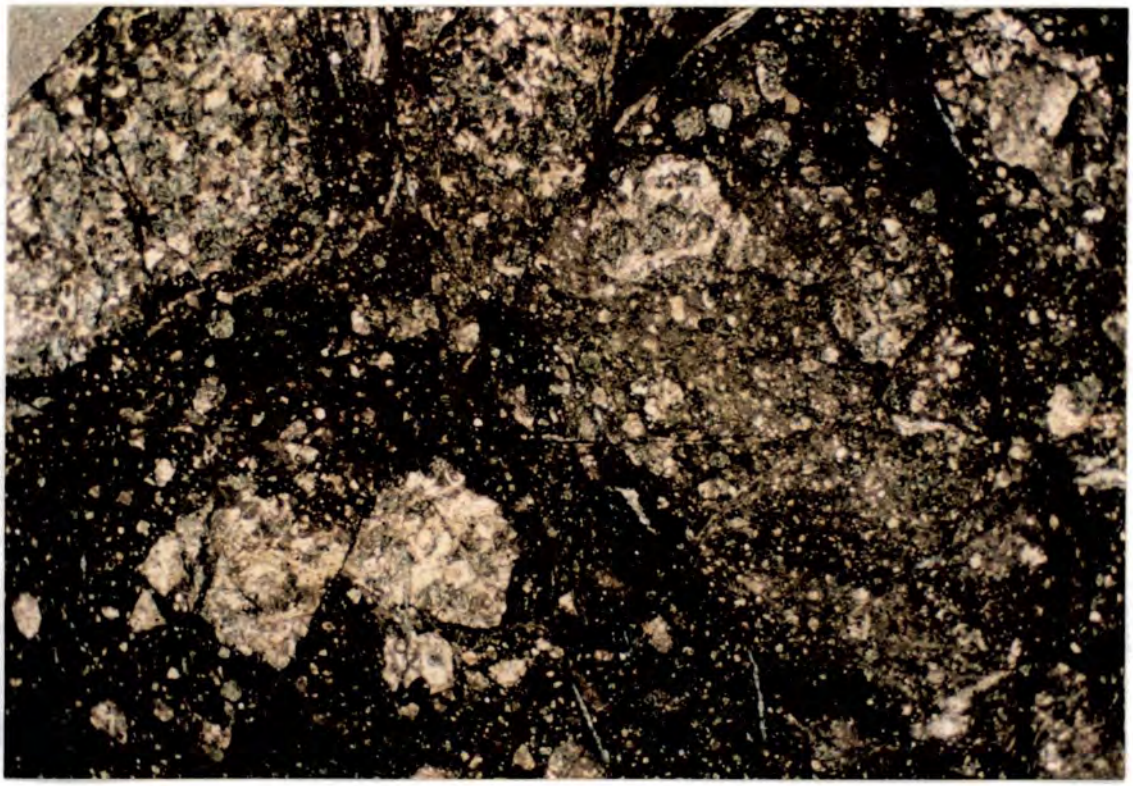

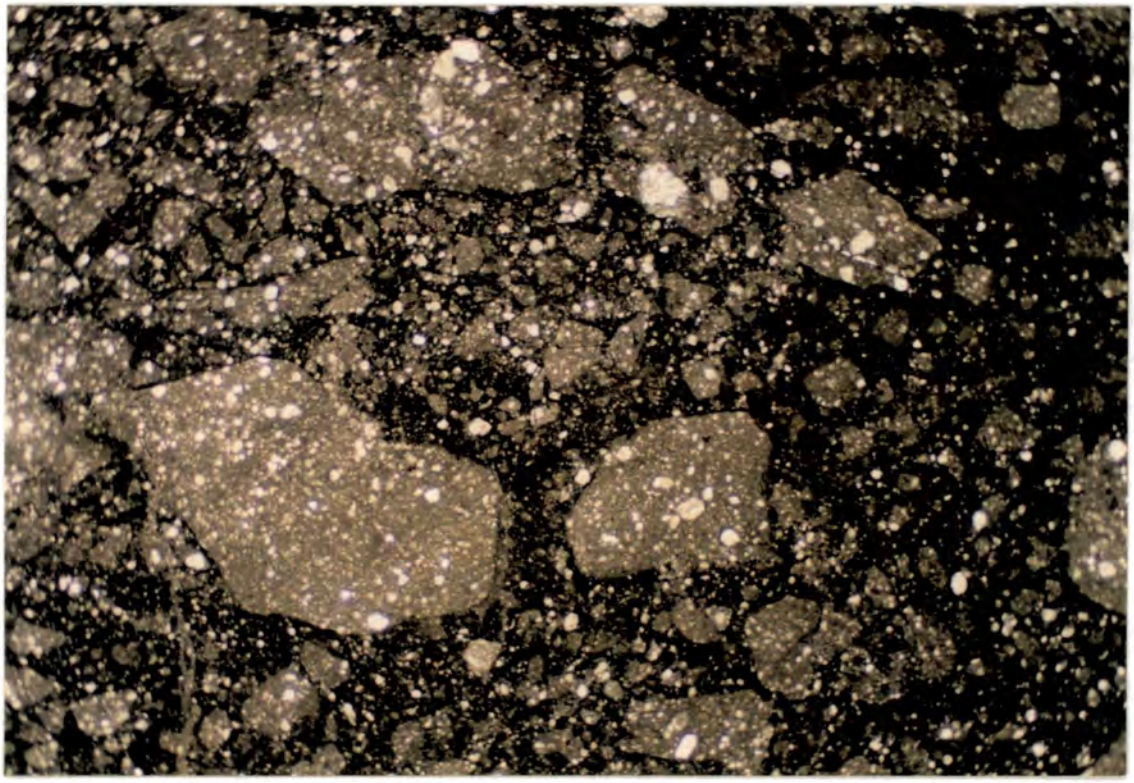

Figure 5.6 Photomicrograph of sample 12x (see Section 5.2.9).
Field of view is 15mm.

Figure 5.7 Field photo of a discrete minor fault developed within the gouge zone along the thrust contact between the Urgonian and the Miocene.

clasts composed of earlier gouge fabrics. The renewed cataclasis produced a younger fault gouge which has larger maximum clast sizes. The whole gouge texture is stained blue with the clasts containing older gouge fabrics slightly lighter in colour. Using high power objectives it can be seen that the individual carbonate clasts within the gouge have not taken up the stain suggesting that they are composed of dolomite. The blue stain occurs around the edges of the clasts in the finest grained material. X-ray diffraction of this gouge shows it to be composed of over 90% dolomite with traces of calcite. Under reflected light, tiny amounts of pyrite can be seen as grains less than 0.02mm in diameter.

Section 5.2.10 Sample 12x- Discussion

The sample has undergone cyclic deformation involving both DMT and cataclasis. Early cataclasis and grain size reduction indicating high strain rates and fluid flow was followed by DMT indicating low strain rates and induration of the gouge. The indurated gouge then underwent further cataclasis followed by another stage of induration. This cyclic deformation and fluid flow seems to have been caused by the development of discrete minor faults within the indurated gouge fabric.

The predominance of dolomite in the gouge composition suggests that the wall-rock precursor to the fault gouge was dolomite. The blue stained material around the dolomite clasts is suggested to be ferroan calcite on the evidence which is presented later in Section 5.2.13. No ferroan calcite has been found within the Urgonian limestones within the wall rocks to this fault zone. Also, no pyrite has been found within the Urgonian wall-rocks to the fault zone. This suggests that fluids have passed through this gouge zone which have interacted with material from outside of the Urgonian limestones. Ferroan calcite and pyrite precipitated from these fluids. Sources for these fluids are suggested in Chapter 6.

Section 5.2.11 Sample 12h

Figure 5.8 shows the microstructure of sample 12h which comes from the same gouge zone as sample 12x. The microstructures are essentially similar to those described from sample 12x. However in this sample, the texture is cut by a set of extensional fractures which are filled with ferroan calcite. The ferroan calcite crystals are generally euhedral with straight crystal margins. In some of the extensional fractures however, the calcite is fibrous with the fibres being aligned sub-parallel to the fracture long-axis. Areas of euhedral "blocky" calcite occur along these extensional fractures where there are steps in the trajectory of the fracture and also in the centre of the extensional fracture fill in a zone parallel to the margin of the fracture. Under

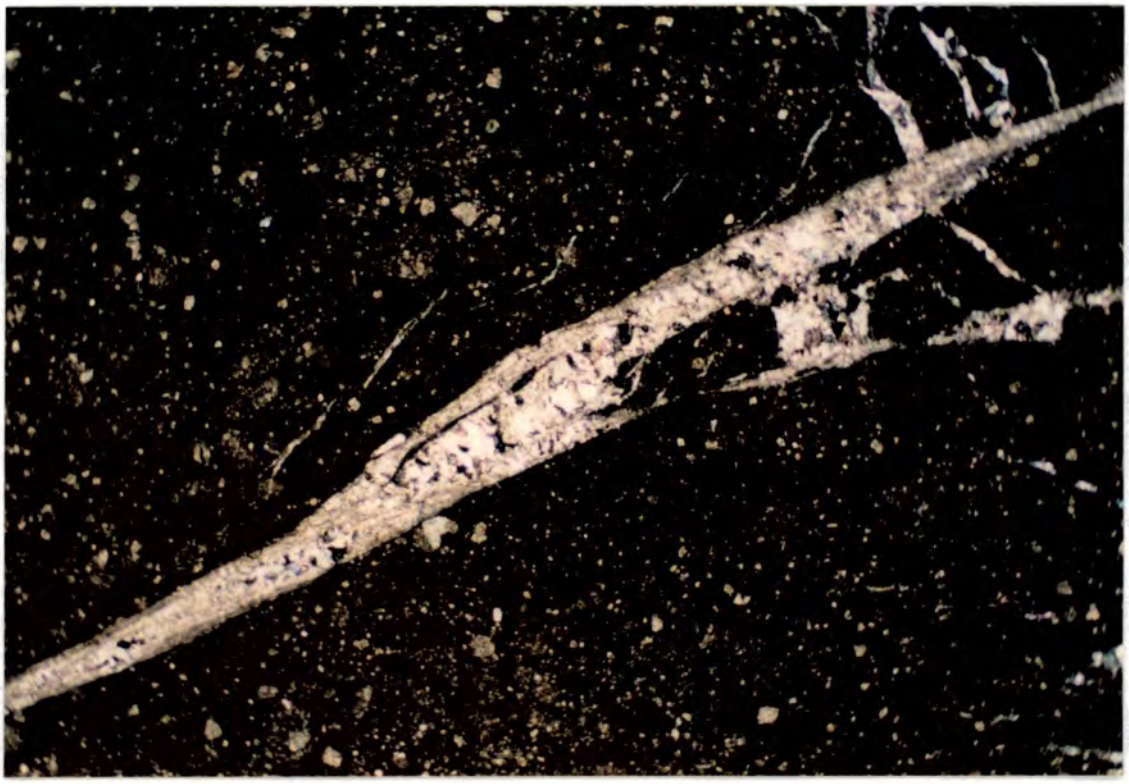

Figure 5.8 Photomicrographsof sample 12h (see Section 5.2.11).
Field of view is 15mm.

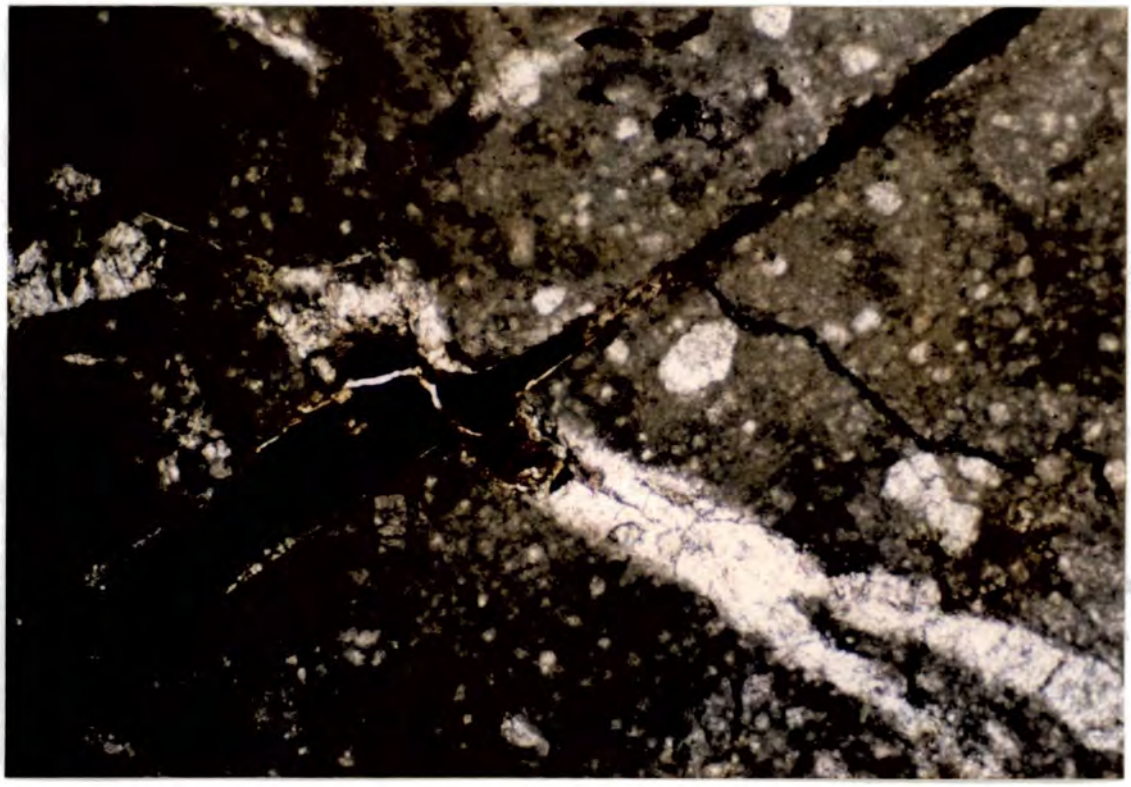

cathodoluminescence, the calcite is dully luminescent and the areas of "blocky" calcite can be seen to be weakly zoned. Some of the fractures are filled with amorphous, opaque material which under reflected light can be seen to be brown in colour. This material is bitumen infilling the fractures. Also thin extensional fractures are associated with these bitumen deposits. The fracture filling material is colourless in plane-polarised light and exhibits extinction under cross-polarised light, indicating that anisotropic crystalline material is present. When viewed under UV-fluorescence, the extensional fractures fluoresce brightly suggesting that they may be filled with free oil as well as crystalline material. Unfortunately the mounting resin used in the thin sections also fluoresces, and it may be that the resin has infiltrated the sample during thin section preparation. To investigate this possibility, a double polished wafer of the sample was prepared so that the mounting resin would find it difficult to infiltrate into the specimen. Similar fluorescent extensional fractures are also visible within the double polished wafer. Thin sections were also prepared with a non-fluorescing resin called Samtollite. The extensional fractures continued to show weak fluorescence. The evidence presented above suggests that presence of free oils is likely; however more reliable results could be achieved using Gas-chromatography mass-spectrometry. However the time limitations of this study prohibited the use of this technique.*

Sample HW 10 which is taken from the same carbonate gouge zone as 12h and 12x, was viewed under a scanning electron microscope (see Figure 5.9). Large clasts up to 120 microns across appear within the gouge surrounded by a fine-grained matrix. At higher magnifications it can be seen that the clast is composed of many smaller sub-angular clasts of carbonate which are less than 8 microns across. The nature of the contacts between the grains cannot be seen clearly. Inter-granular pore spaces exist up to around 2-5 microns across.

Section 5.2.12 Sample 12h- Discussion

Extensional fractures within this sample have acted as pathways for the migration of fluids saturated with respect to ferroan calcite. This fluid may have infiltrated the intergranular pore spaces between the gouge clasts, precipitating ferroan calcite during the induration of the gouge. This ferroan calcite cement may be the material which has stained blue. The zoned nature of the ferroan calcite within the extensional fractures when viewed under cathodoluminescence, indicates that the crystal grew during the evolution of pore water compositions. In the areas of "blocky" euhedral calcite, precipitation occurred relatively slowly compared to the rate of fracture opening so that the crystals grew into fluid-filled pore spaces. In other cases, the fibrous nature of the calcite is due to calcite precipitation keeping up with shear

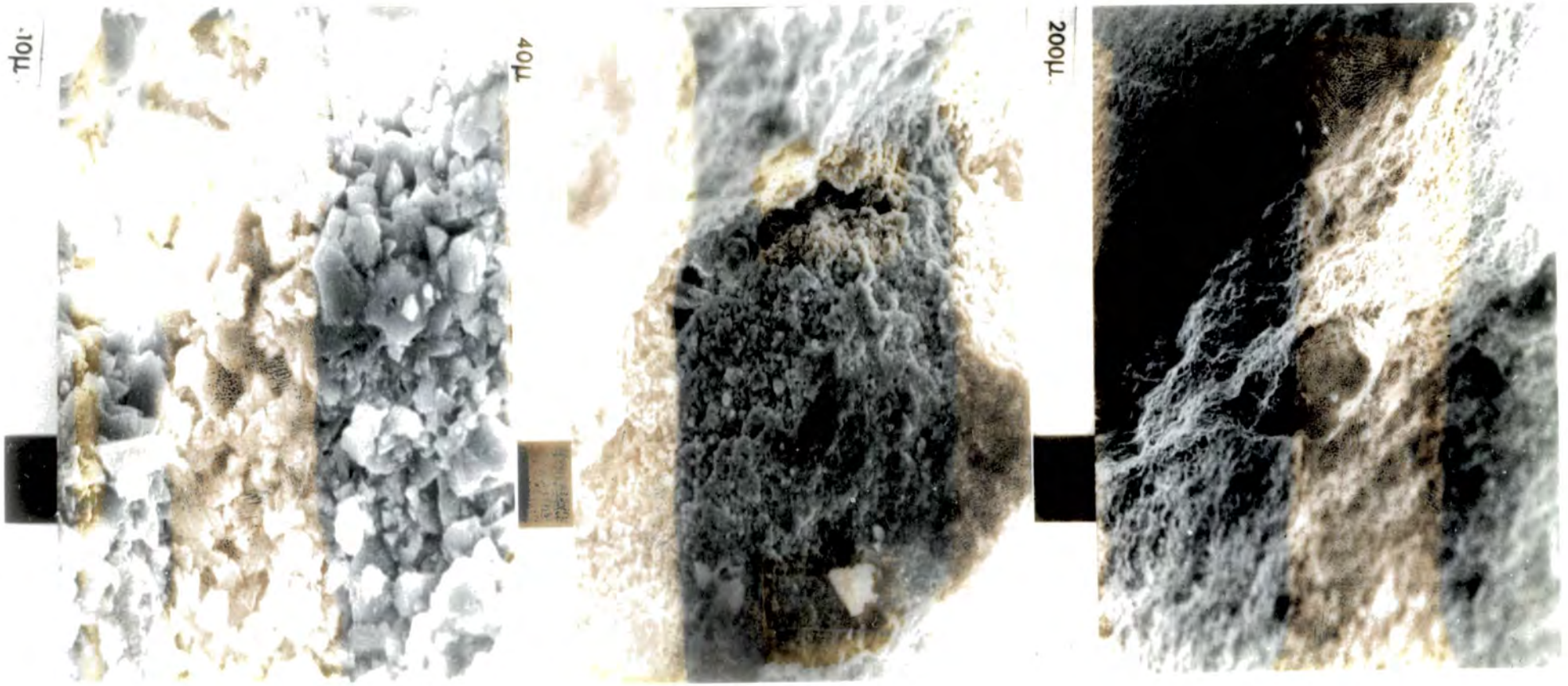

Figure 5.9 SEM image of the fine-grained carbonate gouge developed along the thrust contact between the Urgonian and Miocene rocks (see Section 5.2.11). (Sample HW10).

displacements taking place across a fracture (Durney & Ramsay, 1973). The rate of cement precipitation was relatively fast compared to the rate of fracture opening. Elongate fibres are produced during this process as calcite precipitation occurs syntaxially on to the pre-existing crystal terminations. Fracture porosity became sealed almost as soon as it was formed. The width of open, fluid-filled fractures was at any time only a fraction of the full thickness of calcite present today. The rate of cement precipitation is generally thought to be controlled by the chemical situation within the fluid and the fluid flux within the pore space. In the absence of extremely high flow rates within the fractures, which are difficult to envisage, the extensional fractures filled with fibrous ferroan calcite are evidence for relatively slow deformation and fracture opening compared to the extensional fractures filled with euhedral ferroan calcite. In Chapter 6, ^{18}O and ^{13}C stable isotopic evidence is presented which suggests that the ferroan calcite within these extensional fractures was precipitated from a fluid which was derived from outside the immediate wall-rocks to the extensional fractures. This evidence suggests that these extensional fractures filled with fibrous ferroan calcite are different from those described by Durney & Ramsay, (1973) which are said to form in response to the transport of material by diffusional processes from the immediate wall-rocks into the extensional fractures.

Small amounts of pyrite were also precipitated within the fractures from the migrating pore fluids. The presence of brightly fluorescing material within the fractures partially filled with crystalline material may indicate the presence of free oils in the fractures, although this feature should be subjected to further study. The presence of bitumen indicates that hydrocarbons were present at one stage. Bitumens form from the breakdown of hydrocarbons when lighter hydrocarbons are released for migration, and during the hardening of hydrocarbons during thermal diagenesis or bacterial breakdown oxidation by surficial waters (Teichmuller, 1987; Robert, 1988). In all cases the presence of hydrocarbon before bitumen production can be inferred. Significant amounts of bitumen have not been found in the wall-rocks to the fault zone. These observations suggest that hydrocarbons were present in the fluids which were migrating through the gouge zone, and may have been derived from deeper in the section where the thermal maturation of organic matter is an important process.

Scanning electron microscope (SEM) images of this sample have failed to reveal the nature of the grain-to-grain contacts within the carbonate gouge. It therefore cannot be decided if cement precipitation or grain indentation by chemical compaction is the process by which the gouges became indurated. SEM studies have however, revealed that in some instances the gouges contain inter-granular porosity up to 2-5 microns wide. However, it is not certain how connected these pore spaces are, or even if they

exist away from the surface of these gouges.

Section 5.2.13 Sample 12c

Figure 5.10 shows the microstructure of sample 12c, which comes from the zone of sheared molasse in the footwall to the gouge zone where sample 12x and 12h came from (see Figure 3.19). At outcrop, the sheared molasse is foliated and cut by a set of discrete minor faults as shown in Figure 5.11. The texture has the geometry of an S-C fabric. Sample 12c includes the microstructure of a minor fault which cuts across the pre-existing foliation. The sample consists of a large clast of carbonate, 5cm by 2cm, which occurs within the foliated molasse. The carbonate material is a fault gouge which stains pink. It contains similar microstructures to those described from along the minor faults within the Urgonian described in Chapter 4. Surrounding the carbonate gouge clast, is black sheared and foliated molasse material. At outcrop this material can be seen to be a fine-grained gouge which contains clasts of carbonate and siliciclastic material. The foliation is defined by closely spaced pressure dissolution seams and dips at around 30^{o} towards the ESE. SEM images shown in Figure 5.12 show that striations exist on the foliation surfaces. At the contacts between the carbonate gouge and the black gouge composed predominantly of material from the molasse, pressure dissolution seams are developed. The carbonate gouge clasts are cut by a set of extensional fractures which are oriented in a plane orthogonal to the WNW-ESE transport direction of the thrust derived from the collection of fault plane lineation data (see Section 2.5.4). The fractures do not penetrate into the molasse material, but thin towards the edges of the carbonate clasts, terminating at points. These extensional fractures are filled with ferroan calcite cement which exhibit a zoned texture. On the margins of the fractures, euhedral acicular crystals 0.5mm by 0.05mm occur with their long-axis perpendicular to the fracture margin. In the centre of the ferroan calcite fill, equigranular crystals exist. Under cathodoluminescence, the base of the acicular crystals on the fracture margins are dully luminescent; brightly luminescent calcite forms the crystal terminations and the equigranular crystal in the centre of the fracture fill. Under reflected light, brown coloured bitumen can be seen concentrated along the pressure dissolution seams within the sample. A double polished wafer was made from sample 12c and under ultra-violet fluorescence, brightly fluorescing extensional fractures which may be filled with free oil can be seen associated with the bitumen (see Section 5.2.11 for discussion). Also pyrite can be seen within the extensional fractures filled with ferroan calcite.

Section 5.2.14 Sample 12c- Discussion

Although no recognisable lithologies or fossils occur within the carbonate material

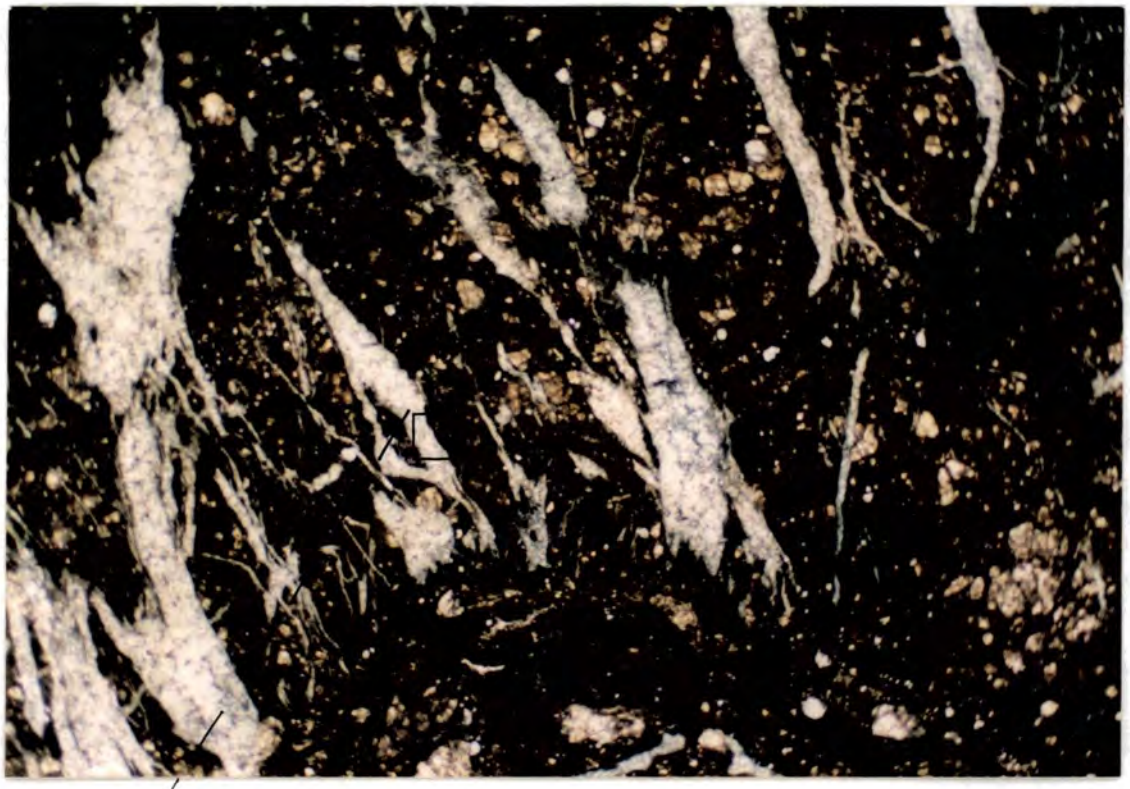

Figure 5.10 Photomicrograph of sample 12c (see Section 5.2.13).

Field of view is 15mm.

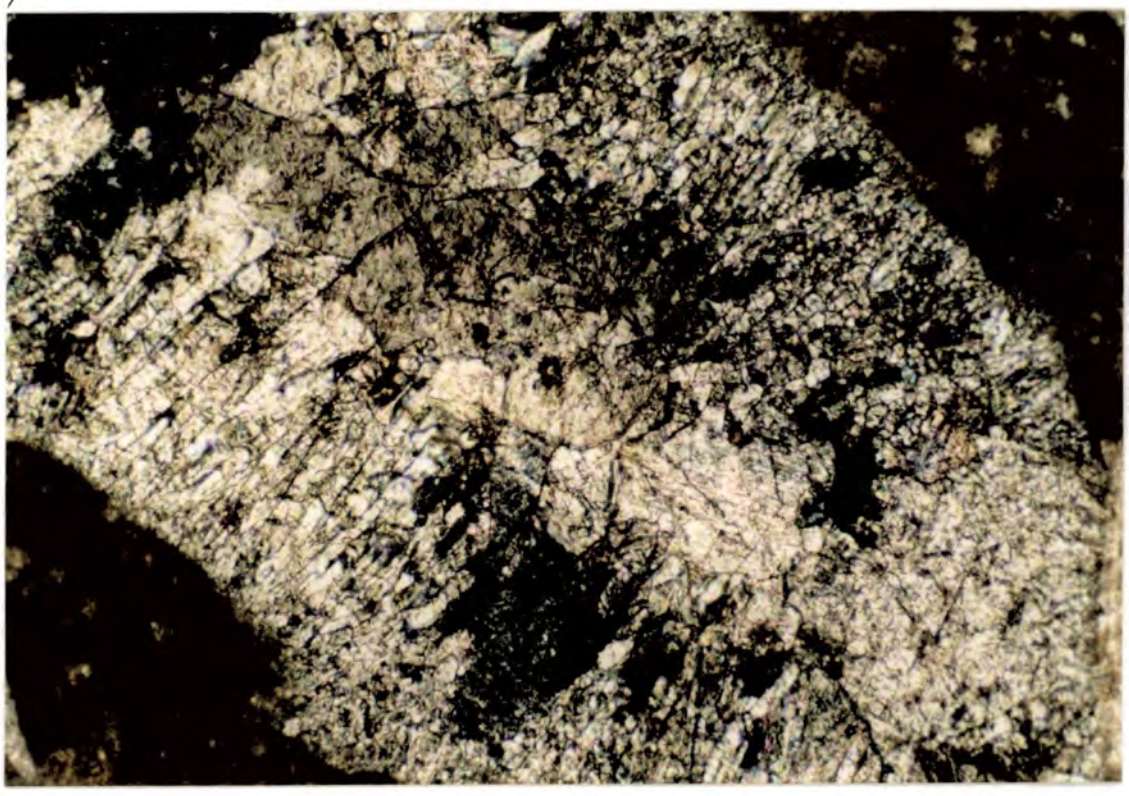

Figure 5.11 Field photo of discrete minor faults cutting across the deformed and foliated Miocene rocks along the thrust contact between the Urgonian and Miocene rocks. **Penknife is 5cm long. (See Section 5.2.13).** See Figure 3.19 for location.

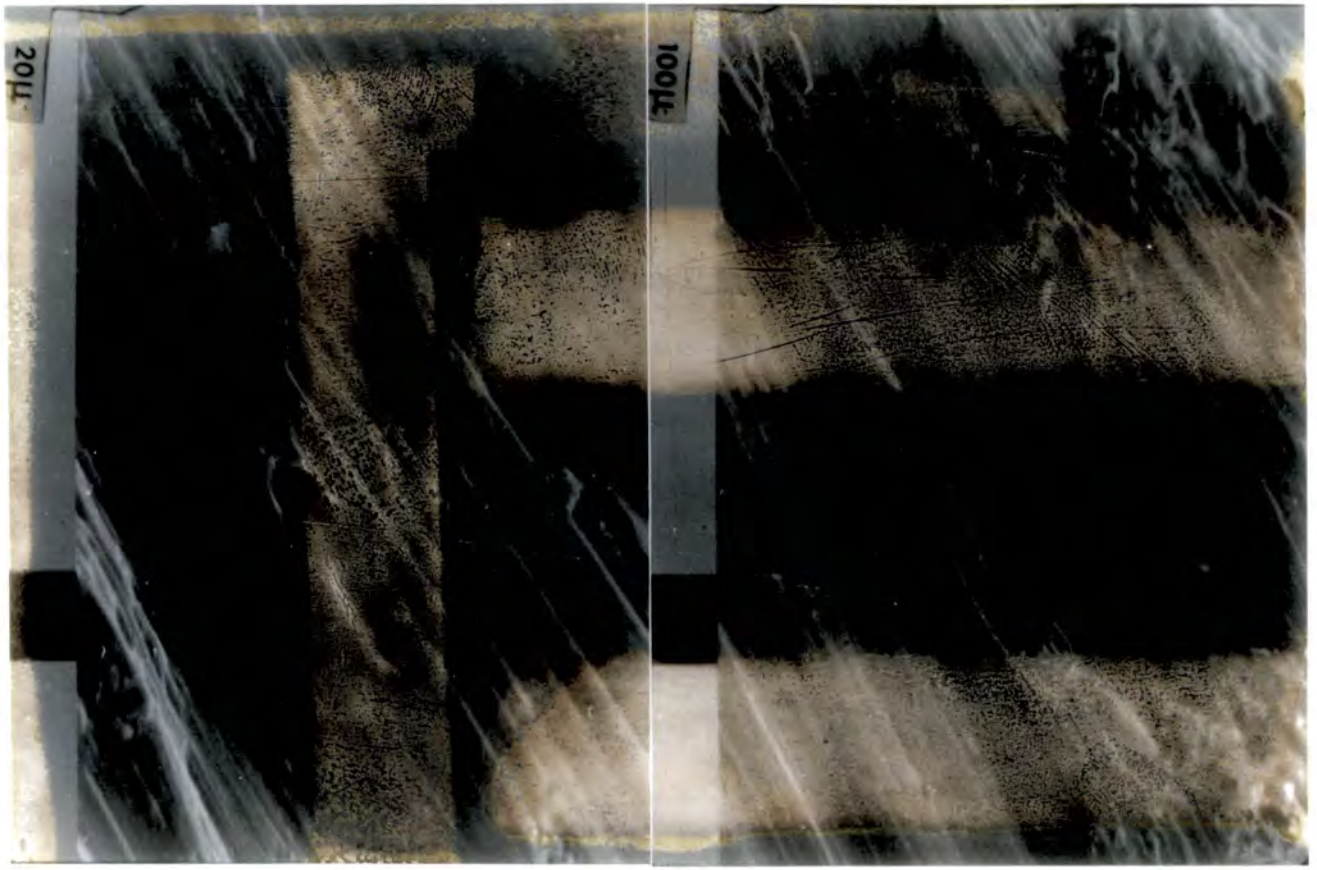

Figure 5.12 SEM images of the foliation surfaces in the Miocene rocks along the thrust contact between the Miocene and Urgonian rocks. (See Section 5.2.13).
Foliation surfaces deformed by pressure dissolution. Displacement, later in the deformation produces the striations.

making up this sample, the carbonate is probably derived from Cretaceous limestones as no massive carbonate formations occur within the Miocene. The similarity of the microstructures between this sample and samples from the minor faults within the Urgonian described in Chapter 4, indicates that the carbonate gouge clasts may have been derived from the Urgonian. This indicates that the zone of sheared molasse is part of the deformation zone which developed after the formation of the fault zones within the Urgonian limestones. They cut across and re-deformed these fault zones, incorporating the material which shows the microstructural textures of the early fault zones. Also the microstructures of the early fault zones within the Urgonian were indurated and impermeable to fluids flowing during the later deformation. This is indicated by the fact that the carbonate gouge does not stain blue and was therefore not infiltrated by the fluids which infiltrated the blue stained gouge. Extensional fracture porosity was needed to allow the pyrite and ferroan calcite saturated fluid and the fluid which contained hydrocarbons to flow through the pink-stained gouges. The hydrocarbons may have been undergoing migration at a different time from the fluids which precipitated ferroan calcite, because the two materials have not been found together within an individual fracture. Conversely, hydrocarbons and ferroan calcite saturated fluids may have co-existed as a two phase fluid. The presence of hydrocarbons may have restricted the precipitation of calcite in certain fractures so that the bitumens and ferroan calcite now exist in separate fractures. Cross-cutting relationships are ambiguous so that it cannot be demonstrated which of these possibilities is correct.

After the migration of the hydrocarbons, a phase of pressure dissolution occurred which seems to have concentrated the bitumen along pressure dissolution seams. Significant densities of these pressure dissolution seams are only found within the fault zone. They represent part of the fault zone deformation which occurred after hydrocarbon migration. This relationship suggests that the hydrocarbon migration occurred during the deformation and not subsequent to it.

The zoned nature of the calcite filling the extensional fractures in the carbonate clast indicates that slight variations in the cation geochemistry of the pore fluid. The ratio of iron and manganese in particular is thought to exert controls on the luminescence character of the material (Fairchild, 1983; Machel, 1985). The zones under cathodoluminescence may also reflect changes in the rate of crystal growth (Ten Have & Heijnen, 1985). The textures within the extensional fractures filled with ferroan calcite can give us information on the deformation history. The pointed terminations of the extensional fractures towards the edges of the carbonate clast suggests that the clast margins were in existence and rheological contrasts existed between the carbonate and the surrounding material at the time of extensional fracture formation.

The material outside the clast at this time is likely to have been deformed molasse material but this cannot be proved as grain size reduction along the clast margin has destroyed textural evidence for the earlier deformation. The fibrous to "blocky" transition in the texture of the ferroan calcite within the extensional fractures can also give insights into the deformation. The fibrous calcite has formed because calcite deposition has kept pace with the opening of the fracture (see Section 5.2.12). It also suggests that the fracture was opening slowly relative to the rate of migration of the pore fluid responsible for the cement precipitation. The "blocky", euhedral crystals within the centre of the extensional fracture-fill, suggest that fracture opening occurred relatively quickly relative to the rate of fluid migration. As discussed in Section 5.2.12, this may mean that the extensional fractures opened slowly to start with and then suddenly widened. It could, however, mean that the rate of fluid migration was initially fast so that cement precipitation kept pace with fracture opening, and then slowed. As discussed in Section 5.2.12, in the absence of extremely high flow rates, a change in the strain rate is the favoured model for producing these textures.

Deformation within the black molasse-derived material involved grain size reduction to produce gouges and the friction-dominated scratching of gouge clasts against indurated foliation surfaces to produce striations. These are the textures developed along the discrete minor faults.

The attitude of the extensional fractures and the pressure dissolution seams suggests that a component of flattening has occurred during the deformation with the maximum flattening direction normal to the attitude of the fault zone as a whole. However, this does not fully describe the finite strain within the fault zone because the gouge zones have presumably caused a component of simple shear within the fault rocks.

As a whole this portion of the fault zone displays similar textures to those described in Chapter 4. The ideas presented in Section 4.4 can be successfully applied here to discuss the deformation style and fluid flow within this portion of the thrust zone. However, the presence of discrete minor faults at outcrop which clearly cross-cut earlier textures, as shown in Figure 5.7, adds another aspect to the picture. The textures along these minor faults within the deformed molasse material indicate the action of DMT and cataclasis so that episodic fluid migration along these faults probably occurred (see Section 5.2.10). The textures away from the minor faults within the carbonate gouge clasts suggest a similar but earlier style of deformation. If the formation of such minor faults occurs during fault zone displacement then these faults may form early in the deformation, be destroyed by later deformation and then

form again in a cyclic fashion. The appearance of these minor faults produces temporal and spatial changes in the deformation and fluid flow within the fault zone.

Section 5.2.15 Sample 12g

Figure 5.13 shows the microstructure of sample 12g which occurs within the 60cm thick carbonate gouge zone along the thrust contact between the Miocene and the Urgonian rocks (see Figure 3.19). The texture is mainly composed of blue-stained carbonate gouge. Clasts up to 1mm across contain the texture of an early blue-stained gouge which became indurated before further cataclasis isolated the clasts. Also clasts up to 3mm across whose texture is that of a pink-stained carbonate gouge are cut by extensional fractures filled with calcite. These pink-stained clasts were also indurated before further cataclasis isolated the clast. The whole texture is cut by red iron oxide-rich pressure dissolution seams. Fractures associated with the pressure dissolution seams are translucent in transmitted light but fluoresce a dull burgundy colour under UV-Fluorescence. This material is as yet unidentified.

Section 5.2.16 Sample 12g- Discussion

Induration and permeability reduction in the pink-stained gouges occurred prior to deformation and fluid flow within the blue stained gouges. This is indicated by the fact that the pink clasts were isolated by brittle fracture which can only occur in materials which exhibit a certain elastic strength. Also the pink clasts were not infiltrated by the fluids which precipitated the material which has stained blue.

Section 5.2.17 Sample 12a

Figure 5.14 shows the microstructure of sample 12a which is a carbonate clast within the zone of sheared molasse. The clast is composed of a relatively undeformed limestone which contains a variety of grains. Carbonate peloids and bryozoan fragments occur together with sub-angular quartz grains which show undulose extinction and the development of internal sub-grains. These grains are held together by a calcite cement. This is a sample of the Senonian limestones which occur stratigraphically between the Urgonian limestones and the Miocene molasse. The block of limestone at the extreme western end of Figure 3.19, where samples Fw1, Fw2, Fw3 and Fw4 were taken, is also composed of Senonian limestones. Sample 12a is cut by a series of fractures. Figure 5.14 shows a set of extensional fractures filled with blue-stained ferroan calcite, cutting across an earlier extensional fracture containing pink-stained calcite. These extensional fractures filled with ferroan calcite formed after a phase of grain size reduction and gouge production within the

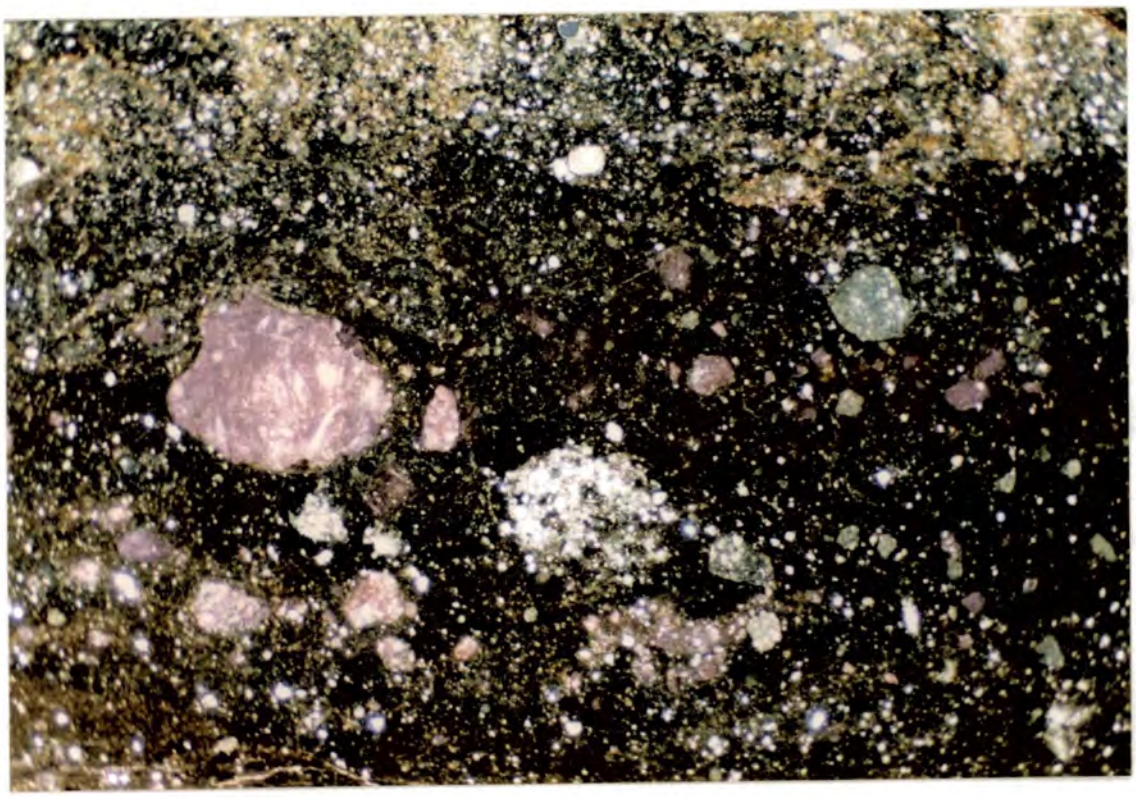

Figure 5.13 Photomicrograph of sample 12g (see Section 5.2.15).
Field of view is 15mm.

Figure 5.14 Photomicrograph of sample 12a (see Section 5.2.17).
Field of view is 15mm.

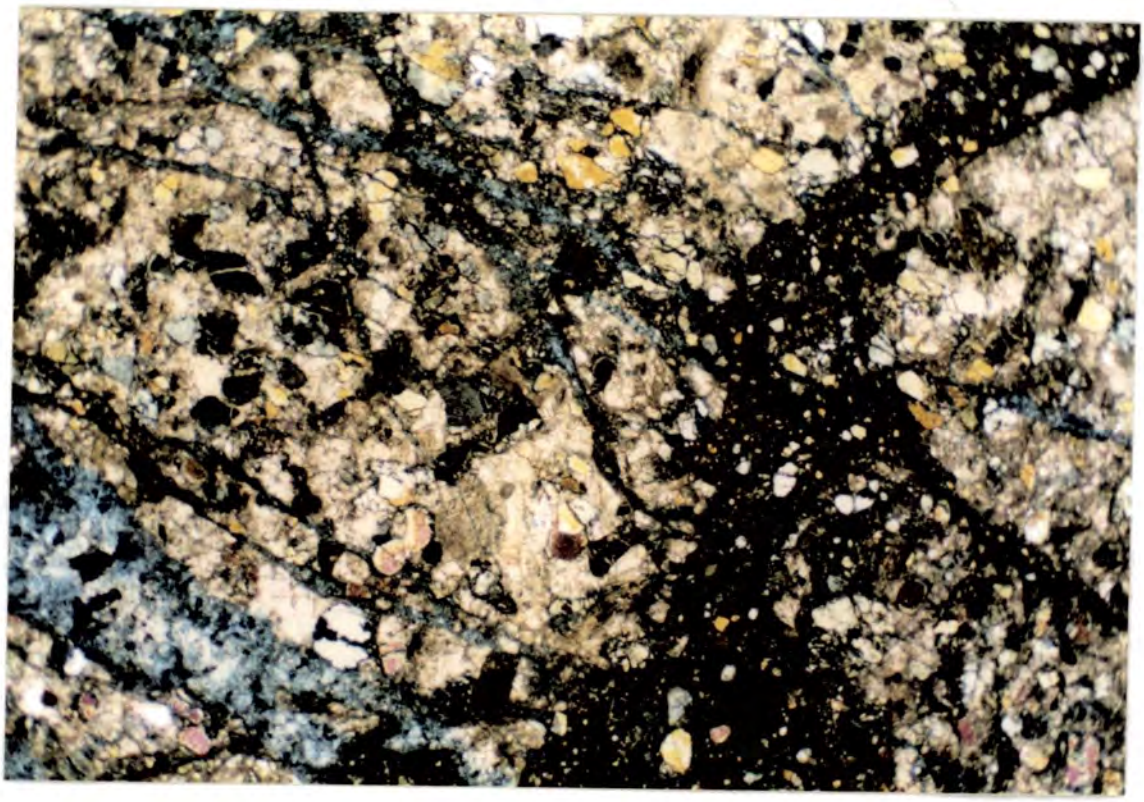

limestone. Both sets of extensional fractures show euhedral "blocky" crystals and the extensional fractures filled with ferroan calcite exhibit drusy fabrics with small crystals on the fracture margins and large crystals in the centre of the fracture-fill. Both sets of extensional fractures are non-luminescent under cathodoluminescence. No evidence for the existence of bitumens or hydrocarbons can be seen. Rare opaque grains can be seen to be pyrite under reflected light within the extensional fractures filled with ferroan calcite.

Section 5.2.18 Sample 12a- Discussion

The early deformation and fluid flow in this sample involved extensional fracturing and the migration of fluids saturated with respect to calcite. This calcite precipitation had occluded the fracture porosity before cataclastic gouge production, extensional fracturing and the flow of fluids saturated with respect to ferroan calcite had begun. The euhedral crystals and drusy fabrics within these extensional fractures indicate that fluid migration and crystal growth occurred in fluid-filled fracture porosity. At first sight the extensional fractures filled with ferroan calcite within this sample seem to be related to the extensional fractures filled with ferroan calcite described from the samples along the thrust contact between the Miocene and the Urgonian rocks. However, these extensional fractures filled with ferroan calcite are non-luminescent and are not associated with bitumens in contrast to the examples along the thrust contact between the Urgonian and Miocene rocks. In Section 6.3 it will be shown that the ferroan calcite infilling these two contrasting extensional fracture sets also have different $\delta^{13}C$ and $\delta^{18}O$ stable isotopic signatures. It will be suggested that the fill to these two extensional fracture sets may record fluid flow which occurred at different times during the structural evolution of the Rencurel Thrust Zone and in different locations on the restored section of the thrust zone.

Section 5.2.19 Sample 64

This Section describes the lithology of the Miocene molasse which is exposed well away from the thrust zone, 300 metres to the west along the D103 road at grid reference 8469 3139. This sample is described to complete the picture of pre-faulting lithologies which has been built up by the descriptions of the Urgonian wall-rock lithologies in Chapter 4 and the Senonian limestones in Section 5.2.17. The sample is a fine-grained well-sorted sandstone. X-ray diffraction analysis of the sample has revealed the presence of quartz, muscovite, calcite, chlorite, feldspar, kaolinite and dolomite. In thin section at least 60% of the sample is composed of sub-angular quartz grains which have a maximum grain size of around 0.1mm. The quartz grains have uneven margins and contain pyrite inclusions. Sericitised and poorly preserved

feldspars now make up around 30% of the texture. The feldspars have very irregular margins and some examples have intracrystalline pore spaces. These textures suggest that the feldspars have undergone a phase of chemical dissolution. This dissolution may also have formed the irregular margins to the quartz grains. Abundant flakes of muscovite also occur. The muscovite is generally not bent or distorted around the other grains. Filling the pore spaces between these grains is a blue-stained ferroan calcite cement. The mica flakes project into the areas of ferroan calcite. The ferroan calcite also surrounds remnants of feldspar grains and fills holes within the feldspar grains. Chlorite can be seen within the areas of feldspar dissolution. Also glauconite accumulations exist within the original intergranular pore spaces, which are now filled with ferroan calcite.

Section 5.2.20 Sample 64- Discussion

The mineralogy and internal textures of the grains suggest they were derived from metamorphic rocks which contained quartz, plagioclase, muscovite and pyrite. The presence of glauconite suggests that the sediment was deposited in a marine environment. Mechanical compaction of the sandstone does not seem to have been significant, as mica grains are generally not distorted. This gives a clue as to when the diagenetic ferroan calcite was precipitated in the pore spaces. Feldspar dissolution and filling of the pore spaces must have occurred at shallow burial depths, otherwise the muscovite flakes would have become bent and distorted as burial took place. Distortion of the muscovite flakes would occur due to the re-packing of grains to fill the secondary porosity during mechanical compaction. The chlorite and kaolinite may be the breakdown products of the feldspar dissolution. The sandstone was cemented by ferroan calcite filling secondary porosity before significant burial took place.

SECTION 5.3 DISCUSSION OF DEFORMATION AND FLUID FLOW ALONG THE THRUST CONTACT BETWEEN THE URGONIAN AND THE MIOCENE ROCKS

The areas of deformation described in this Chapter exhibit microstructures which are essentially similar to the microstructures described in Chapter 4. This Section will compare and contrast the microstructures preserved along the minor faults within the Urgonian and preserved along the thrust contact between the Urgonian and the Miocene. This information will then be used to discuss the deformation style and the fluid flow which occurred along the thrust contact between the Miocene and the Urgonian.

Section 5.3.1 Microstructures produced by cataclasis along the thrust contact between the Urgonian and the Molasse.

The four main styles of microstructure produced along the minor faults within the Urgonian described in Section 4.4.1, are also important along the thrust contact between the Urgonian and the Miocene. Thin zones of fine-grained fault gouge and single extensional fractures filled with cement can both be recognised and occur on the same scale as those described from the minor faults within the Urgonian. Zones of wall-rock breccia are also present, but where they grade into areas of poorly-sorted gouge, the gouge zones are generally much thicker than those described along the minor faults within the Urgonian. The gouge zone along the thrust contact between the Miocene and the Urgonian is around 60cm wide compared to the gouge zones along the minor faults which are around 5-10cm wide. Also the microstructures are different in the two widths of gouge. The largest clasts within the 60cm thick gouge zone are composed of indurated fine-grained gouge contrasting with the clasts of predominantly wall-rock limestone along the minor faults within the Urgonian.

Important processes within the gouge zone along the thrust contact between the Urgonian and the Miocene seem to be grain size reduction so that original wall-rock lithologies cannot be recognised, and cyclic induration and cataclasis producing re-worked gouge clasts. As discussed in Section 4.4.1, cataclasis is the process which will increase fluid flow along this gouge zone. However, the influx of fluids promote the processes of DMT which work towards sealing the fault zone. The role of independent particulate flow in the deformation is not clear as grain re-packing is difficult to recognise within these samples. The implications of this are discussed in Section 4.5.

Section 5.3.2 Microstructures produced by the action of DMT along the thrust contact between the Urgonian and the Molasse.

Areas of cement in former fracture porosity and pressure dissolution seams are found along the minor faults within the Urgonian and along the thrust contact between the Urgonian and the Molasse. The areas of fine-grained material which show evidence for being washed around by migrating fluids are not commonly found along the thrust contact between the Urgonian and the Miocene.

The fluid chemistry is different with more negative Eh ferroan calcite and pyrite saturated pore waters and hydrocarbons, as opposed to calcite saturated pore waters along the minor faults in the Urgonian.

As discussed in Section 4.4.2, pressure dissolution causing chemical compaction, together with cement precipitation both work towards reducing the permeability of the fault rocks.

Section 5.3.3 Insights into the faulting mechanisms from deformation mechanism studies along the thrust contact between the Miocene and the Urgonian

The microstructures along the thrust contact between the Miocene and the Urgonian are essentially similar to those along the minor faults within the Urgonian. The discussion of faulting mechanisms presented in Section 4.5 can also be applied to the fault rocks described in this Chapter. This Section summarises the observations from Section 4.5 which can also be applied to the fault rocks discussed here and also points out some other conclusions which can be drawn.

Section 5.3.3.1 Nature of the cyclic deformation along the thrust contact between the Urgonian and the Miocene.

The microstructures show that DMT and cataclasis were active deformation mechanisms. A range of strain rates great enough to activate DMT and cataclasis was therefore active along this part of the Rencurel Thrust Zone. Strain rate changes occurred in a cyclic manner as evidenced by cross-cutting relationships between microstructures characteristic of DMT and cataclasis. The actual range of strain rates and form of the cyclic deformation is not clear. The microstructures and strain accommodation are dominated episodes of high strain rate cataclastic deformation. DMT occurred between the episodes of cataclasis. The destructive nature of the cataclasis leads to incomplete evidence for a more complicated model for the deformation. The model for the nature of the cyclic deformation is therefore only a simplest case which is likely to be incomplete. Importantly, the role of frictional grain boundary sliding without fracture within this part of the fault zone is also open to question (see Section 4.5.1). It is not clear how much of the deformation was accommodated by the action of this deformation mechanism. As discussed in Section 4.7, this may lead to uncertainty concerning the completeness of any proposed deformation mechanism path.These are essentially the same conclusions which can be drawn for the minor faults within the Urgonian.

Section 5.3.3.2 The mechanical and chemical effects of fluid influx.

The influx of fluids promoted fracture processes and promoted DMT along the thrust contact between the Urgonian and the Miocene rocks. It may also have promoted the

action of independent particulate flow. Seismic pumping may have been active in causing fluid migration. These conclusions are essentially similar to those drawn from study of the minor faults within the Urgonian described in Chapter 4. See Section 4.5.4 for a more detailed discussion.

Section 5.3.3.3 Spatial and temporal changes in the position of deformation.

Study of the thrust contact between the Urgonian and the Miocene highlights two instances when the changing position of deformation is important.

Firstly, discrete minor faults within the gouge zone along the thrust contact between the Miocene and the Urgonian rocks, cut across earlier textures which have already undergone induration and permeability reduction. This suggests that fluid flow would be localised along the minor faults during fracturing events which occur along their length. The development of these minor faults within pre-existing gouge zones therefore causes temporal and spatial changes in deformation and fluid flow during the history of the gouge zone.

Secondly, on a larger scale, the thrust contact between the Urgonian and the Miocene seems to have cut across the pre-existing zone of minor faults within the Urgonian. The evidence for this is the existence of pink-stained clasts of carbonate gouge with microstructures similar to those seen to be being disaggregated from the minor faults within the Urgonian. These clasts were indurated and relatively impermeable during deformation and fluid flow along the thrust contact between the Miocene and the Urgonian. Figure 5.15 shows the distribution of samples within the Rencurel Thrust Zone which show evidence for being infiltrated by ferroan calcite. The ferroan calcite is restricted to the thrust contact between the Miocene and the Urgonian. The flow of fluids saturated with respect to ferroan calcite and pyrite carrying hydrocarbons, occurred after the cessation of fluid flow and deformation which occurred along the minor faults within the Urgonian. The fluids were localised along a 2-3 metre thick zone along the thrust contact between the Miocene and the Urgonian rocks, structurally underneath the zone of impermeable minor faults within the Urgonian. Deformation along this thrust contact did not fracture the Urgonian limestones and fault rocks along the minor faults within the hanging-wall to this part of the thrust zone. The evidence for this is that no ferroan calcite has been found within the Urgonian. This suggests that the indurated and impermeable fault rocks of the minor faults within the Urgonian acted as a migration barrier during deformation and fluid flow along the thrust contact between the Urgonian and the Miocene.

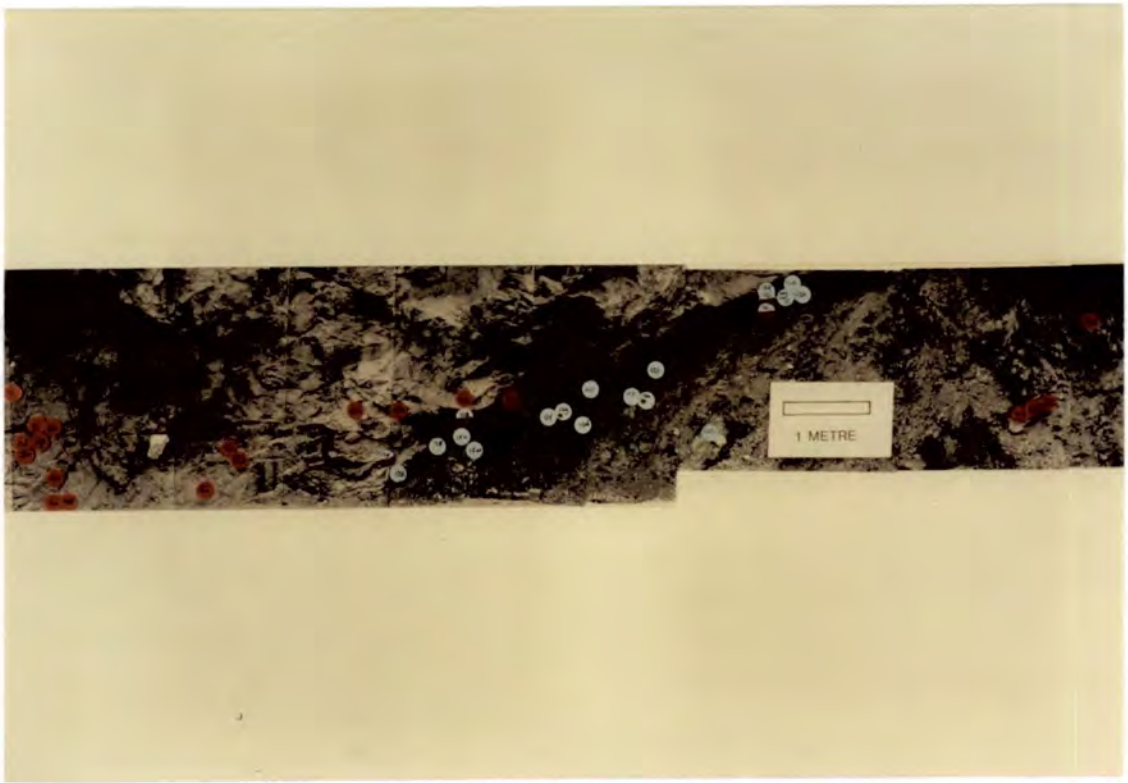

Figure 5.15 Distribution of samples containing ferroan calcite within the Rencurel Thrust Zone.

Red dots - Samples contain Calcite cements
Blue dots - " " Ferroan Calcite cements
½ red / ½ blue - Top of sample contains calcite. The bottom contains Ferroan calcite cements.
Blue dots with red spots - Calcite-rich gouge clast contained in a sample of ferroan calcite-rich gouge.

Section 5.3.4 Fault Zone Model

This Section incorporates some of the points made during the discussion of the deformation along the minor faults within the Urgonian (see Section 4.6). This information is combined with points raised in the discussion of the samples from along the thrust contact between the Urgonian and the Miocene presented in this Chapter. What follows is the presentation of a model for the spatial and temporal changes in fluid migration and deformation which occurred during the development of the Rencurel Thrust Zone. The model can only be applied in full to the Urgonian limestones, due to the level of exposure within the thrust zone.

Deformation of the Urgonian began with the development of minor faults. Fluids saturated with respect to calcite underwent episodic migration in areas where episodic fracturing occurred during high strain rate deformation. The role of grain boundary sliding without fracture as a deformation mechanism is not clear. Fluid flow would have occurred during the action of this mechanism due to the dilatant nature of the deformation as clasts move past each other opening intergranular pore spaces. Fluid flow would have promoted the action of DMT processes which occurred during slow strain rate episodes, sealing the fault rocks. At any time during the deformation, localised deformation occurred along fault zones, whilst the terminations of faults were marked by zones of more distributed deformation. Cross cutting relationships indicate that fault zones grow into tip zones. Distributed deformation and fluid flow had ceased within the tip zones before they were penetrated by localised fault zones. However, fluid flow and sealing events occurred simultaneously within fault zones and the areas of deformation at their terminations. Also the permeability of any individual area of the actively deforming minor faults within the Urgonian, varied during the microstructural evolution.

The minor faults within the Urgonian had ceased to be part of the deformation and fluid flow system before they were cut by the deformation which was to form the thrust contact between the Urgonian and the Miocene. Fluids migrating during episodic fracture events within this growing zone of localised deformation contained hydrocarbons and were saturated with respect to ferroan calcite and pyrite. Fluid flow would also have occurred during the action of grain boundary sliding without fracture as a deformation mechanism but the importance of this is difficult to assess. Fluid flow was, however, confined to the localised deformation zone, underneath the zone of minor faults within the Urgonian, which were relatively impermeable at this time. The deformation at this time did not involve widespread fracturing of this zone of minor faults. The influx of fluids may also have promoted the action of DMT which will have worked towards lithifying the gouge. The temporal changes in deformation

mechanism produced temporal variations in the permeability of the fault rocks. Cross-cutting relationships indicate that temporal and spatial changes in the deformation occurred. This would have caused temporal and spatial changes in the permeability during the history of the fault rocks. The action of DMT at the end of the deformation finally sealed the Rencurel Thrust Zone.

Section 5.3.5 Comparison of the microstructures of the thrust contact between the Urgonian and the Miocene rocks with those of the minor faults within the Urgonian

This Section discusses possible reasons why the microstructures and thickness of the gouge zone along the thrust contact between the Urgonian and the Miocene are different from those of the minor faults in the Urgonian.

The predominance of indurated gouge making up the large clasts along the thrust contact between the Urgonian and the Miocene rocks, as opposed to predominantly wall-rock clasts along the minor faults in the Urgonian suggests two things. Firstly, grain size reduction has reached a more advanced state along the thrust contact between the Urgonian and the Miocene, so that it is now more difficult to recognise wall-rock lithologies. Secondly, induration of the gouge was occasionally well developed along the thrust contact between the Urgonian and the Miocene. The strength of the contacts between the gouge clasts were occasionally as strong as the internal strength of the carbonate clasts themselves. When this level of induration was achieved, further high strain rate deformation involved the fracturing of indurated gouges producing large clasts of re-worked gouge, rather than further reducing the size of the individual carbonate clasts. As discussed in Section 4.5.1, at other times the gouge may have been more poorly indurated and high strain rate deformation may have been accommodated by grain boundary sliding without fracture.

Section 5.3.6 Localisation of displacement onto a single gouge zone

This Section addresses the question of why the majority of the displacement in the Rencurel Thrust Zone may have become localised along the thrust contact between the Miocene and the Urgonian.

As described in Section 4.5.1 as the grain size reduction occurs during fault displacement, the localisation of displacement onto a single gouge zone may be demoted by the following.

1) Gouges may become more difficult to deform by the action of dependent particulate flow as a deformation mechanism. This is due to the decrease in stress concentrations at grain-to-grain contacts retarding fracture.

2) The efficiency of DMT processes may be increased by the shorter diffusion distances involved in fine-grained materials promoting induration of the gouge and an increase in strength.

However, in Section 4.5 and 4.8 it is suggested that when a gouge reaches a certain thickness and grain size of gouge, the localisation of displacement onto a single fault zone can be promoted by the following.

1) Strain rate partitioning.

2) High fluid pressures concentrated in the dense arrangement of sealed fault rocks which exist around a larger fault zone.

3) Relative strain hardening which may occur in the smaller gouge zones.

4) The low yield strength of fine-grained gouges undergoing frictional grain boundary sliding without fracture.

It may be that threshold levels exist in the factors controlling the deformation, which can change the balance between processes promoting and demoting fault zone localisation.

For example, consider the level of induration of a fault gouge. If a gouge achieves a level of induration during the action of DMT where the strength of grain-to-grain contacts becomes as great as the internal strength of the carbonate forming the clasts, renewed high strain rate deformation may take the form of fracturing the indurated gouge or the wall-rocks to the fault zone. In either case the grain size distribution of the gouge is altered because of the production of large clasts of either wall-rock or indurated gouge. The result would for a time, remove the retarding effect of small grain sizes on dependent particulate flow. The gouge zone could once again undergo grain size reduction during dependent particulate flow, until the grain size reduction once again causes strain hardening of the gouge and the cessation of fracturing. If induration processes are indeed fully lithifying the material, the permeability reduction which follows from such lithification, may lead to the build up of fluid pressures and the promotion of fault zone localisation.

Alternatively, if the gouge is only poorly indurated then the deformation may switch to frictional grain boundary sliding without fracture. The low yield strength of a fine-grained gouge undergoing the action of this deformation mechanism may lead to the localisation of displacement onto a single fault zone.

Section 5.3.7 Insights into the seismicity of the fault zone gained from the structural geology of the fault zone.

Figure 5.7 shows the nature of the discrete minor faults which are present within the gouge zone along the thrust contact between the Urgonian and the Miocene. The small size of these shears may be used to suggest something of the seismogenic nature of these fault zones. It has been suggested that large magnitude earthquakes occur along large faults whilst small magnitude earthquakes occur along small faults (Sibson, 1989). The minor faults within the gouge zones would certainly have released elastic strain energy and would have experienced stress drops because their microstructures indicate the action of brittle failure processes during the cataclastic periods of their deformation history. Earthquakes would have been produced during the deformation, but the magnitude of the earthquakes would probably be have been so small that if viewed on a large scale, the deformation would effectively have been aseismic. However these minor faults only represent the last few increments of deformation within this part of the fault zone. One cannot be sure if the earlier deformation history of the gouge involved displacement along similar small localised zones, because cataclasis has destroyed the textural evidence for the earlier deformation. It may be that large areas of the gouge zone were ruptured by large magnitude faulting events which caused widespread fracturing. Or it may be that the deformation of gouge zones changed with time perhaps activating deformation mechanisms such as frictional grain boundary sliding without fracture, which would have been almost completely aseismic. The deformation also may have involved a combination of these faulting styles. The basic problem here is that the seismogenic nature of the Rencurel Thrust Zone during its deformation history is not known. Thrust zones within neotectonic foreland thrust belts are known to produce earthquakes of significant size (King & Yielding, 1984). However, it may not be appropriate to assume that this style of faulting applies to all foreland thrust belts. For example variations in faulting style occur even within individual seismogenic fault systems. An example would be the highly seismogenic and aseismic portions of the San Andreas Fault System (Sibson, 1989). Not understanding the seismogenic nature of the Rencurel Thrust Zone is not a trivial problem when it is remembered that the fault has around 2km of displacement along it. Also the magnitude of earthquakes will control seismic pumping which is suggested to be the process responsible for driving fluid migration along fault zones.

The spatial variation in deformation and fluid flow which is recorded in exhumed fault zones such as the Rencurel Thrust Zone, may give some clues as to the seismogenic nature of ancient faults. The Rencurel Thrust Zone has been suggested to have accumulated the majority of its displacement along a 2-3 metre thick zone along the thrust contact between the Urgonian and the Miocene. In Figure 5.15 it was shown that this zone is characterised by ferroan calcite cement which is not found in the other parts of the fault zone. The fluids involved in the deformation along this gouge zone did not leak out into other parts of the fault zone because of the existence of early faults on the margins of the gouge zone, which were fault seals at this time. Deformation along the 2-3 metre wide gouge zone did not induce widespread fracturing within the rocks outside the gouge zone. Fluids saturated with respect to ferroan calcite did not enter the rocks outside the gouge zone. If the deformation along this gouge zone involved large releases of elastic strain energy and the production of significant sized earthquakes, it is surprising that the wall-rocks to the gouge zone were not also fractured. Evidence from neotectonic fault zones including those in foreland thrust belts, suggests that aftershocks to earthquakes do not occur along the main fault trace, but fracture the wall-rocks to the fault trace (King & Yielding, 1984; Sibson, 1989). This line of reasoning suggests that the seismogenic nature of the Rencurel Thrust zone when it was accumulating the majority of its displacement, involved releases of elastic strain energy so small, that the wall rocks to the 2-3 metre wide active part of the fault zone, were not fractured. It may be that in order to produce the 2km of displacement now seen along the fault, faulting events and displacement may have been occurring almost continuously. The fault zone was effectively undergoing fault creep. The small stress drops required by this model also suggest that seismic pumping may have occurred only over short distances, but would have been active almost continuously, so that large scale fluid fluxes could still have been achieved.

CHAPTER 6 THE NATURE OF THE FLUIDS INVOLVED IN THE DEFORMATION ALONG THE RENCUREL THRUST ZONE.

SECTION 6.1 INTRODUCTION

In Chapters 4 and 5, the existence of calcite and ferroan calcite cements together with minor amounts of pyrite filling former fracture porosity have been described and discussed. They indicate that fluids saturated with respect to calcite, ferroan calcite and pyrite have migrated through the fracture porosity, precipitating material as cement. Further evidence for migrating fluids takes the form of internal sediment now filling former fracture porosity. The presence of bitumen within the fractures along the thrust contact between the Urgonian and the Miocene rocks indicates that hydrocarbons were also present within the pore fluids involved in the deformation. This chapter is aimed at further elucidating the nature of the fluids involved in the deformation. Section 6.2 describes a study using X-ray diffraction techniques. Section 6.3 presents the results of ^{18}O and ^{13}C stable isotope analysis.

SECTION 6.2 X-RAY DIFFRACTION (XRD) STUDIES WITHIN THE RENCUREL THRUST ZONE

XRD studies were carried out to augment the petrological observations of fluid involvement in the deformation. As with petrological studies, any mineral found within the fault rocks, but not within the wall-rocks to a particular deformation zone, will be the result of the breakdown of wall-rock minerals or the precipitation of new minerals within the fault rocks.

The wall-rocks and fault rocks to various elements of the Rencurel Thrust Zone were subjected to XRD analyses. This study is described in the following Sections.

Section 6.2.1 XRD studies of the minor faults within the Urgonian.

Fault zones 9, 4 and 5 were selected for study (see Figure 3.19). Bulk samples of the gouge and undeformed wall-rock along each of the faults were compared. Specimens were sawn in half, and samples were taken using a standard dentists drill from one of the sawn faces. A thin section was prepared from the other sawn face so that the wall-rock samples could be shown not to include vein-fill material. The samples were drilled from hand specimens 9f, 4a and 5ci.

Section 6.2.2.Results

The mineralogies of all the gouges, and all the wall-rocks showed various combinations of calcite and dolomite. No XRD peaks representing the presence of other minerals were found. The XRD equipment at Durham can detect quartz and pyrite down to 1-2% and clays down to around 5%.

Section 6.2.3 Discussion

The actual percentages of calcite versus dolomite in the gouges are probably heavily influenced by the mineralogy of the original wall-rock carbonate. No previously undescribed minerals or alteration products were identified along the minor faults using XRD techniques. Petrological descriptions of the fault rocks in Chapter 4 indicate that calcite is found as a new mineral filling fracture porosity along these fault zones. These cements are cross-cut by later fault zone deformation indicating that they precipitated syn-kinematically from fluids saturated with respect to calcite.

Section 6.2.4 Thrust contact between the Urgonian and the Miocene.

Two samples were studied from this part of the fault zone. One sample was taken from the black sheared Miocene molasse in hand specimen 12c (see Section 5.2.13 for microstructural description). The other sample came from hand specimen 64 of the undeformed Miocene molasse from grid reference 8469 3139 (see Section 5.2.19 for petrological description). The hand specimens were sawn in half. One sawn face was made into a thin section whilst the other was sampled using a dentists drill.

Section 6.2.5 Results

The fault rock in sample 12c contained quartz, calcite, muscovite, chlorite, felspar, illite kaolinite and dolomite. The undeformed Miocene in sample 64 contained the same mineralogies; however, the chlorite and the mica peaks were lower in amplitude and spread over a greater range of 2 theta (θ). Greater percentages of calcite and dolomite were found within the fault rock.

Section 6.2.6 Discussion

No new minerals can be proved to exist within the fault rocks of sample 12c using XRD techniques. Kaolinite may be a cement, but is equally likely to have been derived from the breakdown of the feldspars. The illite may have resulted from the breakdown of muscovite. These possible breakdown minerals cannot be demonstrated

to occur along microstructures which are syn-kinematic. Their occurrence is not confined to within the fault rocks. Fault zone fluids cannot be invoked to explain their presence. They may be related to recent sub-aerial weathering of the outcrops. The higher concentrations of calcite and dolomite may be related to original wall-rock mineralogical variations or the preferential cementation of the fault zone by carbonate cements.

Section 6.2.7 Summary of XRD studies within the Rencurel Thrust Zone.

XRD studies combined with petrological studies have shown that calcite, ferroan calcite, pyrite and hydrocarbons were the main components which were transported within fluids migrating syn-kinematically within the Rencurel Thrust Zone. The recognition of minerals using XRD without the support of textural observations, cannot be used to infer the chemistry of the syn-kinematic fluids. XRD cannot simply differentiate between carbonate minerals derived from grain size reduction of the wall-rocks, and new carbonate minerals precipitated within the fault zone.

SECTION 6.3 ^{18}O AND ^{13}C STABLE ISOTOPIC STUDY OF THE RENCUREL THRUST ZONE

Section 6.3.1 Introduction

The structural studies described in Chapters 4 and 5 have outlined the spatial and temporal changes in the deformation, fluid migration and fluid composition which occurred during the incremental development of the Rencurel Thrust Zone. This information allows the ^{13}C and ^{18}O stable isotopic techniques to be used in a systematic manner. Areas of the fault zone which have interacted with fluids of different compositions at different times can be sampled separately. This methodology can be applied at an outcrop scale, sampling different elements of the fault zone geometry, or on a smaller scale sampling individual elements of the texture of a fault rock. This is analogous to the way ^{18}O and ^{13}C stable isotopes are used in studies of diagenesis in carbonate sedimentary rocks. Elements of the rocks which have formed under different diagenetic conditions such as allochems or different fracture-filling cement generations are sampled separately. This methodology allows the maximum amount of information to be extracted from the study (Hudson, 1977; Dickson and Coleman, 1980; Arthur et al., 1983; Tucker & Wright, 1990).

In the case of the Rencurel Thrust Zone, different fracture-filling cement generations and fault generations identified by structural studies were sampled separately. The smallest area possible to sample using a 0.9mm diameter drill bit was around 1.2mm

across. The veins which were generally not much wider than 1.2mm thus could only provide a bulk sample of the cements which filled them. Also only bulk samples of the fine-grained gouges could be achieved using this sampling technique. These bulk samples therefore represent an average value for the material. Conclusions drawn from these values must therefore be tempered with this knowledge. Where possible individual elements of the rock textures were sampled, such as areas of dolomite rhombs, skeletal fragments and cements. Bulk wall-rock samples were also taken so that comparisons could be made with the bulk gouge samples. In reality this is probably a good comparison to make because the gouges are in fact composed of a bulk sample of the wall-rock, mixed during grain size reduction.

Section 6.3.2 Stable isotopic investigation of the minor faults within the Urgonian.

Figure 6.1 shows ^{13}C and ^{18}O stable isotopic signatures of samples taken from along the minor faults within the Urgonian. The samples included calcite filling extensional fractures forming veins within the fault gouges, bulk samples of the fault gouge, bulk samples of the wall-rock and separate elements of the wall-rock.

Section 6.3.3 Discussion

The calcite filling veins represented in Figure 6.1 has a dull luminescence and is not zoned (Chapter 4). This suggests that the cation chemistry of the pore waters did not alter significantly during the incremental precipitation of the cement. The stable isotopic variations may also have been insignificant. The percentages of calcite and dolomite within the wall-rocks and gouges are very variable. In Appendix 3, gouges from the minor faults which were predominantly composed of dolomite are indicated. Appendix 3 contains the isotopic data for different fractions of the wall-rock.

The calcite filling veins within the fault zone is relatively depleted in ^{13}C and ^{18}O (values around -4.0 per mil $\delta^{13}C$ and -8.5 per mil $\delta^{18}O$) compared to the other samples from the fault zone, the majority of which plot in the same general area (values around +1-3 per mil $\delta^{13}C$ and -2 to -7 per mil $\delta^{18}O$). The only exception to this being the one sample of calcite filling secondary intercrystalline porosity within the dolomitic wall-rocks which plots in the same general area as the vein filling calcite.

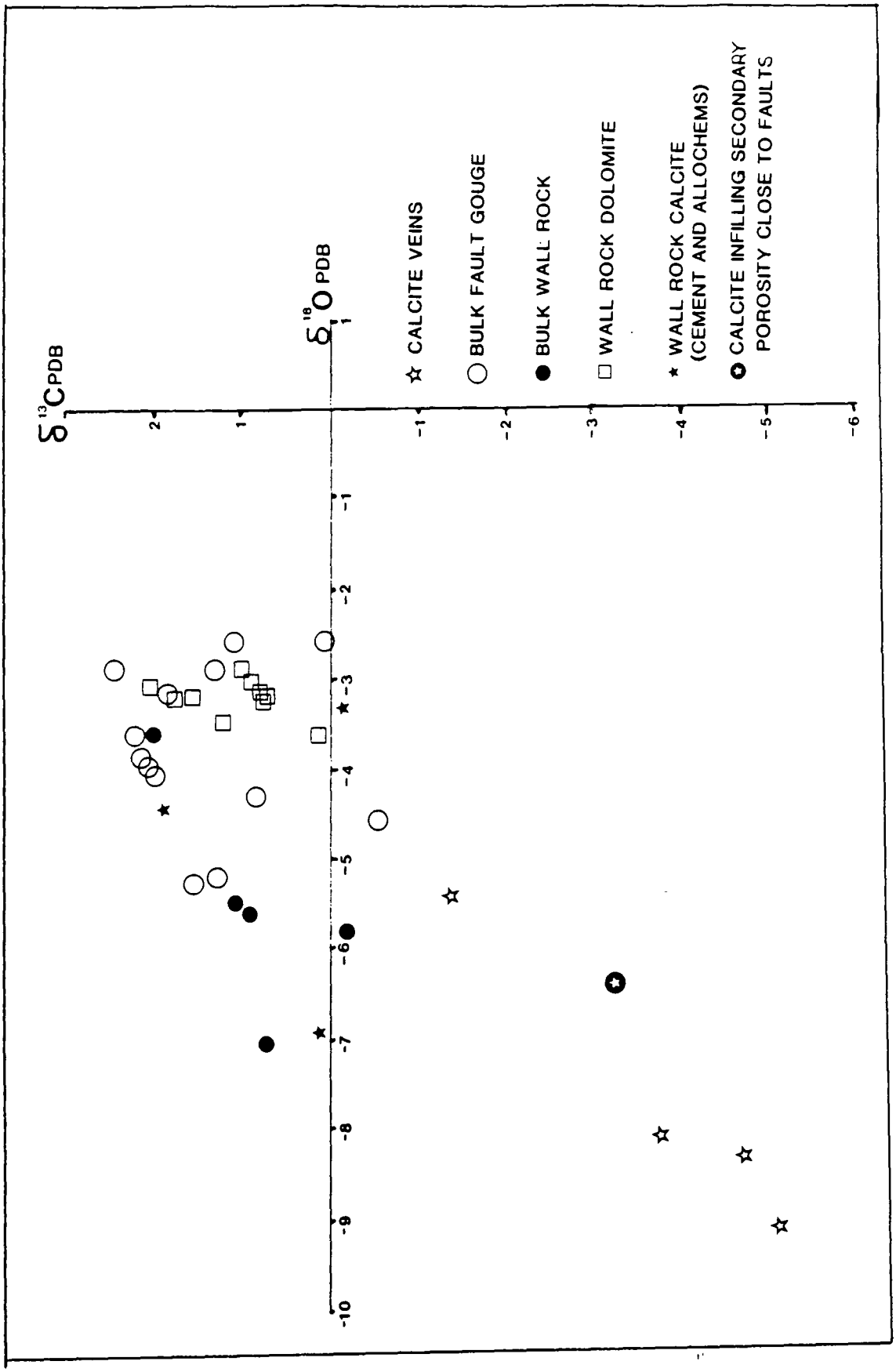

Figure 6.1 Cross-plot of $\delta^{18}O$ and $\delta^{13}C$ stable isotopic data for the minor faults within the Urgonian.

Section 6.3.3.1 Bulk gouge values compared to those of the bulk wall-rocks

The bulk gouge signatures seem to reflect the signatures of the bulk wall-rocks from which they are derived.

Two scenarios exist for fluid migration through these gouges.

Firstly, fluids may have interacted with material from outside the immediate wall-rocks and then been introduced into the gouges by large scale open system migration. Cements of different isotopic signature from those of the immediate wall-rocks may have been precipitated from these fluids or the latter may have altered the isotopic signature of material derived from the wall-rocks through recrystallisation. However, any products of these processes must exist in small quantities as the isotopic signatures of the gouges is the same as those of the wall-rocks.

Secondly, DMT within the gouges may be a closed system process with fluids never interacting with material other than the immediate wall-rocks. Isotopic compositions of newly precipitated intergranular cements or recrystallised material would closely match the signatures of the local wall-rocks which underwent dissolution to provide the material.

No data as yet exist as to the changes in actual flow rates and permeabilities of the gouges which occur during the cyclic deformation which they experienced. Without this input it is difficult to decide whether a diffusion-dominated closed system model, or a high fluid flux open system model is applicable for the gouge induration process. Trace element data may help to elucidate the problem of open or closed system models by providing data on the water to rock ratios. Trace element studies were not carried out due to time constraints but may prove to be a fruitful line of further research. This problem is discussed further in Section 6.3.5.3.

Section 6.3.3.2 Calcite filling the extensional fractures (veins).

The negative values of $\delta^{18}O$ and $\delta^{13}C$ for the calcite filling the extensional fractures within the gouge zones may reflect the input of externally derived fluids. During the diagenesis of organic matter, CO_2 which is light in ^{13}C is generally liberated (Tucker and Wright, 1990). Pore waters which are influenced by the thermal alteration of organic matter in the burial realm therefore develop light $\delta^{13}C$ values. The calcite cements in the extensional fractures discussed here may have been precipitated from pore waters which show the influences of thermal alteration of organic matter. The spore colouration index for the Hauterivian limestones and shales which occur

stratigraphically below the Urgonian rocks in the Rencurel Thrust Sheet is yellow-yellow/orange (see Figure 2.22). This indicates that the rocks are under mature (see Figure 2.23), and that any significant thermal alteration of organic matter must have occurred deeper within the stratigraphic section. A Vitrinite Reflectance value of 1.46% for a sample of Oxfordian carbonate from deeper in the section sampled within the Drac valley at grid reference 8593 2874 on BRGM La Chapelle en Vercors (1967), indicates that thermal alteration was significant enough to take the formation across the oil generation window. Pore waters which show the influence of this organic maturation may have migrated up-section into the minor fault zones within the Urgonian. Coming from deeper in the section it would be expected that the waters would be relatively hot compared with pore waters which had time to equilibrate thermally with their surrounding wall-rocks. If the pore fluids migrated up-dip quickly enough so that they did not equilibrate thermally with the wall-rocks then this may explain why the cements precipitated by the pore waters within the extensional fractures have light ^{18}O values. Figure 6.2 shows that for a pore water of given $\delta^{18}O$ value (SMOW), calcite precipitated from that water becomes progressively depleted in ^{18}O with increasing temperature. An alternative view is that the pore waters did have time to thermally equilibrate with the wall-rocks, but the wall-rock temperatures were still hot enough to precipitate cement with ^{18}O values lighter than the Urgonian wall-rocks. Another scenario could be that the pore waters were simply more depleted in ^{18}O than the waters which existed during formation of the wall-rocks (diagenetically altered sea water for the limestones and deep basinal pore fluids for the dolomites).

The pore waters which infiltrated the extensional fractures along the minor faults within the Urgonian seem to have migrated up dip from an area undergoing thermal alteration of organic matter. The pore fluids may have been migrating quickly enough to retain relatively high temperatures which were inherited from deeper in the section or may simply have had a composition which was light in ^{18}O.

Section 6.3.3.3 Calcite cements filling secondary intercrystalline porosity within the dolomites

The calcite cements which fill secondary intercrystalline porosity within the dolomites (described in Section 4.3.4.2) share the same isotopic signatures as the calcite cements filling the extensional veins. Petrographically the two calcites are similar, both being non-luminescent. The crystal silts within the secondary porosity indicate that the pore fluids responsible for cement precipitation were undergoing migration at significant velocities at the time. This may support the scenario presented in Section 6.3.3.2 that the light ^{18}O signatures may be due to the fact that the fluids

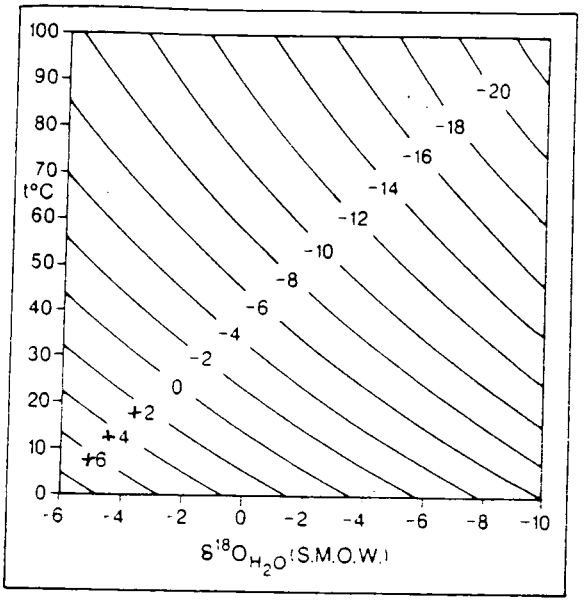

Figure 6.2 Equilibrium relationship between $\delta^{18}O$ of calcite, temperature and $\delta^{18}O$ of water; x-axis represents $\delta^{18}O$ values of water (SMOW); y-axis represents temperature between 0 and 100°C. The curved lines represent constant $\delta^{18}O$ values (PDB) for calcite. (From Tucker & Wright, 1990).

were relatively hot, having migrated fast enough so that they did not have time to equilibrate thermally with the wall-rocks. However, this is only tentatively suggested.

The secondary intercrystalline porosity was formed before the faulting because the dolomites are cut by the cataclasis along the fault zones. This all suggests that the fluids migrating through extensional fracture porosity within the fault zones, and then percolated out of the fault zones and through wall-rock porosity. The fracture porosity and the secondary intercrystalline porosity in the wall-rocks became occluded by the precipitation of calcite cements from these pore waters.

Section 6.3.3.4 Implications

The timing of the deformation along these faults can give insights into the manner by which the rocks underwent burial and thermal alteration. The minor faults within the Urgonian accommodate only small displacements and structural studies have shown them to have been active early in the history of the Rencurel Thrust Zone. Yet at this time the effects of thermal maturation seem to be present within the microstructures along these fault zones. This suggests that the thermal alteration due to burial was not induced by thrust sheet loading during emplacement of the Rencurel Thrust Sheet. Also, no large changes in thermal maturity are seen today across major thrusts within the Vercors which is not what would be expected if thrust sheet loading had been the primary cause of burial and thermal alteration (Figure 2.22). This all suggests that maturation of hydrocarbons was already underway before the thrusting. Burial diagenesis and thermal maturation may have been the result of basin subsidence and depositional burial.

Also, the fact that the minor faults in the Urgonian accommodate only small displacements, suggests that the deformation occurred before any significant thrust related uplift of the hanging-wall rocks. This scenario, when combined with the discussions presented in Sections 2.5.4, 6.3.3.2 and 6.3.3.3 suggest that the diagenesis which occurred along these fault zones and in their immediate wall-rocks probably occurred in the burial realm at depth of at least 2km or more beneath foredeep sediments and younger Mesozoic rocks.

Section 6.3.3.5 Summary

The minor faults within the Urgonian seem to have acted as pathways for the up-dip migration of pore waters from deeper in the stratigraphy where thermal maturation of organic matter was underway. The migration occurred through extensional fracture porosity. The same fluid flow system may have been operative during the

deformation of the gouge or alternatively, the gouge may have experienced its own closed system fluid involvement. This is discussed further in Section 6.3.5.3. Pore waters seem to have moved out of the fault zones into the wall-rocks, locally filling wall-rock porosity.

Section 6.3.4 Ferroan calcite filling extensional fractures (veins) along the thrust contact between the Miocene and the Urgonian

Figure 6.3 shows the $\delta^{13}C$ and $\delta^{18}O$ stable isotopic signatures available to aid discussion of fluid flow along the thrust contact between the Urgonian and Miocene. All the wall-rock data for the Rencurel Thrust Zone are also plotted here.

Section 6.3.5 Discussion

The data for the ferroan calcite veins divide into two groups. The first group has $\delta^{13}C$ values between -1 and 1 and $\delta^{18}O$ values between -6 and -8. All these veins occur within blue-stained carbonate gouges. The second group all have $\delta^{13}C$ values between 0 and -1 and $\delta^{18}O$ values between -2.5 and -3.5. All these veins with the exception of sample 12cv occur within clasts of Senonian limestone caught up in the fault zone. Sample 12cv is a blue-stained carbonate gouge clast with ferroan calcite veins, surrounded by a coating of gouge derived from the Miocene molasse. Notes taken during the sampling record that the veins were thin and difficult to sample and that the sample may have become contaminated with material from the gouge derived from the Miocene. The isotopic signature of the gouge derived from the Miocene is plotted in Figure 6.3 and shows a similar signature to 12cv which reinforces the idea that the sample became contaminated in the way described above. Thus, there seem to be two sets of ferroan calcite veins distinguishable using the stable isotopes of ^{18}O and ^{13}C, one found in gouges and one found within Senonian limestones.

Section 6.3.5.1 Ferroan calcite veins within the blue-stained carbonate gouges.

The ferroan calcite fill to these veins is zoned under cathodoluminescence (Section 5.2.13). The stable isotopic values discussed here are likely to represent average values for the calcite due to the crude sampling technique.

The calcite in these veins share the same $\delta^{13}C$ values as the wall-rocks but have lighter $\delta^{18}O$ values. The veins are found in association with hydrocarbons which, because of the low maturity levels of the wall-rocks at the present erosion level of the fault zones suggest that the pore fluids migrated up-dip along the fault zone. It is suggested that the light $\delta^{18}O$ values for the vein calcite may be the result of

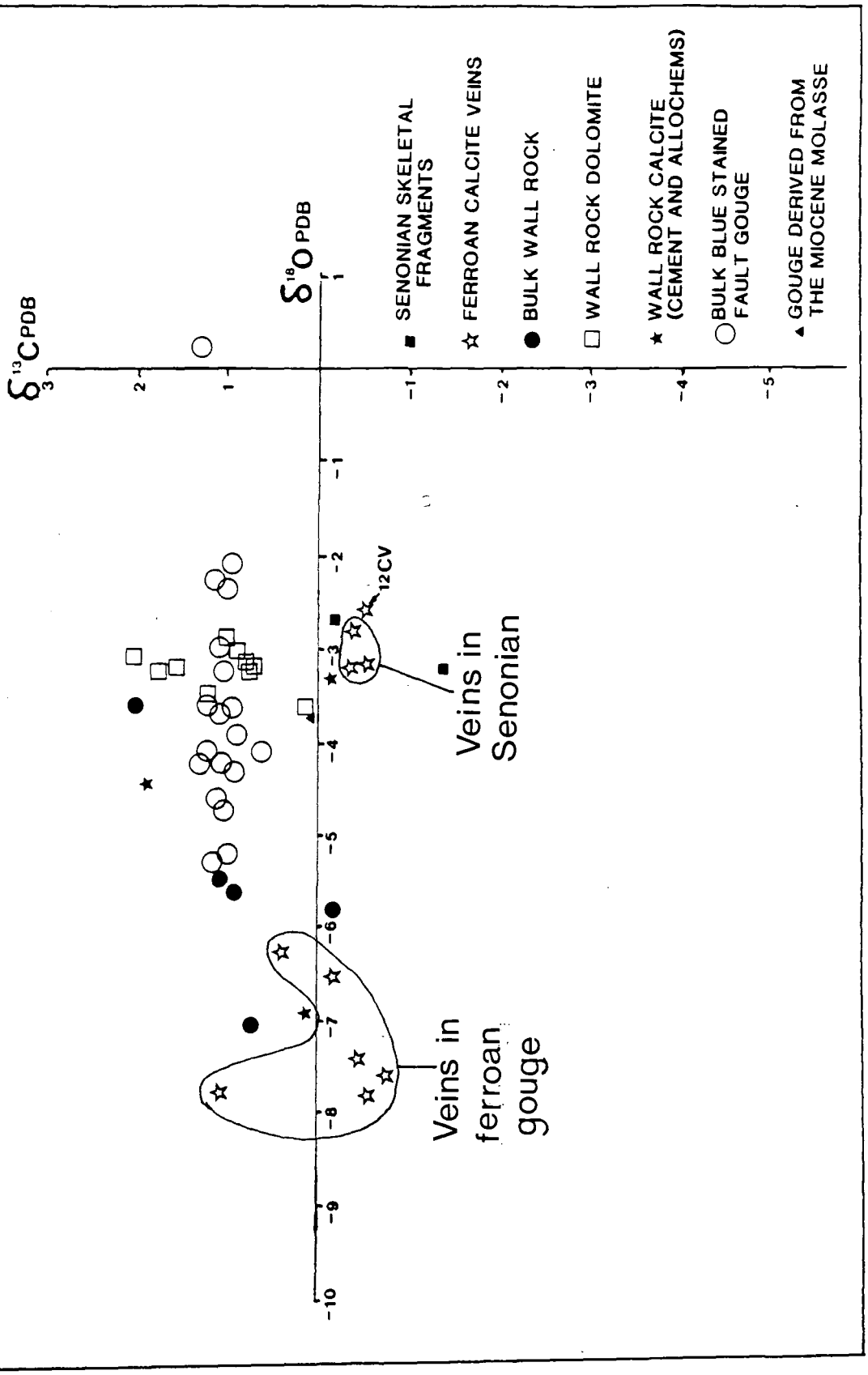

Figure 6.3 Cross plot of $\delta^{18}O$ and $\delta^{13}C$ stable isotopic data for the thrust contact between the Miocene and the Urgonian.

precipitation from pore waters which migrated up-dip carrying hydrocarbons. If the fluid migration velocities were high enough, these pore waters would have been relatively hot, hence the light $\delta^{18}O$ values (Section 6.3.3.2). The actual temperatures may be estimated using the graph in Figure 6.2 if an $\delta^{18}O$ composition for the pore water is assumed, but no evidence is available as to the pore water composition. This data could be attained by the ^{18}O stable isotopic analysis of the contents of fluid inclusions within the calcite if they can be found. However, the time constraints on this study did not allow the collection of these data. Alternatively, it may be that the ferroan calcite was precipitated from waters which were diagenetically altered and were depleted in ^{18}O (Section 6.3.3.2).

The fault rocks have a high density of pressure dissolution seams within them suggesting that the wall-rock material within the fault rocks would have been a source of ^{13}C for the pore fluids within the fault zone. This may be why the $\delta^{13}C$ values are similar to those of the wall-rocks. The high levels of pressure dissolution may have swamped the pore fluids with relatively heavy ^{13}C, masking the existence of light ^{13}C in the upward migrating pore water derived from areas undergoing organic maturation. The $\delta^{13}C$ values are typical values for a marine limestone (+1 to -1 per mil) and so the Jurassic marine limestones deeper in the section could equally well have been the source of the ^{13}C.

Section 6.3.5.2 Ferroan calcite veins within the clasts of Senonian limestone

These veins are not zoned under cathodoluminescence. The stable isotopic composition of the pore water is therefore likely to have remained relatively constant.

The timing of vein formation within the Senonian limestone clasts is thought to have occurred before the advent of widespread cataclasis and gouge production as discussed in Section 5.2.18. Unfortunately, the Senonian limestones are not well exposed in the immediate footwall to the Rencurel Thrust Zone. This makes it difficult to decide exactly when the veins formed. They may have formed early in the development of the Rencurel Thrust Zone or even before this time. Whichever of these scenarios is correct, the veins still record some of the diagenetic history of the area which was to become part of the Rencurel Thrust Zone. The $\delta^{13}C$ and $\delta^{18}O$ values for the calcite fill to the veins closely match those of the Senonian limestones and the Urgonian limestones. The ferroan calcite may have been precipitated from waters which either reflect the isotopic signature of the immediate wall-rocks or the isotopic signatures of an externally derived fluid which precipitated cement with similar isotopic values to the wall-rocks. It is not as yet clear whether the fluid circulation was in an open or closed system. If the system was open to externally

derived fluids, the relatively enriched $\delta^{13}C$ and $\delta^{18}O$ values for the calcite suggest that the waters did not move up-dip from significantly lower in the stratigraphy where higher temperatures existed and thermal alteration of organic material may have been occurring. This would have resulted in relatively light $\delta^{18}O$ and $\delta^{13}C$ values. The pore waters may have been derived from the down-dip migration of Tertiary sea water. The area of the Vercors was experiencing marine sedimentation throughout Aquitanian to Tortonian times (Debrand-Passard et al., 1984). If the veins formed early in the deformation along the Rencurel Thrust Zone at the same time as the veins along the minor faults within the Urgonian, comparison of the two sets of isotopic signatures suggests that stratified diagenesis was occurring as illustrated in Figure 6.4.

The hot pore fluids showing influences of the thermal alteration of organic matter within the lower parts of the stratigraphy would be unable to migrate up-dip because of the generally low porosity and permeability of the rocks below the Senonian limestones. For example the Hauterivian and Valanginian limestones and shales are generally fine-grained and compacted, containing little porosity. Also only small displacement faults of small dimensions would have existed at this time in the material which was to become involved in the Rencurel Thrust Zone. Deformation along the minor faults may not have produced fracture porosity which was sufficiently interconnected to allow large scale fluid migration along the fault zone.

The range of $\delta^{18}O$ values for the probable early veins suggests further complexity concerning the possible stratification of the pore water circulation. Figure 6.2 shows that for a pore water of given $\delta^{18}O$ (SMOW) composition, calcite precipitated at a given temperature will be around 6 per mil more positive in $\delta^{18}O$ than calcite precipitated from the same composition pore water which is 30°C higher in temperature. The $\delta^{18}O$ values for the calcite veins along the minor faults within the Urgonian are around 6 per mil more negative than the ferroan calcite veins within the Senonian which are suggested to have formed penecontemporaneously. Both vein sets may have been formed when the developing Rencurel Thrust Zone had accumulated only small displacements. The veins forming in the Urgonian would have been around 500-300 metres deeper than the veins forming in the Senonian which can be predicted by partially restoring the structural cross-section for the Rencurel Thrust shown in Figure 3.2. Unfortunately the exact stratigraphic position of the blocks of Senonian limestone caught up in the fault zone are not known, so that one cannot be more precise about the restoration of the fault zone. If the $\delta^{18}O$ of the pore water was the same over this depth range of stratigraphic section, it can be inferred that the pore waters were 30°C hotter in the Urgonian extensional fractures than the Senonian extensional fractures. This gives a paleogeothermal gradient in the ground water of between 30°C per 500 metres and 30°C per 300 metres which is a very high value.

This may support the idea that the pore waters were migrating up-dip from deeper in the section into the extensional fractures within the Urgonian. The pore waters were migrating at a velocity great enough so that they did not equilibrate thermally with the temperatures of the Urgonian wall-rocks.

Many assumptions are involved in the reasoning which lead to this conclusion. The most important assumptions include homogeneous pore water compositions across this depth range, equilibrium fractionation of the calcite during precipitation, the validity of the restoration of the fault zone geometry, the penecontemporaneous formation of the two vein sets early in the deformation, the validity of assuming that pore waters within the extensional fractures in the Senonian rocks were static and temperature of the pore water exerting the primary control on the isotopic signature of calcite cements.

Section 6.3.5.3 Comparison of the wall-rock isotopic signatures with those of the bulk gouge

The wall rock data and the blue-stained fault gouge data (Figure 6.3) plot in the same general area of the cross plot. This suggests that the bulk gouge isotopic signatures reflect the signatures of the original wall-rock from which they were derived. Either no recrystallisation of the gouge material has occurred or recrystallisation did not alter the isotopic composition. This same situation occurs in the gouges along the minor faults within the Urgonian (see Section 6.3.3.1). However, these gouges are stained blue and it was suggested in Section 5.2.12 that the staining was the result of the presence of ferroan calcite cements filling the intergranular pore spaces within the gouge. The wall-rocks to this gouge were suggested to be Cretaceous limestones at the time of the deformation and fluid flow, and these rocks contain little iron. The fluids from which the ferroan calcite precipitated probably interacted with material containing iron lying outside the fault zone and the immediate wall-rocks to the fault zone. The nearest source of ferrous iron would probably have been ferroan calcite cements and clays within the Miocene molasse sediments (see Section 5.2.19). Negative Eh pore fluids containing ferrous iron are also commonly associated with the diagenesis of organic matter which is thought to have been occurring deeper within the section (Tucker & Wright, 1990). This seems to rule out the possibility of closed system pore water circulation within the fault gouges which was suggested in Section 6.3.3.1 to be a possible reason why the bulk gouge signatures so closely matched those of the rocks from which they were derived by grain size reduction. This suggests that the cements make up such a small percentage of the volume of the gouge that their isotopic signature is masked by the isotopic signature of the wall-rock material in the gouge. It is also possible that the ferroan calcite cement thought to be

filling the intergranular pore spaces within the gouge has isotopic signatures very close to that of the wall-rocks.

Section 6.3.5.4 Summary

Ferroan calcite veins within the blue-stained gouges formed when the Rencurel Thrust had already accumulated large displacements. Relatively hot fluids may have been moving up-dip into the fault zone, precipitating relatively light $\delta^{18}O$ calcite and carrying hydrocarbons. Alternatively, the pore waters may have been diagenetically altered and depleted in ^{18}O. The action of intense pressure dissolution in the fault zone may have driven relatively heavy ^{13}C from the wall-rocks into the pore fluids which may have masked any relatively light $\delta^{13}C$ pore waters derived from the influence of organic maturation occurring deeper in the section. The resulting cements have $\delta^{13}C$ values which reflect those of the wall-rocks, or those of marine limestones which occur deeper in the section.

The ferroan calcite veins within the Senonian may have formed during the early history of deformation along the Rencurel Thrust Zone when only small displacements had accumulated. They seem not to have been connected to the fluid circulation system which may have existed contemporaneously deeper in the stratigraphy because they do not show signs of the effects of thermal alteration of organic matter which occurs in the veins formed lower in the stratigraphy. This may be because no well developed fault zone conduit was available to allow the pore waters to pass through the low permeability stratigraphy below the Senonian. The pore waters may have been derived from sea water which may have been at the surface at this time. This model is summarised in Figure 6.4.

Comparison of the $\delta^{18}O$ isotopic values between the ferroan calcite veins in the Senonian and the calcite veins within the Urgonian in conjunction with consideration of a partially restored cross-section of the fault zone highlights the difficulties in constraining the causes of $\delta^{18}O$ variation in the fault zone. It may be that the light $\delta^{18}O$ values indicate the rapid up-dip migration of pore waters from deeper in the section.

The gouge signatures are comparable to the wall-rock signatures yet the presence of intergranular cements rich in ferrous iron indicates that open system pore water circulation existed within the gouges. This suggests that the cements are simply not volumetrically important enough or have isotopic compositions similar to the wall-rocks so that they do not radically alter the bulk gouge signatures.

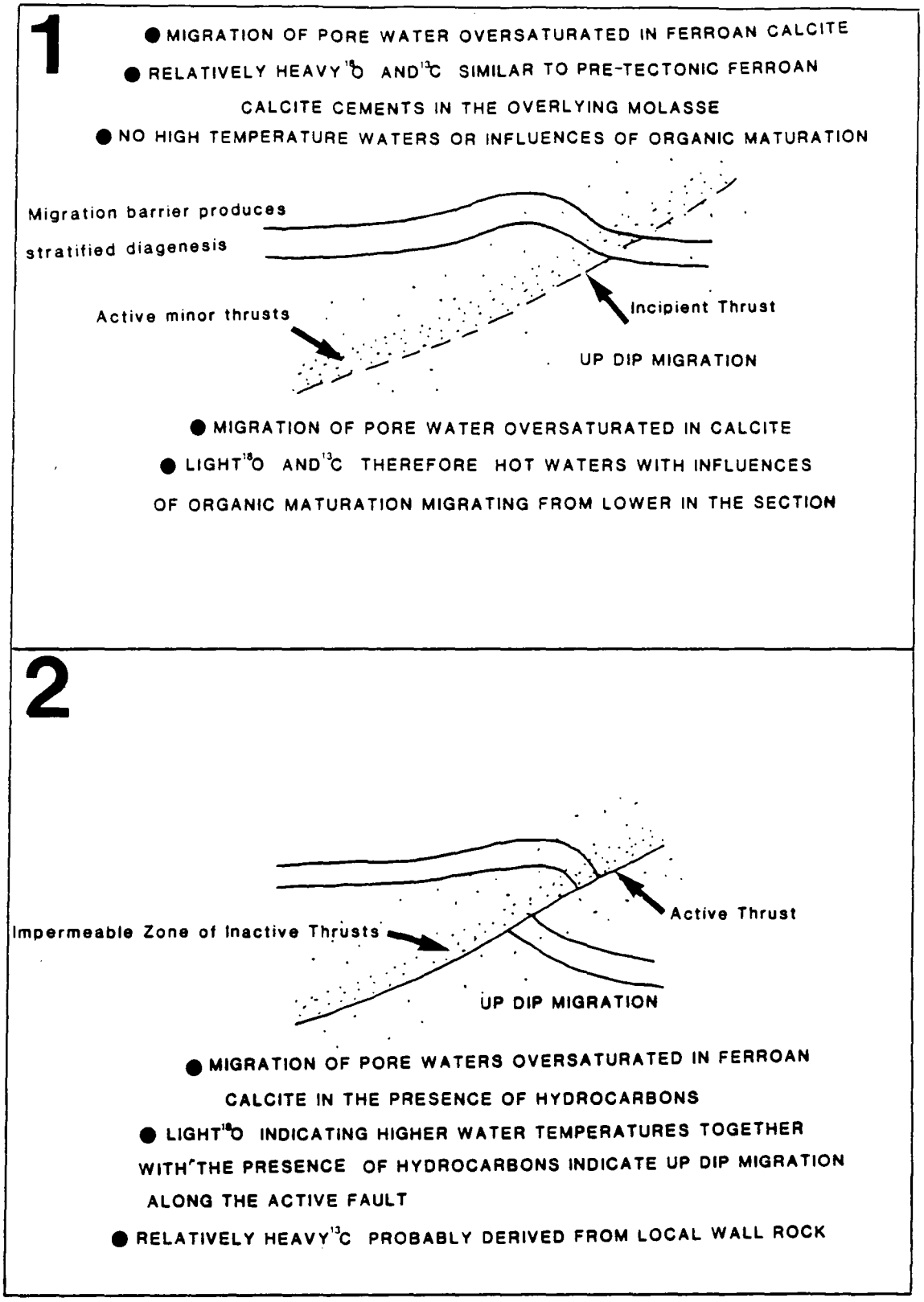

Figure 6.4 Model for the structurally controlled fluid flow through the Rencurel Thrust Zone.

Section 6.4 DISCUSSION

This Chapter suggests that only simple major changes in the pore fluid composition occurred during the deformation. In reality changes in fluid composition were probably more complex than this but their occurrence has not been recognised because the sampling procedure has been too coarse or the pore fluids migrated through the thrust zone without leaving significant petrological or geochemical signatures.

CHAPTER 7 PRESENT DAY PERMEABILITY OF ROCKS WITHIN THE RENCUREL THRUST ZONE

Section 7.1 INTRODUCTION

In Chapters 4 and 5 it is suggested that the porosity and permeability of the rocks in the Rencurel Thrust Zone has changed during microstructural evolution. It is not possible to state the actual values for porosity and permeability which existed during the deformation but relative values of porosity and permeability have been suggested in Chapters 4 and 5.

It is, however, possible to measure the permeability of the rocks which exist today within the Rencurel Thrust Zone. When these values are compared with the permeabilities of rocks from outside the thrust zone the effect which the fault zone may have had on sub-surface fluid migration after the cessation of deformation can be assessed. This chapter presents the results of such a study performed using a mini-permeameter.

Section 7.2 TECHNIQUES

Section 7.2.1 Sample collection and preparation

Hand specimens of the fault rocks from the Rencurel Thrust Zone, which deforms the lower parts of the Urgonian limestones were collected. Samples were also collected from the Gorges de la Bourne at grid reference 312 845 where the lower part of the Urgonian limestones are exposed away from the Rencurel Thrust Zone. The stratigraphy of this part of the Urgonian is given in Arnaud-Vanneau (1980). The samples were broken to present a freshly fractured clean face with no weathering effects.

Section 7.2.2 The equipment and technique.

The mini-permeameter measures the flow rate and injection pressure of compressed air within rock samples in order to determine permeability. The equipment was borrowed from Shell Research B.V., and consists of a portable suitcase-sized box which contains equipment which produces a supply of compressed air. Samples were analysed in the laboratory but the portability of the device also allows it to be used in the field. The specifications of the mini-permeameter can be found in Clelland, (1984).

In simple terms the instrument introduces compressed air into a sample from a pump at 0.1bar. The pump and the measuring valves are connected to the sample by means of a flexible plastic hose with a gun arrangement which is placed against the sample. A good seal between the sample and the gun is achieved by using a close-cell foam tip to the gun, which allowed slight deformation in order to adjust to slight irregularities on the surface being measured. Introduction of the compressed air to the sample was by means of a valve operated by a trigger on the gun. The flow rate of the compressed air was measured and the instrument gave a digital read-out of the result in cc/min. The flow rate was recorded once the reading had stabilised which was usually took <2 minutes. The flow rate was transformed into a permeability reading by means of the empirical relation given in equation 1.

$$\log_{10}k = 0.99(\log_{10}F) - 0.38 \qquad (1)$$

(where k=permeability in millidarcies; F= flow rate in cc/min)

This relationship was derived by measuring the flow rate of core plugs whose permeability was known through standard core analysis (Clelland, 1984). At the injection pressure of 0.1bar, the equipment is capable of resolving permeability measurements down to around 5 millidarcies (Chandler, 1989).

Section 7.3 RESULTS

The results of this study are shown in Appendix 2. The permeability recorded from the fault rocks is generally well below 5 millidarcies. These values are below the resolution of the equipment so that the actual permeability values are not shown in Appendix 2. The permeability values for the undeformed carbonates ranges from <5 millidarcies up to 220 millidarcies.

Section 7.4 CONCLUSIONS

The values of permeability for the fault rocks are generally below the detection limit of the equipment. The permeability values of the wall-rocks are generally above the detection limit of the equipment and occasionally reach values approaching those of oil and gas reservoirs (Dreyer et al., 1990). The fault rocks are significantly less permeable than the undeformed carbonates. The Rencurel Thrust Zone contains material which would be capable of being a seal to fluid flow in the sub-surface.

CHAPTER 8 CONCLUSIONS

1) The Vercors forms part of a foreland thrust belt, which is relatively well constrained structurally and stratigraphically compared to other foreland thrust belts (Sections 2.1 - 2.4).

2) The thrust geometries are influenced by pre-existing basin structures and stratigraphic variations (Section 2.5).

3) Post Miocene erosion during and after isostatic and thrust related uplift has exhumed the structures within the thrust belt (Section 2.5.4). Reasoning involving the interpretation of thermal maturation data for organic matter within the Vercors (Figure 2.22) suggests that the thickness of Miocene foredeep sediments prior to uplift and erosion may have been around 2.5km assuming a paleogeothermal gradient of 25°C/Km and 1.3km assuming a 35°C/Km paleogeothermal gradient.

4) The Urgonian limestones and the structures within the Vercors were potential reservoir rocks and structural traps prior to uplift and erosion. The rocks presently at the surface were never buried deeper than the diagenetic realm.

5) Thermal maturation studies indicate that hydrocarbon maturation may have occurred deeper in the section prior to thrusting (Section 2.5.4).

6) The Rencurel Thrust is an important regional structure and emplaces Mesozoic carbonates on to Miocene molasse rocks (Section 3.1).

7) The Rencurel Thrust sheet is heterogeneously internally deformed by thrusts and folds. Pre-existing faults are truncated by thrusts. Large thrusts within the thrust sheet such as the Ferrière Thrust and the Chalimont Thrust show a complex geometrical development history involving changes in the displacement localisation (Section 3.4). Structural data suggest that all the thrusts within the thrust sheet were formed during one kinematically linked phase of thrusting and can all be used in developing models of deformation and fluid flow through the thrust sheet. Individual thrust zones are generally less than 10cm wide and were formed by the action of DMT and cataclasis. The wall-rocks to individual thrusts are relatively undeformed by cataclasis. Syn-kinematic fluid migration can be demonstrated to have been controlled by the production of fracture porosity. This suggests that temporal and spatial changes in the deformation will produce temporal and spatial changes in the fluid migration.

8) The Rencurel Thrust changes its geometrical relationship to the stratigraphy along

strike and shows a complex internal geometry (Sections 3.5.2 and 3.5.3). The Rencurel Thrust Zone is composed of an array of minor faults within the Urgonian limestones which overlies a gouge zone which is at least four metres wide and which lies along the thrust contact between the Miocene and the Urgonian rocks. Structural data suggest that all the minor thrusts within the Rencurel Thrust Zone were formed during one kinematically linked phase of thrusting and they all can therefore be used in developing models of the deformation and fluid flow through the thrust zone (Section 3.5.4). Cross-cutting relationships exist which suggest that individual parts of the fault zone were deforming at different times. This suggests that the position where syn-kinematic fluid flow occurred may also have changed with time.

9) Deformation within the Rencurel Thrust Zone locally produced breccias but more commonly discrete gouge zones (Section 4.1 and Chapter 5). Syn-kinematic fluid migration cannot be proved to have occurred through these breccia zones (Section 4.2.2). The discrete gouge zones form a dense array of minor faults within the Urgonian rocks (Section 4.3); (Figure 3.19). Both extensional and compressional faults can be found within the Rencurel Thrust Zone (Section 4.3.3). Individual fault zones are less than 10cm wide and their wall-rocks are relatively undeformed. The wall-rocks do contain small fault zones coated in fault gouge which are less than 2cm across. These faults are difficult to spot at outcrop. The 4 metre wide gouge zone which exists along the thrust contact between the Miocene and the Urgonian contains discrete minor fault zones less than 1cm wide which cut across the early gouge fabric (Sections 5.2.9 & 5.2.13). All of these fault zones contain microstructures which indicate that DMT and cataclasis have been the dominant deformation mechanisms (Sections 4.4.1 and 4.4.2). Fault plane features include lineations in the form of striations but no mineral stretching fibres were found. Cements filling former fracture porosity and bitumen within the fault zones suggest that syn-kinematic fluid migration accompanied the deformation. The existence of crystal silts and washed in debris filling former fracture porosity suggests that fluids were migrating at significant velocities during the deformation. These features can also be used as geopetal structures when they fill only the bottom of pore spaces with the higher parts of the pore spaces filled with cement (Section 4.3.2.3).

10) Cataclastic processes are dilatant and initially increase the porosity and permeability of the fault zones (Section 4.4.1). DMT initially works towards destroying porosity and reducing the porosity and permeability of the fault zones. Cataclasis, however, causes grain size reduction and allows fluid influx both of which promote the action of DMT and sealing of the fault zone (Section 4.4.1). DMT increases the strength of the weak areas where deformation may formerly have been accommodated by sliding without fracture. This promotes the action of cataclasis and

generates fracture porosity (Section 4.4.2). It is not clear whether cement precipitation or chemical compaction is the dominant process causing gouge induration (Section 5.2.12). The dominant process of fracture porosity occlusion is cement precipitation and not the mechanical closure of the fractures. The existence of fibrous calcite in some of the veins may indicate that calcite precipitation kept pace with the opening of fracture porosity. Some pressure dissolution seams within the wall-rocks may be the result of burial related compaction. The seams appear to have acted as pathways for the migration of fluids causing burial dolomitization prior to thrusting (Section 5.2.2).

11) Complex cross-cutting relationships exist between the microstructures in the fault zones which suggests that the deformation involved cyclicity between DMT and cataclasis as the dominant deformation mechanism. This suggests that the porosity and permeability of the fault rocks change significantly during incremental deformation and microstructural evolution. Episodes of significant fluid flow during dilatant cataclastic events separate times when the fault zone is sealed due to the action of DMT (Section 4.6).

12) The role of frictional grain boundary sliding (independent particulate flow) during the deformation is not clear due to the difficulty of recognising grain re-packing. This causes problems when trying to assess the faulting mechanisms and deformation mechanism paths for the fault zones. Gouge zone deformation probably involved independent particulate flow and re-fracturing of gouge indurated by the action of DMT (Section 4.5); (Figure 4.19). Cataclasis destroys evidence for earlier deformation textures which further complicates the problem of assessing deformation mechanism paths for the fault zones.

13) The nature of the cyclic deformation is difficult to assess. A range of strain rates existed which was great enough to allow both DMT and cataclasis to be dominant deformation mechanisms at different times. However, the actual range of strain rates and the duration of individual levels of strain rate are not clear (Section 4.5.2 & 4.7).

14) Conclusions (12) and (13) make it difficult to propose realistic models to predict the actual permeability of the fault zones during the deformation (Section 4.5.2).

15) The mechanical effects of fluid influx into the fault zones is not clear. Fluid pressures may have exceeded lithostatic pressures inducing hydraulic fracturing. Alternatively the fluids may have been migrating due to fluid pressure gradients between the interiors of dilatant fractures and the wall-rocks (Section 4.5.4). Fluid influx also promotes the action of certain deformation mechanisms (Figure 4.19).

16) Spatial changes in the deformation occurred. At the scale of an individual minor fault within the Urgonian, the terminations of the faults may have undergone deformation during the growth in dimension of the faults during displacement accumulation. However, the faults grow into areas which have previously undergone deformation at the termination of the fault. The deformation at the fault termination has ceased to be accommodated by fracturing and is lithified by the action of DMT before the area is cut by the growing fault zone (Section 4.6). On the scale of the entire Rencurel Thrust Zone, deformation involving fracturing along the minor faults within the Urgonian had ceased and the fault rocks had become lithified before significant deformation and fluid flow occurred within the area which was to become the thrust contact between the Urgonian and the Miocene rocks (Section 5.3.4). During the deformation of the area which was to become the thrust contact between the Urgonian and the Miocene rocks, deformation did not produce fracturing of the hanging-wall Urgonian rocks. Fluid migration occurred within some parts of the fault zone simultaneously with the existence of fault sealing elsewhere within the fault zone.

17) The localisation of displacement involving fracturing into individual parts of the Rencurel Thrust Zone whilst other areas were abandoned may have been enhanced by strain rate partitioning between thin and thick fault zones, high fluid pressures concentrated in areas containing a high density of sealed microstructures and the rheological nature of the material exposed to the deformation (Section 5.3.6). This may have important implications for modelling the development of arrays of minor faults (Section 4.9).

18) The spatial and temporal changes in the deformation which occurred during the development of the Rencurel Thrust Zone occurred during a change in the composition of the pore fluids involved in the deformation. XRD and petrological studies have shown that calcite, ferroan calcite, pyrite and hydrocarbons exist within the fault zone and record the passage of pore fluids (Section 6.2).

Early deformation along the minor faults within the Urgonian was accompanied by the migration of pore waters saturated with respect to calcite. Stable isotopic studies (Section 6.3) indicate that these pore waters may have showed the influence of organic maturation which when combined with thermal maturation studies of the area suggest that the fluids were moving up-dip from deeper in the section. The faults only accommodate small displacements, which suggests that significant thermal maturation of organic matter occurred prior to the thrust related burial and loading (Section 6.3.3.4). They may have either been relatively hot or may have interacted with material which had light $\delta^{18}O$ values (Section 6.3.3.2). These pore waters leaked out

of the fault zones and locally occluded secondary porosity within the wall-rocks (Section 6.3.3.3). These pore waters may have existed simultaneously, but were spatially separated from pore waters involved in the deformation higher within the stratigraphy within the Senonian limestones. These pore fluids were saturated with respect to ferroan calcite and do not show significant influence of organic maturation, high temperatures or interaction with a supply of light $\delta^{18}O$. The separation of these two pore waters may be due to the fact that at this early stage in the deformation, the Rencurel Thrust Zone was not fully developed and was not as yet an efficient fluid conduit between different levels in the stratigraphy. The variation in $\delta^{18}O$ values between these two vein sets may be controlled by the temperature difference between the pore fluids they contained. The high gradient in temperature suggested by the $\delta^{18}O$ values may support the idea that rapid up-dip pore water migration occurred. The velocity of migration may have been fast enough so that the pore waters did not have time to equilibrate thermally with the wall-rocks prior to cement precipitation (Section 6.3.5.2).

Later deformation within the Rencurel Thrust Zone was accompanied by the migration of hydrocarbons and pore waters saturated with respect to ferroan calcite and pyrite which thermal maturation studies of the wall-rocks suggest may have migrated from deeper in the stratigraphy. The ferroan calcite precipitated from these pore fluids has light $\delta^{18}O$ values which may be due to up-dip pore water migration such that the waters did not have time to equilibrate thermally with the wall-rocks prior to cement precipitation. Alternatively, the pore waters may have been diagenetically altered so that they were depleted in ^{18}O. The $\delta^{13}C$ values of the cements may reflect the $\delta^{13}C$ values of the carbonate gouge and wall-rock material which was undergoing intense pressure dissolution in the fault zone at this time (Section 6.3.5.1).

These late pore fluids flowed through fracture porosity which existed within the material which was to become the thrust contact between the Urgonian and Miocene rocks. The porosity available at this time was restricted to fractures beneath the array of minor faults within the Urgonian which were sealed during this stage of the fluid flow. The pore fluids did not flow across this structurally produced migration barrier so that the potential structural trap in the form of the hanging-wall anticline to the thrust could not have been filled by hydrocarbon migration along this pathway. The rocks above the thrust zone will also not have been diagenetically altered by the fluids migrating up the fault zone at this time. Open system fluid migration was involved in the deformation of the gouges, but the products were too small volumetrically to effect significantly the isotopic signatures of the bulk gouge samples (Section 6.3.5.3). The deformation within the thrust zone directly controlled the diagenesis of

the fault zone and some aspects of the regional diagenetic patterns in the stratigraphy (Section 5.3.4).

19) The migration of fluids saturated with respect to ferroan calcite and pyrite in the presence of hydrocarbons was restricted to the area which was to become the thrust contact between the Miocene and the Urgonian rocks. The deformation which produced the fracture porosity which allowed this fluid migration did not fracture the hanging-wall rocks to permit fluid influx. This suggests that relatively large volumes of rock were not fractured during the deformation, such that the release of elastic strain energy as seismic waves may have been on a small scale. On a regional scale the Rencurel Thrust Zone may have been the site of fault creep. No evidence has been found for large releases of energy during large scale fracturing events so that the 2km of displacement which exists along the Rencurel Thrust Zone may have accumulated without the existence of large magnitude earthquakes (Section 5.3.7). at shallow depths.

20) The fault rocks in the Rencurel Thrust Zone exposed at the surface today are significantly less permeable than the Urgonian limestones exposed at surface which show permeabilities up to around 220 millidarcies. The fault zone may have been a fault seal controlling fluid flow at depth before it was exhumed by erosion during and after isostatic uplift (Chapter 7).

REFERENCES

Argand, E. (1916) Sur l'arc des Alpes Occidentales. Eclog. Geol. Helv. **14**, 145-191.

Arnaud, H. (1981) De la plate-forme urgonien au basin vocontien: le Barrémo-Bédoulien des Alpes occidentales entre Isére et Buech (Vercors Méridional, Diois oriental et Devoluy). Géologie Alpine, mém. **11**, 3 volumes, 804p.

Arnaud-Vanneau, A. (1980) Micropaléontologie, paléo-écologie et sédimentologie d'une plate-forme carbonatée de la marge passive de la Téthys: l'Urgonien du Vercors septentrional et de la Chartreuse (Alpes occidentales). Géologie Alpine, mém. **10**, 3 volumes, 874p.

Arnaud-Vanneau, A. & Arnaud, H. (1990) Hauterivian to Lower Aptian carbonate shelf sedimentation and sequence stratigraphy in the Jura and northern Sub-Alpine Chains (south eastern France and Swiss Jura). In: M.E. Tucker et al. (eds) Carbonate Platforms: Facies, Sequences and Evolution. Spec. Publs int. Ass. Sediment. **9**, 203-233.

Arthur, M.A., Anderson, T.F., Kaplan, I.R., Veizer, J. & Land, L.S. (1983) Stable Isotopes in Sedimentary Geology. Soc. econ. Paleont. Miner. Short Course No. **10**.

Bathurst, R.G.C. 1975. Carbonate sediments and their diagenesis, 2nd edition, Elsevier Scientific Publishing Company, New York, 658p.

Bathurst, R.G.C. (1987) Diagenetically enhanced bedding in argillaceous platform limestones: stratified cementation and selective compaction. Sedimentology, **34**, 749-778.

Bayer, R., Cazes, M., Dal Piaz, G.V., Damotte, B., Elter, G., Gosso, G., Hirn, A., Lanza, A., Lombardo, B., Mugnier, J-L., Nicolas, A., Thouvenot, F., Torrielles, G. & Vilien, A. (1987) Prémiers résultants de la traversée des Alpes Occidentales par sismique reflexion verticale (Programme ECORS-CROP), Compte Rendus de L'Academie des Sciences Paris **305**, 1461-1470.

Beach, A. (1981a) Thrust structures in the eastern Dauphinois Zone (French Alps), north of the Pelvoux Massif. J. Struc. Geol. **3**, 299-308.

Beach, A. (1981b) Thrust tectonics and cover-basement relations on the northern margin of the Pelvoux Massif, French Alps. Eclog. Geol. Helv. **74**, 471-479.

Borradaille, G.J. (1981) Particulate flow and the generation of cleavage. Tectonophysics **72**, 306-321.

Boyer, S. & Elliott, D. (1982) Thrust Systems. Bull. Am. Ass. petrol. Geol. **66**, 1195-1230.

BRGM (Bureau des Recherches Géologiques et Minières) (1967) Carte géologique de la France a 1:50 000, feuille La Chapelle en Vercors.

BRGM (Bureau des Recherches Géologiques et Minières) (1968) Carte géologique de la France a 1:50 000, feuille Charpey.

BRGM (Bureau des Recherches Géologiques et Minières) (1975) Carte géologique de la France a 1:50 000, feuille Romans-sur-Isére.

BRGM (Bureau des Recherches Géologiques et Minières) (1978) Carte géologique de la France a 1:50 000, feuille Grenoble.

BRGM (Bureau des Recherches Géologiques et Minières) (1983) Carte géologique de la France a 1:50 000, feuille Vif.

Briggs, R.C. & Troxell, H.C. (1955) Effects of the Arvin-Tehachipi Earthquake on spring and stream flows. In: Earthquakes in Kern County during 1952 (Ed. G.B. Oakeshoff) Calif. Div. Mines and Geol. Bull. **171**, 81-97.

Burley, S.D., Mullis, J. & Matter, A. (1989) Timing diagenesis in the Tartan Reservoir (U.K. North Sea): constraints from combined cathodoluminescence microscopy and fluid inclusion studies. Marine and Petroleum Geology **6**, 98-120.

Butler, R.W.H. (1982) The terminology of structures in thrust belts. J. Struc. Geol. **4**, 239-245.

Butler, R.W.H. (1983) Balanced cross-sections and their implications for the deep structure of the N.W. Alps. J. Struc. Geol. **5**, 125-137.

Butler, R.W.H. (1986) Thrust tectonics, deep structure and continental subduction in the Alps and Himalayas. Journal of the Geological Society. **143**, 857-873.

Butler, R.W.H. (1988) The geometry of crustal shortening in the Western Alps. In: Sengor, A.M.C. (ed) Tectonic evolution of the Tethyan regions. Proc. Nato Ad. Inst., Istanbul, Turkey. **C259**, 43-76.

Butler, R.H.W. (1989) The influence of pre-existing basin structure on thrust system evolution in the Western Alps. In: Cooper, M.A., Williams, G.D., (eds) Inversion Tectonics. Spec. Pub. Geol. Soc. Lond. 105-122.

Butler, R.W.H. in press. Thrust evolution within previously rifted regions: an example from the Vercors, French Sub-Alpine Chains. Memoria Societa Geologica Italiana, **389**.

Butler, R.W.H. in prep. Structural evolution of the western Chartreuse fold and thrust system, N.W. French Sub-Alpine Chains.

Chandler, M.A., Goggin, D.J. & Lake, L.W. (1989) A mechanical field permeameter for making rapid, non-destructive permeability measurements. J. sedim. Petrol. **59**, 613-635.

Clelland, W. (1984) Measurement and analysis of small scale permeability distributions in sandstones. Unpublished Ph.D. Thesis, University of Heriott Watt.

Collet, L.W. (1927) The structure of the Alps. Edward Arnold & Co. London. p289.

Debelmas, J. & Lemoine, M. (1970) The Western Alps: paleogeography and structure. Earth Sci. Rev. **6**, 221-256.

Debelmas, J. & Kerchove, C. (1980) Les Alpes Franco-Italiennes. Géologie. Alpine. **4**, 21-58.

Debelmas, J. (1983) Alpes du Dauphine. Masson, Paris, New York, Barcelone, Milan, Mexico, Sao Paulo. p198.

Debrand-Passard, S., Courbouliex, S. & Lienhardt, M.J. (1984) Synthése Géologique du sud-est de la France. Mémoire Bureau de Recherche géologiques et minières. Volumes **125-6.**

Dickson, J.A.D. & Coleman, M.L. (1980) Changes in carbon and oxygen isotopic compositions during limestone diagenesis. Sedimentology **27**, 107-118.

Dorobek, S. (1989) Migration of orogenic fluids through the Siluro-Devonian Helderberger Group during late Paleozoic deformation: constraints on fluid sources and implications for the thermal histories of sedimentary basins. Tectonophysics **159**, 25-45.

Dreyer, T., Scheie, A. & Walderhaug, O. (1990) Minipermeameter-based study of permeability trends in channel sand bodies. Bull. Am. Ass. petrol. Geol. **74**, 359-374.

Durney, D.W. & Ramsay, J.G. (1973) Incremental strain measured by syntectonic fibre growths. In: Gravity and Tectonics (Ed. by K.A. DeJong & R. Scholten) New York, John Wiley and Sons. 67-96.

Fairchild, I.J. (1983) Chemical controls of cathodoluminescence of natural dolomites and calcites: new data and review. Sedimentology **30**, 579-583.

Gidon, M. (1979) Carte Géologique simplifée des Alpes occidentales (Leman a Digne) a 1:25 000 BRGM. Ed. by Didier-Richard, Grenoble.

Gillchrist, R., Coward, M. & Mugnier, J.L. (1987) Structural inversion and its controls: examples from the Alpine Foreland and the French Alps. Geodinamica Acta (Paris). **1**, 5-34.

Gillchrist, R. (1989) Mesozoic basin development and structural inversion in the external French Alps. Unpublished Ph.D. Thesis, University of London.

Giroir. G., Merino, E. & Nahon, D. (1989) Diagenesis of Cretaceous sandstone reservoirs of the South Gabon Rift Basin, West Africa: mineralogy, mass transfer and thermal evolution. J. sedim. Petrol. **59**, 482-493.

Goguel, J. (1963) L'interpretation de l'arc des Alpes occidentales. Bull. Soc. Geol. France **5**, 20-33.

Graciansky, P.C., Bourbon, P., Chenet, P.Y., de Charpal, O. & Lemoine, M. (1979) Genèse et evolution comparée de deux marges continentales passives: Marge Iberique

de l'Océan Atlantique et Marge Européene de la Téthys dans les Alpes Occidentales, Bull. Soc. Geol. France, Paris Series 7, **21**, 663-674.

Haq, B.U., Hardenbol, J. & Vail, P.R. (1987) Chronology of fluctuating sea-levels since the Triassic. Science **235**, 1156-1167.

Harding, T.P. & Tuminas, A.C. (1989) Interpretation of footwall (lowside) fault traps by reverse faults and convergent wrench faults. Bull. Am. Ass. petrol. Geol. **72**, 738-757.

Heim, A. (1921) Géologie der Schweiz. 2/1 Tauchnitz, Leipzig. 259-476.

Hudson, J.D. (1977) Stable Isotopes and limestone lithification. J. Geol. Soc. Lond. **133**, 637-660.

King, G. and Yielding, G. (1984) The evolution of a thrust fault system: processes of rupture initiation, propagation and termination in the 1980 El Asnam (Algeria) earthquake. Geophys. J. Roy. Astron. Society **77**, 915-933.

Knipe, R.J. (1989) Deformation Mechanisms - Recognition from natural tectonites. J. Struc. Geol. **11**, 127-146.

Lemoine, M., Bas, T., Arnaud-Vanneau, A., Arnaud, H., Dumont, T., Gidon, M., Graciansky, D. E., Rudkiewicz, J. L., Megard-Galli, J. & Tricart, P. (1986) The continental margin of the Mesozoic Tethys in the Western Alps. Mar. Pet. Geol. **3**, 179-199.

Machel, H.G. (1985) Cathodoluminescence in calcite and dolomite and its chemical interpretation. Geosciences Canada **12**, 139-147.

Menard, G. (1979) Relations entre structures profondes et structures superficiélles dans le sud-est de la France: éssai d'utilisation de donnés geophysiques. Thése de 3ème Cycle, Université de Grenoble.

Menard, G. & Thouvenot, F. (1984) L'anomalie gravimetrique d'Ivréa: résultant d'un écaillage de la lithosphère européenne? Sci. Geol. Bull. Strasbourg 37, **1**, 23-27.

Mitra, S. (1988) The effects of deformation mechanisms on reservoir potential in the Central Appalachians Overthrust Belt. Bull. Am. Ass. petrol. Geol. **72**, 536-554.

Montadert, L., de Charpal, O., Roberts, D.G., Guennoc, P. & Sibuet, J.C. (1979) North-east Atlantic Passive Margins: rifting and subsidence processes. In: Deep drilling results in the Atlantic Ocean: Continental margins and paleo-environment. (Ed. by S. Talwani, O. Hay and D. Ryan) Amer. Geoph. Union. Washington D.C., Maurice Ewing Series **3**, 154-186.

Mugnier, J.L., Arpin, R. & Thouvenot, F. (1987) Coupes équilibrées a travers le massif sub alpin de la Chartreuse. Geo. Acta. (Paris). **1**, 125-137.

Perrier, G. & Vialon, P. (1980) Les connaissances geophysiques sur le sud-est de la France: implications geodynamiques. Géologie Alpine **56**, 13-20.

Ramsay, J.G. (1963) Stratigraphy, structure and metamorphism in the western Alps. Proc. Geol. Assoc. **74**, 357-391.

Robert, P. (1988) Organic metamorphism and geothermal history. Microscopic study of organic matter and thermal evolution of sedimentary basins. D. Reidel Publishing Company, Dordrecht, Holland. 311p.

Roberts, G. (1990) Structural controls on fluid migration in Foreland Thrust Belts. In: Petroleum and Tectonics in mobile belts (Ed. J.Letouzey) Editions Technip, Paris 193-210.

Rutter, E. (1976) The kinetics of rock deformation by pressure solution. Phil. Trans. R. Soc. London **A283**, 203-219.

Sibson, R.H., Moore, J.McM., Rankin, A.H. (1975) Seismic pumping - A hydrothermal fluid transport mechanism. J. Geol. Soc. Lond. **131**, 653-659.

Sibson, R.H. (1977) Fault rocks and fault mechanisms. J. Geol. Soc. Lond. **133**, 191-213.

Sibson, R.H. (1981) Fluid flow accompanying faulting: Field evidence and models. In: Earthquake prediction: an international review (Ed. Simpson, D.W. and Richards, P.G). 593-603.

Sibson, R.H. (1986). Brecciation processes in fault zones: inferences from earthquake rupturing. Pageoph. **124**, 159-175.

Sibson, R.H. (1989) Earthquake faulting as a structural process. J. Struc. Geol. **11**, 1-14.

Smith, D.A. (1966) Theoretical consideration of sealing and non-sealing faults. Bull. Am. Ass. petrol. Geol. **50**, 363-374.

Smith, D.A. (1980) Sealing and non-sealing faults in Louisiana Gulf Coast Salt Basin. Bull. Am. Ass. petrol. Geol. **64**, 145-172.

STATIS Stereonet Programme. Stimpson, I. unpublished. U.C. Cardiff.

Teichmuller, M. (1987) Recent advances in coalification studies and their application to geology. In: Coal and coal bearing strata: recent advances (Ed. A.C. Scott). Geological Society Special Publication **32**, 127-169.

Ten Have, T. & Heijnen, W. (1985) Cathodoluminescence activation and zonation in carbonate rocks: an experimental approach. Geol. Mijn. **64**, 297-310.

Tricart, P. & Lemoine, M. (1986) From faulted blocks to megamullions and megaboudins: Tethyan heritage in the structure of the Western Alps. Tectonics **5**, 95-118.

Trumpy, R. (1960) Paleotectonic evolution of the central and western Alps. Bull. Geol. Soc. Am. **71**, 843-901.

Tucker, M.E. & Wright, V.P. (1990) Carbonate Sedimentology. Blackwell Scientific Publications. 482p.

Vieban, F. (1983) Installation et evolution de la plate-form Urgonien (Hauterivian a Bedoulien) du Jura méridional aux chaines sub alpines (Ain) Savoie, Haute Savoie, Thése 3e Cycle, Grenoble.

Walsh, J.J. & Watterson, J. (1988) Analysis of the relationship between displacement and dimensions of faults. J. Struc. Geol. **10**, 437-462.

Wanless, H.R. (1979) Limestone response to stress: pressure solution and dolomitization. J. sedim. Petrol. **49**, 437-462.

Weber, K.J. & Daukoru, E. (1975) Petroleum Geology of the Niger Delta. Proceedings of the Ninth World Petroleum Congress **2**, 209-221.

Weber, K.J., Mandl, G., Pilaar, W.F., Lehner, F. & Precious, G. (1978) The role of faults in hydrocarbon migration and trapping in Nigerian growth fault structures. Proc. 10th Annual Offshore Technology Conference, Houston, Texas. **4**, 2643-2653.

Welbon, A. (1988) Deformation styles and localisation of thrust faults in the external French Alps. Unpublished Ph.D. University of Leeds.

White, S.H. (1976) The effects of strain on the microstructures, fabrics and deformation mechanisms in quartzites. Phil. Trans. R. Soc. Lond. **A283**, 69-86.

Wojtal, S. & Mitra, G. (1986) Strain hardening and strain softening in fault zones from foreland thrusts. Geol. Soc. Am. Bull. **97**, 674-687.

Woodward, N.B., Wojtal, S., Paul, J.B. & Zadins, Z.Z. (1988) Partitioning of deformation within several external thrust zones of the Appalachian Orogen. J. Geol. **96**, 351-361.

Zweidtler, D. (1985) Genése des gisements d'asphalte des formations de la Pierre Jaune de Neuchatel et des calcaires Urgoniens du Jura (Jura Neuchatelois et nord-vaudois). Thése Université Neuchatel, 107pp.

Appendix 1

Structural data for the Rencurel Thrust Sheet

Structural data was collected from the Rencurel Thrust Sheet during mapping of the area which is presented in Figure 3.1. The majority of the structural data was collected during summer of the second year of the study. Approximately 6 weeks was spent at the locality of the Rencurel Thrust Zone described in detail in this thesis (Grid Reference 8472 3139). This time was spent collecting structural data for the Rencurel Thrust Zone, collecting samples and preparing the structural log presented in Figure 3.19. Three hundred and five structural measurements were taken of which one hundred and seventy two were located on the structural log presented in Figure 3.19. Marking faults onto the black and white photo montage was done in the field. The procedure was very time consuming as the faults were not easily visible from a distance of more than approximately one metre. From this distance the geometry of the faults and their position on the photo montage were difficult to mark so that a large amount of time was needed to walk back and forth across the road to check the position of faults and then accurately mark them onto the photo montage. Figure 3.19 brings out these problems as faults are generally not visible on the lower photo montage. One hundred and ten samples were taken from this fault zone. Each sample was orientated by marking a dip and strike onto a prominent plane on each possible sample. Many orientated blocks did not become samples because they disintegrated during collection with a hammer and chisel. The marking of the localities of structural measurements and the localities of samples onto the black and white photo montage was also difficult and time consuming due to the problems with visibility of the faults mentioned above. Detailed outcrop descriptions were also carried out during this time. Sample collection and locating the samples on the photo montage took approximately two weeks. Marking the faults onto the photo montage and carrying out outcrop descriptions took around two and a half weeks. Marking the position of one hundred and seventy two structural measurements on the photo

montage took one week. The rest of the time was spent collecting more structural data and taking photos of the outcrop. The duration of these individual parts of the study are only approximate because the studies were all underway at the same time. A further five weeks was spent producing the map in Figure 3.1. Seventy samples were taken, three hundred and twenty seven structural measurements were made, structural logs along all the road sections where as many faults as possible which were visible at outcrop were marked, outcrop descriptions were carried out and the position of stratigraphic boundaries and the position of faults were mapped.

In the laboratory all samples were re-orientated by mounting the blocks on plasticine and rotating them to a position indicated by a compass clinometer. All thin sections came from the vertical plane orientated 114°-194°. Around one hundred thin sections measuring five centimetres by seven centimetres were prepared. These sections took approximately three weeks to obtain twelve from the technical staff.

Lineation data is presented in the form of plunge and plunge direction (Table 1). Fault plane data is presented in the form of a strike and dip, the dip direction being 90° clockwise from the strike (Table 2). Table 3 presents combined lineation and fault plane data for the points marked on the un-interpreted part of Figure 3.19.

The structural data is also presented in the form of contoured stereonets in Figures 3.20 and 3.21.

Section 1 The Rencurel Thrust Zone

Section 1.1 Thrust contact between the Urgonian and Miocene rocks.

73 lineations were measured from 69 fault planes which all existed within the 4 metre thick gouge zone which is exposed

along the thrust contact between the Urgonian and the Miocene rocks. Two distinct sets of faults existed as shown in Figures 3.20 and 3.21. One set of faults dips towards the east-south-east with lineations plunging in the same direction. Another set dips towards the west-north-west with lineations also dipping towards the west-north-west. The first set mirror the attitude of the Rencurel Thrust Zone as a whole whilst the other set of faults have the geometry of Reidel faults. Displacements along the Reidel faults were measured from five examples, all of which had top to the west kinematic indicators and had a maximum value of 30cm. The majority of displacement within the Rencurel Thrust Zone probably occurred at this locality which is suggested by the presence of Miocene rocks on one side of the zone and Urgonian rocks on the other (See Figure 5.1). The displacement along the Rencurel Thrust Zone is around one kilometre. This was estimated by projecting units down the plunge of the structure. The value of displacement is the sum of the displacements along the minor faults preserved today and also faults which formed earlier in the displacement history and have been disrupted by later deformation within the fault zone. The spread of lineation plunge directions of the Reidel faults and those dipping towards the east is around 30^{o}. This may simply reflect the natural spread of movement directions which occur along a fault whose large displacement has resulted from the addition of many small increments of deformation.

Section 1.2 Array of minor faults in the Urgonian within the Rencurel Thrust Zone

Ninety four lineations were measured from ninety one fault planes along the road section which extends around 100 metres into the hanging-wall of the thrust contact between the Urgonian and the Miocene rocks. Kinematic indicators were found on around ten faults, all of which indicate a top to the west movement sense, regardless of whether the fault was dipping to the west or to the east. The westward dipping faults may be "Reidels" which also exist within the gouge zone along the thrust contact between the Urgonian and Miocene rocks. No eastward vergent backthrusts

were found. Displacements were measured from five faults, the maximum being around 50cm. The orientation of lineations along these minor faults is very close to the orientations of lineations from along the thrust contact between the Urgonian and Miocene rocks. This suggests that the lineations at the two localities were produced during one kinematically linked phase of thrusting and the array of minor faults within the Urgonian must be included in any models which aim to describe the deformation within the Rencurel Thrust Zone. The spread of movement directions indicated by the lineations at locality 3 (Figures 3.20 and 3.21) may simply represent the natural range of movement directions which exist during the many increments of deformation which produced such an array of faults.

Section 1.3 Discussion

It is interesting that lineation orientations and spread of the data are very similar between the thrust contact between the Urgonian and Miocene rocks and the array of minor faults within the Urgonian, yet fault plane orientations are not. Fault plane orientations in the array of minor faults within the Urgonian which developed early (locality 3 on Figure 3.21) are spread over around 90^{o} whereas they are spread over only around 30^{o} at the thrust contact between the Urgonian and Miocene rocks which developed late in the deformation (locality 2 on Figure 3.21). The relative timing of the faults at these two localities is discussed in Chapter 5. The faults along the thrust contact between the Urgonian and Miocene rocks only represent the last few increments of deformation within the Rencurel Thrust Zone as microstructural evidence suggests that earlier faults existed but became disrupted by later deformation. The orientations of these early faults cannot be measured and therefore their orientations do not play a major role in governing the spread of fault plane orientations which can be measured today. This may suggest that during the displacement history of an evolving fault zone a change occurs in the factors which combine to determine the orientations of new fault planes which develop. Early in the deformation history a wide spread of fault plane orientations can develop

whilst still maintaining a tightly constrained movement direction. In parts of the fault zone exposed to further deformation the early spread of plane orientations is erased and new fault planes can form in only a small range of orientations. The development of small scale lateral ramps is restricted to the early displacement history of a fault zone.

Section 2 The Rencurel Thrust Sheet

Section 2.1 Faults around Pont de Goule Noire

Seventy lineations were measured from forty five minor faults along 200 metres of road section. Most of the faults had gouge zones less than 10cm wide and four that were measured had displacements of less than one metre. However, three of the faults had gouge zones up to 40cm wide and had displacements in the order of tens of metres. Actual displacements were difficult to measure because of the paucity of bedding indicators for the small faults and the limited size of exposures for the larger faults.

Section 2.2 Footwall to the Chalimont Thrust

Data were collected along 50 metres of road section from 41 minor faults which cut the Urgonian limestones and the Hauterivian interbedded limestones and lime-mudstones. Fault displacements were measured from four of the minor faults where offset of bedding was visible. The maximum measured displacement was 90cm. The presence of both backthrusts and foreland-directed thrusts is indicated by kinematic indicators such as inclined pressure dissolution seams, calcite steps and offsets of bedding. The Chalimont Thrust Zone accommodates several hundred metres of displacement, the exact figure being uncertain because the footwall cut-off and the hanging-wall cut-off to the fault do not exist within the same exposure.

Section 2.3 Ferriere Thrust Zone

Fifty lineations were measured from fifty fault planes along 30 metres of road section. The thrust zone accommodates displacements in the order of hundreds of metres, the actual amount being difficult to assess because of the lack of exposure.

Section 2.4 Valchevriere Thrust Zone

Twenty two lineations were measured from twenty two fault planes developed within the the thrust zone. The thrust zone has a gouge zone up to 40cm thick and accommodates displacements approaching one hundred metres. All the faults measured came from within this gouge zone or from minor faults with gouge zones less than 10cm thick which exist less than 2 metres into the hanging-wall and 1 metre into the footwall of the thick gouge zone. The measurements were confined to this small area because the rest of the thrust zone was not well exposed.

Section 2.5 Discussion

Individual localities within the Rencurel Thrust Sheet exhibit the same movement directions of thrusting towards the west-north-west. This is the same movement direction recorded by the lineations developed within the Rencurel Thrust Zone. This suggests that individual fault zones with displacements in the order of hundreds of metres, tens of metres and less formed during one kinematically linked phase of thrusting within the Rencurel Thrust Sheet and Rencurel Thrust Zone. All the faults must be considered in attempting to assess the structural evolution of this suite of deformed rocks. Localities 1, 3, 4 and 5 where measurements were not taken from a single thick gouge zone and where displacements in the order of hundreds of metres or more were involved show fairly constant movement directions but a large range of fault plane orientations. This may be explained by the reasoning presented in Section 1.3 of this Appendix where it is suggested that as an area is progressively deformed the range of orientations which in which new fault planes develop becomes more restricted. The Valchevriere Thrust

Zone where most of the data was taken from along a single gouge zone indicates that this process may also occur along thrusts which have less than one hundred metres displacement as opposed to the kilometre scale displacements which occur along the Rencurel Thrust.

Appendix 1 Structural data for the Rencurel Thrust Sheet

Lineation data is presented in the form of plunge and plunge direction (Table 1). Fault plane data is presented in the form of a stike and dip, the dip direction being 90° clockwise from the strike (Table 2). Table 3 presents combined lineation and fault plane data for the points marked on the un-interpretedpart of Figure 3.19.

LINEATION DATA FOR THE RENCUREL THRUST SHEET									
Lineations from the Ferriere Thrust.									
16 136	16 148	22 030	02 084	18 104	51 098	12 130	12 146	20 125	20 134
12 138	16 140	12 150	30 062	03 155	00 156	03 089	42 284	12 085	20 258
17 098	20 098	17 104	16 096	10 280	12 091	05 110	24 311	40 280	09 106
20 120	40 285	45 293	12 309	03 170	08 125	00 120	15 280	25 110	00 165
45 114	30 090	05 215	00 270	30 290	50 270	48 277	38 120	08 170	35 290
Lineations from the Valchevriere Thrust Zone.									
45 084	42 090	46 100	35 100	40 101	40 081	40 074	45 087	30 067	55 090
45 082	38 050	52 090	60 070	60 115	50 098	48 100	45 109	40 104	39 104
45 094	32 094								
Lineations from the thrust in the HW to the Ferriere Thrust. (Above gorge).									
25 160	30 164	30 135	31 162	30 150	50 150				
Lineation data from faults in the HW to the Rencurel Thrust.									
35 290	45 314	38 310	29 292	60 090	28 272	28 288	45 243	50 293	40 117
15 090	38 284	30 268	24 270	31 274	32 266	08 095	36 290	30 292	25 089
36 089	40 100	22 095	10 290						
Lineation data from the road section around Pont de Goule Noire.									
45 318	40 346	32 355	50 330	62 355	40 357	20 340	18 120	25 115	05 170
20 100	32 010	50 024	30 133	35 110	40 110	62 110	55 315	35 332	20 309
27 354	10 325	25 344	37 346	50 360	40 354	60 339	35 360	43 352	38 010
20 012	42 018	70 355	51 316	55 330	05 160	30 320	35 330	15 320	30 320
21 292	70 254	06 280	10 320	00 294	60 110	70 105	45 118	08 300	11 120
09 304	18 289	11 237	44 270	08 140	14 130	25 132	00 310	10 170	00 085
30 099	20 078	70 120	40 117	20 115	20 102	15 115	30 129	20 143	40 128
Lineation data from the road section in the hanging wall to the Rencurel Thrust.									
65 309	59 305	55 268	51 083	19 180	00 067	25 258	25 255	42 280	30 270
42 270	03 260	54 102	60 080	69 063	16 083	30 103	10 104	12 102	37 143
42 089	15 106	25 277	18 273	20 268	43 270	09 254	35 272	29 290	24 272
41 260	22 268	33 248	30 280	10 109	22 285	02 285	15 355	40 272	07 251
19 285	56 092	34 296	07 288	06 260	70 072	22 278	08 252	18 080	18 258
32 296	28 100	08 276	35 296	20 287	64 264	38 258	02 100	30 256	25 230
43 270	60 270	52 274	49 110	50 092	30 098	18 104	30 100	10 080	35 104
40 100									
Lineation data from the Rencurel Thrust Zone.									
75 106	80 100	42 107	79 274	68 269	25 144	65 334	38 107	62 321	69 325
71 279	24 117	40 100	15 104	19 110	53 254	64 280	25 105	25 104	22 098
11 098	79 271	20 106	20 100	10 104	30 116	19 100	10 101	55 292	50 278
35 238	32 089	15 100	20 090	54 272	40 120	30 090	65 255	25 108	32 108
36 098	80 100	75 109	15 105	44 270	10 120	40 090	20 270	65 280	52 316
25 102	18 105	21 092	20 292	25 130	40 090	45 310	37 100	07 120	40 114
28 105	80 258	65 252	60 303	40 249	70 292	62 219	80 104	62 284	45 332
36 120	40 094	20 110							

Table 1

	FAULT PLANES FROM THE RENCUREL THRUST SHEET								
Fault planes from the Ferriere Thrust Zone									
332 32	320 35	338 32	338 32	344 31	088 38	200 33	035 15	193 28	066 26
052 24	070 28	034 16	100 65	084 50	010 10	206 40	190 40	094 50	028 20
100 90	190 25	280 55	220 65	276 80	160 40	165 30	245 20	182 52	318 50
080 55	350 20	290 50	305 15	355 50	048 49	030 45	030 55	040 60	175 32
210 75	170 50	170 59	200 49	174 68	176 50	340 65	360 55	355 55	343 69
Fault planes from Belv de Valchevriere.									
022 52	004 45	350 48	038 40	028 40	028 42	040 55	006 45	020 48	038 51
015 60	012 50	030 70	360 52	007 40	345 65	010 60	004 50	050 50	031 40
060 60	010 32								
Fault planes in the footwall to the Chalimont Thrust									
109 70	055 40	150 40	145 75	149 60	150 49	279 72	305 70	140 75	360 30
092 30	160 60	166 50	178 80	195 78	175 75	184 85	176 88	172 74	165 90
330 96	360 85	355 80	183 40	166 45	221 50	160 60	180 50	190 25	204 70
339 85	180 30	145 55	180 80	264 40	230 32	199 80	204 75	200 65	190 32
160 60									
Fault planes from around Pont de Goule Noire									
106 06	044 25	127 03	100 07	010 03	056 52	019 70	025 70	020 25	011 25
040 40	040 20	040 30	195 20	348 38	350 50	287 43	001 15	354 22	334 10
054 50	085 30	038 44	190 65	166 55	130 50	183 50	157 50	170 50	178 62
170 65	180 70	210 60	189 60	165 65	189 79	180 85	200 78	191 65	210 51
170 65	321 50	160 66	215 55	165 45					
Fault planes from the road section in the hanging-wall to the Rencurel Thrust									
360 45	255 72	246 64	227 69	004 51	021 43	067 63	052 68	050 60	089 72
086 71	090 67	325 46	251 49	073 50	084 62	246 61	100 64	097 65	075 56
278 58	072 80	030 53	009 65	352 46	100 50	100 45	078 80	029 72	025 72
037 68	040 20	006 69	004 65	000 31	290 01	008 32	164 11	035 18	016 41
017 43	008 65	358 45	015 35	010 10	008 13	350 50	012 35	009 55	029 37
018 45	017 32	030 30	050 21	172 21	284 32	202 22	195 25	260 50	084 85
091 45	081 75	103 50	089 21	252 53	257 42	246 41	254 85	273 85	230 62
230 62	254 58	110 15	152 12	146 14	072 32	027 15	192 30	124 53	112 64
315 46	151 41	144 30	205 10	036 30	007 56	222 38	355 54	270 70	269 68
002 21									
Fault planes from the Rencurel Thrust									
011 76	012 79	010 42	190 82	192 64	360 27	175 75	195 36	210 69	198 71
180 69	183 75	357 30	019 45	042 10	063 30	198 68	185 70	038 30	050 35
004 22	075 20	182 71	036 19	340 25	006 11	019 31	324 32	032 10	199 53
173 50	350 40	020 15	324 20	360 30	360 30	019 30	008 32	076 31	022 10
035 81	305 40	225 52	350 20	352 40	104 50	200 71	176 62	018 20	025 25
140 20	330 40	015 40	185 50	360 40	357 18	356 30	017 54	200 80	200 75
210 60	200 50	192 70	010 75	194 59	205 60	360 30	003 37	045 25	

Table 2

Fault planes from the road section in the hanging-wall to the Rencurel Thrust located on Fig. 3.19

	1	2	3	4	5	6	7	8	9	10
1	360 45	255 72	246 64	227 69	004 51	021 43	067 63	090 67	325 46	251 49
11	073 50	084 62	246 61	100 64	097 65	075 56	278 58	072 80	030 53	009 65
21	352 46	100 50	100 45	078 80	029 72	025 72	037 68	040 20	006 69	004 65
31	000 31	290 01	008 32	164 11	035 18	016 41	017 43	008 65	358 45	015 35
41	010 10	008 13	350 50	012 35	009 55	029 37	018 45	017 32	030 30	050 21
51	172 21	284 32	202 22	195 25	260 50	084 85	091 45	081 75	103 50	089 21
61	252 53	257 42	246 41	254 85	273 85	230 62	254 58	110 15	152 12	146 14
71	072 32	027 15	192 30	124 53	112 64	315 46	151 41	144 30	205 10	036 30
81	007 56	222 38	355 54	270 70	269 68	002 21				

Lineation data from the road section in the hanging wall to the Rencurel Thrust located on Fig. 3.19

	1	2	3	4	5	6	7	8	9	10
1		65 309	59 305	55 268	51 083	19 180	00 067	25 258		
11		25 255	42 280	30 270	42 270			03 260		54 102
21					60 080	69 063		16 083		
31										30 103
41	10 104	12 102				37 143	42 089			15 106
51				25 277	18 273	20 268	43 270	09 254		
61	35 272	29 290	24 272	41 260	22 268	33 248	30 280			
71	10 109			22 285	02 285	15 355	40 272		07 251	19 285
81	56 092	34 296								

Table 3

Sample	lithology	Flow rate	Millidarcies
507.0	DOLOMITE	23.9	6.0
512.0	LIMESTONE	6.7	2.4
516.0	DOLOMITE	19.9	4.4
529.0	DOLOMITE	100.0	39.8
535.0	DOLOMITE	20.0	5.7
535.0	DOLOMITE	42.0	14.5
538.0	DOLOMITE	14.0	3.3
543.0	DOLOMITE	564.0	220.0
547.0	DOLOMITE	206.0	81.4
552.0	GRAINSTONE	51.5	18.3
555.0	GRAINSTONE	8.0	0.9
559.0	GRAINSTONE	20.5	5.9
573.0	LIMESTONE	50.4	17.8
579.0	GRAINSTONE	1.6	0.4
580.0	GRAINSTONE	4.0	1.5
586.0	GRAINSTONE	21.0	6.2
589.0	DOLOMITE	21.0	8.5
590.0	DOLOMITE	55.0	22.0
595.0	DOLOMITE	35.0	14.0
596.0	DOLOMITE	79.5	31.7
599.0	DOLOMITE	14.0	5.6
605.0	DOLOMITE	27.4	11.0
609.0	DOLOMITE	330.0	129.8
612.0	DOLOMITE	18.8	7.6
615.0	LIMESTONE	105.0	41.7
618.0	LIMESTONE	5.0	2.0
621.0	LIMESTONE	160.0	63.4
626.0	LIMESTONE	13.0	5.2
508.0	LIMESTONE	14.1	5.7
520.0	LIMESTONE	40.0	16.2
520.0	LIMESTONE	36.0	14.6
523.0	LIMESTONE	50.0	20.0
523.0	LIMESTONE	40.0	16.0
540.0	LIMESTONE	115.0	45.7
540.0	LIMESTONE	85.0	33.8
540.0	LIMESTONE	27.0	10.9
540.0	LIMESTONE	59.0	23.6
23A	FAULT ROCK	0.4	
9D	FAULT ROCK	0.3	
9D	FAULT ROCK	1.3	
9D	FAULT ROCK	2.4	
9D	FAULT ROCK	0.9	
9D	FAULT ROCK	0.1	
12H	FAULT ROCK	7.5	
12H	FAULT ROCK	6.2	
12F	FAULT ROCK	0.8	
12F	FAULT ROCK	0.9	
12F	FAULT ROCK	1.1	
12A	FAULT ROCK	1.8	
12A	FAULT ROCK	1.4	
8L	FAULT ROCK	0.6	
8L	FAULT ROCK	0.7	
8L	FAULT ROCK	0.8	
12R	FAULT ROCK	1.4	
12R	FAULT ROCK	0.9	
12R	FAULT ROCK	1.1	
19.9-5	FAULT ROCK	1.5	
19.9-12	FAULT ROCK	0.9	
19.9-12	FAULT ROCK	0.4	
19.9-12	FAULT ROCK	1.0	
19.9-13	FAULT ROCK	1.1	
19.9-13	FAULT ROCK	0.3	
19.9-13	FAULT ROCK	0.2	
19.9-13	FAULT ROCK	0.1	

Appendix 2 Permeability data

These data are discussed in Chapter 7.

Appendix 3 Stable isotopic data

Isotopic compositions are reported here in the standard δ notation (Tucker &Wright 1990). All samples are reported in permil relative to the internationally accepted standard, PDB. Some references to oxygen isotopic compositions of pore-waters are given relative to SMOW, as is standard practice. Sample analysis was carried out by M. Savell at the BP laboratories, Sunbury-upon-Thames using standard techniques. Samples were collected using a dentist's drill from thin-sections and the sawn faces of hand-specimens. Dolomites were reacted with anhydrous concentrated phosphoric acid for 18 minutes whilst calcites were reacted for 4 minutes. The reaction temperature was 70°C.

The use of bulk samples of wall-rock and gouge which included both calcite and dolomite made it necessary to correct the oxygen data for both a 100% calcite composition and a 100% dolomite composition. Both figures were calculated for the samples of mixed mineralogy. The predominance of calcite or dolomite in a sample was determined petrographically. If a sample was predominantly calcite it was reacted for 4 minutes, or 18 minutes if it was predominantly dolomite. In the following tables, if a reaction time of 4 minutes is indicated the sample was predominantly calcite. If the reaction time is indicated as 18 minutes the sample was predominantly dolomite. In some instances the same sample was reacted at both reaction times to give an estimate of the importance of the reaction time to the measured isotopic composition. Repeat analyses were perfomed on some samples in order to estimate analytical accuracy.

Sample	Time	13C	18O (C)	18O (D)	Sample type
12J	18	1.1	-4.3	-4.7	BBSG
19/9 (1)	4	1.0	-1.7	-2.1	BBSG
repeat	18	1.0	-1.1	-2.1	
12H (4)	4	0.6	-3.7	-4.1	BBSG
12H (5)	4	1.0	-2.0	-2.4	BBSG
12M	18	1.0	-3.2	-3.7	BBSG
12Y (1)	4	1.2	-5.0	-5.4	BBSG
12i (4)	18	-0.1	-3.0	-2.6	BBSG
12H (4)	4	0.6	-3.7	-4.1	BBSG
repeat	18	0.6	-3.9	-4.5	
12H (5)	4	1.0	-2.0	-2.4	BBSG
repeat	18	1.1	-1.8	-2.5	
12Y (1)	4	1.2	-5.0	-5.4	BBSG
repeat	18	1.3	-4.6	-5.2	
HW10 (1)	18	1.2	-3.0	-3.6	BBSG Transect across sample
HW10 (2)	18	1.2	-3.5	-4.1	BBSG 3cm
HW10 (3)	18	1.8	-1.5	-1.7	BBSG 5cm
HW10 (4)	18	0.9	-3.7	-4.4	BBSG 7cm
HW10 (5)	18	1.3	0.9	0.2	BBSG 9cm
HW10 (6)	18	1.3	-2.6	-3.0	BBSG12cm
HW10 (7)	18	1.1	-3.1	-3.7	BBSG 15cm
12g	18	1.0	-2.9	-3.3	BBSG
12f	18	1.1	-1.9	-2.3	BBSG
Fw5	18	1.0	-4.9	-5.2	BBSG

Table 1: Bulk blue-stained gouges (BBSG) from along the thrust contact between the Miocene and the Urgonian.

Sample	Time	13C	18O (C)	18O (D)	Sample type
12Y3	18	1.5	-4.6	-5.2	BPSG
4a (3)	18	1.3	-2.3	-2.9	BPSG
12c	18	-0.6	-4.2	-4.6	BPSG
8h (2)	18	1.0	-2.2	-2.6	BPSG (dolomite)
8dii	18	2.2	-3.5	-3.9	BPSG (dolomite)
8l (1)	18	1.5	-2.8	-3.2	BPSG (dolomite)
repeat	18	1.6	-2.5	-2.9	
8l (2)	18	1.7	-2.9	-3.3	BPSG (dolomite)
8h (1)	18	1.8	-2.6	-3.0	PSG in vein (dolomitised)
8i (2)	18	2.1	-3.6	-4.0	BPSG (dolomite)
repeat	18	2.1	-3.5	-3.9	
8di (2)	18	2.1	-3.4	-3.9	BPSG (dolomite)
12i (1)	18	0.1	-7.2	-7.6	BPSG
12JP	18	0.6	-5.5	-6.0	BPSG

Table 2: Bulk pink-stained gouges (BPSG) from the minor faults within the Urgonian. Pink-stained gouge (PSG).

Sample	Time	13C	18O (C)	18O (D)	Sample type
8h (5)	18	1.8	-2.9	-3.3	BWR (dolomite)
repeat	18	1.8	-3.0	-3.4	
8h (3)	18	2.1	-2.6	-3.0	BWR (dolomite)
repeat	18	2.0	-2.9	-3.3	
599	18	0.2	-5.2	-5.6	Dolomite L. Bourne Gorge
repeat	18	0.4	-5.1	-5.5	
8di (1)	18	2.4	-2.6	-3.0	BWR (dolomitised)
8h (4)	18	2.1	-3.3	-3.7	BWR (dolomitised)
3N (2)	18	0.9	-5.2	-5.6	BWR (limestone)
3L (2)	18	-0.4	-4.9	-5.3	BWR (limestone)
12Q (1)	18	0.7	-6.6	-7.1	BWR (Dolomitised)
12u (2)	18	2.1	-4.8	-5.2	Dol. rhombs along stylolite
2ai (1)	18	0.2	-3.3	-3.7	WRD
repeat	18	0.4	-3.2	-3.6	
3n (1)	18	1.4	-3.1	-3.5	WRD
3l (1)	18	1.6	-3.0	-3.4	WRD
574	4	1.8	-4.4		BWC Lower Bourne Gorge
FW4 (2)	4	-0.1	-2.6		SSF
12c (1)	4	0.0	-3.7		Miocene Molasse Gouge
623	4	0.1	-7.0		BWC Lower Bourne Gorge
2IA (2)	4	-0.1	-3.3		Neomorphic Spar
FW7	4	-1.3	-3.2		SSF
9f (6)	4	-3.2	-6.4		Calcite in 2nd porosity
12a (4)	18	-0.3	-5.5	-5.8	Neomorphic calcite spar
9f (1)	18	0.9	-2.2	-2.6	Samples across fault zone
repeat	18	0.9	-2.0	-2.4	lcm
9f (2)	18	1.1	-2.5	-2.9	3cm
9f (3)	18	1.1	-2.6	-3.0	7cm
9f (4)	18	0.8	-2.6	-3.0	10cm
repeat	18	0.8	-2.8	-3.2	
9f (5)	18	0.8	-2.8	-3.2	15cm

Table 3: Bulk wall-rock (BWR); Wall-rock dolomite (WRD); Unaltered Senonian skeletal fragments (SSF); Bulk wall-rock calcite (BWC).

Sample	Time	13C	18O (C)	18O (D)	Sample type
12MP	4	0.6	-3.3	-3.7	PCBSG
12MC	4	1.0	-3.9	-4.3	LCBSG
19/9 (1)c	4	0.9	-3.6	-4.0	LCBSG
12i (3)	4	1.2	-4.2	-4.6	LCBSG
12JC	18	1.3	-3.8	-4.2	LCBSG
12J (1)	18	1.0	-5.1	-5.5	Wall-rock clast BSG
19/9 (1)c	4	0.9	-3.6	-4.0	LCBSG
repeat	18	1.0	-3.4	-4.0	
12MP	4	0.6	-3.3	-3.7	PCBSG
repeat	18	0.6	-3.3	-3.9	
12MC	4	1.0	-3.9	-4.3	LCBSG
repeat	18	1.2	-3.0	-3.7	
12i (3)	4	1.2	-4.2	-4.6	LCBSG
repeat	18	1.3	-4.0	-4.7	
4a (2)	18	0.8	-3.7	-2.3	CPSG
12gp	18	-0.2	-4.0	-4.4	PCBSG
12fp	18	0.4	-2.0	-2.4	PCBSG
repeat	18	0.5	-3.0	-3.4	
12w	18	1.3	-4.6	-5.2	Wall-rock clast PSG
8i (2)c	18	2.2	-3.3	-3.7	CPSG (dolomite)

Table 4: Pink clasts in blue-stained gouge (PCBSG); Light clasts in blue-stained gouge (LCBSG); Clasts in pink-stained gouge (CPSG); Pink-stained gouge (PSG); Blue-stained gouge (BSG).

Sample	Time	13C	18O (C)	18O (D)	Sample type
19/9 1V	4	-0.8	-7.7		FCV
19/9 1A	4	-0.5	-7.5		FCV
12HV 2	4	-0.2	-6.5		FCV
12HV 1	4	-0.6	-7.8		FCV
FW4 (1)	4	-0.4	-3.3		FCV
12A (1)	4	-0.4	-2.8		FCV
12cv	4	-0.5	-2.6		FCV
12A (3)	4	-0.5	-3.2		FCV
12U (1)	4	1.0	-7.8		FCV
FW5 (1)	4	0.4	-6.3		FCV
4A (1)	4	-1.4	-5.4		CV
8DIIV	4	-3.8	-8.1		CV
8HV	4	-5.1	-9.2		CV
8H6	4	-4.8	-8.4		CV

Table 5: Ferroan calcite veins (FCV); Calcite veins (CV).

Sample number	9f2 (2 theta values)	9f1 (2 theta values)	Mineral
Comment	Wall-rock	Fault gouge	
	25.7		Dolomite
	28.1	28	Dolomite
	34.4		Calcite
	36	36	Dolomite
	39	39	Dolomite
	41.2	41.1	Dolomite
	43.5	43.6	Dolomite
	48.1	48	Dolomite
	52.6	52.6	Dolomite
Sample number	5Ci2 (2 theta values)	5Ci1 (2 theta values)	Mineral
Comment	Wall-rock	Fault gouge	
	27		Calcite
	31.1	31	Quartz
	34.4	34.4	Calcite
	36.1	36	Dolomite
	42.2	42.1	Calcite
		48	Dolomite
	50.8	50.8	Calcite
	56	56	Calcite
	57.2	57.1	Calcite
Sample number	Sheared Molasse (2 theta)	64 (2 theta values)	Mineral
Comment	Fault Gouge	100 Metres in Footwall	
		7.3	Chlorite
	10		Glauconite
	10.2	10.2	Mica
	14.6	14.6	Chlorite/Kaolinite
	19.9	20.8	Muscovite
		21.9	Chlorite
	23.1	23.1	Mica
	24.2	24.2	Quartz
		26.8	Calcite
	28.2	28.2	Serpentinite/Clinochrysolite
	29.3	29.3	Chlorite/Kaolinite
	31.1	31.1	Quartz
		32.1	Feldspar
	32.6	32.4	Feldspar
	34.5	34.3	Calcite
	35.2	34.7	Mica
	36.2	36	Dolomite
	37	36.9	Chlorite
		38.6	Pyrite?
	41	41	Mica
	42.1	42.1	Calcite/Mica
	42.9	42.7	Quartz
	44	44.1	Kaolinite
	46.2	46.1	Calcite
		46.2	Quartz
	47.2	47.2	Quartz
	48.3	48.2	Dolomite

	49.8	49.8	Quartz
	51	50.7	Calcite
	53.5	53.4	Mica
		56	Calcite
	57.5	57.1	Calcite
		59.1	Quartz

SAMPLE NUMBER	LOCALITY (SEE FIGURE 3.19)	ORIENTATED THIN SECTION	CALCITE CEMENT	FERROAN CALCITE CEMENT	HYDROCARBONS	CATHODOLUMINESCENCE MICROSCOPY	REFLECTED LIGHT MICROSCOPY	ULTRA-VIOLET FLUORESCENCE MICROSCOPY	STABLE ISOTOPES Appendix 3	X-RAY DIFFRACTION Appendix 4	MINI-PERMEAMETER Appendix 2
12a	FAULT ZONE 12	x		x	x	x	x	x			x
12a(1)		x		x		x	x	x	x		x
12a(3)		x		x		x	x	x	x		
12a(4)		x	x			x	x	x	x		
12b		x				x	x	x			
12c		x	x			x	x	x	x		
12cv		x		x		x	x	x	x		
12d		x				x	x	x			
12e		x				x	x	x			
12f		x		x		x	x	x	x		x
12f		x		x		x	x	x	x		x
12fp		x	x			x	x	x	x		
12g		x		x	x	x	x	x	x		
12gp		x	x			x	x	x	x		
12h		x		x	x	x	x	x			x
12h(4)		x		x		x	x	x	x		
12h(5)		x		x		x	x	x	x		
12h4		x		x		x	x	x	x		
12h5		x		x		x	x	x	x		
12hv1		x		x		x	x	x	x		
12hv2		x		x		x	x	x	x		
12i(1)		x	x			x	x	x	x		
12i(3)		x		x		x	x	x	x		
12i(4)		x		x		x	x	x	x		
12j		x		x		x	x	x	x		
12j		x		x		x	x	x	x		
12jc		x		x		x	x	x	x		
12jp		x	x			x	x	x	x		
12k		x				x	x	x			
12l		x				x	x	x			
12m		x		x		x	x	x	x		
12mc		x		x		x	x	x	x		
12mc		x		x		x	x	x	x		
12mp		x	x			x	x	x	x		
12mp		x	x			x	x	x	x		
12n		x				x	x	x			
12o		x				x	x	x			
12r		x				x	x	x			x
12u1		x				x	x	x	x		
12v(1)		x				x	x	x			
12v(2)		x				x	x	x	x		
12w		x	x			x	x	x	x		
12y(1)		x		x		x	x	x	x		

Appendix 5 Laboratory techniques

SAMPLE NUMBER	LOCALITY (SEE FIGURE 3.19)	ORIENTATED THIN SECTION	CALCITE CEMENT	FERROAN CALCITE CEMENT	HYDROCARBONS	CATHODOLUMINESCENCE MICROSCOPY	REFLECTED LIGHT MICROSCOPY	ULTRA-VIOLET FLUORESCENCE MICROSCOPY	STABLE ISOTOPES Appendix 3	X-RAY DIFFRACTION Appendix 4	MINI-PERMEAMETER Appendix 2
12y(1)		x		x		x	x	x	x		
12y3		x	x			x	x	x	x		
19/9 .5	FAULT ZONE 12	x				x	x	x			x
19/9.12		x				x	x	x			x
19/9.13		x				x	x	x			x
19/9/1c		x		x		x	x	x			
19/9/1v		x		x		x	x	x	x		
19/9/1a		x		x		x	x	x	x		
									x		
4a(1)	FAULT ZONE 4	x				x	x	x			
4a(2)		x	x			x	x	x	x		
4a(3)		x	x			x	x	x	x		
4b		x				x	x	x			
4c		x				x	x	x			
4d		x				x	x	x			
9d	FAULT ZONE 9	x				x	x	x			
9f(1)		x	x			x	x	x	x		
9f(2)		x	x			x	x		x		
9f(3)		x	x			x	x	x	x		
9f(4)		x	x			x	x	x	x		
9f(5)		x	x			x	x	x	x		
9f(6)		x	x			x	x	x	x		
8di(1)	FAULT ZONE 8	x	x			x	x	x	x		
8di(2)		x	x			x	x	x			
8dii		x	x			x	x	x	x		
8diiv		x	x			x	x	x	x		
8h(1)		x	x			x	x	x	x		
8h(2)		x	x			x	x	x	x		
8h(3)		x	x			x	x	x			
8h(4)		x	x			x	x	x			
8h(5)		x	x			x	x	x			
8h(6)		x	x			x	x	x	x		
8hv		x	x			x	x	x	x		
8i(2)		x	x			x	x	x	x		
8i(2)c		x	x			x	x	x	x		
8l		x	x			x	x	x			x
8l(1)		x	x			x	x	x	x		
8l(2)		x	x			x	x	x	x		
3a	FAULT ZONE 3	x				x	x	x			

Appendix 5 Laboratory techniques

SAMPLE NUMBER	LOCALITY (SEE FIGURE 3.19)	ORIENTATED THIN SECTION	CALCITE CEMENT	FERROAN CALCITE CEMENT	HYDROCARBONS	CATHODOLUMINESCENCE MICROSCOPY	REFLECTED LIGHT MICROSCOPY	ULTRA-VIOLET FLUORESCENCE MICROSCOPY	STABLE ISOTOPES Appendix 3	X-RAY DIFFRACTION Appendix 4	MINI-PERMEAMETER Appendix 2
3b		x				x	x	x			
3c		x				x	x	x			
3l(1)		x	x			x	x	x			
3l(2)		x	x			x	x	x			
3n(1)		x	x			x	x	x			
3n(2)		x				x	x	x			
4a(1)	FAULT ZONE 4	x	x			x	x	x			
4a(2)		x	x			x	x	x			
4a(3)		x	x			x	x	x			
4b		x				x	x	x			
4c		x				x	x	x			
4d		x				x	x	x			
2a	FAULT ZONE 2	x				x	x	x			
2b		x				x	x	x			
2c		x				x	x	x			
2ai(1)		x	x			x	x	x			
2IA(2)		x				x	x	x	x		
fw4(1)	FAULT ZONE 12	x		x		x	x	x	x		
fw5(1)		x		x		x	x	x	x		
fw4(2)		x	x			x	x	x			
fw7		x				x	x	x			
HW 10(1)	FAULT ZONE 12	x		x		x	x	x	x		
HW 10(2)		x		x		x	x	x	x		
HW 10(3)		x		x		x	x	x	x		
HW 10(4)		x		x		x	x	x	x		
HW 10(5)		x		x		x	x	x	x		
HW 10(6)		x		x		x	x	x	x		
HW 10(7)		x		x		x	x	x	x		
574	L. Bourne gorge	x	x			x	x	x	x		
623		x	x			x	x	x	x		
64	D531 Road	x		x		x	x	x		x	
5ci	FAULT ZONE 5	x	x			x	x	x		x	
5cii		x				x	x	x			
5cii		x				x	x	x			

Appendix 6

Plane polarised light and cathodoluminescence photomicrographs of an extensional fracture within the Ferriere Thrust Zone. The calcite infilling the fracture is zoned which suggests that the crystals grew into a fluid filled cavity. (See Section 3.3.1).

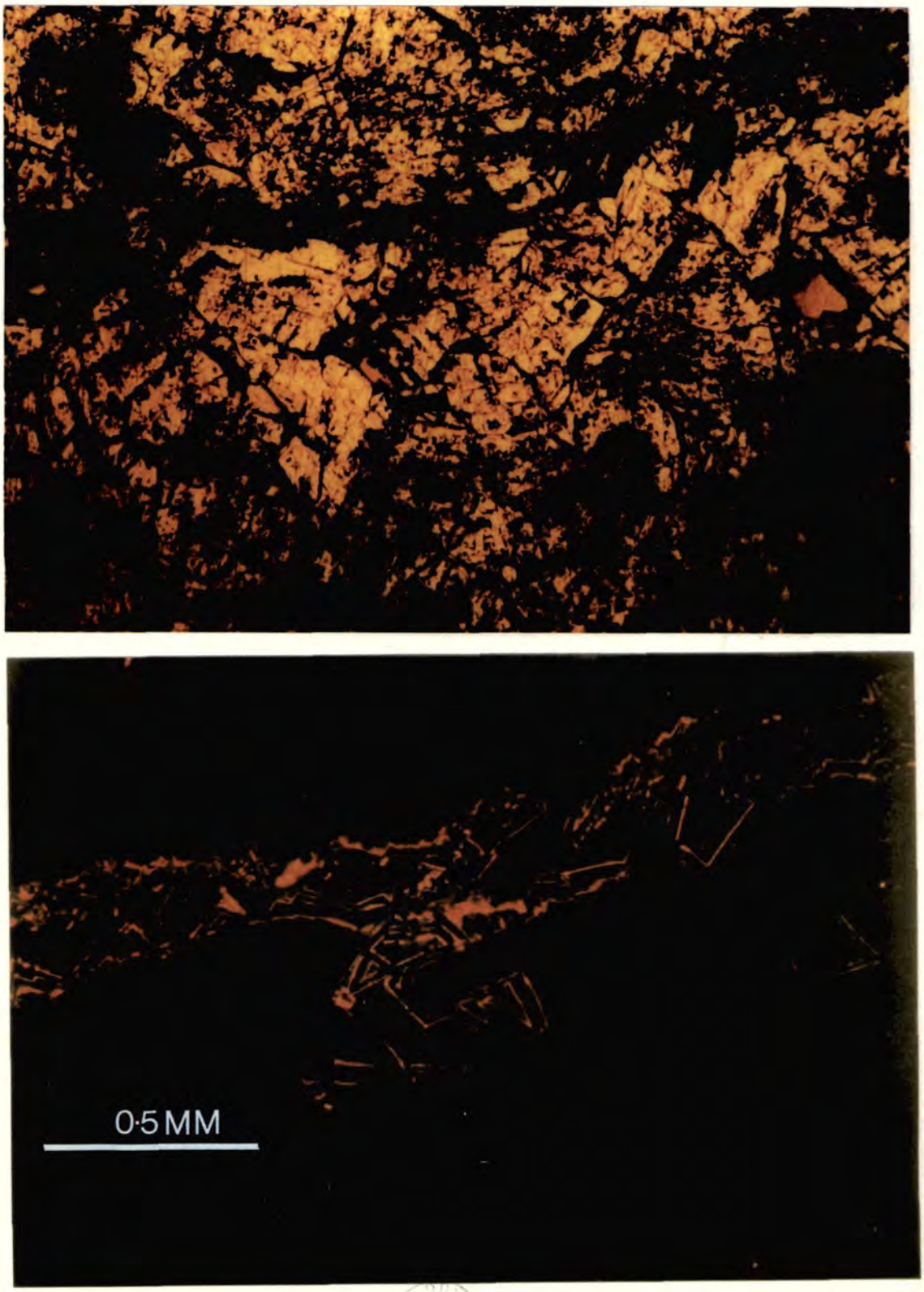

Appendix 7

Vitrinite reflectance and spore colouration methodology.

At the start of the study, samples of all the formations which compose the stratigraphy within the Vercors were collected, so that thermal maturity studies could be attempted. Spores and vitrinite were not found within the majority of formations in the Vercors. However, the Hauterivian and Valanginian limestones and lime-mudstones contain very small amounts of spores and fragments of vitrinite. Also, samples of the Oxfordian shales contained small amounts of vitrinite. The Oxfordian sample from the Drac valley was of too high maturity for spores to be useful.

In the second and third summers of the study, more samples of the Hauterivian and Valanginian were collected from around the Vercors. Around 20 samples were collected from near Die to the south of the Vercors, the eastern margin of the Vercors bordering the Drac Valley, exposures within the Vercors Plateau and from the western Vercors in the core of the Beauregard-Baret Anticline. The samples were ground down to grain sizes of around 4-5mm and then the carbonate was removed by immersion in dilute Hydrocloric Acid. The residues were then mounted in epoxy resin blocks which then had polished surfaces prepared. The sample preparation and polishing was carried out by the author. Only five of the samples were found to contain organic material which was suitable for estimations of thermal maturity. Spore colours were estimated with the aid of Prof. M. Jones (University of Newcastle - upon-Tyne) who is an experienced worker in this field. Quantitative spore colour analysis was not possible at Newcastle at the time of the study. The vitrinite reflectance value of 0.45% for sample 2 (See Figure 2.22) was a mean value calculated from around 15 individual measurements of reflectance. The maximum value was around 0.46% and the minimum was around 0.44%. The sample also contained spores which had the same colour as spores in reference samples from the north east of England which also had a vitrinite reflectance value of around 0.45%. The vitrinite reflectance value of 1.45% gained from the Oxfordian sample

taken from the Drac Valley was gained from 11 individual reflectance measurements which had a similar small range of deviation as the Hauterivian sample 2.

Appendix 8

Discussion of the aims and conclusions of the project: implications for future work

The aims listed in Chapter one of this thesis were designed to guide the study. They were not considered to be research objectives which could be fully achieved within the tenure of a three year PhD studentship. The conclusions presented in Chapter eight of this thesis describe how far the research has progressed within the three years of study. The conclusions are useful in that they highlight aspects of the research which have led to "dead ends". The conclusions also serve another purpose in that they highlight specific aspects of the research which warrant more detailed studies using different approaches. These future lines of research are often not apparent at the outset of the study, although it may be that they prove to be of great importance. This Appendix discusses problems with certain aspects of the research and suggests the approach which future studies could usefully apply to progress further with the research aims listed in Chapter one of this thesis.

Conclusions 1-5 highlight the importance of understanding the faulting environment which is to be studied. Thermal maturation studies can give a crude maximum burial depth and background temperature at which the rocks now exposed at the surface were deformed. This type of study must be performed because it allows the conclusions of the study to be usefully applied elsewhere, the exposed part of the Rencurel Thrust Zone being an analogy for a sub-surface migration pathway for hydrocarbons and diagenetic fluids and also fault seals. Work has started assessing the deformation and diagenetic histories of neotectonic fault zones where the seismicity of the fault zone is known and some of the deformation has occurred within a few hundreds of metres from the surface. The observation that the Vercors contains a simple regional structure may suggest that the processes active along thrusts within the area may have progressed in their simplest forms. This simplest case scenario must be established before

studies in more complicated areas can be undertaken. A paper is now in preparation which is designed to compare and contrast the deformation and diagenetic histories of "simple" thrust zones such as the Rencurel Thrust Zone with that which occurs in areas where pre-existing basin structure is complicated (See Appendix 9).

The description of the environment which the faulting occurred in was not listed as a primary research aim because this type of study will highlight different avenues of research for each individual fault zone. Although this type of study is essential, specific research objectives concerning the faulting environment cannot be stated until the faulting environment has been established. Regional structural studies and burial data are essential parts of the study of the deformation and diagenetic histories around fault zones.

Conclusions 6-8 indicate the dimensions of the area which was involved in the deformation to be studied. A full appreciation of the deformation and diagenetic histories around fault zones can only be achieved if the whole picture can be seen. Once the extent of the deformation has been recognised, only then is it possible to assess the scale on which temporal and spatial changes in the permeability of the fault zone may be recognised in the field. Detailed structural studies in the field are essential parts of the study of the deformation and diagenetic histories of exhumed fault zones. The insights gained from such studies should be applied to sub-surface fault zones. Studies have begun to compare exhumed fault zones on the mainland UK with fault zones at depth under the North Sea which can only be studied from cores and other sub-surface analysis methods.

Conclusions 9-14 begin to address assessment of the processes which induce changes in the permeability of fault zones during deformation which was the second aim listed in Chapter one. Cataclasis and diffusive mass transfer (DMT) are the dominant processes which induce porosity and permeability changes within the Rencurel Thrust Zone. The way in which these processes operate may be radically altered in other fault zones due to

magnitude within the vicinity of the portion of the Rencurel Thrust Zone now exposed at the surface although larger earthquakes may have been occurring deeper, down-dip along the fault zone.

Conclusions 16 and 17 suggest that the diagenetic history of the rocks surrounding fault zones may be directly controlled by the geometrical development of the fault zone. This was the fourth research aim listed in in Chapter one. The rocks in the hanging-wall of the Rencurel Thrust Zone were not subjected to diagenesis in the influence of the pore-waters and hydrocarbons which were migrating through the fault zone late in its deformation history. The hanging-wall rocks were separated from these fluids by the relatively impermeable higher parts of the Rencurel Thrust Zone which formed early in the deformation history. Again, more case studies are needed to suggest whether this is a general rule for fault zones or not.

Conclusion 18 confirms that fluids are involved in the deformation along the Rencurel Thrust Zone. The nature of the solute precipitated from the fluids involved in migration through the Rencurel Thrust Zone has been well established using petrographic, X-ray diffraction and stable isotopic data. The solute data can be used to infer the nature of the pore fluids and the environment of precipitation of mineral phases. The pore fluid composition can be inferred to have changed with time. The inferred fluid compositions can be interpreted as resulting from the interaction of the fluids with rocks which have certain mineralogical, organic and stable isotopic compositions. Also the inferred fluids compositions may suggest that the fluids have interacted with material within which the thermal alteration of organic material was occurring. The fluids may also have reached saturation with respect to the solute over a range of temperatures as great as 30°C. The carbonate fault gouges may also have been shown to be composed of material derived from the grain size reduction of the wall-rocks. The gouges have not been re-crystallised in the presence of fluids with a composition such that the solute derived from them would have an isotopic

differences in many aspects including fluid pressure, strain rate, lithology and depth of faulting. Each fault zone to be considered must be subject to microstructural analysis. For example in Appendix 9, faulting in the Hauterivian limestones and lime-mudstones involved the production of fracture porosity by cataclasis and the precipitation of relatively large volumes of cement during the action of DMT. Deformation in Urgonian dolomites involved the same deformation mechanisms but the volume of cement precipitated in fracture porosity was limited. Whether this pattern is related to the size of pore spaces produced by fracturing or whether cement precipitation was in some way enhanced within the Hauterivian is not clear. **Conclusion 19** may suggest that cataclastic deformation in the Rencurel Thrust Zone was not accompanied by seismic shocks of significant magnitude in the portion of the Rencurel thrust Zone presently exposed at the surface. Future work should concentrate on trying to provide case studies of the type of deformation which develops in certain lithologies, at certain strain rates, fluid pressures and faulting depths. The provision of more case studies is of prime importance. The role of microstructural evolution is also stressed. The manner in which cyclic deformation in fault zones develops is central to understanding microstructurally controlled porosity and permeability changes within deforming rocks. Lithological cycles leading to rheological cycles is an important line of future research.

Conclusion 15 highlights the difficulties which arise when trying to assess whether the fluids control the deformation (the "Sibson valve model") or vice-versa (the "Sibson pump model"). Future work should concentrate on recognising the products of deformation caused by hydraulic fracturing. Also the collection of paleo-pore pressure data from fluid inclusions is important. The recognition of flow velocities in fracture filling pore waters also needs to be developed. This thesis presents some preliminary results which indicate that pore waters may be capable of transporting crystal silts during their flow through fracture porosity (Chapter 4). **Conclusion 19** suggests that the fluid flow was unlikely to have been driven by earthquakes of significant

Petroleum and Tectonics in Mobile Belts
© J. Letouzey (Editor) and Editions Technip, Paris 1990, p. 193 à 210

STRUCTURAL CONTROLS ON FLUID MIGRATION IN FORELAND THRUST BELTS

G. ROBERTS[1]

ABSTRACT

The Ferriere Thrust zone in the French Sub-Alpine Chains Foreland Thrust Belt shows a complex displacement localisation history as demonstrated by the cross-cutting relationships between different elements of the fault zone geometry. Early distributed deformation resulted in extensional fracturing. Later shear fractures became localised along these early extensional fractures, resulting in the formation of mesoscale thrust faults. These early faults then became rotated during distributed folding before large displacement thrusts cut through all the pre-existing structures. The preserved microstructures indicate that cataclasis and diffusional mass transfer were the dominant deformation mechanisms. The deformation mechanisms and the displacement localisation history of the Ferriere Thrust Zone may be compared to present day seismically active faults.

From the permeability characteristics of the microstructures developed in each element of the fault zone geometry, a model of syntectonic pore water migration during the incremental evolution of the fault zone is proposed. Early pore water migration occurs through a pervasive, distributed extensional fracture porosity system. The fracture porosity is occluded by the precipitation of zoned carbonate cements. Later pore water migration occurs within actively deforming localised faults and areas of distributed deformation during episodes of both aseismic, low strain rate deformation involving diffusional mass transfer and during coseismic, high strain rate deformation involving cataclasis. Non-deforming portions of the fault zone represent barriers to fluid migration due to impermeable, fine-grained gouge and sealed extensional fracture porosity which exist in these areas.

INTRODUCTION

This paper is concerned with the mechanical evolution and syntectonic fluid flow characteristics of thrust faults from external foreland thrust belts. Recent studies (Woodward et al. 1988, Ghisetti 1987, Engelder 1984, Wojtal and Mitra 1986) have shown that thrust faults in foreland thrust belts are not simple planar features. They consist of zones up to 100 metres wide containing an array of mesoscale faults. The density of these faults increases into the centre of the fault zone where shortening involving many kilometres of displacement can often be demonstrated. Gouge zones which can be several metres across are produced during such displacement. The internal geometry of such fault zones is produced by processes which include the propagation of the tips of faults into already deformed zones (Coward and Potts 1983, King and Yielding 1984, Cox and Scholz 1988, Elliott 1976), and by the modification of pre-existing fault zone geometries during thrust sheet translation (Wojtal and Mitra 1986). Displacement is acquired incrementally during a repeated seismic

(1) University of Durham, Department of Geological Sciences, Science Laboratories, South Road, Durham DH1 3LE, United Kingdom.

cycle (Sibson 1989, King and Yielding 1984). Deformation mechanisms include cataclasis and diffusional mass transfer (Knipe 1989). Within the French Sub-Alpine Chains, the Ferriere Thrust Zone shows an internal geometry indicating a complex displacement localisation history, where the style and spatial extent of the deformation can be documented to have changed through time. This is shown by examination of the cross-cutting relationships which exist between elements of the fault zone geometry such as mesoscale fault arrays and distributed cataclastic deformation. This combined with documentation of the occurrence of microstructures indicative of cataclasis and diffusional mass transfer allows description of the fault zone evolution. Cyclicity between distributed and localised deformation and between diffusional mass transfer and cataclasis can be demonstrated and this has important implications for modelling the mechanical development of foreland thrust structures.

Fault zones are often invoked as fluid migration pathways, and the syntectonic migration of fluids is well documented (Reynolds 1987, Kerrich and Hyndman 1986, Sibson 1981, Sibson et al. 1975). Mitra (1988) has demonstrated that micro-structures can control the porosity and permeability of deformed rocks including fault zones in the Appalachian fold and thrust belt. However, given the importance of syntectonic fluid migration, (Sibson 1975) the fluid flow characteristics of actively deforming fault zones must also be assessed. A combined study involving examination of the types of microstructure which occur in the fault zone to allow assessment of their deformation mechanisms and fluid flow characteristics, together with recognition of the mesoscale cross-cutting relationships in fault zones, allows the spatial changes in permeable and impermeable areas within fault zones during progressive deformation to be inferred. This paper draws attention to the complexities of modelling the mechanical evolution and fluid migration characteristics of fault zones.

GEOLOGICAL BACKGROUND

The Vercors is part of a foreland thrust belt which is developed in the French Sub-Alpine Chains (Goguel 1948, Gidon 1981, Butler 1987, Mugnier et al. 1987, Butler 1989). The relatively simple structural geometries represent the last few kilometres of west-north-west directed shortening in the Alps (Butler 1987) (see Figure 1). Eocene/Oligocene age normal faults offset the stratigraphy, and these faults are cut by post-middle Miocene thrust structures (Butler 1987), with both ages of fault activity being constrained stratigraphically (BRGM 1967, BRGM 1978, BRGM 1983, Butler 1987). Basement is probably not involved in this thin-skinned thrust belt (Bayer et al. 1987, Mugnier et al. 1987), which is thought to detach along the basement cover contact where Triassic evaporites exist. Mesozoic times saw the deposition of a carbonate sequence from the Lower Triassic to the Upper Cretaceous (Arnaud et al. in press) onto continental crust which was undergoing crustal extension during part of this time, related to the opening of Tethys (Graciansky et al. 1979, Lemoine et al. 1986). This sequence is overlain by Tertiary foredeep clastic sediments. The whole succession is involved in the thrust structures. The Mesozoic rocks consist of organic-rich interbedded limestones and shales with several thick carbonate shelf sequences. Along strike in the Annecy sector of the Sub-Alpine Chains, bitumen seeps can be found indicating the maturation and migration of hydrocarbons within the thrust belt (Zweidler 1985). The thrust belt has been exhumed by erosion since Miocene times during uplift related to isostatic adjustment of the lithosphere after thrusting ceased. For background information on the Sub-Alpine Chains and the Alps see Debelmas and Kerchove (1980), Butler (1988), Debelmas and Lemoine (1970), Ramsay (1963), Arnaud et al. (in press) and the Bulletin de la Societe Geologique de France Nos. 4 and 5 (1988 vol. IV).

In the Vercors, field structural mapping and sample collection were undertaken in the Gorges de la Bourne, and the Ferriere Thrust was selected for detailed study. The fault is exposed on the D 531 road between La Balme de Rencurel and Villard de Lans at grid reference 8497 33125 on Carte 3235 Ouest, Serie Bleu, 1:25,000, Villard de Lans. The fault

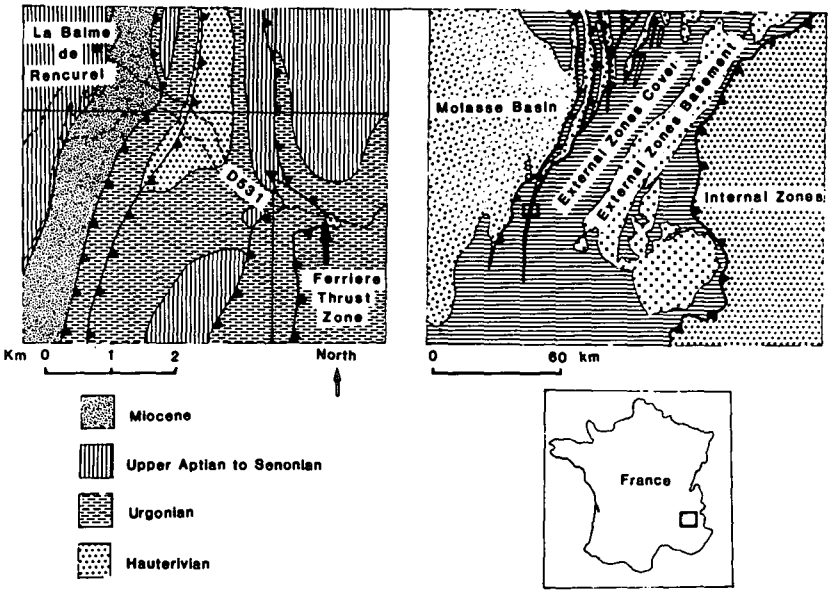

FIG. 1. Location map for the Ferriere Thrust Zone, Vercors, French Sub-Alpine Chains.

emplaces Hauterivian interbedded limestones and shales onto Barremian age limestones, locally termed the Urgonian. The Urgonian is locally dolomitised (Vieban 1983). Detailed mapping indicates that the fault probably represents around 300 metres displacement.

MESOSCALE STRUCTURAL EVOLUTION OF THE FERRIERE THRUST ZONE

Figure 2 shows the Ferriere Thrust at outcrop. The thrust is not a single fault plane but consists of a zone of extensional fracturing and mesoscale faulting around 50 metres wide. The cross-cutting relationship which exists between generations of faults, and also between the faults and extensional fractures, indicate that the deformation changed its style and spatial extent during progressive deformation. Detailed structural observations were made at outcrop of the Ferriere Thrust Zone to document the time relationships between these structures in order to allow qualitative description of the structural evolution of the fault zone.

A detailed structural log of the outcrop is shown in Figure 2, which indicates the style, position and chronology of the different deformation styles which occurred during the evolution of the Ferriere Thrust zone gained by interpretation of the structural log.

Extensional fracturing occurred during the early history of the fault zone as indicated by the carbonate cement-filled extensional fractures that exist pervasively throughout the outcrop. Mesoscale faulting then became the dominant deformation mechanism, as indicated by the fact that crystalline fill to the early extensional fractures is cut by the cataclastic faults. These early faults then became rotated into a downward facing attitude during flexural slip folding which occurred in the hanging wall to the overall thrust zone. Pressure dissolution was the dominant deformation mechanism during folding, as shown by the presence of pressure dissolution seams within the fold geometry. The early thrusts are now preserved on the steep limb of the westward vergent fold. Later thrusts then cut through the earlier structures during the last stages of deformation. One of these thrusts emplaces older Hauterivian limestones and shales on to younger Urgonian dolomites.

Deformation changed its nature and position with time during the evolution of the Ferriere Thrust Zone. This change in the displacement localisation means that areas where structurally-controlled fluid migration occurred would have also changed style, position and spatial extent through time along the Ferriere Thrust Zone. This will be discussed below.

Sample in figure five A

Sample in figure six B

Sample in figure seven C

Sample in figure eight D

1 m

Hangingwall ramp indicated by bedding plane cut offs.

H H

Footwall ramp indicated by bedding plane cut offs.

F F

FIG. 2. Photo montage and structural interpretation of the Ferriere Thrust Zone. Urgonian Limestone which has been locally dolomitised has been overthrust by Hauterivian interbedded limestones and shales.

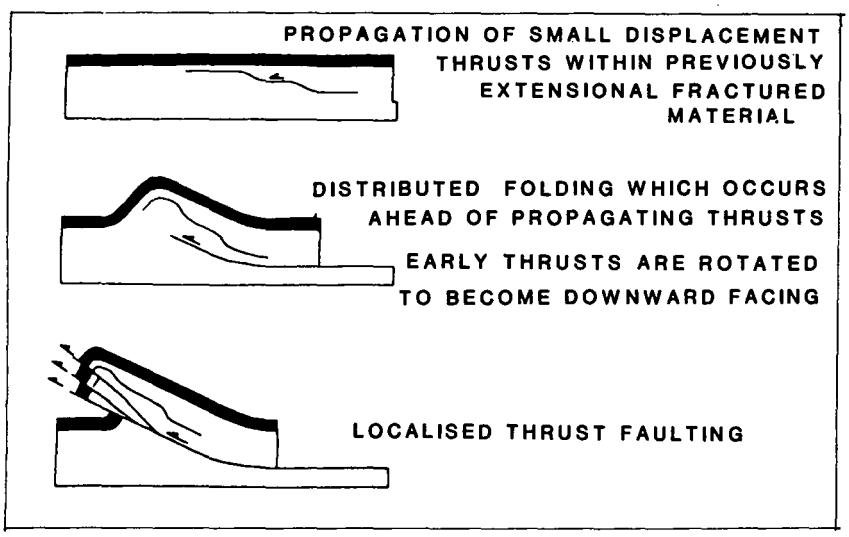

FIG. 3. The evolution of structural style seen in the Ferriere Thrust Zone.

DEFORMATION MECHANISM AND SYNTECTONIC FLUID FLOW CHARACTERISTICS OF THE FERRIERE THRUST ZONE

The dominant deformation mechanisms which were active within the Ferriere Thrust Zone were assessed by examining the microstructures found at outcrop. The location of samples is given in Figure 2. The syn-tectonic nature of fluid flow was also assessed during this microstructural analysis. The Ferriere Thrust Zone is dominated by microstructures characteristic of cataclastic deformation. Extensional fracturing and shear fracturing with associated gouge production are the dominant deformation mechanisms. Microstructures indicating the action of diffusional mass transfer are less prevalent in the part of the fault zone which is exposed. Figure 4 shows the textural and permeability characteristics which would have been dominant in the Ferriere Thrust Zone during and after the operation of such deformation mechanisms. The microstructures found in the samples are described below, and the deformation mechanisms and fluid flow characteristics were assessed using the guidelines in Figure 4. The aim was to describe the characteristic deformation mechanisms and fluid flow characteristics for the different ages of mesoscale deformation summarised in the displacement localisation history shown in Figure 3.

Microstructures and Permeability Characteristics of Areas Distant from Large Shear Fractures

The Urgonian in the footwall to the thrust is a coarse dolomite with inclusion-rich centres to individual crystals; the latter may be relics of the original foraminiferal grainstone texture seen at other localities. A patchy inter-crystalline porosity is present within the dolomite mosaic, the pore spaces being up to 0.25mm across and poorly interconnected.

Deformation resulted in a system of thin (0.3mm wide) fractures which cut across the earlier rock texture. Two sub-groups of fracture have been identified:-

(a) Fractures which have been completely filled by euhedral dolomite rhombs (see Figure 5). Under cathodoluminescence, the dolomite rhombs show alternating bright and dull luminescing zones which reflect subtle changes in overgrowth composition due to fluctuations in the pore water chemistry during dolomite precipitation.

(b) Fractures which show zoned crystalline fill and fine-grained material along the length of the same fracture (see Figure 6). A combined stain of Alizarin red S and potassium ferricyanide shows the vein fill to be dolomite along the edge of the fractures, with calcite spar towards the centre. The fine-grained material is very angular and poorly sorted.

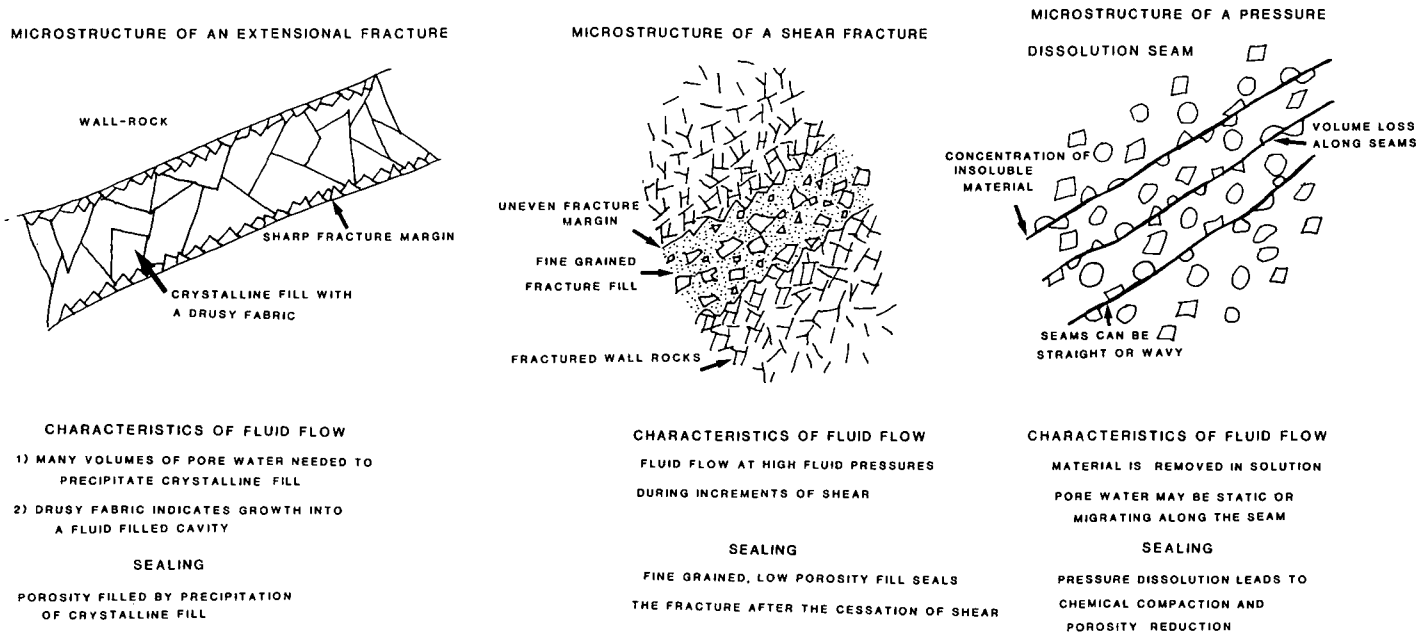

FIG. 4. Summary of the microstructures and permeability characteristics of microstructures developed within the Ferriere Thrust Zone.

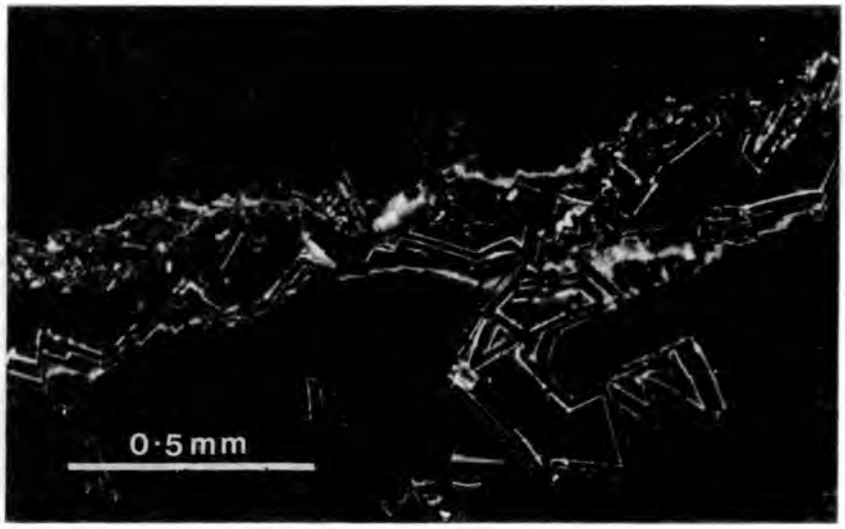

FIG. 5. A photomicrograph under cathodoluminescence of an extensional fracture filled by zoned dolomite cement. The wall-rocks are composed of a coarse dolomite mosaic.

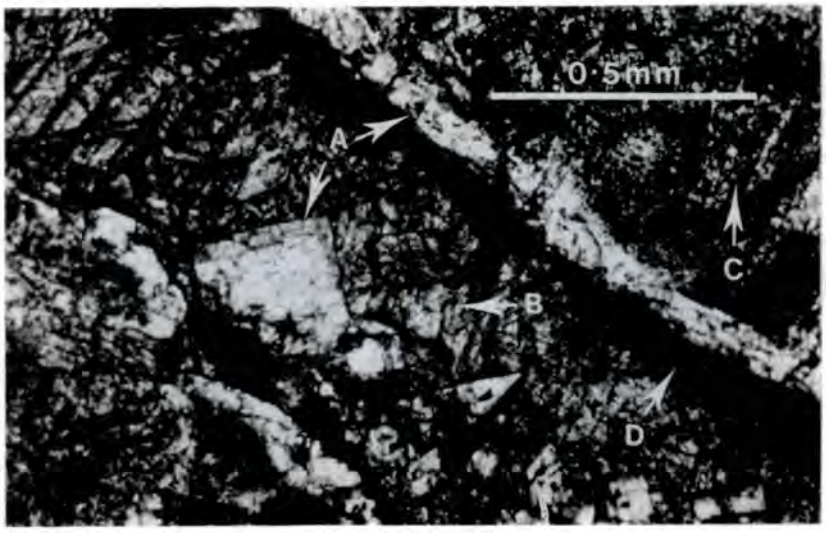

FIG. 6. A photomicrograph of an extensional fracture filled with zoned cement. A. Syntaxial dolomite cement B. Calcite cement, C. Coarse dolomite mosaic, D. Gouge.

Electron microprobe analysis has shown the fine-grained material to be calcite rich. The crystalline vein fill does not occur along some parts of the fracture.

These textures are characteristic of extensional fractures. The resultant fracture porosity was filled with pore water from which the crystalline vein material precipitated. Later in the deformation history, after the precipitation of the calcite, cataclasis during later shearing produced the fine-grained gouge material along the edges of the fracture.

Extensional fracturing was an important deformation mechanisms within the fault zone. The zoned crystalline cement in fractures is consistent with a change in the pore water chemistry during precipitation, both during dolomite precipitation and during precipitation of later cements from dolomite-saturated to calcite saturated waters. Mass balance calculations carried out during studies of cementation in carbonate rocks have shown that many volumes of pore fluid are needed to precipitate such carbonate cements (Bathurst 1975). These extensional fractures must therefore contain effective porosity and permeability for a period of

time long enough to allow the migration of large volumes of pore water. Further evidence of long lived porosity within these fractures occurs within the microstructure of the crystalline fracture fill. The dolomite cement has the form of euhedral crystals lining the sides of the open fractures during migration of the calcite-saturated pore water. The dolomite crystals show no sign of cataclastic deformation which might be expected if the fracture walls had moved together during fracture closure. The fracture porosity remained open throughout precipitation of the crystalline cement.

Microstructures and Permeability Characteristics of the Early Small Displacement Thrusts

Figure 7 shows a negative image of a thin section taken from a sample located on a small displacement, early thrust fault. The sample shows a significant change in style of deformation across its width. Towards the right of the specimen, blocks of intact dolomite are separated by shear fractures with fine grained material developed along them. Moving to the left towards the thrust fault, there is an increase in the density of fractures. The blocks of intact dolomite crystals decrease in size, and the percentage of fine-grained material in the rock increases until it dominates the fabric. This area of fine-grained material contains clasts of early-lithified fine-grained material. Some of the fractures separating blocks of dolomite have intact areas of calcite crystals developed along them. Dissolution seams occur within this specimen. They occur around blocks of surviving dolomite crystals and within the thick accumulation of fine-grained material towards the top of the specimen.

These textures are characteristic of cataclastic shear fractures (Engelder 1974, Knipe 1989). Cataclastic shear fracturing occurs during times of high fluid pressure as discussed below. Cataclasis in the form of shear fracturing has played an important role in the deformation of this sample producing the fine-grained gouges seen. The presence of calcite crystals within the gouge developed along some of these fractures suggests that extensional fractures with their crystalline fill existed before shear fracturing occurred. These shear fractures may have become nucleated along early extensional fractures. Further evidence for this exists in the microstructures described above, where the edges of extensional fractures can be seen to localise shear displacements (see Figure 6). The composition of the gouges has been shown by electron microprobe analysis to be calcitic and this is consistent with gouge production during shear fracturing occurring after precipitation of calcite in extensional fractures. Some early-formed gouges have been reworked during later increments of deformation and incorporated as clasts within younger gouge zones, indicating the incremental nature of the acquisition of cataclastic shear fracture strains.

Microstructures and Permeability Characteristics of the Late Cross Cutting Large Displacement Faults

Figure 8 shows a negative image of a thin section from the centre of the fault zone, located in Figure 2. A zone of fine-grained lithified material at least 20mm thick occurs along the fault. This fine-grained area includes clasts ranging up to 0.1mm in diameter. The largest clasts are few in number, around 20 of them visible in a field of view 5mm across. A foliation is developed through alternations of bands of coarser and finer gouge. The borders of these areas of different grain size are defined by red pressure dissolution seams. Clasts of earlier-formed lithified fine-grained material exist within this zone. The microstructure displayed by these clasts is complex indicating a previous history of deformation by fracturing and diffusional mass transfer. The whole texture of the 20mm thick gouge zone is cut by 1mm wide extensional fractures. These fractures have pressure dissolution seams running along their margins. These extensional fractures have a tension gash geometry in relation to the shear sense on the fault.

These textures are also characteristic of cataclastic shear fractures (Engelder 1974, Knipe 1989). Within these fault zones, large displacements have occurred by shear fracturing. This has led to the thick accumulation of gouge seen. This fracturing has reworked gouges which were

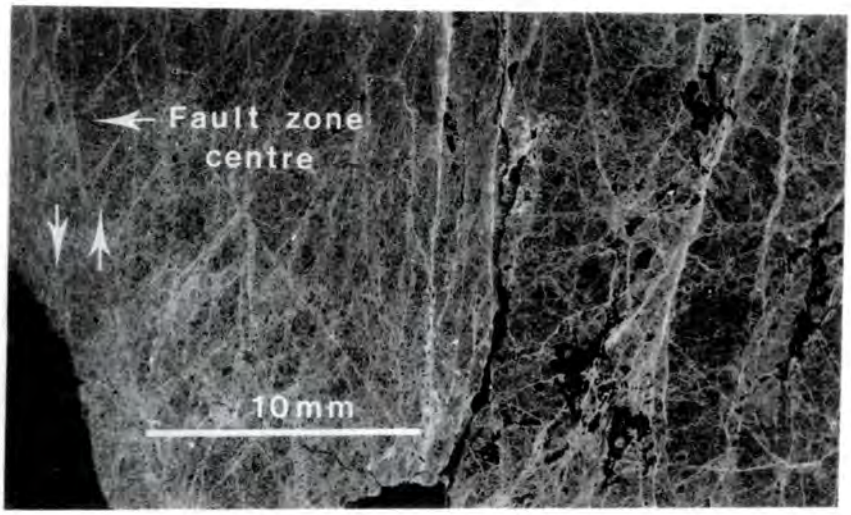

FIG. 7. Microstructures of an early displacement thrust showing a transition from isolated shear fractures into gouge. Dolomitic wall rock has survived between the isolated shear fractures. Print from a thin section.

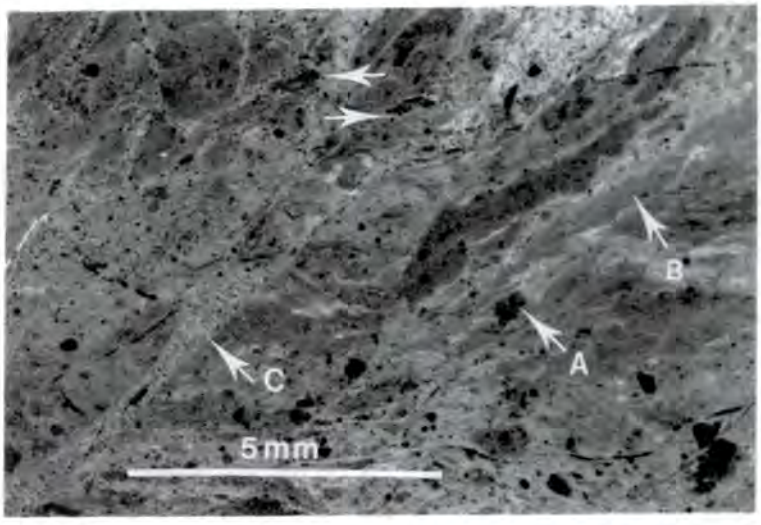

FIG. 8. Gouge of a late displacement thrust. A. Reworked lithified gouge clast. B. Fine-grained gouge. C. Extensional fracture filled with gouge. Print from a thin section.

produced during earlier increments of deformation. These early gouges may have undergone lithification perhaps by a process of diffusional mass transfer which will be discussed below. The lithified gouges were then broken into clasts by later shear fracturing. The resultant texture then underwent pressure dissolution to produce the red foliations within the gouge before extensional fracturing occurred. Then a final phase of pressure dissolution produced the red seams lining the edges of the extensional fractures. The final texture is the result of many increments of deformation.

DISCUSSION

The style of deformation exhibited by the Ferriere Thrust Zone, where episodes of diffusional mass transfer, extensional fracturing and shear fracturing occur may be consistent with the style of displacement acquisition which occurs on seismically active faults known from the geophysical and geodetic studies carried out on neotectonic thrust systems such as the El Asnam Thrust system in Algeria, by King and Yielding (1984). Deformation occurs during a seismic cycle. The

majority of displacement is acquired during high displacement rate events during which earthquakes are produced. Immediately before and after such events, displacement is also accumulated during low bulk strain rate deformation accommodated by small magnitude foreshock and aftershock earthquakes. Large periods of time exist where no earthquake related displacement is actively accumulating along such a fault. The finite fault displacement is the sum of many increments of deformation which occurs during repeated seismic cycles. The fault zone will therefore contain textures showing microstructural evidence for many increments of deformation. These changes in the nature of fault movement may be an important control on syn-tectonic fluid migration.

In order to assess the mechanical behaviour and fluid migration during such coseismic deformation within fault zones, the microstructures of the deformed rocks must be considered. The high strain rates during coseismic deformation suggest that cataclasis would be the dominant deformation mechanism (Knipe 1989). The action of cataclasis would produce thick accumulations of gouge. The gouge would be produced during a slip increment of very short duration and would have a repeat time many orders of magnitude greater. The duration of slip and the repeat time would be a result of the characteristic earthquake magnitude which occurs on the fault (Sibson 1989). Changes in the coseismic displacement along the fault would produce lateral changes in the nature of the gouge. Repeated increments of coseismic deformation with similar displacement variations would produce changes in the fault zone geometry along its length, as described by King and Yielding (1984) in their description of the Al Asnam Thrust System, Algeria.

During such cataclastic deformation along a fault, high fluid pressures and the migration of fluids between areas where fluid pressure gradients exist would occur within actively slipping portions of the fault. Sibson et al. (1975) have outlined the process by which fluids are tectonically pumped along fault zones into areas where fault slip is about to occur and then away from the area after fault slip has ceased. Rising tectonic stresses produce dilatant elastic deformation in the form of extensional fractures. Relatively low fluid pressures exist within the fractures so that fluids flow into them. When the influx of fluid creates fluid pressures great enough to overcome the frictional strength of the area, fault slip occurs. Fault slip is accompanied by a stress drop and the relaxation of dilatant elastic strains. The extensional fractures close and the fluid they contain is expelled. This causes a drop in fluid pressure within the fault zone, a rise in the frictional forces acting on the fault and eventually the cessation of fault slip.

It is interesting to speculate about the manner by which this fluid pressure assisted fault slip moves along the fault zone. Archuleta (1984) has shown the slipping portion of a fault surface migrates at velocities in the order of a few kilometres per second during modelling of the 1979 Imperial Valley Earthquake along the San Andreas Fault System. It seems that the zone of high fluid pressure therefore must also migrate at such velocities. The nature of pathways through which the fluids enter and leave the zone of high fluid pressure in areas of fault slip during such a short time period remain unclear. Etheridge et al. (1984) envisaged a process where there is exchange of fluid between grainscale porosity and fractures during deformation, the direction of flow being determined by local fluid pressure gradients. A similar process to that described by Sibson et al. (1975) probably induces the flow of fluids between fractures and grainscale porosity. Fluids may be drawn into the fault zone using these pathways as the slipping portion of the fault approaches and expelled as fault slip occurs and microfractures close due to the relaxation of elastic extensional fracture strains. Fluid migration would occur towards areas of relatively low fluid pressure which include the wall-rocks and the neighbouring area of the fault which is about to undergo fault slip where fluids are actively being drawn in due to rising stress and dilatant elastic deformation. This provides a mechanism for achieving wholesale mass transfer of fluids along an active fault zone.

The thick accumulation of gouge along the mesoscale faults within the Ferriere Thrust Zone indicates the action of cataclasis at high strain rates during coseismic displacement. Coseismic fluid migration within the Ferriere Thrust Zone will have occurred at high fluid pressures during the short-lived events in the order of seconds or less and would have recurred on a time scale which would be several orders of magnitude greater.

Pressure dissolution seams occur within the thick gouge zones the Ferriere Thrust Zone indicating that diffusional mass transfer was also active as a deformation mechanism during the displacement history in addition to cataclasis. Kerrich (1978), Rutter (1983) and Knipe (1989) have pointed out that diffusional mass transfer operates at low strain rates, suggesting that the Ferriere Thrust Zone acquired displacement over a range of strain rates great enough to activate cata- clasis and diffusional mass transfer as deformation mechanisms.

The possibility exists that cyclicity may have occurred between cataclasis and diffusional mass transfer along the thrusts within the Ferriere Thrust Zone, representing deformation which occurs during the seismic cycle where large strain rate fluctuations are known to occur (Sibson 1989). Lithified gouge clasts occur as elements of the textures of later formed gouges. Lithification may occur as a result of chemical compaction by pressure dissolution or by precipitation of cement. If lithification is the result of such processes of diffusional mass transfer, then it may suggest that lithification occurs during slow strain rate aseismic creep between high strain rate seismic events involving cataclasis.

Clearly, diffusional mass transfer was an active deformation mechanism outside of localised gouge zones, evidenced by the existence of fracture filling cements and stylolites. Work is continuing to identify the detailed nature of the sources and sinks for material involved in diffusional mass transfer in the Ferriere Thrust Zone.

Diffusional mass transfer may have played an important role in both the deformation which occurred between seismic slip events on the fault, and in fluid migration within the Ferriere Thrust Zone.

The Nature of the Fault Zone between Slip Increments

Very low permeabilities in the order of less than 10 nannodarcies at 15 bars and 0.3 nannodarcies at 220 bars confining pressure have been demonstrated in clay-rich gouges from the San Andreas Fault System by Chu and Wang (1981). The extremely fine-grained nature of the gouges from the Ferriere Thrust Zone, together with evidence of lithification of gouges between slip increments suggests that they also have a very low permeability. It is therefore likely that fluid migration will be severely impeded by the impermeable nature of gouges during times when the fault zone is not undergoing active displacement.

Summary

The mesoscale faults within the Ferriere Thrust Zone have been shown to exhibit both low strain rate and high strain rate deformation during the action of diffusional mass transfer and cataclasis respectively. This is consistent with the behaviour of seismically active faults which deform at varying rates during a seismic cycle (Sibson 1989).

The exposed portion of the Ferriere Thrust Zone accumulated displacement during episodes of coseismic cataclastic deformation with fluid migration at high fluid pressures, and during aseismic slip with fluid migration during diffusional mass transfer. Displacement also involved episodes of both localised and distributed deformation. Periods of time may also have existed where no displacement was actively accumulating and the undeforming zone represented a barrier to fluid migration. Fluid migration along such a fault zone will therefore change spatially and with time during its displacement history. This will be discussed below.

Implications for Syn-Tectonic Fluid Flow within the Ferriere Thrust Zone

In this section the mesoscale deformation history and likely seismogenic character of the fault zone is combined with the microstructural permeability

assessment to provide a qualitative pore-water migration model for the exposed portion of the Ferriere Thrust Zone.

Early in the deformation history, extensional fracturing occurred pervasively throughout the area which would later be cut by the fault zone. The fractures contained porosity filled with pore waters from which carbonate cement precipitated, eventually filling the pores. Therefore the extensional fracture system must have been well interconnected to allow significant pore-water migration. Rye and Bradbury (1988) have described a similar situation from a thrust zone in the Pyrenees where fluid wall-rock interactions occurred pervasively throughout an area where extensional fracturing took place. Similar pervasive fluid wall-rock interaction may have occurred in the Ferriere Thrust zone and this is being subjected to further study. The zonation of dolomite and calcite filling the fractures is evidence of a change in the pore-water chemistry during the fluid migration history. This may indicate a change in the nature of pathways and source areas of the migrating pore-waters. Fracture porosity occlusion by cement precipitation or further fracturing events may have been responsible for this change. The euhedral form of the early cement phases suggests that the extensional fractures were never fully closed during cement precipitation, since this would have crushed the crystalline cement. Occlusion of the fracture porosity and resultant changes in the fracture system interconnectedness during mechanical compaction of the fracture system does not seem to have been an important process within the exposed portion of the Ferriere Thrust Zone. Extensional fracture porosity which underwent repeated episodes of mechanical opening and closing as described by Sibson et al. (1975) for seismic pumping of fluids along fault zones, may exist elsewhere within the unexposed parts of the Ferriere Thrust Zone. The precipitation of carbonate cements seems to have been the dominant mechanism of fracture porosity occlusion. The rate of fracture porosity occlusion will be controlled by the rate of cement precipitation.

Fine-grained gouges along the margins of the extensional fractures were produced by shear fracturing. Shear fractures nucleated along the pre-existing extensional fractures with the earlier cements being cut by the shear fracturing. The calcite-rich composition of the gouge indicates that extensional fracture porosity had already been occluded by dolomite and calcite cement precipitation prior to shear fracturing. This implies that a time lapse occurred between extensional and shear fracturing. The time lapse was long enough to allow precipitation of carbonate cements within the extensional fractures. This has important implications for modelling the transition between pervasive, distributed strains in tip line folds accommodated by extensional fracturing to localised strains along faults accommodated by shear fracturing (Coward and Potts 1983, Williams and Chapman 1983). The timing of extensional and shear fracturing is an important consideration when assessing the interconnectedness of the permeability of the two fracture systems. If the extensional fracture porosity has already been occluded prior to shear fracturing the two fracture systems will not be interconnected and the extensional fracture system would be a barrier to fluid migration. The extensional and shear fracture system must be distinguished and their relative timing must be considered before any assessment of their interconnectedness can be made.

During the subsequent history of the fault zone, the style of deformation changed and shear fracturing became the dominant deformation mechanism during initial attempts to propagate an earthquake rupture or fault tip into the area. Shear fracturing nucleated along the margins of extensional fractures and thrust faults with a few centimetres displacement began to grow. The cataclastic gouges found along these faults indicates that their displacements were acquired during high strain rate coseismic deformation. This represents a change in the displacement localisation in the fault zone between pervasive, distributed displacement accommodated by extensional fracturing to displacement along many small offset thrust faults characterised by shear fracturing. The faults developed ramp flat geometries in the Hauterivian hangingwall rocks due to the anisotropy of the interbedded limestone and shale. Fracture-controlled fluid flow changed accordingly so that fluid-rock interactions occurred along a spaced, localised and linked system of laterally

continuous zones along these faults. Fluid flow occurred at high fluid pressures along actively slipping portions of the faults. The faults represent planar seals to fluid migration when they are not active due to the fine grained, low permeability nature of the gouge which is developed along them. Only short segments of any faults are slipping at any one time so that fluid flow at high fluid pressures occurs within the actively slipping zone bounded by impermeable fine-grained gouge produced during previous slip increments. High fluid pressures within slipping segments of the Ferriere Thrust Zone may have been dissipated at the cessation of rupture propagation by migration of the fluids into grainscale porosity and microcracks in the wall rocks which would have a relatively low fluid pressure compared with the fault zone. The dissipation of fluid pressures by the migration of fluids along the fault zone as suggested by Sibson et al. (1975) seems unlikely because of the low permeability of the gouges which are found along the Ferriere Thrust Zone.

The displacement localisation then changed again within the fault zone. Flexural slip folding occurred which rotated earlier structures and produced downward-facing thrusts and vertical bedding within the Hauterivian limestones and shales. The bedding within the massive Urgonian is difficult to trace so that it is unclear whether such deformation may have been triggered by the anisotropic bedding within the Hauterivian limestones and shales or whether it is simply difficult to recognise within the Urgonian. The action of diffusional mass transfer in the form of pressure dissolution as the dominant deformation mechanism is indicated by the presence of pressure dissolution seams which is consistent with deformation occurring aseismically. Volume was lost by the mass transfer of material in solution away from the pressure dissolution seams. The pathways and sinks for the migrating fluids remain unclear but may lie elsewhere within the fault zone or within grainscale porosity and fractures within the wall rocks. Folding may have occurred due to the propagation of thrusts and their associated tip line folds into the area as described by Williams and Chapman (1983) from examples within the Variscan thrust belt of Great Britain and Coward and Potts (1983) from the Moine Thrust Belt. Folding accommodates deformation at the terminations of actively-deforming faults so that the Ferriere Thrust Zone may have experienced the synchronous action of distributed folding dominated by diffusional mass transfer and localised faulting dominated by cataclasis in different parts of the fault zone during one increment of displacement. This means that fluid migration may have occurred between areas of distributed deformation dominated by pressure dissolution and volume loss, to areas where fracturing and volume gain by the precipitation of carbonate cements was occurring. Possible migration paths would have included parts of the fault zone actively undergoing slip and cataclasis. Migration would have been driven by the pressure gradients created between these two areas.

Late thrusts can be seen to cut the steep limb of the fold developed within the Hauterivian hangingwall rocks. These faults have gouge zones up to 100mm thick and one of them emplaces the Hauterivian onto the Urgonian. These factors imply that these thrusts may accommodate large displacements. Gouges, extensional fractures and pressure dissolution seams are the microstructures developed within the fault zone. This indicates that deformation became localised onto large displacement thrusts where episodes of both coseismic high strain rate deformation involving cataclasis and aseismic low strain rate deformation by the action of diffusional mass transfer occurred. Fluid flow also occurred through extensional fractures which were produced during the translation history of the fault.

CONCLUSIONS

(a) The Ferriere Thrust Zone is a 50 metre thick zone where fracturing and diffusional mass transfer were the dominant deformation mechanisms. The fault zone accommodates around 300 metres displacement.

(b) Cross-cutting relationships exist between the mesoscale structures developed within the fault zone, and imply that the displacement localisation changed through time involving both distributed and localised deformation. Early distributed, pervasive extensional

fracturing is replaced by mesoscale thrust faulting as the dominant deformation mechanism. These thrusts are later rotated during distributed flexural slip folding which may have occurred synchronously to thrust displacement elsewhere in the thrust zone. Large displacement, localised thrusts then cut earlier structures and accommodate the last phases of displacement.

(c) During each stage in the displacement history of the fault zone, different deformation mechanisms are dominant. Resulting microstructures can be used to decide whether deformation occurred seismically and also to decide what effect the deformation had on fluid migration during each stage of the incremental development of the thrust zone.

(d) Early pore-water migration occurred through a pervasive extensional fracture system. Changes in the pore-water chemistry can be inferred from the existence of zoned carbonate cements filling the fractures. Porosity existed within the fractures throughout their cementation history as demonstrated by the undeformed nature of the early cement phases. Occlusion of the fracture porosity occurred through the precipitation of carbonate cements and not through mechanical compaction of the fracture system.

(e) Shear fractures nucleated along the margins of the extensional fractures and produced cataclastic gouges which include fragments of the carbonate cements which were precipitated within the extensional fractures. This represents the propagation of an earthquake rupture or tip of the fault zone into the area. Pore-water migration through the extensional fractures examined ceased prior to shear fracturing as evidenced by the inclusion of calcite cement into the gouge.

(f) Pore-water migration along the shear fractures probably occurred at high fluid pressures during coseismic deformation and also during aseismic deformation involving diffusional mass transfer. Non-slipping segments of the fractures were impermeable barriers to pore-water migration due to the fine-grained nature of the gouge which fills them.

(g) In che hangingwall to the fault, early structures became rotated by flexural slip folding. Pore-water may have migrated out of the area due to the predominance of pressure dissolution as a deformation mechanism.

(h) Large displacement localised thrusts then cut through pre-existing structures. Pore-water migration occurred both at high fluid pressures during cataclastic high strain rate coseismic deformation and during low strain rate aseismic deformation involving diffusional mass transfer, and through extensional fracture porosity which was produced during slip along the fault zones. Several periods of extensional and shear fracturing occurred along these faults, as demonstrated by the cross-cutting relationships preserved in the microstructures of the fault rocks. Displacement and pore-water migration along these faults must therefore have occurred episodically. Non-slipping segments of the faults represented fine-grained barriers to fluid migration.

The mechanical evolution of foreland thrust structures can be assessed by comparing their deformation mechanisms and displacement localisation histories with seismically active fault zones. Syn-tectonic fluid flow can be modelled in fault zones by firstly considering the preserved microstructures and assessing their permeability characteristics during the seismological event which they represent, and then by documenting the spatial changes in actively deforming areas by unravelling the geometrical evolution of the fault zone.

ACKNOWLEDGEMENTS

I am most grateful to Rob Butler, Sue Bowler, David Hunt, Jonathan Henton and Maurice Tucker for discussions and comments on the manuscript. I should also like to thank Carole Blair and Jeanette Finn for typing this paper and Maurice Tucker for completing the diagrams in my absence. This study was undertaken during the tenure of a BP studentship at Durham. I am also grateful to Clare Milsom and James Porter for assistance during fieldwork.

REFERENCES

Arnaud-Vanneau, A. and Arnaud, H., in press, Hauterivian to Lower Aptian carbonate shelf sedimentation and sequence stratigraphy in the Jura and northern Sub-Alpine Chains (South-eastern France and Swiss Jura). In: M.E. Tucker et al. (Editors), Carbonate Platforms, International Association of Sedimentologists Special Publication N. 9.

Archuleta, R.J., 1984, A faulting model for the 1979 Imperial Valley Earthquake, Journal of Geophysical Research, 89, No. B6, p. 4559-4585.

Bathurst, R.G.C., 1975, Carbonate sediments and their diagenesis, 2nd edition, Elsevier Scientific Publishing Company, New York, 658 p.

Bayer, R. et al., 1987, Premiers resultants de la traversee des Alpes Occidentals par sismique reflexion verticale (Programme ECORS-CROP), Compte Rendus de L'Academie des Sciences Pris, 305, p. 1461-1470.

B.R.G.M., 1967, Carte Geologique de la France au 1/50,000, Feulle, La Chapelle en Vercors, Bureau de Recherches Geologiques et Minieres, Orleans.

B.R.G.M., 1978, Carte Geologique de la France au 1/50,000, Feulle, Grenoble, Bureau de Recherches Geologiques et Minieres, Orleans.

B.R.G.M., 1983, Carte Geologique de la France au 1/50,000, Feulle, Vif, Bureau de Rechereches Geologiques et Minieres, Orleans.

Butler, R.W.H., 1987, Thrust evolution within previously rifted regions: An example from the Vercors, French Sub-Alpine Chains, Mem.Soc.Geol.Italia. 38, (in press 1989).

Butler, R.W.H., 1988, The geometry of crustal shortening in the Western Alps, In: Sengor, A.M.C. (Editor), Tectonic evolution of the Tethyan Regions, Proc. Nato Ad. Inst., Istanbul, Turkey, C259, p. 43-76.

Butler, R.W.H., 1989, The influence on pre-existing basin structure on thrust system in the Western Alps, In: M.A. Cooper and G.D. Williams (Editors), Inversion Tectonics, Geological Society, London Special Publications, p. 105-122.

Bulletin de la Societe Geologique de France, Nos. 4 and 5, 1988, Volume IV.

Carte 3225 Ouest, Serie Bleu, 1/25,000, Villard de Lans.

Chu, C.L. and Wang, C.Y., 1981. Permeability and Frictional properties of San Andreas Fault gouges, Geophysical Research Letters, 8, no. 6, p. 565-568.

Cox, S.J.D. and Scholz, C.H., 1988, On the formation and growth of faults: an experimental study, Journal of Structural Geology, 10, no. 4, p. 413-430.

Coward, M.P. and Potts, G.J., 1983, Complex strain patterns developed at the frontal and lateral tips to shear zones and thrust zones, Journal of Structural Geology, 5, no. 3/4, p. 383-399.

Debelmas, J. and Lemoine, M., 1970, The Western Alps: Palaeogeography and structure, Earth Science Reviews, 6, p. 221-256.

Debelmas, J. and Kerchove, C., 1980, Les Alpes France-Italiennes, Geologie Alpine, 56, p. 21-58.

Elliott, D., 1976, The energy balance and deformation mechanisms of thrust sheet, Philosophical Transactions of the Royal Society of London, A283, p. 289-312.

Engelder, J.T., 1974, Cataclasis and generation of fault gouge, Geological Society of America Bulletin, 85, p. 1515-1522.

Etheridge, M.A., Wall, V.J. and Cox, S.F., 1984, High fluid pressures during regional metamorphism and deformation: Implications for mass transport and deformation mechanisms, Journal of Geophysical Research, 89 B6, p. 4344-4358.

Ghisetti, F., 1987, Mechanisms of thrust faulting in the Gran Sasso Chain, Central Appenines, Italy, Journal of Structural Geology, 9, no. 8, p. 955-967.

Gidon, M., 1981, Les deformations de la couverture des Alpes Occidentales externes dans la region de Grenoble: Leurs rapports avec celles du socle, C.R., Acad. Sci. Paris, 292, p. 1057-1060.

Goguel, J., 1948, Le Role des failles de dechrochment dans le massif de la Grande Chartreuse, Bull. Soc. Geol. France, 18, p. 277-235.

Graciansky, P.C. et al., 1979, Genese et evolution comparee de deux marges continentales passive: marge Iberique de l'ocean Atlantique et marge Europeene de la Tethys dans les Alpes Occidentales, Bull. Soc. Geol. France, Paris, 7, XXXI, p. 663-674.

Kerrich, R., 1978, An historical review and synthesis of research of pressure solution, Zentbl Miner. Geol. Palaont, 5, p. 512-550.

Kerrich, R. and Hyndman, D., 1986, Thermal and fluid regimes in the Bitterroot Lobe Sapphire block detachment zone, Montana: Evidence from $^{18}O/^{16}O$ and geological relations, Geological Society of America Bulletin, 97, p. 147-155.

King, G. and Yielding, G., 1984, The evolution of a thrust fault system: processes of rupture initiations, propagation and termination in the 1980 El Asnam (Algeria) earthquake. Geophysical Journal of the Royal Astronomical Society, 77, p. 915-933.

Knipe, R.J., 1989, Deformation Mechanisms - recognition from natural tectonites, Journal of Structural Geology, 11, 1/2 p. 127-146.

Lemoine, M., et al., 1986, The Continental Margin of the Mesozoic Tethys in the Western Alps, Marine and Petroleum Geology, 3, p. 179-146.

Mitra, S., 1988, Effects of deformation mechanisms on reservoir potential in the Central Appalachians Overthrust Belt, American Association of Petroleum Geologists Bulletin, 72, p. 536-554.

Mugnier, J.L., Arpin, R. and Thouvenot, F., 1987, Coupes Equilibrees a travers le massif sub alpin de la Chartreuse, Geodinamica Acta, (Paris), 1, no. 2, p. 125-137.

Ramsay, J., 1963, Stratigraphy, Structure and Metamorphism in the Western Alps, Proceedings of the Geologists Association, 74, p. 357-391.

Reynolds, S.J., 1987, Structural aspects of fluid-rock interactions in detachment zones, Geology, 15, p. 362.

Rutter, E.H., 1983, Pressure solution in nature, theory and experiment, Journal of the Geological Society of London, 140, p. 725-740.

Rye, D.M. and Bradbury, H.J., 1988, Fluid flow in the crust: an example from a Pyreneean thrust ramp, American Journal of Science, 288, no. 3, p. 197-235.

Sibson, R.H., Moore, J.M. and Rankin, A.H., 1975, Seismic Pumping - a hydrothermal fluid transport mechanism, Journal of the Geological Society, London, 131, p. 653-659.

Sibson, R.H., 1981, Fluid flow accompanying faulting: Field evidence and Models. In: D.W. Simpson and P.G. Richards (Editors), Earthquake Prediction, An international review, p. 593-603.

Sibson, R.H., 1989, Earthquake faulting as a structural process, Journal of Structural Geology, 11, no. 1/2, p. 1-14.

Vieban, F., 1983, Installation et evolution de la plate-form Urgonienne (Hauterivian a Bedoulien) du Jura meridional aux chaines sub alpines (Ain) Savoie, Haute Savoie, These 3e cycle, Grenoble.

Williams, G. and Chapman, T., 1983, Strains developed in the hangingwalls to thrusts due to their slip/propagation rate: a dislocation model, Journal of Structural Geology, 5, no. 6, p. 563-571.

Wojtal, S. and Mitra, G., 1986, Strain hardening and strain softening in fault zones from foreland thrusts, Geological Society of America Bulletin, 97, p. 674-687.

Woodward, N.B., Wojtal, S., Paul, J.B. and Zadins, Z.Z., 1988, Partitioning of deformatoin within several external thrust zones of the Appalachian orogen, Journal of Geology, 96, p. 351-361.

Zweidler, D., 1985, Genese des gisements d' asphalte des formations de la Pierre Jaune de Neuchatel et des calcaires Urgoniens du Jura (Jura neuchatelois et nord-vaudois). These Universite Neuchatel, 107 pp.

PETROLEUM AND TECTONICS IN MOBILE BELTS

Edited by
Jean LETOUZEY
Institut Français du Pétrole

Publication in English

Organized by
Institut Français du Pétrole

Commercial quantities of oil and gas have been discovered in several fold and thrust belts. Around the world these zones, which for several years have been the main target of oil exploration, are arousing new interest with the development of new ideas and techniques.

The principal problems in folding oil in such complex areas are to accurately locate the structural traps and determine if they lie in a potentially productive area.

This volume contains a selection of papers presented during the 4th IFP Exploration Research Conference, held in Bordeaux, November, 14-18, 1988.

They focus mainly on: geodynamics of thrust belts and associated basins; new approaches to compressional structures; physical models, balanced cross-sections, case histories of thrust belts and foreland basins.

CONTENTS

1990, 1 vol., hardback, 210x275 mm, 224 p., 162 figs., 6 photos ..... FF 336
ISBN 2-7108-0579-0 COLLECTION COLLOQUES ET SÉMINAIRES, N° 47

ÉDITIONS TECHNIP 27 RUE GINOUX 75737 PARIS Cedex 15 • FRANCE •
TELEX : EDITECP 200375 F • FAX 33 (1) 45 75 37 11 • **TÉL : 33 (1) 45 77 11 08**

Appendix 9

Deformation and diagenetic histories within transfer zones between foreland thrust faults: An example from the area around the Col de la Bataille, Vercors, French Sub-Alpine Chains.

Introduction

A transfer zone between the two major thrusts exists in the area around the Col de la Bataille. In this area, the mountain front structure consists of the Pont en Royans Anticline in the north, and the Beauregard-Baret Anticline in the south. Borehole data show that the Beauregard-Baret Anticline is underlain by a thrust (Figure 2.12, in thesis). The Pont en Royans Anticline is also likely to be underlain by a splay from the Voreppe Thrust, exposed to the north. The anticlines are arranged en echelon (see Figure 1). This suggests that the displacement responsible for producing the mountain front structure in Royans is transferred from the thrust underlying the Pont en Royans Anticline in the north to the thrust underlying the Beauregard-Baret Anticline in the south. The transfer zone between the two structures lies in the area around the Col de la Bataille where a set of early normal faults is known to exist (Butler, in press). It has been suggested that pre-existing normal faults may serve to localise later compressional deformation by fault reactivation or cause widespread deformation and complex thrust geometries (Welbon, 1988). The Col de la Bataille shown in Figure 2.18 (Chapter 2), has been cited as a locality where a complex thrust geometry has developed due to the existence of a pre-existing normal faults (Butler in press). It is suggested here that the pre-existing normal fault at the Col de la Bataille may have, at least in part, controlled the position of the transfer zone between the Pont en Royans Thrust and the Beauregard-Baret Thrust. It has been suggested that the areas around offset segments of fault zones contain long-lived barriers to rupture propagation during seismogenic faulting (King & Yielding, 1984; Sibson, 1986). The offset of fault segments may be initiated in part by pre-existing heterogeneities in the geology

before the onset of deformation. The pre-existing normal fault at the Col de la Bataille which is thought to have disrupted the later compressional deformation producing a complex thrust geometry, may be an example of such a heterogeneity. Further controls on the position of the transfer zone at the Col de Bataille may be en echelon offsets in the buried Isere Fault as discussed in Section 2.5.

The structures exposed around the Col de la Bataille provide an opportunity to examine the deformation and diagenetic histories of a compressional structure associated with a pre-existing normal fault which lies in a transfer zone between two major thrusts. This will allow comparisons and contrasts with "simple" thrust zones such as the Ferriere and Rencurel Thrust Zones to be drawn. The "simple" thrust zones mentioned above, which are discussed in this thesis are examples where pre-existing structures do not seem to have played an important role in controlling the geometrical development of the fault zone. Also the exposures described from these thrusts lie along segments of the thrusts away from transfer zones. Sibson (1986) has suggested that complex structurally-controlled mineralisation is preferentially sited in areas between offset fault segments. Thus, it is important to examine the deformation and diagenetic histories in such zones of offset and compare these to data from along fault segments to fully understand the links between deformation and fluid flow in the sub-surface along strike within a thrust system.

This Appendix presents data from a study carried out at the Col de la Bataille during the tenure of this PhD study. Thirty orientated thin-sections were prepared to aid this study, the sample sites being carefully located onto a black and white photo-montage which is represented here by a line drawing. The positions of all the faults which were visible at outcrop were also marked onto the the photo-montage whilst in the field. This study formed a major part of the study undertaken during the tenure of this PhD, the work being presented at conferences abroad and in the UK.

Geological setting of the Col de la Bataille

The Col de la Bataille is situated at the southern termination of the Royans district (see Figure 1). In this area, the Beauregard-Baret Anticline dies out towards the north and Mesozoic rocks are hidden beneath a cover of Eocene/Oligocene and Miocene rocks. The Eocene/Oligocene continental clastic deposits show growth sequences into normal faults, which exist on the limbs of the Beauregard-Baret Anticline. These faults are probably related to the formation of the Rhone-Bresse Basin. Miocene shallow marine sandstones, siltstones and limestones were deposited in the Bas Dauphine Foreland Basin which developed during Alpine compressional tectonics. The Eocene/Oligocene and post mid-Miocene stratigraphy is folded around the Beauregard-Baret Anticline and lie in the footwall to a thrust which underlies the mountain front structures exposed at the surface which run from just north of the Col de la Bataille, close to Pont en Royans and north along the western margin of the Mesozoic rocks exposed within the Vercors. South of Pont en Royans, the mountain front is defined by the Beauregard-Baret Anticline which lies to the west of the Col de la Bataille. This suggests that in post mid-Miocene times, thrusts and thrust-related anticlines were growing in the Royans district. Spore colouration is yellow/yellow-orange within the Hauterivian rocks at the Col de la Bataille. This indicates that the structure was at a burial depth in the order of 1-3km during the deformation before thrust-related and post-thrusting isostatic epeirogenic movements uplifted the structure allowing erosion to exhume the structure. Compressional structures are well exposed in a road-cut at the Col de la Bataille shown in Figure 2. These exposures provide an opportunity to examine the structural styles and the controls on syn-kinematic fluid flow which exist at depth in a transfer zone between two major thrusts.

Structures exposed around the Col de la Bataille

Figure 1B shows a detailed map of the area around the Col de la Bataille. The Pont en Royans Thrust which terminates in this area. To the north large stratigraphic separation occurs across the thrust, with Mesozoic rocks being thrust upon Miocene rocks. The thrust, although not exposed is presumably a fairly localised zone of deformation (<100 metres wide) as bedding less than 200 metres from the thrust returns to horizontal on the backlimb of the hanging-wall anticline. At the southern termination of the Pont en Royans thrust, in the area around the Col de la Bataille, many small zones of high compressional strain can be found associated with pre-existing normal faults in an area around 5km across No single thrust with large stratigraphic separation can be mapped. The high strain zones marked on Figure 1 consist of zones of intense folding and minor thrusts. They are particular marked in thin-bedded units such as the U. Aptian "Lumachelle" bioclastic limestones, U. Cretaceous limestones and Hauterivian limestones and lime-mudstones. The massive Barremian "Urgonian" limestones and dolomites are also highly deformed by minor thrust arrays. High strain zones associated with pre-existing normal faults are not found to the north along the trace of the Pont en Royans Thrust. An explanation for the association between pre-existing normal faults and later zones of high compressional strains may be achieved by interpretation of the structures exposed at the Col de la Bataille.

Around the Col de la Bataille compressional deformation is distributed over a wide zone (500-600 metres) in the form of a folding associated with minor thrusts. The pre-existing normal fault which exists at the Col de la Bataille, down-throws relatively hard-to-deform massive Urgonian limestones against relatively easy-to-deform Hauterivian interbedded limestones and lime-mudstones. The rheological contrast across this early normal fault may have formed a barrier to thrust related displacement and forced the production of wide zone of compressional damage. The

geometry of the structures at the Col de la Bataille are described below.

The area around the Col de la Bataille is an example of a wide zone of deformation which exists at the southern termination of a major thrust. Rheological contrasts across individual faults within the set of early normal faults in this area may have formed a barrier to the propagation of displacements associated with the Pont en Royans Thrust. Compressional displacements produced high strain zones associated with individual pre-existing normal faults. Compressional displacement was distributed over a large number of localities existing in a zone around 5km across. To the south, compressional displacements were accommodated by slip along the Beauregard-Baret Thrust.

Structural geometries exposed at the Col de la Bataille

Figure 3 shows a line drawing of a black and white photo-montage from the road section (see Figure 2) at the Col de la Bataille. Bedding, the orientation of faults and the location of over fifty samples were located on the photo-montage in the field. Faults were only marked if fault rocks were visible at outcrop. This methodology removes the possibility of marking fractures produced by unloading of the rocks during uplift and fractures produced by excavating the road section as faults. This procedure can only produce a minimum fault density as faults may be missed which may bias the study. Examination of thin-sections taken from away from the areas of fault rock show that the wall-rocks to the faults are relatively undeformed with sedimentary and diagenetic features such as cement and skeletal fragments visible. This suggests that the majority of faults can be seen at outcrop and that marking only faults visibly lined with fault rocks does not bias the study too adversely. Kinematic indicators were available for many of the faults in the form of calcite steps on fault planes, offsets of bedding and inclined pressure dissolution seams within the fault rocks. The bedding which is shown on the line drawing marks the limits of the exposure.

Figure 5 shows a field photo of the western end of the section where a pre-existing normal fault exists. The fault downthrows the Urgonian limestones against the Hauterivian interbedded limestones and lime-mudstones. For 20-30 metres to the east and west of the normal fault a dense array of minor thrusts exists, the part of which exists in the Hauterivian rocks being shown in Figures 6 & 7. The steeply-dipping Hauterivian rocks in the footwall to this normal fault contain thrusts which have been rotated along with bedding during the folding seen in Figure 3, so that they are now also steeply dipping. These faults were probably formed in a similar attitude and at the same time as the minor thrust at the eastern end of the section shown in Figure 3. All of these early structures including the steep bedding are cut by a set of thrusts dipping at around 25-40^{o} to the east indicating that they post-date folding.

Compressional deformation at the Col de la Bataille which lies in a transfer zone between two major thrusts began with the production of small displacement thrusts. These thrusts were rotated by folding which now occurs in the hanging-wall of a relatively large displacement backthrust (Figures 3 & 4). These rotated structures were then cut by a series of west-directed thrusts (Figures 5, 6 & 7). This suggests that structurally-controlled fluid flow associated with compressional deformation associated with a pre-existing normal fault, may occur in a wide zone 500-600 metres wide and that in the centre of this zone, complex temporal changes in the position of structurally influenced syn-kinematic fluid migration may occur.

Microstructural evolution within the Col de la Bataille (See Figures 8-13)

This Section describes the microstructures, deformation mechanisms and syn-kinematic fluid migration in the Hauterivian rocks involved in the structure at the Col de la Bataille. Figures 8 and 9 show detailed views of the material developed along the

faults within the Hauterivian rocks. The calcite along the faults exhibit euhedral crystal forms which form drusy fabrics which suggest that the calcite grew into fluid filled cavities. Porosity still exists within some of the fractures. The calcite has been deformed by cataclastic processes after it crystallised with striations, developed on the fault surfaces. Developed at right angles to the lineations are extensional fractures which have been healed by calcite which is cut by some of the striations. The microstructure of the area shown in Figure 9 is shown in Figure 10. Under cathodoluminescence the microstructure of this fault rock and indications of the nature of fluid involvement is displayed well. The Figure shows a plane-polarised light and cathodoluminescence view of calcite found lining the fault. An early phase of fracturing allowed fluid influx from which precipitated non-luminescent calcite which completely sealed the available porosity in the fault zone. The calcite fault rock was then re-deformed by fracturing allowing the influx of pore waters from which precipitated a phase of brightly-luminescent calcite. This brightly-luminescent calcite sealed the newly-formed fracture porosity. Further cataclastic deformation and greater damage along the fault zones is shown in Figure 12. Grain size reduction of the style of microstructures shown in Figure 10, that is, a fracture-filling calcite fault rock has produced a fault gouge. This fault gouge then became indurated, probably by precipitation of cement in intergranular pore spaces or pressure dissolution leading to chemical compaction and grain indentation, before renewed extensional fracturing occurred. This produced extensional fracture porosity which allowed the influx of pore waters from which non-luminescent calcite was precipitated causing porosity occlusion.

Deformation along the faults within the Hauterivian limestones and lime-mudstones involved significant dilatancy, influx of pore waters and cement precipitation, which occurred in several phases (Figures 8, 9, 10 & 11). The deformation also involved cataclastic grain-size reduction probably during frictional fault slip (Figure 12). Figure 13 shows a fault surface developed within the Urgonian limestones. Cataclastic grain size reduction has produced

a fault gouge. DMT has indurated the fault rock probably due to the action of cementation and pressure dissolution leading to chemical compaction.

The overprinting phases of cataclasis and diffusive mass transfer will have produced significant changes in the porosity and permeability of the fault rocks in the same way as discussed in the following manner. The dilational nature of fracturing increases the porosity and permeability of the fault zones promoting fluid flow. However, intense fracturing leading to the formation of cataclastic fault gouge textures involves grain size reduction which also reduces the size of intergranular pore spaces, leading to a reduction of permeability. The influx of fluid into the fracture porosity aids the mass transport of material in solution which may lead to the precipitation of porosity occluding cements within the fault zone. The material involved in mass transfer may be provided by the action of pressure dissolution which also leads to a reduction in porosity and permeability due to chemical compaction and a reduction in the size of available pore spaces. Cementation and pressure dissolution may be especially marked in rocks with small grain sizes such as fault gouges, where the small grain sizes reduce the distances involved in diffusional processes.

Conclusions

Syn-kinematic fluid flow in a transfer zone between two major thrusts and in the vicinity of pre-existing normal faults may be complex.

Around individual pre-existing normal faults, fracture porosity may be produced over a wide area several hundreds of metres across. This is in contrast to fracturing along localised major thrust zones such as the Rencurel Thrust Zone described in this thesis where deformation may be confined to zones of only around 100 metres across. Individual fractures and faults may undergo a complex textural evolution leading to episodic fluid flow. Also, faults and fractures may not all be deforming synchronously.

Early faults and fractures may be sealed before the initiation of structurally-controlled episodic fluid migration along later generations of faults and fractures. This may lead to temporal changes in the position of fluid migration associated with compressional deformation around individual pre-existing normal faults. Temporal and spatial changes in structurally-controlled fluid flow due to microstructural evolution and fault propagation sequences have also been recognised along major thrust zones, away from transfer zones such as the Rencurel and Ferriere Thrust Zones.

The major influence which pre-existing basin structures exert in controlling temporal and spatial changes in fluid flow during active compressional deformation, seem to be in producing complex thrust geometries. The microstructural controls on the evolution of porosity and permeability are generally similar.

Complex compressional deformation histories associated with pre-existing normal faults exist at a number of localities at the southern termination of the Pont en Royans Thrust. These localities are distributed over an area around 5km across. Fluid flow associated with this compressional deformation will also be distributed over an area around 5km across. This is in contrast to fluid flow associated with compressional deformation around "simple" thrust zones such as the Ferriere and Rencurel Thrust Zones which exist away from thrust terminations. Here, fluid flow associated with compressional deformation is thought to be confined to a zone less than 100 metres across.

Along strike in the thrust system in the Vercors, variations in structurally-controlled fluid flow occur. Transfer zones seem to be wide areas of deformation and structurally controlled fluid flow (<5km across). Along individual fault segments structurally-controlled fluid flow is confined to thin zones (<100 metres). This information may prove important in assessing the regional geometry of seals to conduits to fluids such as hydrocarbons and diagenetic brines.

Figure 1. Geological map of the Vercors showing the location of the Col de la Bataille. A thrust can be mapped south of Pont en Royans which is thought to carry Mesozoic rocks in its hanging-wall onto the Miocene rocks of the Bas Dauphine Foreland Basin. Approaching the Col de la Bataille stratigraphic relationships suggest that an early normal fault downthrows massive Urgonian limestones against Hauterivian interbedded limestones and lime mudstones. This fault is exposed in a road section at the Col de la Bataille (see Figure 2) and has the same trend as normal faults which are associated with Eocene/Oligocene growth sequences at the northern termination of the Beauregard-Baret Anticline. Approaching the Col de la Bataille, no major thrust related repetition of the stratigraphy exists. In this area the thrust merges into a wide zone of folding and intense minor thrusting. Starred localities indicate areas where intense compressional strains in the form of folding and minor faulting are situated.

Figure 2. View looking west onto the Col de la Bataille. Note the existence
of:-
A- A normal fault which downthrows the white Urgonian limestones against Hauterivian limestones and lime mudstones.
B- A thrust emplacing vertically-bedded Urgonian limestones onto gently dipping Urgonian limestone in the footwall.
C- The well exposed road section through the structure.

Figure 3. Line drawing of the black and white photo-montage from the road section (see Figure 2) at the Col de la Bataille.

Figure 4. Backthrust accommodating more than five metres of displacement. No match of bedding across the fault within the exposure. The backthrust also has at least 60cm of fault gouge developed along it. This relatively large displacement thrust separates the gently dipping eastern portion of the section where bedding is only gently dipping and only minor thrusts exist which displacements of less than one metre and fault rock thicknesses of

less than 10cm, from the western end where bedding is dipping steeply towards the west and a relatively high density of thrusts exists (See Figures 6&7). The lens cap is 50mm in diameter.

Figure 5. Field photo of the western end of the section where a pre-existing normal fault exists. The hammer is 40cm long.

Figures 6 & 7. Field photos of the steeply-dipping Hauterivian rocks in the footwall to this normal fault. The rocks are cut by early thrusts which have been rotated into a steeply dipping attitude by folding. A late set of thrust can be seen to cut across the steep bedding indicating that they post-date the folding. The hammer is 40cm long.

Figure 8. Detailed view of the material developed along the faults within the Hauterivian rocks, the coin being 2cm in diameter.

Figure 9. Detailed view of the calcite lining a fault within the Hauterivian. (S)- Striations developed on the fault surfaces. (E)- Developed at right angles to the lineations are extensional fractures which have been healed by calcite which is cut by some of the striations.

Figure 10. Plane-polarised light and cathodoluminescence photomicrographs of the microstructure of the area shown in Figure 9.

Figure 11. Plane polarised light and cathodoluminescence view of the microstructure of the fault shown in Figure 3. The microstructure is similar to that shown in Figure 10.

Figure 12. Plane-polarised light and cathodoluminescence photomicrographs of the indicating further cataclastic deformation along the fault zones.

Figure 13. Detailed view of a fault surface which is developed within the Urgonian which has been dolomitised prior to the

thrust related deformation. The coin is 2cm in diameter. Fracturing has led to grain size reduction of the carbonate wall-rocks so that the fault is coated in cataclastic fault gouge containing large angular fragments contained within a fine-grained matrix. The fault gouge is now indurated probably due to cement precipitation or chemical compaction during pressure dissolution. The thickness of this fault rock is generally less than 5cm thick and exists within relatively undeformed wall-rock where the pre-deformational texture of the the sedimentary rock containing skeletal fragments and cements is still visible.

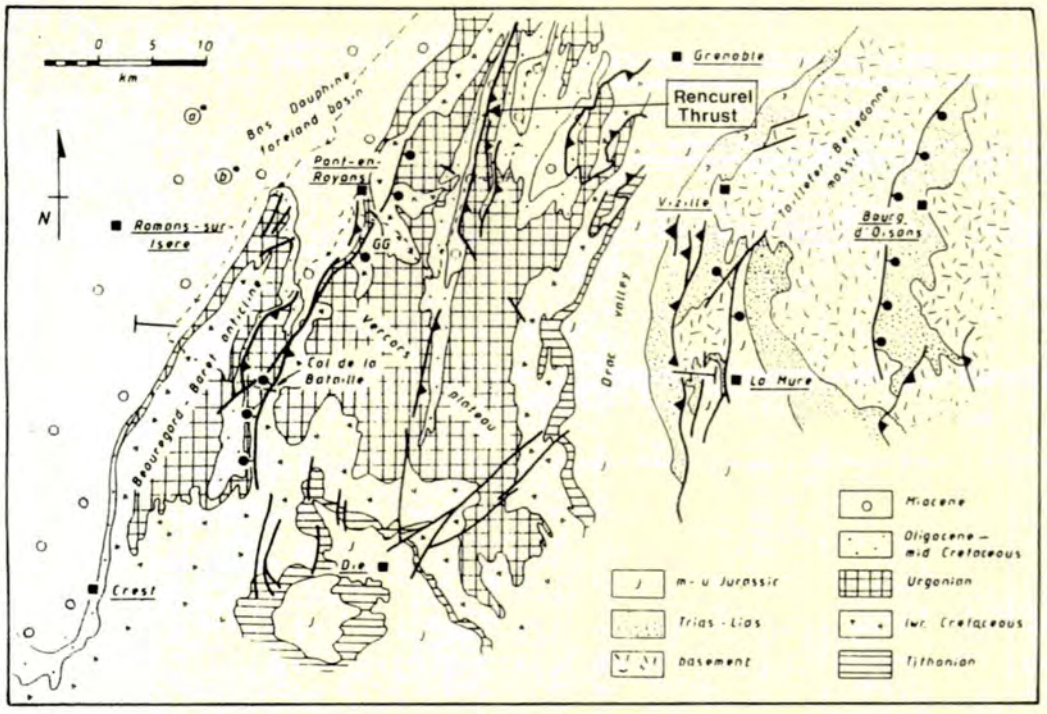

FIGURE 1**A**

FIGURE 2

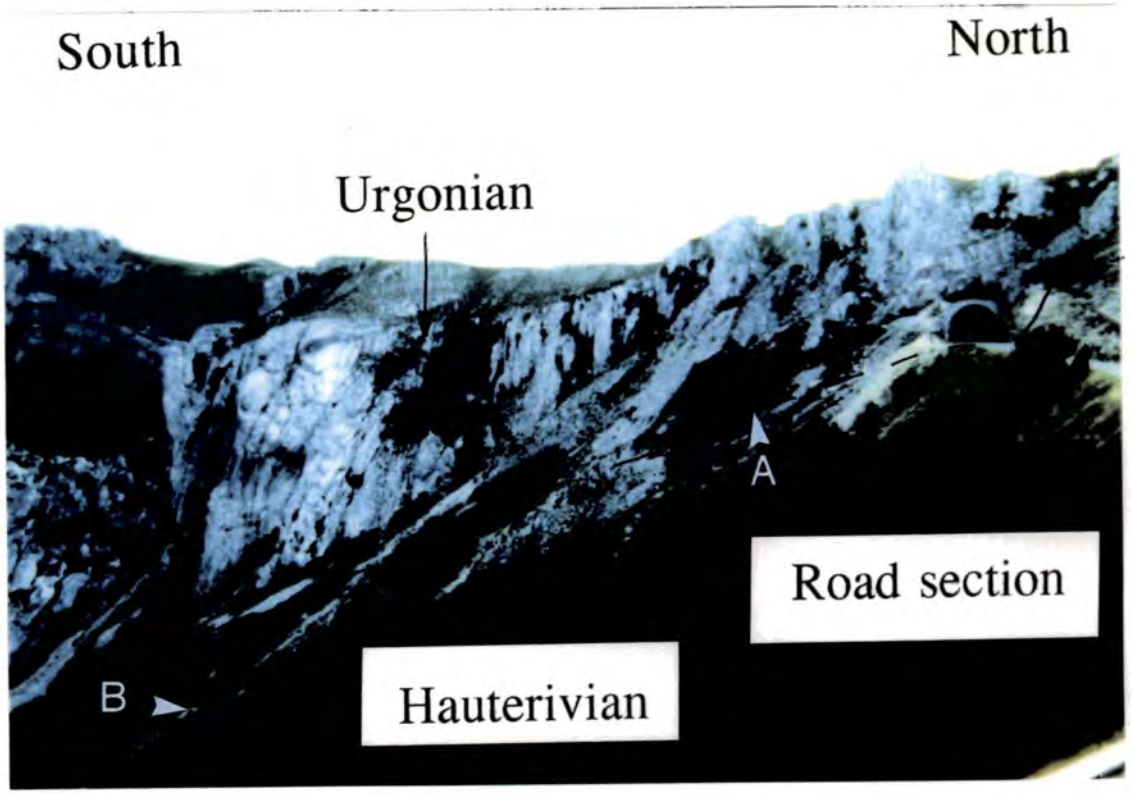

FIGURE 1B

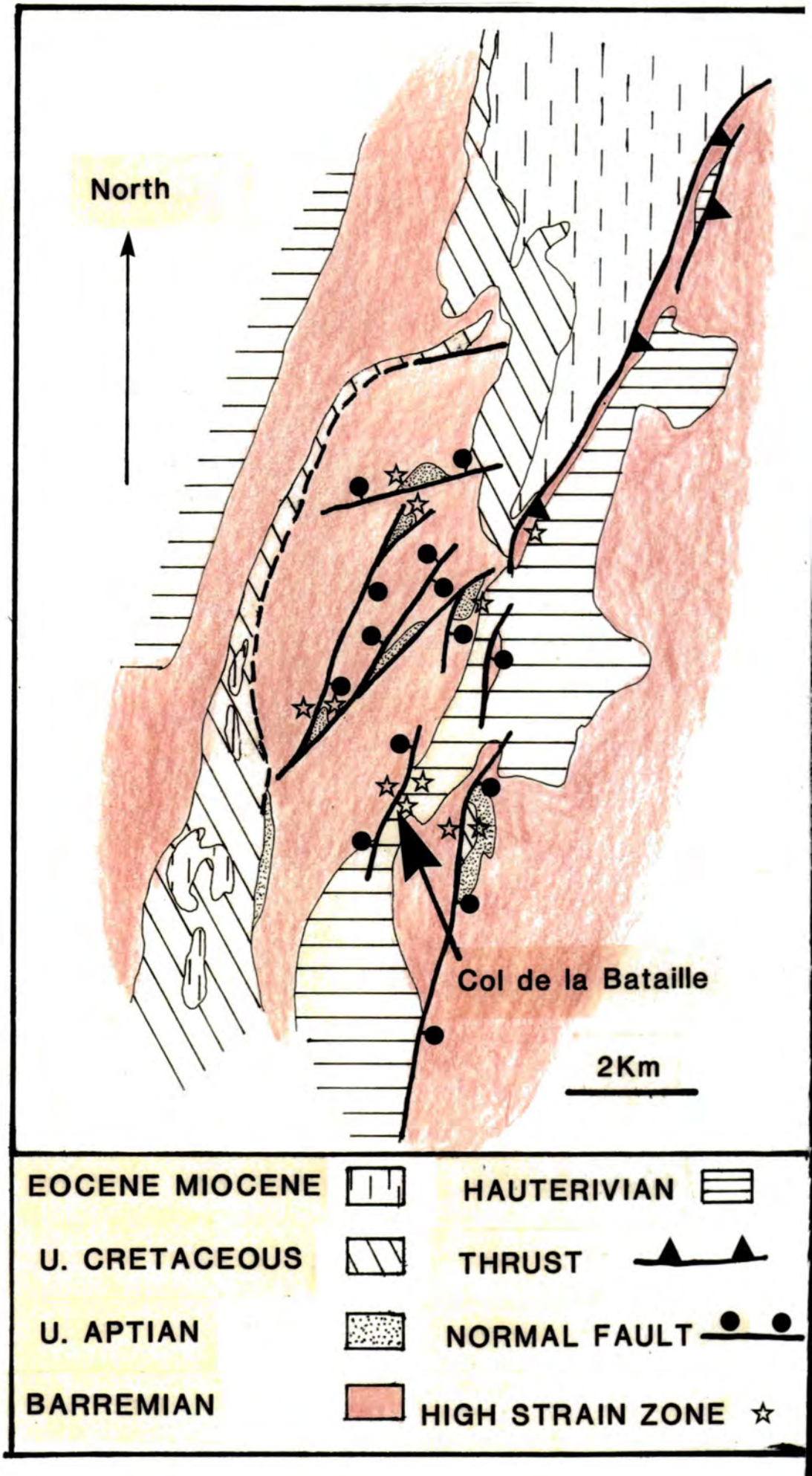
North
Col de la Bataille
2Km
EOCENE MIOCENE
U. CRETACEOUS
U. APTIAN
BARREMIAN
HAUTERIVIAN
THRUST
NORMAL FAULT
HIGH STRAIN ZONE

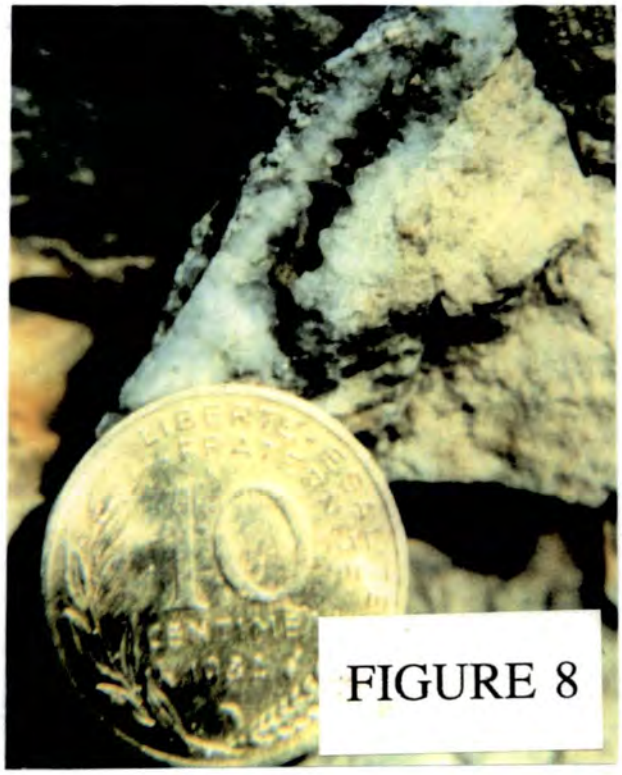

FIGURE 8

FIGURE 9

FIGURE 10

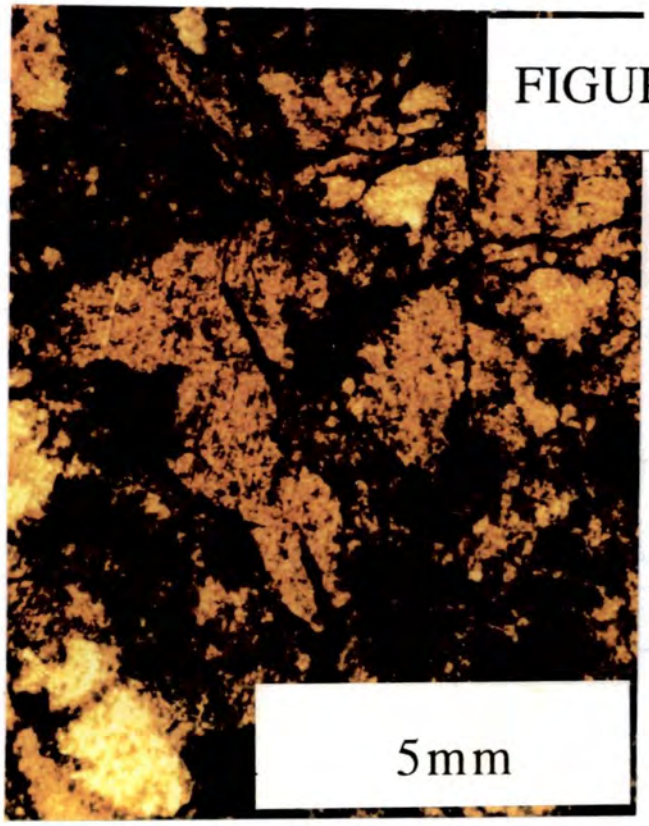

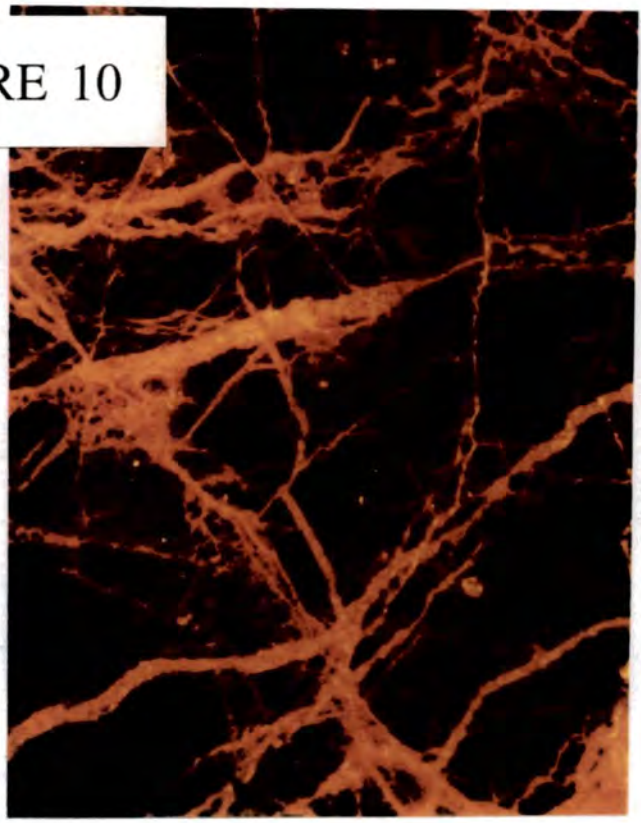

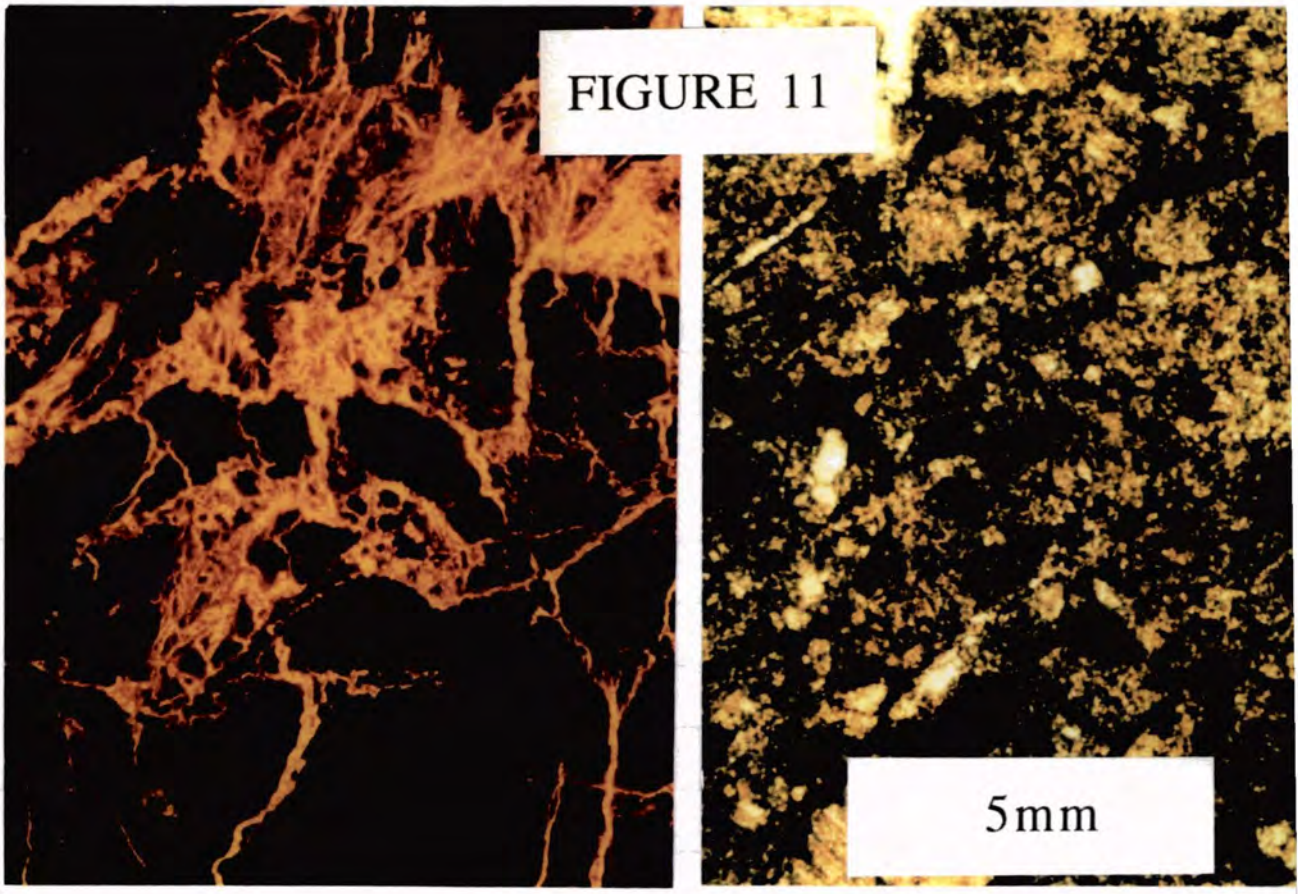
FIGURE 11
5mm

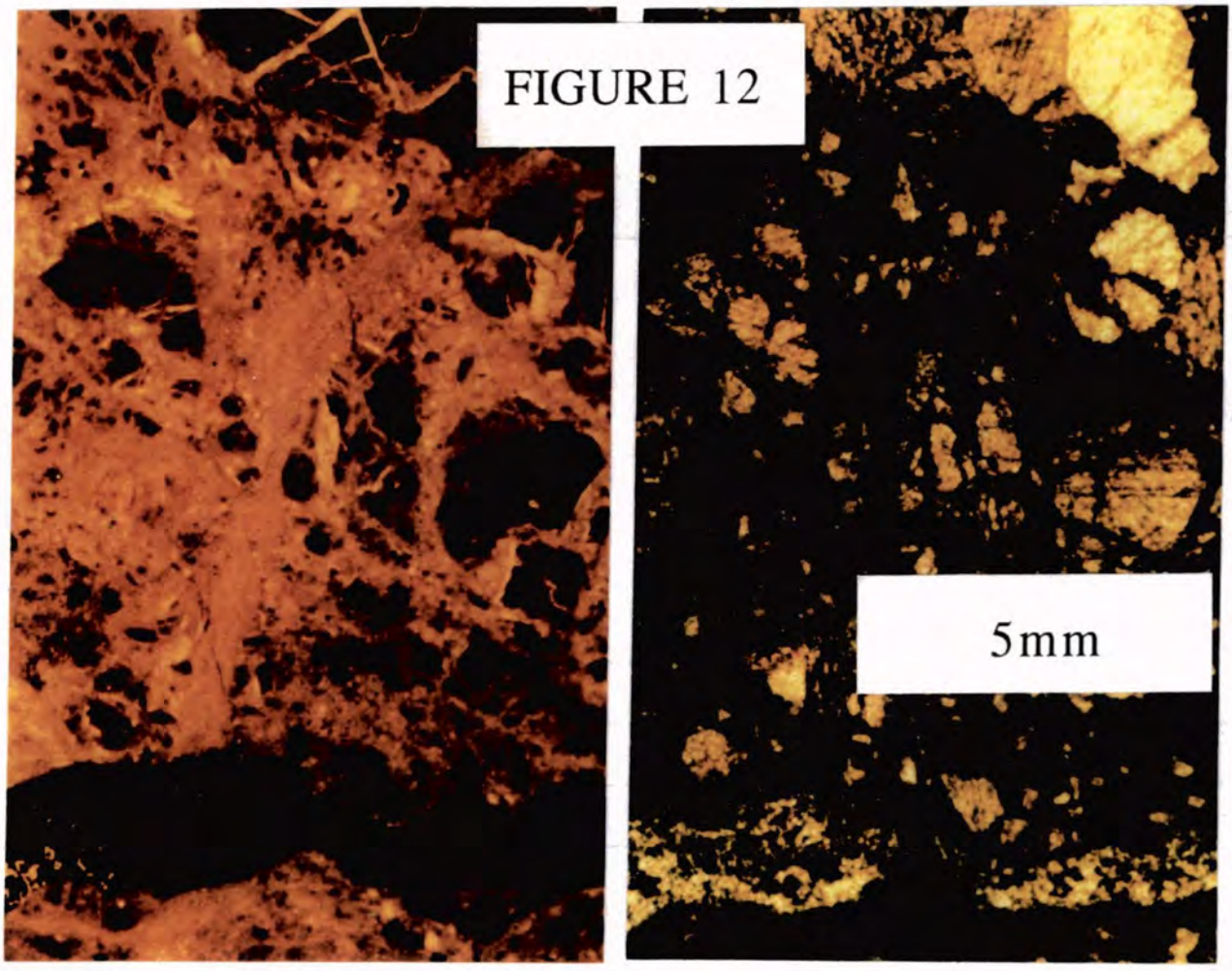
FIGURE 12
5mm

FIGURE 3.1 GEOLOGICAL MAP OF THE AREA SOUTH EAST OF LA BALME DE RENCUREL

KEY TO SYMBOLS

- Bedding
- Bedding,vertical
- Bedding,horizontal
- Bedding,overturned
- Lineation,with amount of plunge
- Contact,observed
- Contact,position uncertain
- Thrust fault,major displacement,observed
- Thrust fault,major displacement,position uncertain
- Thrust fault,major displacement,position very uncertain
- Thrust fault,minor displacement,observed
- Thrust fault,minor displacement,position uncertain
- Dip of fault plane
- Younging direction of the stratigraphy
- Anticline,fold axial plane showing dip and strike
- Syncline,fold axial plane showing dip and strike
- Early steep fault with dip

Scale

0 500 1000

Metres

- Line of section See Figure 3.2
- Contour lines every 100 metres
- Spot height
- Road
- Cliffs
- River Bourne

Grid North

1° 50' West Magnetic North

- Miocene Molasse, Burdigalien
  Conglomerates, sandstones and thin-bedded limestones
- Albian-Senonian. 250 metres.
  Quartz rich thin-bedded limestones. Glauconite and Phosphates.
- "Lumachelle" Bedoulian-Gargasian-Clansayesian
  Thin-bedded bioclastic limestone. 20 metres.
- "Urgonian" Barremian L.Aptian Massive white limestones
  Rudists and Foraminifera. Locally dolomitised. 300 metres.
- Hauterivian Interbedded limestones and lime mudstones. Echinoids.

Stratigraphy after BRGM 1983 Vif, Arnaud Vanneau 1980, Debelmas 1983 and Debrand Passard et al. 1984

Boundaries were marked with the aid of BRGM 1983 Vif. This was needed because the areas outside of the Gorges de la Bourne were poorly exposed.